The role of open-shell environments on the spectroscopy of complex spin architectures : wavefunction-based studies

Pablo Roseiro

▶ **To cite this version:**

Pablo Roseiro. The role of open-shell environments on the spectroscopy of complex spin architectures : wavefunction-based studies. Theoretical and/or physical chemistry. Université de Strasbourg, 2023. English. NNT : 2023STRAF032 . tel-04259690

HAL Id: tel-04259690

https://theses.hal.science/tel-04259690v1

Submitted on 26 Oct 2023

HAL is a multi-disciplinary open access archive for the deposit and dissemination of scientific research documents, whether they are published or not. The documents may come from teaching and research institutions in France or abroad, or from public or private research centers.

L'archive ouverte pluridisciplinaire **HAL**, est destinée au dépôt et à la diffusion de documents scientifiques de niveau recherche, publiés ou non, émanant des établissements d'enseignement et de recherche français ou étrangers, des laboratoires publics ou privés.

Université de Strasbourg

UNIVERSITÉ DE STRASBOURG

EDSC École Doctorale des Sciences Chimiques

ÉCOLE DOCTORALE DES SCIENCES CHIMIQUES

Institut de Chimie UMR 7177

THÈSE présentée par :

Pablo ROSEIRO

soutenue le : **8 septembre 2023**

pour obtenir le grade de : **Docteur de l'université de Strasbourg**

Discipline/ Spécialité : Chimie / Chimie Théorique

The role of open-shell environments on the spectroscopy of complex spin architectures: wavefunction-based studies.

THÈSE dirigée par :

M. Vincent ROBERT	Professeur, Université de Strasbourg, France

RAPPORTEURS :

M. Celestino ANGELI	Professeur, Università degli Study di Ferrara, Italy
Mme. Carmen JIMENEZ CALZADO	Professeure, Universidad de Sevilla, Spain

---

AUTRES MEMBRES DU JURY :

M. Cyrille TRAIN	Professeur, Université Grenoble Alpes, France
Mme. Nathalie VIART	Professeure, Université de Strasbourg, France

INVITÉS :

Mme. Nadia BEN AMOR	Docteure, Université Toulouse III, France

“Il en faut peu pour être heureux.”

—Baloo, *Le Livre de la Jungle*

Acknowledgements

Cette thèse n'aurait jamais eu lieu sans un nombre conséquent de personnes. Il m'est cher de les remercier dans les paragraphes qui suivent.

Avant toute chose, non pas une personne mais une valeur : je suis très reconnaissant d'avoir eu la chance de suivre une scolarité gratuite du début à la fin de mon cursus. L'éducation est à mes yeux un droit ineffaçable, dont l'accès doit être donné à tous. J'ai ainsi pu découvrir et apprécier la science, ce dont je suis grandement redevable.

L'ordre n'a que peu d'importance, cependant j'aimerais commencer par remercier mon directeur de thèse, Vincent. Lorsque je suis venu dans ton bureau en décembre 2019, je me suis dit que j'apprécierai faire ma thèse sous ta supervision. Nous voilà trois ans plus tard et je suis toujours aussi heureux d'avoir pris cette décision. Tu es à mes yeux le directeur de thèse idéal, tant du point de vue scientifique que du point de vue humain. J'ai énormément appris et grandi à tes côtés. Pour cela, je ne te remercierais jamais assez. Merci. Merci d'avoir fait de ces trois années une balade agréable. Merci pour ton encadrement strict mais constructif. Merci pour toutes ces belles discussions à la pause-café, dans ton bureau, en congrès, et pour toutes ces chouettes activités et sorties. Merci d'avoir aidé le scientifique en moi à s'épanouir, en m'offrant liberté et autonomie, tout en me protégeant. Simplement, merci d'avoir été mon directeur.

En parlant de vie de laboratoire, j'aimerais remercier toute l'équipe du LCQS pour la bonne ambiance pendant ma thèse. Merci à Manu pour toutes ces discussions passionnantes et d'être toujours aussi plein d'entrain pour parler de science. Merci à Chantal pour toutes ces questions sur le spin-orbite, mais surtout d'être si avenante et aidante avec les jeunes chercheurs. Merci à Roberto pour ses questions pertinentes et sa bienveillance à l'envers des doctorants. Merci à Guillaume d'être un informaticien si réactif et gentil, et pour toutes les heures passées ensemble à essayer de débugger et/ou d'installer certains programmes. Merci à Thomas pour toutes nos discussions non-scientifiques et les débats qui en suivaient.

Il m'est important de souligner la chance que j'ai eu de commencer ma thèse dans un

environnement riche en doctorants brillants qui sont devenus de chers amis. Merci à Oussama pour sa bonne humeur contagieuse, toutes les blagues, les heures passées à discuter de science au tableau, les discussions sincères. Merci à Filip pour sa gentillesse, toutes les idées débattues ensemble et d'être toujours partant pour une activité sportive ou culinaire. Merci à Lucie pour sa chillance hors du commun, pour toutes les discussions de Python et d'être ma super voisine de bureau.

Finalement, j'aimerais remercier les deux autres personnes qui ont grandement marqué ma thèse. Tout d'abord Sajanthan. Tu es vraiment une personne unique au monde, je ne pensais pas que la Kasteel et la quantique allaient si bien ensemble avant de te rencontrer. Outre la blague, je suis infiniment reconnaissant pour ta bienveillance, tes conseils et ta bonne humeur. Tu es un ami cher à mes yeux et ma thèse aurait été entièrement différente si tu n'avais pas été là pour me guider à mes débuts. Merci pour ces deux ans et demi passés ensemble, à discuter de science, de la vie, d'un peu tout, toujours dans la joie, le respect et l'écoute.

Enfin, le petit dernier, que je considère comme mon second mentor de thèse : Saad, le grand singe de Franche-Comté. Merci beaucoup de m'avoir guidé sur la voie, cher Rafiki. Tu es un primate d'exception et un ami précieux. J'aimerais te remercier pour tout, les discussions scientifiques et d'orientation, les blagues douteuses, ta participation active à la vie du labo, nos innombrables sorties sportives et culturelles, ta bienveillance et ton envie de science. Ces deux ans en ta compagnie étaient une sorte de rêve scientifique et je mesure la chance que j'ai eue. Je sais que nos chemins se recroiseront et cela m'enchante, j'ai hâte de voir toutes les merveilles que tu comptes faire au labo.

Il m'est important de remercier Nadia, mon mentor dans les calculs de fonctions d'onde étendue et dans les méthodes de localisation. J'ai appris énormément, de la programmation en Fortran à l'utilisation habile du bash et de vi, en passant par toutes ces méthodes développées à Toulouse.

J'aimerais remercier ma famille : Papa, Maman, Luce et Félix. Vous avez toujours soutenu mes envies scientifiques et m'avez inspiré de nombreuses fois. J'ai eu la chance d'être soutenu financièrement et socialement pendant mon éducation, tout en me laissant de la liberté, ce qui m'a aidé à devenir un adulte accompli, et désormais

un scientifique accompli. Merci beaucoup. Merci à Luce, ma sœur adorée, d'être aussi gentille et passionnée. J'ai hâte d'assister à ta thèse, dans trois ans. Merci à Félix, mon chat mignon, qui m'a toujours réconforté et aidé à coup de câlins et de miaulements. En quatre mots, merci à ma famille.

Il m'est aussi cher de remercier ma future belle-famille, grâce à qui j'ai découvert la Franche-Comté, ses coutumes et sa beauté. Merci à Christine et Jörg pour tout votre soutien, pour m'avoir accepté si simplement dans la famille et pour être tout bonnement extraordinaires. Merci à Renée et Louis pour toutes les parties de tarot, les histoires rigolotes et les plats délicieux. Merci à Béné et Manue de nous avoir hébergé à Agadir afin de faire une pause dans ma rédaction. C'était une aventure incroyable.

J'ai eu la chance d'être entouré scientifiquement, familialement mais aussi socialement. Les nombreuses personnes qui suivent sont mes amis chers, entrés dans ma vie pour y rester.

Toitoine, Marie, Marie, Julia, Alex, Louis, Tagir, Roman... Que dire de cette équipe fantastique, si ce n'est que ce sont tous.tes des amis profondément chers à mon cœur, avec qui j'ai partagé cinq années de joie et de galères. Heureusement que vous étiez là pendant cette thèse, je vous aime fort et n'ai pas les mots.

Chaque jour au labo était un plaisir grâce à l'ambiance qui y règne mais aussi grâce à la team du midi. Nous avons joué un nombre phénoménal de parties pendant 2 ans et demi, Skull King, Tichu et j'en passe. Merci à Baptiste, Gaël, Jordan, Nico et William d'avoir passé toutes ces heures à jouer et à se changer les idées.

En parlant de jeux, je souhaiterais remercier Dylan, Jordan et Dim, mes fidèles comparses de jeux-vidéos. Pendant près de 10 ans, nous nous sommes retrouvés en ligne afin d'oublier le travail et de s'amuser. J'espère que nous continuerons dans le futur, pour un max de feed&fun.

J'aimerais aussi remercier Flo, mon meilleur ami de longue date. Même si nous étions à plus de 700km, nous trouvions toujours le temps de nous retrouver une ou deux fois par an. Merci pour toutes ces discussions, sorties cinéma et entrain dans la vie.

Merci aussi à mon club de Kung-Fu et en particulier à Ethan, Léa, Niels et Bruno, grâce à qui j'ai pu amplement décompresser physiquement de la thèse. J'ai beaucoup appris et me suis bien amusé.

J'aimerais remercier ma psychologue, Mme Gollner, qui m'a aidé à surmonter une dépression à la moitié de la thèse et à grandir pour être une meilleure personne.

Merci à toutes les personnes qui m'ont accompagné pendant la thèse, pour n'en citer que quelques-unes, merci à : Anne-Charlotte, Franck, Maria, Masha, Paula, Elise, Jaison, Théo, Eloïse, Solal, Laurent, Leïla, Anne, Jean, Laura, Nikita, Jonathan, Benjamin, Guillaume, Vincent, Thomas, Essenam, Regina, Karina, Helena. J'ai forcément oublié du monde mais sachez que je vous remercie tous.tes d'avoir brillé un moment dans ma vie.

Certain.e.s semblent avoir droit à un traitement de faveur, c'est le cas de Marine, Jordan, Hannah, Lior, Elisabeth et Adrien. Vous êtes des personnes géniales, inspirantes et bienveillantes. Merci pour ces années d'amusement, de brunch et jeux en tout genre, de blagues et de bonne humeur.

Finalement, j'aimerais terminer par remercier ma fantastique fiancée, Alexia. Bientôt cinq ans ensemble et je suis toujours aussi heureux. Tu es une personne incroyable. Tu m'as connu dans les moments heureux mais aussi les tristes. Aussi, tu as continué à me soutenir en restant à l'écoute et en m'aidant. Je ne te remercierai jamais assez de faire partie de ma vie et de l'illuminer dans la joie et l'humour. Je t'aime.

Table of Contents

Papers

[1] Roseiro, P.; Robert, V. *Phys. Chem. Chem. Phys.* **2022**, *24*, 15945-15950

[2] Roseiro, P.; Ben Amor, N.; Robert, V. *ChemPhysChem* **2022**, *23*, e202100801

[3] Roseiro, P.; Petit, L.; Robert, V.; Yalouz, S. *ChemPhysChem* **2023**, *24*, e202200478

[4] Roseiro, P.; Yalouz, S.; Brook, D. J. R.; Ben Amor, N.; Robert, V. *Inorg. Chem.* **2023**, *62*, 5737-5743

Acronyms

Acronym	Meaning
AO	Atomic Orbital
AS	Active Space
BO	Born-Oppenheimer
C-G	Clebsch-Gordan
CAS	Complete Active Space
CASPT2	Complete Active Space second-order Perturbation Theory
CASSCF	Complete Active Space Self-Consistent Field
CFT	Crystal Field Theory
CI	Configuration Interaction
CMO	Canonical Molecular Orbital
CT	Charge Transfer
DDCI	Difference Dedicated Configuration Interaction
FCI	Full Configuration Interaction
FOIS	First Order Interacting Space
HDVV	Heisenberg-Dirac-Van Vleck
HF	Hartree-Fock
HOMO	Highest Occupied Molecular Orbital
IC	Internal Conversion
ISC	InterSystem Crossing
LCAO	Linear Combination of Atomic Orbitals
LFT	Ligand Field Theory
LIESST	Light Induced Excited Spin State Trapping
LMCT	Ligand-Metal Charge Transfer
LMO	Localized Molecular Orbital
LUMO	Lowest Unoccupied Molecular Orbital
MCSCF	Multi-Configurational Self-Consistent Field
MLCT	Metal-Ligand Charge Transfer
MO	Molecular Orbital
MOT	Molecular Orbital Theory

Acronym	Meaning
MP2	second-order Möller-Plesset
MRCI	Multi-Reference Configuration Interaction
NEVPT2	N-Electron Valence state second-order Perturbation Theory
PT2	second-order Perturbation Theory
QC	Quantum Chemistry
QCo	Quantum Computing
QDPT	Quasi Degenerate Perturbation Theory
RS-PT	Rayleigh-Schrödinger Perturbation Theory
SCF	Self-Consistent Field
SCO	Spin CrossOver
SF	Singlet Fission
SOC	Spin-Orbit Coupling
VT	Valence Tautomerism
WFT	WaveFunction Theory

Résumé en Français

Cette thèse étant rédigée en Anglais, une traduction équivalente à 10% du manuscrit se doit d'être réalisée en Français. Ainsi les parties majeures de la thèse, l'Introduction, les Résumés et les Conclusions des divers Chapitres sont traduits ci-dessous. Seule la partie du Chapitre 1 concernant les méthodes fonction d'onde a été traduite avec plus de détail, de part son possible intérêt pour un étudiant débutant la chimie quantique.

INTRODUCTION: Comme tous les êtres humains, nous attachons une importance singulière à notre environnement. Nous organisant en société, nous avons toujours été confrontés à la notion d'environnement. Socialement, nous nous réunissons en groupes dont chaque membre partage des intérêts communs avec les autres. Il s'agit d'un environnement social. Ces intérêts sociaux peuvent être considérés comme des paramètres qui définissent les individus. Dans la recherche de meilleures conditions de vie, nous rejoignons un groupe lorsque nous pensons que son environnement nous sera bénéfique, soit parce qu'il renforce nos croyances, soit parce qu'il nous apporte des avantages. À cet égard, lorsque différentes personnes rejoignent un même groupe, elles influencent indirectement ses caractéristiques. Mais alors qu'un groupe est façonné par les personnes qui le compose, celui-ci influence également ses membres. D'un point de vue économique, les entreprises rassemblent des salariés pour maximiser leur productivité. Les organisations non gouvernementales ont besoin de plus de personnes pour améliorer leur impact. Sur le plan politique, les partis se renforcent à mesure que des personnes les rejoignent. Sur le plan scientifique, la manière dont un enseignant transmet son savoir influence directement l'environnement scientifique des étudiants et peut encore les influencer une fois qu'ils sont devenus des scientifiques à part entière. Dans notre langage courant, nous utilisons le terme "environnement" pour désigner la Nature. La Nature est l'un des plus simples exemples de l'influence réciproque de l'homme sur son environnement. Nous l'avons détruite petit à petit, en tuant des espèces, en modifiant les écosystèmes, en la façonnant à notre guise, en lui jetant nos déchets... En ce sens, nous avons une profonde influence sur notre environnement. Pourtant, nous sommes toujours influencés par la nature, de notre naissance à notre mort. Si l'on se réfère au rapport

du GIEC de 2023,[1] il ne fait aucun doute que nous serons encore plus influencés par la Nature, en raison de notre comportement désastreux sur la Terre en tant qu'espèce. Mettant de côté des opinions personnelles, la notion d'environnement est un concept important en chimie. L'environnement chimique se définit à de multiples échelles.

Il peut tout d'abord être défini à l'échelle macroscopique. En chimie générale, l'environnement désigne le milieu dans lequel une espèce chimique évolue et peut influencer ses propriétés et son comportement. Il peut être vu comme l'ensemble des facteurs qui entourent une molécule ou un ion, c'est-à-dire les autres atomes ou molécules proches, les molécules de solvant, la température, la pression, le champ magnétique... Les molécules de solvant qui entourent une molécule peuvent modifier sa réactivité, sa solubilité et d'autres propriétés.[2] En thermochimie, il existe de nombreux exemples où le pH, la pression et la température peuvent favoriser ou défavoriser la réactivité d'une molécule.[3, 4, 5] En outre, la modification de l'environnement par l'utilisation d'un autre solvant peut jouer un rôle important dans les propriétés spectroscopiques d'une molécule, telles que ses spectres d'absorption ou d'émission (par exemple, le solvatochromisme). Cette définition se veut une image globale qui considère l'environnement comme un continuum périodique.

On peut alors définir l'environnement à une échelle plus petite, c'est-à-dire une portée autour de la molécule concernée. En chimie organique, l'empilement π et les liaisons hydrogène sont de bons exemples. Alors qu'une seule molécule *pi*-conjuguée occupe l'espace de façon aléatoire, la présence d'une autre molécule *pi*-conjuguée dans son environnement permet une interaction non covalente (chevauchement d'orbitales) qui empile les deux molécules. La spectroscopie de la première molécule peut alors être modifiée en fonction de son empilement π. D'autre part, certaines molécules ont des fréquences rotationelles plus élevées en phase gazeuse en comparaison avec celles en solution, en raison d'interactions non covalentes avec les molécules voisines, par exemple des liaisons H, des interactions de Van Der Waals... Cette notion d'environnement doit être différenciée de celle des réactions chimiques, où des liaisons covalentes sont rompues et créées. Dans ce cas, la notion d'"environnement réactionnel" se rattache à la première définition, un environ-

nement global.

En raccourcissant encore les distances d'interaction, on peut proposer une autre définition pour l'environnement, telle qu'elle est habituellement utilisée en chimie inorganique. Un composé de coordination est, dans sa forme la plus simple, un ion métallique entouré de molécules de ligands par des liaisons covalentes de coordination. L'environnement des ligands est généralement considéré comme l'environnement chimique du centre métallique, un "environnement de coordination". Historiquement, l'importance de l'environnement de coordination a été décrite par différentes théories. D'une part, la Théorie du Champ Cristallin (TCC),[6, 7] qui approxime l'ion métallique comme une charge positive ponctuelle et son environnement de coordination comme un champ électrique d'anions figés, considère leur interaction comme purement électrostatique. Cette théorie décrit correctement la levée de dégénérescence des orbitales métalliques d et f par la géométrie du milieu environnant. La séparation des orbitales métalliques dépend directement de la nature et de la géométrie de l'environnement de coordination, ainsi que de la nature de l'ion métallique et de son état d'oxydation. La structure électronique du complexe (haut spin ou bas spin), et plus particulièrement de l'ion métallique, est ainsi influencée par son environnement de coordination. D'autre part, la Théorie du Champ de Ligands (TCL), inspirée de la TCC et de la Théorie des Orbitales Moléculaires (TOM), décrit à la fois les interactions électrostatiques et les liaisons covalentes de coordination par l'utilisation d'orbitales moléculaires. Elle décrit la structure électronique du centre métallique et les caractéristiques de liaison, en fonction du type d'environnement. Ces deux théories visent à représenter l'influence de l'environnement de coordination sur un ion métallique.

À toutes les échelles, l'environnement peut avoir une influence sur les systèmes d'intérêt. Comprendre et quantifier cette influence est la clé de la rationalisation scientifique des propriétés des composés. Cependant, la notion d'environnement reste vague et l'environnement est souvent approximé ou même négligé. De plus, la chimie quantique ne peut pas se permettre de prendre en compte la description complète de l'environnement dans ses calculs. Ainsi, différentes approximations sont utilisées pour le prendre en compte intrinséquement (par exemple, les conditions périodiques pour les matériaux, les modèles de continuum polarisables pour les

solvants...). Cela permet d'obtenir des résultats plus physiques à un coût acceptable. Cependant, l'importance de l'environnement est parfois mal décrite et les quantités évaluées s'en retrouvent biaisées.

L'état de spin d'un environnement peut influencer la structure électronique d'une molécule, et la spectroscopie qui en résulte. En outre, différents schémas de couplage de spin peuvent apparaître, influençant davantage les interactions entre le site d'intérêt et son environnement. Des scénarios particulièrement intéressants apparaissent dans les systèmes à couche ouverte. C'est le fil rouge qui a guidé mes recherches au cours des trois dernières années. Cette thèse aborde deux questions liées au rôle de l'environnement sur la spectroscopie des architectures de spin, l'une en photochimie organique (1) et l'autre en magnétochimie inorganique (2). Elle est organisée comme suit.

Le Chapitre 1 introduit tous les éléments et méthodes nécessaires à la compréhension des deux autres Chapitres. Toutes les inspections de cette thèse sont basées sur la théorie de la fonction d'onde. Ainsi, ce Chapitre commence par la section (1.1), avec une présentation du problème électronique du point de vue de la théorie de la fonction d'onde. Les principaux ingrédients de la fonction d'onde utilisés dans cette thèse sont rappelés. Ensuite, dans la section (1.2), une brève introduction est donnée aux méthodes basées sur la fonction d'onde, afin d'introduire l'importance de la corrélation et des méthodes post-Hartree-Fock. Les méthodes d'interaction de configuration (IC) et de champ multi-configurationnel auto-consistent (MultiConfigurational Self Consistent Field - MCSCF) sont présentées pour mieux comprendre les deux méthodes de choix utilisées dans ce travail : la méthode du champ autocohérent de l'espace actif complet (Complete Active Space Self Consistent Field - CASSCF) et la méthode d'interaction de configuration par différence dédiée (Difference Dedicated Configuration Interaction - DDCI). La localisation est un concept important en chimie quantique qui permet une meilleure lisibilité des fonctions d'onde et une réduction possible du coût des calculs. Elle est donc exposée dans la section (1.3), et la méthode DoLo de localisation est brièvement présentée. La section (1.4) rappelle les opérateurs de spin et plusieurs éléments de l'algèbre de spin, par exemple les coefficients de Clebsch-Gordan. Enfin, la section (1.5) se termine par une introduction au concept de modèles en chimie quantique et aux Hamil-

toniens modèles qui en résultent. L'Hamiltonien de Heisenberg-Dirac-Van Vleck, un Hamiltonien modèle de choix pour les systèmes magnétiques, termine la section et ce Chapitre.

Le Chapitre 2 est consacré à un processus photophysique, la fission du singulet (Singlet Fission - SF). La SF est un phénomène prometteur qui nécessite au moins un dimère (covalent ou non) pour produire deux excitons après l'absorption d'un seul photon. Ce phénomène a suscité un intérêt croissant de la communauté au cours de la dernière décennie, tant du point de vue expérimental que théorique. De nombreuses conditions ont été théoriquement démontrées pour que le phénomène de SF se produise. L'une d'entre elles est la "condition thermodynamique", relative au positionnement des niveaux d'énergie des chromophores. Cependant, alors qu'il faut au moins deux chromophores pour que le phénomène se produise, de nombreux groupes théoriques prédisent de possibles candidats en calculant la spectroscopie d'un seul monomère, sans tenir compte de son voisin. Nous nous sommes demandé dans quelle mesure l'environnement immédiat d'un monomère donné peut moduler sa spectroscopie. Plus précisément, nous nous sommes concentrés sur l'influence de la structure électronique et de la structure de spin de cet environnement sur un monomère donné. Cela a soulevé les questions suivantes :

1) Le spin et la charge de l'environnement ont-ils une influence sur la condition thermodynamique du phénomène de la fission du singulet ? Comment peut-on quantifier et expliquer cette influence ?

Pour répondre à ces questions, le Chapitre 2 commence par présenter le phénomène de SF et ses applications dans la section (2.1). Ensuite, dans la section (2.2), un Hamiltonien modèle est développé. Il est basé sur un modèle minimal de deux molécules de dihydrogène, avec une molécule considérée "active" (dont la structure électronique peut se relaxer) et l'autre considérée comme un "environnement" gelé (dont la structure électronique est gelée dans un état donné). Les influences du spin et de la charge de l'environnement sur la spectroscopie du monomère actif sont mis en évidence et dimensionnés. Ce Chapitre se conclut et propose une autocritique dans la section (2.3).

Le Chapitre 3 se concentre sur un phénomène particulier : la *spinmérie*. La TCC et la TCL considèrent les ligands d'un composé de coordination comme un environ-

nement figé autour de l'ion métallique. En fonction de sa géométrie et de sa nature, cet environnement de coordination peut influencer le spin, l'état électronique et l'état d'oxydation de l'ion métallique. La versatilité du spin de l'ion métallique, c'est-à-dire sa capacité à changer d'état de spin en cas de modification de son environnement, est un effet important que l'on retrouve dans les complexes à transition de spin (Spin CrossOver - SCO). Cependant, ce phénomène se base sur la considération d'un environnement qui agit comme un champ moyen et est séparé du centre métallique. Cette considération est acceptée et prouvée dans le cas de ligands à couche fermée, mais elle est plus discutable dans le cas de ligands à couche ouverte, et plus particulièrement pour des ligands radicalaires. L'environnement généré par des ligands radicalaires présente une variabilité de spin en raison des couplages entre radicaux, ce qui remet en question la séparation entre l'ion métallique et son environnement. Ceci nous conduit aux deux questions suivantes :

2) Quelles sont les limites de la séparation entre un environnement de coordination et un ion métallique à transition de spin, lorsque l'environnement est aussi de spin variable ? Quelle est l'influence résultante sur la spectroscopie du complexe de coordination ?

Deux entités de spin variable couplées peuvent donner lieu à des scénarios inhabituels. L'un de ces scénarios est le phénomène de *spinmérie*. Ce phénomène peut être considéré comme une analogie de la mésomérie, les différentes structures de résonance étant des distributions d'états de spin locaux différents. Les principaux ingrédients de la *spinmérie* ont été identifiés comme étant la présence d'au moins deux entités de spin variable couplées. Cela engendre des états de spin total qui sont des superpositions de différents états de spin locaux. Alors que le spin total reste un nombre quantique pur, les spins locaux ne le sont plus. Néanmoins, les différents couplages entre les états de spin locaux des deux entités génèrent le même état de spin total. En ce sens, ce phénomène se produit même en l'absence des bien connus couplages spin-orbite. La *spinmérie* ouvre de nouvelles perspectives sur la notion d'environnement dans les composés de coordination et sur la conception de nouveaux dispositifs de spin-Qubits. Le Chapitre 3 commence, dans la section (3.1), par une introduction aux systèmes SCO et aux phénomènes connexes, par exemple le piégeage d'états de spin excité induit par la lumière (Light Induced Excited Spin

State Trapping - LIESST). Cela permet de mieux comprendre le phénomène de tautomérie de valence (Valence Tautomerism - VT) et ses ingrédients : les ions SCO et les ligands non innocents. Enfin, le phénomène de *spinmérie* est présenté plus en détail et des applications possibles aux ordinateurs quantiques et aux Qubits sont suggérées. La section suivante (3.2) présente une étude du phénomène de *spinmérie* basée sur un Hamiltonien modèle. Elle est basée sur un ion SCO d^2 (ou d^8) "artificiel", coordonné à deux ligands radicalaires, et est limitée aux interactions d'échange. Des structures d'état de spin inhabituelles sont observées et deux règles guidant l'apparition d'une *spinmérie* importante sont dérivées. La section suivante (3.3) est une étude *ab initio* d'un complexe oxoverdazyle de Co(II), à travers des méthodes basées sur la fonction d'onde (CASSCF et DDCI). Des états fondamentaux et des premiers états excités atypiques, car présentant un faible effet *spinmérique*, sont calculés. Il s'agit de la première observation *ab initio* de *spinmérie* dans un complexe de coordination. Ensuite, la section (3.4) présente une étude *ab initio* d'un complexe oxoverdazyle de Fe(II), en utilisant la même approche que dans la section (3.3). Alors que le spectre de basse énergie dépeint un schéma de Heisenberg-Dirac-Van Vleck (HDVV) habituel, les états quintuplet plus élevés sont des superpositions d'états de spin triplet et quintuplet locaux sur le Fe(II). Cette observation est la conséquence d'un phénomène de *spinmérie à l'état excité*. La modification du diagramme de Tanabe-Sugano d^6 par ce dernier effet est discutée, ce qui stimule de nouvelles perspectives pour les environnements de spin variables. Une manipulation de la *spinmérie* par le biais de l'effet LIESST est suggérée, ce qui permettrait de concevoir de possibles candidats de spin-Qubits. Enfin, la section (3.5) conclut le Chapitre par une autocritique.

Des conclusions et des perspectives clôturent enfin ce travail.

Chapitre 1: L'objectif de ce Chapitre est de présenter tous les éléments et méthodes nécessaires pour comprendre les développements théoriques ultérieurs des Chapitres 2 et 3. Il est divisé en cinq sections. Dans la section (1.1), le problème électronique et ses composantes sont présentés. Une attention particulière est accordée à la correction des éléments de matrice construits sur une base d'orbitales

non orthonormées. Dans la section (1.2), la méthode Hartree-Fock est brièvement présentée afin d'introduire les méthodes post-Hartree-Fock utilisées dans ce travail. Les méthodes CASSCF et DDCI sont expliquées dans la sous-section (1.2.5). La dernière partie de cette section donne quelques mots sur la théorie des perturbations. Dans la section (1.3), le concept de localisation et les approches *a priori* et *a posteriori* sont expliqués. La méthode DoLo, une méthode *a posteriori* utilisée dans le Chapitre 3, est présentée. Dans la section (1.4), les opérateurs de spin et les équations importantes du couplage de spin sont rappelés. Enfin, la section (1.5) présente, en quelques mots, le concept de modèles en chimie quantique et les Hamiltoniens modèles qui en résultent. Un bref commentaire est donné sur les Hamiltoniens effectifs, qui ne sont pas utilisés dans ce travail, et sur l'Hamiltonien de Heisenberg-Dirac-Van Vleck, qui est largement utilisé pour rationaliser les comportements magnétiques.

Le problème électronique:

L'objectif principal de la chimie quantique est de résoudre l'équation de Schrödinger. Dans cette optique, nous recherchons des solutions de l'équation de Schrödinger non relativiste :

$$\hat{H}|\Psi\rangle = E|\Psi\rangle \tag{1}$$

où $\hat{H}$ est l'opérateur Hamiltonien.

Un électron pèse environ 1836 fois moins que les protons et les neutrons. C'est le principal argument en faveur de l'approximation de Born-Oppenheimer (BO) : compte tenu du rapport de masse, on peut s'attendre à ce que le mouvement des électrons soit instantané par rapport à celui du noyau (composé de nombreux protons et neutrons). On peut donc supposer que les mouvements électroniques et nucléaires dans les molécules peuvent être traités séparément. Cela simplifie fortement les calculs moléculaires et permet de séparer la chimie quantique en deux points de vue : statique ou dynamique. Le point de vue statique considère les noyaux figés dans l'espace et étudie les structures électroniques (équation de Schrödinger électronique). Le point de vue dynamique suppose que le problème de la structure électronique a été résolu et étudie la dynamique nucléaire (équation de Schrödinger pour les mouvements nucléaires).

Dans le cadre de ce travail, nous nous intéressons au problème électronique pour les systèmes à géométrie gelée. Nous nous concentrerons uniquement sur l'Hamiltonien électronique $\hat{H}_e$ et la fonction d'onde Ψ_e.

Méthodes basées sur la fonction d'onde:

Venant de la chimie expérimentale, je peux affirmer que l'interprétation générale d'une molécule dans son état fondamental est souvent la configuration obtenue en remplissant $\frac{N}{2}$ OM avec N électrons de l'OM la plus basse (en énergie) à l'OM la plus haute. Ce concept s'inspire du principe d'Aufbau (qui s'applique aux atomes et aux ions) selon lequel "*un maximum de deux électrons sont placés dans les orbitales dans l'ordre croissant de l'énergie orbitalaire : les orbitales de plus faible énergie sont remplies avant que les électrons ne soient placés dans les orbitales de plus haute énergie*".[8]

Instinctivement, les chimistes représentent l'état fondamental d'une molécule comme une fonction d'onde mono déterminantale. C'est la base de l'approximation Hartree-Fock (HF) : supposer que la fonction d'onde à N-électrons exacte d'un système peut être approximée par un seul déterminant de Slater. Il est inutile de décrire l'approximation Hartree-Fock en plus de détails, car elle fait déjà l'objet d'une abondante littérature. Cependant, HF reste le point de départ de presque toutes les méthodes de chimie quantique et il est intéressant de commenter certains de ses points.

De mon point de vue, l'idée la plus intéressante que porte HF est de considérer que chaque électron du système à N-électrons "ressent" un champ moyen dû à la présence des $N-1$ autres électrons. Cela permet de découpler le problème à haute dimension de la fonction d'onde en plusieurs problèmes de dimensionnalité inférieure. Pour résoudre ce problème non linéaire et obtenir la racine la plus basse, il faut obtenir la meilleure fonction d'onde, comme le stipule le principe variationnel.

Pour ce faire, HF utilise une procédure appelée le champ autoconsistant (Self-Consistent Field - SCF). En bref, cette procédure commence par une estimation des OM à partir de laquelle le champ moyen, généré par $N-1$ électrons, (et le champ constant des noyaux) vu par chaque électron dans une OM est calculé, ce qui permet d'obtenir la valeur propre du système. En promouvant un électron dans

une OM virtuelle, il est possible d'évaluer l'énergie d'une OM virtuelle. Ensuite, les OM sont modifiées et la procédure est répétée itérativement, jusqu'à ce que l'autoconsistance soit atteinte (c'est-à-dire que le champ moyen ne change pas et est minimisé). Au final, on obtient l'énergie HF de l'état fondamental du système et son ensemble orthonormé d'OM.

Inconvénients d'Hartree-Fock:

Cependant, si l'on passe d'un système à $2N$ électrons à un système à $2N-1$ électrons, HF devient incapable de traiter le système. La même chose se produit lors de la recherche d'un état à couches ouvertes. Le concept de déterminant unique est limité à un déterminant entièrement doublement occupé. Ainsi a vu le jour la méthode Hartree-Fock non restreinte,[9] qui est capable de traiter les systèmes à couches ouvertes. Cependant, un nouvel inconvénient est apparu en raison de l'utilisation d'un seul déterminant pour décrire une couche ouverte, la contamination de spin : une fonction d'onde mono-déterminantale n'est pas une fonction propre satisfaisante de l'opérateur de spin total $\hat{S}^2$, et les états propres obtenus sont donc contaminés par le spin.

Un autre problème possible dans la méthode HF est l'approximation du champ moyen elle-même. Il s'agit d'une approximation puissante qui a son lot de responsabilités. En effet, elle apporte une moyenne des répulsions électron-électron en considérant l'interaction d'un électron avec un champ moyen généré par $N-1$ électrons. HF ne tient donc pas compte des fluctuations des répulsions électron-électron. Ces fluctuations sont particulièrement importantes dans la description des interactions faibles. Un exemple connu est la mauvaise description de H_2 à la limite de dissociation. En effet, la corrélation est nécessaire pour décrire avec précision certains phénomènes physiques.

Corrélation:

Il est important de présenter un concept majeur dans les méthodes de chimie quantique : l'énergie de corrélation. L'UICPA la définit comme "*la différence entre l'énergie Hartree-Fock calculée pour un système et l'énergie non relativiste exacte de ce système*".[10] Elle est due à la représentation approximative des répulsions électron-électron dans la méthode HF, également appelée corrélation de Coulomb.

HF remplace les interactions électron-électron instantanées par une interaction moyenne d'un électron avec un champ moyen de $N-1$ électrons. La méthode HF étant une méthode mono-déterminantale, elle peut être considérée comme une optimisation sous contrainte de l'équation de Schrödinger exacte non relativiste : elle ne tient pas compte de la corrélation électronique. Il est nécessaire de retrouver cette corrélation manquante, ce qui nécessite des méthodes post-HF décrites plus loin. Cependant, avant d'avancer, il est nécessaire de préciser trois faits :

1) La corrélation dépend fortement de la base utilisée. L'énergie non relativiste exacte (E_{exact}) d'un système nécessite un ensemble d'orbitales atomiques (OA) infini, ce qui est trop coûteux sur le plan informatique. Par conséquent, la corrélation est calculée à l'aide d'un ensemble fini d'OA suffisamment grand pour être considéré comme complet. En raison de la dépendance à la base, les comparaisons entre les méthodes doivent être effectuées dans le même ensemble de base complète.

2) Ainsi, la définition UICPA de l'énergie de corrélation (E_c) est généralement définie comme le gain d'énergie E par rapport à HF (E_{HF}).[1]

$$E_c = E_{HF} - E \tag{2}$$

3) L'énergie de corrélation est souvent divisée en deux types : la corrélation dynamique et la corrélation non dynamique (statique). Dans les deux cas, la corrélation est récupérée en passant d'une fonction d'onde mono-déterminantale à une fonction d'onde multi-configurationnelle. En d'autres termes: mélanger plus de déterminants de Slater $|\Phi_I\rangle$ au déterminant HF $|\Phi_{HF}\rangle$.

$$|\Psi\rangle = c_{HF}|\Phi_{HF}\rangle + \sum_I c_I|\Phi_I\rangle \tag{3}$$

Si c_{HF} est proche de 1 et que de nombreux déterminants excités sont ajoutés mais ne donnent qu'une faible contribution, alors la corrélation dynamique est principalement traitée. En revanche, s'il existe des déterminants $|\Phi_I\rangle$ avec des poids c_I proches de c_{HF}, alors la corrélation statique est principalement traitée. Cependant, ces définitions sont particulièrement arbitraires. La limite entre corrélation dynamique et statique n'est pas claire. Les configurations dégénérées et quasi-dégénérées doivent être prises en compte dans la corrélation statique mais qu'est-ce

[1] Toutefois, on peut trouver $E_c = E - E_{HF}$ dans la littérature.

qui définit le critère d'énergie de quasi-dégénérescence ? De plus, les configurations à plus haute énergie qui peuvent être considérées comme des perturbations devraient être prises en compte dans la corrélation dynamique, mais qu'est-ce qui définit les critères d'énergie ? En fin de compte, mon opinion est que chacun doit se satisfaire de sa propre définition. Une approche intéressante de l'arbitraire de ces définitions consiste à s'adapter dynamiquement au système, c'est-à-dire en utilisant l'espace d'interaction du premier ordre (First Order Interacting Space - FOIS). Dans la partie suivante, nous présenterons d'abord la manière de traiter ces deux corrélations, puis les méthodes axées sur la corrélation statique, et ne présenterons pas les méthodes axées sur la corrélation dynamique (Théorie des Perturbations).

Interaction de Configuration:

Au-delà de HF, une méthode de choix pour capturer la corrélation est la méthode dite de l'interaction de configuration (IC), décrite dans le paragraphe précédent. Elle consiste en une expansion de la fonction d'onde en une combinaison linéaire du déterminant fondamental et de déterminants excités. Ensuite, les coefficients c_I sont optimisés en respectant le principe variationnel.

$$\min_{c_I} \frac{\langle \sum_I c_I \Phi_I | \hat{H} | \sum_I c_I \Phi_I \rangle}{\langle \sum_I c_I \Phi_I | \sum_I c_I \Phi_I \rangle} \geq E_0 \tag{4}$$

Il s'agit de l'une des méthodes les plus simples sur le plan conceptuel. En pratique, elle revient à travailler avec $\binom{2K}{N}$ déterminants pour $2K$ spin-orbitales et N électrons. Cela en fait l'une des méthodes de chimie quantique les plus exigeantes en termes de calcul. Une première astuce pour réduire la taille du problème consiste à ne travailler que dans un sous-espace M_s choisi. Par exemple, supposons que nous calculons un état quintuplet ($S = 2$). Alors, en l'absence de tout champ magnétique extérieur, nous pouvons réduire le nombre de déterminants à $\binom{K}{4}\binom{K-4}{\frac{N}{2}-2}\binom{K}{\frac{N}{2}-2}$ en prenant seulement les $M_s = +2$ déterminants. La prise en compte de l'espace d'excitation complet est appelée méthode d'interaction de configuration complète (Full Configuration Interaction - FCI). Par rapport à la théorie HF dans laquelle les OM sont optimisées, cela n'est pas nécessaire dans la méthode FCI car l'amélioration de la fonction d'onde par les excitations est équivalente à la rotation des OM. Cependant, en raison de son énorme facteur d'échelle, cette méthode n'est possible que pour les systèmes de petite taille.

Pour économiser du temps de calcul et traiter des systèmes plus grands, nous devons tronquer l'espace IC. Cela donne lieu à la méthode ICD, limitée aux excitations doubles, à la méthode ICSD, limitée aux excitations simples et doubles, etc... Cependant, un problème important dans la troncature est la perte de la cohérence de taille. Cela signifie que l'énergie de deux sous-systèmes infiniment éloignés doit être égale au double de l'énergie d'un seul sous-système et que la fonction d'onde totale doit être égale au produit de chaque fonction d'onde individuelle, ce qui est perdu par la troncature. C'est pourquoi les méthodes d'IC tronquée doivent être utilisées avec précaution pour étudier la dissociation des molécules. Dans le cas contraire, il est nécessaire d'apporter des corrections appropriées pour retrouver une cohérence de taille.

Méthodes de champ autoconsistant multi-configurationnel:

Il existe des méthodes pour corriger la cohérence de tailles. Nous allons présenter ci-dessous un concept propre aux méthodes multi-configurationnelles, l'espace actif (Active Space - AS), ainsi que les méthodes qui lui sont associées.

Nous avons vu d'une part qu'HF utilise la méthode SCF à travers la rotation des OM pour minimiser l'énergie. D'autre part, une fonction d'onde multidéterminantale comme celle de l'interaction de configuration permet de récupérer l'énergie de corrélation. Néanmoins, nous ne pouvons pas nous permettre le coût de calcul du FCI et la troncature perd la cohérence de taille. Mais conserverions-nous la cohérence de taille si nous faisions une FCI dans un sous-espace plus petit ? C'est ce qui a motivé le développement des méthodes de champ autoconsistant multi-configurationnel (MultiConfigurational Self-Consistent Field - MCSCF). Au lieu de traiter le système dans son ensemble, seule une partie de celui-ci est étudiée à un niveau précis. Ce sous-espace plus petit est le concept de l'espace actif.

Tout comme les chimistes représentent une molécule par ses orbitales de valence, ce que l'on appelle l'espace actif est une tranche du système électronique qui est jugée plus importante que le reste du système, c'est-à-dire pour étudier des propriétés particulières. Il existe plusieurs méthodes MCSCF, mais je ne parlerai que de celle que j'ai utilisée tout au long de mon doctorat, la méthode CASSCF (Complete Active Space Self-Consistent Field). La méthode CASSCF est basée sur la définition

préalable d'un espace actif complet (Complete Active Space - CAS). En ce sens, les OM sont divisées en trois catégories :

- OM virtuelles, toujours vides, dénotées *r*, *s*.
- OM actives, occupation partielle d'électrons, dénotées *a*, *b*.
- OM inactives, toujours doublemenet occupées, dénotées *p*, *q*.

Le CAS est défini par un nombre n d'électrons dans un ensemble k d'OM actives (par exemple CAS[8,7] signifie 8 électrons dans 7 OM). Toutes les excitations possibles à l'intérieur du CAS sont générées (FCI à l'intérieur du CAS). Les fonctions d'onde sont donc construites comme des combinaisons linéaires des déterminants du CAS. Pour éviter les biais, ces déterminants sont traités sur un pied d'égalité, ce qui signifie qu'ils sont considérés comme dégénérés. CASSCF utilise ensuite le principe variationnel pour effectuer une double optimisation sur les OM ψ_i et sur la fonction d'onde CAS $|\Psi_{CAS}\rangle$.

$$\psi_i = \sum_k c_k \, \chi_k \quad \text{and} \quad |\Psi_{CAS}\rangle = \sum_I c_I \, |\Phi_I\rangle \tag{5}$$

où $\sum_I c_I^2 = 1$.

L'énergie du système est ensuite minimisée en suivant cette double optimisation jusqu'à convergence.

$$\min_{c_k, c_I} \frac{\langle \Psi_{CAS} | \hat{H} | \Psi_{CAS} \rangle}{\langle \Psi_{CAS} | \Psi_{CAS} \rangle} \geq E_0 \tag{6}$$

Cela permet de récupérer un grand nombre de corrélation statique et un peu de corrélation dynamique. Il est certain qu'étendre le CAS à la taille du système complet équivaut à faire un FCI (et l'étape d'optimisation des OM sera inutile), ce que nous ne pouvons pas nous permettre. Dans ce sens, CASSCF est un compromis intéressant entre les méthodes SCF et FCI.

Afin d'obtenir davantage de corrélation, il est également possible d'utiliser des méthodes d'interaction de configuration multiréférence (MultiReference Configuration Interaction - MRCI). Contrairement à la méthode d'IC où il n'y a qu'un seul déterminant de référence HF, la méthode MRCI utilise plusieurs déterminants comme référence. Une fois de plus, la troncature est nécessaire pour réduire le coût de calcul. En choisissant les références appropriées, on peut équilibrer la

corrélation entre l'état fondamental et l'état excité, car les excitations simples et doubles génèrent désormais des excitations triples et quadruples. Cependant, le problème de la cohérence de tailles subsiste dans les MRCI tronqués. Après avoir présenté les méthodes MCSCF, on peut voir que ces méthodes génèrent un ensemble d'OM approprié et une fonction d'onde multidéterminante. C'est une bénédiction pour les méthodes MRCI qui ont besoin de bonnes OM de départ. Il est alors possible de transmettre ces fonctions d'onde et ces OM à une méthode MRCI telle que DDCI afin d'obtenir une corrélation plus dynamique. Les méthodes MRCI tronquées sont bien décrites dans la littérature. Pour cette raison, je ne présenterai dans cette thèse que celles que j'ai utilisées ces dernières années, telles qu'elles sont mises en œuvre dans le code CASDI.

Méthodes d'Interaction de Configuration MultiRéférences

Nous allons maintenant discuter des méthodes MRCI implémentées dans le code CASDI et utilisées le long de cette thèse. Afin de générer différents déterminants excités, nous définirons certains termes : les "trous" (h) sont des excitations d'un électron des orbitales inactives vers l'AS ; les "particules" (p) sont des excitations d'un électron de l'AS vers les virtuelles. Ces excitations sont schématisées dans la Figure ci-dessous.

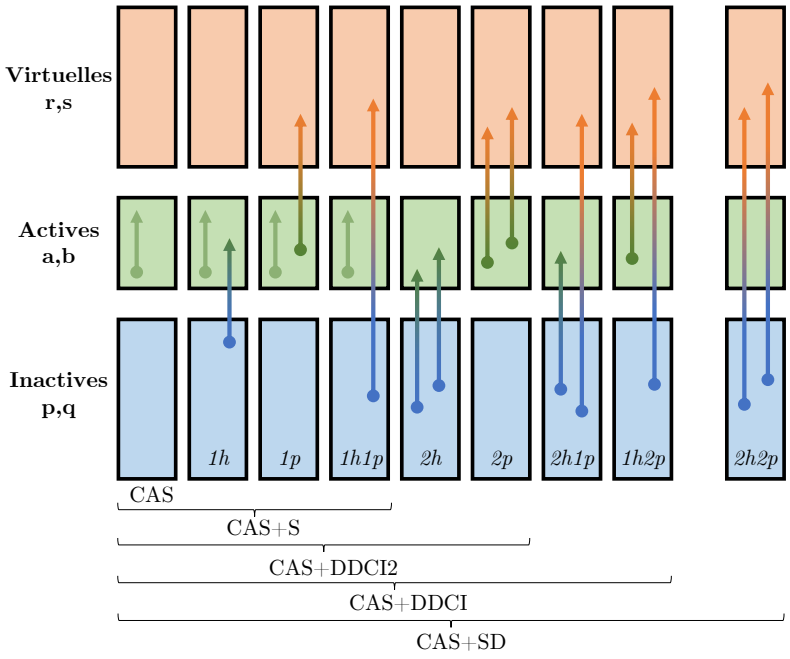

Figure 1: Différents types d'excitation de CAS à CAS+SD.

Commentons maintenant les méthodes MRCI mises en œuvre dans CASDI :

1) *CAS*. Il s'agit d'un calcul CASCI typique. Contrairement à CASSCF où la fonction d'onde et les OM sont optimisées, ici les OM sont gelées et un FCI est calculé dans le sous-espace CAS.

2) *CAS+S*. Il s'agit d'une méthode MRCIS. Elle diagonalise la représentation de l'Hamiltonien dans la base formée par les déterminants CAS et toutes les excitations simples : $1h$, $1p$ et $1h1p$.

3) *CAS+DDCI2*. Il s'agit d'une méthode MRCISD tronquée. Elle travaille avec des déterminants au niveau CAS+S et ajoute des excitations doubles depuis et vers le CAS uniquement, telles que : $2h$ et $2p$.

4) *CAS+DDCI*. Également appelé *CAS+DDCI3*. Il s'agit de la première méthode d'interaction de configuration par différence dédiée, une MRCISD tronquée. Elle utilise tous les déterminants précédents et génère davantage d'excitations doubles : $2h1p$ et $1h2p$.

On peut observer qu'il manque des excitations doubles en dehors du CAS : $2h2p$. En ajoutant ces excitations, on obtient une méthode MRCISD (un calcul CAS+SD dans CASDI). Cependant, ceci n'est pas nécessaire pour la plupart des composés magnétiques. En effet, les excitations $2h2p$, au second ordre de la théorie des perturbations, ne contribuent pratiquement pas aux différences d'énergie des états.

Localisation:

La question de la représentabilité des OM a fait l'objet de discussions au sein de la communauté quantique depuis ses débuts. Deux philosophies ont vu le jour : les OM localisées *vs.* délocalisées. Un Chapitre particulièrement intéressant (p.41-101) de Basis Sets in Computational Chemistry [11] présente les différentes méthodes de localisation et leurs avantages et inconvénients par rapport à la délocalisation. Je vais résumer les points qui me semblent importants dans le cadre de ce travail de thèse.

Dès les années 1930, les orbitales moléculaires localisées (OML) ont intéressé les chimistes quanticiens, car elles permettaient de représenter les liaisons selon le formalisme des liaisons de valence. Cependant, elles limitent les liaisons à une paire

d'électrons localisée entre deux atomes spécifiques, ce qui ne convient pas à de nombreux systèmes, notamment ceux dont les électrons sont délocalisés. Néanmoins, en tant qu'approximation, elle offre de la représentabilité aux étudiants de premier cycle qui étudient la chimie quantique et reste acceptable pour les petites molécules. Au contraire, le succès de la théorie des orbitales moléculaires (TOM) a introduit la notion d'OM délocalisées sur l'ensemble de la molécule. C'est ainsi que sont apparues les orbitales moléculaires canoniques (OMC), qui sont des OM optimisées après un calcul fonction d'onde. Les OMC sont aujourd'hui plus populaires que les OML car la différence entre l'énergie de deux OMC donne la fréquence de la transition électronique associée à ces deux orbitales. Cependant, le fait d'avoir des OM délocalisées est un inconvénient lors de l'analyse de la fonction d'onde, car on ne peut extraire que des informations globales.[2] Les blocs de construction de la fonction d'onde électronique sont les OM.[3] La liberté d'utiliser des OM localisées ou délocalisées vient du fait que l'on peut appliquer une transformation unitaire sur des OM délocalisées pour obtenir des OML, et vice-versa. Cela signifie que toute valeur, en particulier l'énergie, reste intacte, et que seule la structure de la fonction d'onde est modifiée. L'intérêt d'une représentation locale est double. Tout d'abord, elle est utile pour sélectionner les régions moléculaires qui sont physiquement "intéressantes", c'est-à-dire pour étudier les réactions chimiques, les états excités, les systèmes magnétiques, etc. En d'autres termes, elle peut permettre de réduire l'espace actif en ne travaillant qu'avec une sélection d'OML d'intérêt. Cela ouvre la voie à un deuxième avantage, à savoir la réduction possible de la taille de l'espace de référence, ce qui est pratique pour les calculs MRCI. Il existe deux concepts principaux de localisation : *a posteriori* et *a priori*.

Dans les méthodes *a posteriori*, un ensemble d'OMC est préalablement calculé puis transformé par une transformation unitaire pour obtenir des OML. Deux méthodes *a posteriori* populaires sont Foster-Boys,[12] où une fonctionnelle basée sur la position spatiale des OM est minimisée, et Pipek-Mezey,[13] où une fonctionnelle basée sur les charges atomiques partielles est maximisée.

[2]Les informations locales peuvent être trop compliquées à extraire.

[3]Les OM servent de blocs de construction pour les déterminants, ce qui permet de construire davantage la fonction d'onde.

Les méthodes *a priori* sont basées sur l'intuition chimique : une estimation des OML définie par l'utilisateur est utilisée comme point de départ. Ces OML convergent ensuite vers les OMC de référence d'un calcul de la fonction d'onde, à condition que les OML restent aussi locales que possible. Une méthode *a priori* de choix utilisée dans ce travail est mise en œuvre dans la suite de programmes DoLo.[14] Sa spécificité est la séparation des orbitales inactives, actives et virtuelles en trois classes. Il s'agit d'une méthode en deux étapes. La première étape (1) consiste à déterminer une estimation des OML. À partir d'OA non orthogonales, on commence par orthogonaliser chaque classe d'OA (inactive, valence, virtuelle) pour obtenir des OA orthogonales. Ensuite, des combinaisons linéaires d'OA orthogonales, guidées par les informations sur les liaisons et les fragments moléculaires contenus dans la matrice densité à un électron, sont réalisées pour produire des OML non orthogonales. Enfin, les OML non orthogonales sont séparées en classes inactives, actives et virtuelles, et chaque classe est orthogonalisée, avec un ordre de priorité différent.[4] La deuxième étape (2) est l'optimisation des OML. Elle consiste à projeter les OML sur des OMC de référence (après un calcul HF ou CASSCF antérieur). Les OML projetées peuvent perdre leur orthogonalité, une orthogonalisation finale est donc nécessaire. Cette procédure peut ensuite être répétée pour essayer d'augmenter la projection des OML sur les OMC.

Les méthodes *a posteriori* sont plus faciles à mettre en œuvre, mais plus difficiles à utiliser pour identifier les régions physiquement "intéressantes", car elles ne sont pas basées sur l'intuition chimique. Au contraire, cette intuition peut constituer un biais pour les méthodes *a priori*. Il existe de nombreuses autres méthodes de localisation. Un bref exemple est celui de la méthode des orbitales de liaison naturelles [15] et de son extension, l'approche des orbitales moléculaires localisées naturelles,[16] qui produit des OML optimales pour une description de la structure de Lewis. Il est également possible d'effectuer une localisation *a posteriori* "à la main" en procédant à une combinaison linéaire d'OMC choisies.

Enfin, il est important de souligner que toute stratégie d'OML brise la symétrie du système. La symétrie est en effet un allié puissant dans les calculs de chimie

[4] La priorité la plus élevée est accordée aux OML inactives, puis aux OML actives et enfin aux OML virtuelles.

quantique pour réduire leurs coûts. Il faut donc choisir entre l'utilisation d'OML pour clarifier le problème (région moléculaire et OM spécifiques) à l'aide de la localisation ou conserver la facilité de manipulation de la symétrie. Il est important de préciser que les OML peuvent potentiellement réduire la taille de l'espace de référence, et donc le coût de calcul. La mise en œuvre des OML est plus exigeante que l'utilisation de la symétrie, mais elle présente de nombreux avantages, en particulier pour l'analyse qualitative des données.

Modèles:

Il est particulièrement fastidieux de comprendre les propriétés physiques complexes des molécules, telles que le magnétisme moléculaire, le spin ou l'aromaticité, en utilisant l'Hamiltonien exact. Au lieu de cela, on peut simplifier le problème en développant un Hamiltonien modèle ou effectif.

J'aimerais ici résumer l'idée principale derrière les modèles comme suit : "Pourquoi s'embêter à étudier le système dans son intégralité alors que seules certaines de ses propriétés sont intéressantes ?" De fait, la prise en compte de toutes les interactions possibles dans un système peut être préjudiciable, car elle risque d'occulter les informations pertinentes au profit d'informations non pertinentes. L'élimination des éléments inutiles permet d'identifier un nombre minimum de paramètres physiquement sensibles, mais aussi de réduire le coût de calcul à une résolution analytique ou numérique peu coûteuse. La capacité à identifier les paramètres sensibles d'un système ouvre la voie à de nouvelles approches moléculaires et à une analyse plus qualitative des phénomènes. Un modèle est donc une simplification, physique ou non, d'un problème complet qui permet de se concentrer uniquement sur certaines de ses propriétés. C'est un jouet avec lequel les scientifiques peuvent s'amuser, grâce à l'utilisation d'un Hamiltonien modèle.

Un Hamiltonien modèle est défini sur un sous-espace de l'espace exact, un "espace modèle", où différents paramètres sont choisis pour intégrer la physique du problème. En les ajustant, on peut explorer la physique d'une manière plus simple et identifier les paramètres sensibles. Les Hamiltoniens modèles sont nécessaires tant à la communauté expérimentale que théorique. D'une part, les expérimentateurs mesurent les propriétés exactes du système complet, puis traitent leurs données en supposant

un Hamiltonien modèle donné, ce qui permet d'extraire les paramètres physiquement pertinents. D'autre part, les calculs théoriques étant coûteux, on peut développer un Hamiltonien modèle à partir d'un modèle chimique afin de mieux comprendre les mécanismes en jeu. Ces Hamiltoniens sont souvent proposés sur la base d'intuitions chimiques/physiques. Cependant, ils doivent reproduire aussi précisément que possible les valeurs propres d'un "espace cible" de l'Hamiltonien exact. Les énergies et les fonctions d'onde ciblées sont souvent celles des solutions de basse énergie. Il est donc important pour la chimie théorique de fournir des preuves de la validité (ou de l'invalidité) de ces modèles. La validité d'un Hamiltonien modèle dépend du type de ses approximations : une approximation non physique aboutit souvent à un modèle erroné. Lorsqu'un modèle est correct, ses paramètres peuvent être extraits à partir de calculs de premier principe. Lorsqu'un modèle n'est pas valide, c'est-à-dire qu'il ne reproduit pas les propriétés physiques souhaitées du système, les chimistes théoriciens peuvent utiliser différents outils pour corriger et déduire un Hamiltonien modèle plus précis. L'un de ces outils est ce que l'on appelle les Hamiltoniens effectifs. En bref, un Hamiltonien effectif est une contraction de l'Hamiltonien exact dans un espace modèle particulier où toute la physique du problème est prise en compte de manière effective. Comme les Hamiltoniens modèles, les Hamiltoniens effectifs sont beaucoup plus simples que les Hamiltoniens exacts et visent à reproduire des solutions ciblées. Cependant, ils utilisent des paramètres *ab initio*, transformés dans l'espace modèle pour cartographier efficacement le reste du système.

Hamiltonien modèle Heisenberg-Dirac-Van Vleck:

L'Hamiltonien Heisenberg-Dirac-Van Vleck est un Hamiltonien modèle formulé par Heisenberg [17] et amélioré par Dirac [18] et Van Vleck.[19] Développé à l'origine pour mieux comprendre le couplage (anti)ferromagnétique, il est rapidement devenu utile pour traiter un grand nombre de composés ferromagnétiques et antiferromagnétiques. Il peut être dérivé d'un Hamiltonien effectif de l'Hamiltonien exact et/ou d'un modèle de Hubbard généralisé suivi d'une perturbation Rayleigh-Schrödinger au second ordre.[20, 21]

La forme générale[5] de l'Hamiltonien HDVV est :

$$\hat{H}_{HDVV} = -\sum_{i>j} 2J_{ij}\hat{\boldsymbol{S}}_{\boldsymbol{i}}\hat{\boldsymbol{S}}_{\boldsymbol{j}} \tag{7}$$

avec des sites de spin actifs i et j ($s > 0$). Comme $\hat{\boldsymbol{S}}_{\boldsymbol{i}}$ et $\hat{\boldsymbol{S}}_{\boldsymbol{j}}$ sont des opérateurs scalaires, il est possible de réécrire le produit scalaire $\hat{\boldsymbol{S}}_{\boldsymbol{i}}\hat{\boldsymbol{S}}_{\boldsymbol{j}}$ sous une forme plus pratique :

$$\hat{\boldsymbol{S}}_{\boldsymbol{i}}\hat{\boldsymbol{S}}_{\boldsymbol{j}} = \hat{S}_{iz}\hat{S}_{jz} + \frac{1}{2}(\hat{S}_{i+}\hat{S}_{j-} + \hat{S}_{i-}\hat{S}_{j+}) \tag{8}$$

La littérature utilise un coefficient $-2J$, $-1J$, $+1J$ ou $+2J$, ce qui n'est qu'une question d'appréciation. Dans le cadre de ce travail de thèse, le coefficient $-2J$ a toujours été considéré, par commodité. Le terme J_{ij} est le couplage magnétique entre les centres i et j. Il incorpore toute la physique autre du système, telle que l'interaction électron-électron, l'interaction électron-noyau et la structure spatiale du système. Il est important de noter qu'il est valide lorsque le système étudié est principalement constitué d'une configuration neutre (dans le sens d'un transfert de charge négligeable, c'est-à-dire un petit rapport entre l'intégrale de saut divisée par l'intégrale de répulsion coulombienne). Des déviations expérimentales par rapport à l'Hamiltonien HDVV sont parfois signalés dans la littérature. La correction de l'Hamiltonien HDVV par l'ajout d'un terme biquadratique $\sum_{i>j} +2j_{ij}(\hat{\boldsymbol{S}}_{\boldsymbol{i}}\hat{\boldsymbol{S}}_{\boldsymbol{j}})^2$ [22, 23] a permis d'identifier et de prendre en compte le rôle des formes non-Hund dans cette déviation.[24] Cependant, dans les systèmes où la contribution de l'échange direct peut être considérée comme négligeable, l'Hamiltonien HDVV permet de représenter correctement la physique du système. L'une des forces de HDVV est qu'il ne fonctionne qu'avec les degrés de liberté de spin, puisque la dépendance de la partie spatiale est injectée dans les valeurs de la constante d'échange J_{ij}. Cela permet d'extraire la valeur physique du terme de couplage à partir de calculs *ab initio* ou de mesures expérimentales.

[5] La littérature peut ajouter un terme supplémentaire $-\frac{n_i n_j}{4}\hat{I}$ pour fixer l'énergie de l'état de multiplicité de spin le plus élevé à zéro. n_i et n_j sont le nombre d'électrons non appariés sur les sites i et j, et $\hat{I}$ est l'opérateur d'identité.

En prenant comme exemple un système à deux sites A et B de spins respectifs S_A et S_B, on peut dériver les termes suivants.

$$\hat{\boldsymbol{S}} = \hat{\boldsymbol{S}}_{\boldsymbol{A}} + \hat{\boldsymbol{S}}_{\boldsymbol{B}} \tag{9}$$

$$\hat{S}^2 = \hat{S}_A^2 + \hat{S}_B^2 + 2\hat{\boldsymbol{S}}_{\boldsymbol{A}}\hat{\boldsymbol{S}}_{\boldsymbol{B}} \tag{10}$$

L'Hamiltonien HDVV de ce système $\hat{H}_{HDVV} = -2J\hat{\boldsymbol{S}}_{\boldsymbol{A}}\hat{\boldsymbol{S}}_{\boldsymbol{B}}$ peut être réécrit comme suit

$$\hat{H}_{HDVV} = -J(\hat{S}^2 - \hat{S}_A^2 - \hat{S}_B^2) \tag{11}$$

dont les valeurs propres sont

$$E(S, S_A, S_B) = -J[S(S+1) - S_A(S_A+1) - S_B(S_B+1)]. \tag{12}$$

Comme tous les états générés par le couplage S_A et S_B ne diffèrent que par leur spin total S, il est possible de changer l'origine du système pour avoir :

$$E(S) = -JS(S+1) \tag{13}$$

Enfin, on constate que selon le signe de J, l'état de spin le plus élevé ($J > 0$) ou le plus bas ($J < 0$) sera l'état fondamental. Conformément à notre décision d'utiliser une constante de $-2J$, un J positif représente un couplage ferromagnétique tandis qu'un J négatif représente un couplage antiferromagnétique.

Chapitre 2: Ce Chapitre est composé de deux parties. Il commence par une introduction sur le phénomène de SF, ses mécanismes et la façon dont l'environnement est considéré par la communauté. Vient ensuite une étude modèle sur les effets d'un voisin sur les conditions thermodynamiques de la SF. Le modèle est basé sur un dimère de H_2 où la première molécule de dihydrogène représente un environnement gelé ressenti par une deuxième molécule, représentant un chromophore actif de classe I. L'environnement est gelé dans un état de configuration électronique donné, soit un état de spin singulet ou triplet, ce qui signifie que les transferts de charge ne sont pas autorisés. L'influence de différents environnements sur la spectroscopie de la fraction active est étudiée et différentes valeurs de correspondance énergétique $\rho = [E(S_{A,1}) - E(S_{A,0})]/[E(T_{A,1}) - E(S_{A,0})]$ sont obtenues, en fonction du type d'environnement (couche ouverte/fermée et triplet/singulet). Le champ généré par

un environnement singulet améliore le rapport ρ jusqu'à 6% par rapport à un chromophore libre. Ce rapport est encore amélioré lorsque l'environnement est triplet, jusqu'à 10% en comparaison au chromophore libre. Cela indique que la prédiction informatique des candidats de SF qui utilise l'approximation "un seul chromophore" peut laisser de côté certains composés intéressants. Enfin, ce Chapitre est conclu et d'autres critiques personnelles de l'étude sont discutées.

CONCLUSION Chapitre 2: L'importance de la structure de spin de l'environnement sur les états d'énergie d'un chromophore actif à deux électrons a été examinée en construisant un modèle. L'ordre des états du chromophore actif est très affecté par la présence d'un environnement triplet ou singulet. En conséquence, le rapport critique $\rho = [E(S_{A,1}) - E(S_{A,0})]/[E(T_{A,1}) - E(S_{A,0})]$ défini sur les énergies d'excitation des premiers états excités singulet et triplet peut atteindre la limite inférieure $\rho = 2$, signe que la SF est thermodynamiquement possible. Il est important de rappeler que la distance critique $L = 1,9$ Å dans notre modèle est analogue à la distance d'empilement π dans un dimère de systèmes π conjugué (3,5 Å). L'environnement crée un champ électronique qui influence le chromophore actif dès $L = 3$ Å, ce qui équivaut à une séparation de 5,7 Å entre deux pentacènes. Une description simplifiée qui néglige les recouvrements conduit à une modification encore plus profonde de la spectroscopie du monomère actif. En outre, le spin de l'état fondamental change d'un singulet (bas spin) à un triplet (haut spin) lorsque la distance entre le chromophore actif et l'environnement est d'environ 2,5 Å. Cette distance critique est régie par la structure d'un environnement singulet, qui agit comme un champ contrôlant la hiérarchisation des états de spin. L'influence de l'intégrale à deux électrons $[i_A j_A | i_E j_E]$, qui décroit lentement en $1/L$, sur la sous-unité active est réduite lorsque la description devient plus complexe, ce qui ne l'empêche pas de jouer un rôle discriminant entre les différents environnements. Même en l'absence de transferts de charge entre les sous-unités, notre modèle suggère que les effets des environnements de spin doivent être pris en compte. En effet, un environnement triplet favorise la condition thermodynamique de SF, alors qu'un environnement singulet doublement excité à couche fermée défavorise cette condition. À la lumière des nombreuses études approximant la condition énergétique de SF à l'étude d'un seul chromophore, notre modèle met en évidence l'importance d'un second chro-

mophore agissant comme environnement. La simplicité de ce modèle basé sur H_4 apporte des éléments de compréhension et des moyens d'interprétation qui devraient être transférables dans la recherche théorique de candidats à la SF. Enfin, il est important de souligner que ce modèle (disponible en ligne dans l'annexe 2.3) permet d'étudier l'influence d'un chromophore "environnement" gelé 2×2 (2 électrons dans une paire HOMO/LUMO) sur un chromophore "actif" 2×2. Il est alors possible de remplacer les bases de HOMO et LUMO (construites sur la base minimale de l'hydrogène 1s) par n'importe quelle base HOMO_{phys} et LUMO_{phys}. Ce modèle corrige la non-orthonormalité entre les OM à travers la construction des éléments de matrice, ce qui le rend apte à ajouter davantage de physique (par exemple, les OA de carbone 2p), dans l'approximation d'un Hamiltonien modèle 4×4.

Chapitre 3: Ce Chapitre est divisé en quatre parties. Tout d'abord, il introduit le phénomène de *spinmérie*, étudié plus loin dans le Chapitre, en présentant ses différentes composantes clés. La première partie se termine par une brève introduction à l'informatique quantique. Elle se poursuit par une étude d'un Hamiltonien modèle pour la *spinmérie*, avec une extension aux spin-Qubits moléculaires utilisés par l'informatique quantique. Elle est suivie d'une étude *ab initio* basée sur la fonction d'onde d'un complexe oxoverdazyle de Co(II) qui présente un faible effet *spinmérique* dans son état fondamental. Malgré la faible manifestation de *spinmérie* observée dans ce complexe, il s'agit de la première observation *ab initio* de ce mécanisme. Enfin, la dernière partie concerne une étude *ab initio* basée sur la fonction d'onde d'un complexe oxoverdazyle de Fe(II) qui présente de la *spinmérie à l'état excité*. Ceci conduit à un commentaire sur l'influence de la *spinmérie* sur les diagrammes de Tanabe-Sugano (ici uniquement sur le diagramme d^6 octaédrique) et son applicabilité dans l'électronique moléculaire. Ce Chapitre se termine par une conclusion générale et une autocritique.

CONCLUSION Chapitre 3: Les études basées sur l'Hamiltonien modèle et les calculs *ab initio* ont mis en évidence l'émergence d'un phénomène que nous avons nommé la *spinmérie*. Ce phénomène est une superposition de différents états de spin locaux qui génère un état de spin total donné, en ce sens il diffère des effets

de couplage spin-orbite en maintenant le spin total à un bon nombre quantique. Il peut être considéré comme une extension de la mésomérie, les différentes structures de résonance étant des distributions d'états de spin locaux différents. Anticipé par l'algèbre de spin, ce travail met en évidence sa manifestation dans deux complexes *ab initio*. La *spinmérie* repose principalement sur le couplage de deux composants spin variables dont les variations sont identiques. Ici, l'utilisation d'un ion métallique à transition de spin et de deux ligands radicalaires permet de mettre en évidence des comportements *spinmériques*.

En se concentrant sur les interactions d'échange direct, le premier travail a modélisé un complexe construit à partir d'un ion à transition de spin artificiel ($M = d^2$ ou d^8) et de deux ligands radicalaires afin d'étudier les conditions d'émergence de la *spinmérie*. Cela a mis en évidence deux règles pour l'apparition d'une *spinmérie* forte (50/50). Les contributions des transferts de charge (Ligand-Metal/Metal-Ligand Charge Transfer - LM/ML CT) ont ensuite été prises en compte de manière perturbative pour se rapprocher de composés de coordination réalistes et souligner leur influence sur le spectre énergétique.

Le second travail a présenté une inspection *ab initio* d'un premier complexe moléculaire candidat à la *spinmérie* : un ion métallique Co(II) coordonné par deux ligands verdazyle radicalaires. L'ion métallique Co(II) peut subir une transition de $S_M = 1/2$ à $S_M = 3/2$, et les radicaux verdazyle donnent lieu à un environnement dépendant du spin $S_L = 0$ ou $S_L = 1$. Les principaux ingrédients de la *spinmérie* se trouvent dans ce complexe particulier et une faible *spinmérie* ($\sim 0,1\%$) est observée au moyen de calculs basés sur la fonction d'onde. Cela a mis en avant le fait que le champ de ligands généré par un ensemble de radicaux à couche ouverte ne peut pas être considéré comme un champ statique selon la vision habituelle des composés de coordination. Cependant, le comportement *spinmérique* observé est trop faible pour des applications potentielles, mais il élargit l'image traditionnelle du champ cristallin dans les complexes de métaux de transition.

Enfin, le troisième travail est une étude *ab initio* d'un autre candidat pour la *spinmérie* : un ion métallique Fe(II) avec deux ligands verdazyle. L'ion métallique Fe(II) présente une transition de spin de $S_M = 0$ à $S_M = 2$. La transition de spin

de ses ligands ne permet pas la superposition de $S_M = 0$ et $S_M = 2$, mais permet la superposition de $S_M = 1$ et $S_M = 2$. En effet, des états excités présentant cette superposition sont observés et une importante *spinmérie à l'état excité* ($\sim 20\%$) est mise en évidence. Alors que le spectre de basse énergie est facilement rationalisé par un comportement de Heisenberg, la répartition des états excités redistribue les cartes concernant le diagramme d^6 de Tanabe-Sugano. La flexibilité de l'environnement ouvre de nouveaux schémas d'interprétation, contrastant avec la vision couche fermée habituelle du champ cristallin.

La *spinmérie* est un phénomène qui introduit un point de vue différent sur les complexes magnétiques. Sa force réside dans le fait qu'elle est naturellement induite par la structure de la fonction d'onde, ce qui la différencie des effets de couplage spin-orbite. La versatilité de spin des sites locaux est la condition principale pour les applications futures de la *spinmérie*. Par conséquent, la variabilité des états de spin locaux pourrait permettre d'encoder des informations quantiques sur des systèmes moléculaires synthétiques. En sondant expérimentalement la densité de spin locale, ces composés moléculaires pourraient devenir des cibles originales pour la génération de spin-Qubits moléculaires dans de nouvelles architectures d'ordinateurs quantiques. Nous suggérons l'utilisation de l'effet LIESST comme moyen possible de contrôler les composés *spinmériques* et l'information qu'ils encodent.

CONCLUSION DE LA THESE: Ce manuscrit s'articule autour de la notion d'environnement dans des architectures complexes de spin dans les domaines de la photoChimie Organique et de la magnétoChimie Inorganique. Ce qui suit est un bref résumé des principaux résultats et idées.

Dans le deuxième Chapitre, la construction d'un Hamiltonien modèle permet d'évaluer qualitativement l'influence du spin et de la charge de différents environnements sur un chromophore actif. D'un point de vue pratique, ce travail met en évidence le fait que l'approximation du chromophore unique dans la Fission du Singulet (SF) ne reflète pas la réalité et sous-estime le rapport des écarts d'énergie qui régit la condition thermodynamique de la SF. Cela signifie que de nombreux candidats possibles sont ignorés en raison d'un calcul erroné de leur spectre énergétique

et d'une sous-estimation de leur potentiel. Ce point est particulièrement important à l'aube d'une nouvelle ère d'apprentissage automatique et de criblage informatique pour la SF. Le matériau parfait pour la SF n'a pas encore été découvert, et l'on prend le risque de l'exclure en utilisant cette approximation. D'un point de vue fondamental, ce travail met en évidence et quantifie l'influence du spin et de la charge de l'environnement sur la spectroscopie d'un chromophore. Le modèle utilise un nombre minimal de paramètres complété par des évaluations *ab initio* d'intégrales et des modulations significatives du spectre d'énergie sont observées. En complexifiant le modèle (par exemple un glissement-empilement, une rotation...), d'autres types d'environnement peuvent être explorés, au prix d'une plus grande variabilité. Cela constituerait un prochain travail intéressant, permettant d'avoir un aperçu qualitatif des différents empilements de chromophores et des mécanismes en jeu. Cependant, l'augmentation de la variabilité appelle à la prudence : un Hamiltonien modèle trop complexe peut être moins utile que le calcul direct avec un Hamiltonien *ab initio*. Néanmoins, le modèle développé est transférable à l'étude de nombreux systèmes SF de classe I, à condition de fournir des des HOMO et LUMO locales et pertinentes.

Dans le troisième Chapitre, un Hamiltonien modèle et des calculs *ab initio* étudient le phénomène de *spinmérie*. Son émergence ouvre de nouvelles perspectives dans les considérations sur le champ du ligand et les comportements magnétiques. Anticipé par l'algèbre de spin, ce phénomène diffère des effets de couplage spin-orbite parce qu'il maintient le spin total comme un bon nombre quantique. La structure particulière de la fonction d'onde générée par des ligands variables en spin et un centre métallique à transition de spin permet divers schémas de couplage qui, dans les bonnes conditions, conduisent à une superposition significative d'états de spin locaux. L'analyse qualitative des états de spin locaux met en évidence l'apparition de la *spinmérie*. Cependant, ses mécanismes internes restent mal compris. Notre étude avec un Hamiltonien modèle met en lumière l'importance des interactions d'échange directes dans le contrôle de la *spinmérie*. Il s'agit de la première étape d'un long projet visant à trouver de bons candidats pour une manifestation importante de *spinmérie*. D'un point de vue appliqué, la *spinmérie* a de potentielles applications dans la conception de nouveaux spin-Qubits moléculaires, c'est-à-dire pour l'informatique quantique. Pour progresser dans cette direction, plusieurs études sont

nécessaires, telles que la conception de complexes avec une superposition facilement contrôlable et quantifiable d'états de spin locaux, la mesure de la cohérence quantique dynamique et, surtout, des études expérimentales pour sonder la *spinmérie*. D'un point de vue fondamental, ce phénomène représente une nouvelle perspective dans l'interprétation des données magnétiques et dans l'étude des phénomènes induits par une fonction d'onde polyvalente. Une compréhension plus approfondie de la *spinmérie* pourrait être la solution à une interprétation plus correcte des données jugées "non rationalisables" par les modèles magnétiques habituels. Les architectures basées sur un ion métallique à transition de spin coordonné à plusieurs (au moins deux) ligands à couche ouverte sont susceptibles de remettre en question les concepts traditionnels de spin gelé. En conséquence, la *spinmérie* appelle à reconsidérer la vision habituelle des diagrammes de Tanabe-Sugano, en passant d'un "champ de ligands" strict à une considération d'un "champ de ligands à couche ouverte". Toutefois, ce phénomène n'en est qu'à ses débuts et des études théoriques et expérimentales supplémentaires sont nécessaires pour en percer les mystères. De nouveaux projets et collaborations sont en cours pour atteindre cet objectif.

En conclusion, ce travail de doctorat a étudié l'importance des environnements à couche ouverte et leur influence en Chimie Organique et Inorganique. Les calculs fonction d'onde ont fourni un terrain fertile pour de telles recherches, au prix d'un coût de calcul plus élevé. Le calcul et l'analyse approfondis de nos systèmes ont nécessité des outils de travail appropriés, tels que des méthodes de localisation et l'algèbre de spin. D'une part, l'environnement a une influence directe sur la spectroscopie d'une molécule (par exemple un chromophore, un composé de coordination). D'autre part, il joue un rôle majeur dans la composition d'une fonction d'onde polyvalente et des phénomènes induits qui lui sont associés. De mon point de vue personnel, la *spinmérie* est un phénomène passionnant qui donne un nouvel aperçu des composés magnétiques, émergeant de la combinaison de ligands radicalaires avec un ion métallique à transition de spin.

Introduction

Like all human beings, we attach particular importance to our environment. Because we are organized as a society, we have always been confronted with the notion of environment. Socially, we come together in groups where each member shares common interests with the others. This is a social environment. These social interests can be seen as parameters that define individuals. In the search for better life conditions, we join a group when we think that the environment will benefit us, either because it reinforces our beliefs or because it brings us advantages. In this regard, when different people join the same group, they indirectly influence the characteristics of that environment. But since the group is shaped by people, it also influences its members. Economically, companies bring people together to maximise productivity. Non-Governmental Organizations need more people to improve their impact. Politically, parties grow stronger as more people join them. Scientifically, the way in which a teacher transmits her or his knowledge directly influences the students' scientific environment and can still influence them once they have become fully-fledged scientists. In our everyday language, we use the term "environment" to describe Nature. Nature is one of the simplest ways of seeing the reciprocal influence of humans on their environment. We have destroyed it little by little, killing species, modifying ecosystems, shaping it to our own liking, throwing our waste away for nature to deal with... In this sense, we have a profound influence on our environment. Yet, we are always influenced by Nature, from birth to death. Looking at the IPCC report for 2023,[1] there is no doubts that we will be even more influenced by Nature because of our disastrous behaviour on Earth as a species. Putting personal opinions aside, the notion of environment is an important concept in Chemistry. The chemical environment is defined on multiple scales.

First it can be defined at the macro-scale. In general Chemistry, the environment refers to the medium in which a chemical species evolves and which can influence its properties and behaviour. It can be understood as all the factors that surround a molecule or an ion, including other nearby atoms or molecules, solvent molecules, temperature, pressure, magnetic field... The solvent molecules around the molecule may tune its reactivity, solubility, and other properties.[2] In Thermochemistry,

many examples exist where pH, pressure and temperature can favour or disfavour the reactivity of a molecule.[3, 4, 5] In addition, modification of the environment through the use of another solvent can play an important role in the spectroscopic properties of a molecule, such as its absorption or emission spectra (*i.e.*, solvatochromism). This definition is a somewhat global picture which consider the environment as a continuum.

Then one may define the environment at a smaller scale, *i.e.* the range around the molecule of interest. Good examples in Organic Chemistry are π-stacking and H-bonds. Where a π-conjugated molecule would be randomly arranged in space, having another π-conjugated neighbour in its environment allows for a noncovalent interaction (orbital overlaps) which then packs the two molecules together. The spectroscopy of the first molecule may then be tuned depending on its π-stacking. On the other hand, some molecules have high rotational frequencies in the gas phase that can lower in solution due to noncovalent interactions with neighbouring molecules, *e.g.* H-bonds, Van Der Waals interactions... This environment is to be differentiated from the one of chemical reactions, where covalent bonds are broken and created. In this case, the so-called "reaction environment" is then the former, a global environment.

Shortening further the distances of interactions, one may find another definition for the environment, like the usual one in Inorganic Chemistry. A coordination compound is, in its simpler form, a metal ion surrounded by ligand molecules through coordinate covalent bonds. The surroundings of ligands is usually considered as the chemical environment of the metal centre, a "coordination environment". Historically, the importance of the coordination environment was described by different theories. On one hand, the Crystal Field Theory (CFT),[6, 7] which approximates the metal ion as a punctual positive charge and its coordination environment as a static electric field of anions, considers their interaction as purely electrostatic. This theory well describes the breaking of metallic d- and f-orbitals degeneracy due to the geometry of the surrounding environment. The type and strength of the splitting depends directly on the nature and geometry of the environment.[6] The electronic structure of the complex (high- or low-spin) and more particularly of the metal ion

[6]It also depends on the nature of the metal ion and its oxidation state.

will then be influenced by its coordination environment. On the other hand, the Ligand Field Theory (LFT),[25] inspired from CFT and from Molecular Orbital Theory (MOT),[26] describes both electrostatic interactions and coordinated covalent bonding by the use of Molecular Orbitals. It provides information on both the electronic structure of the metal centre and its bonding characteristics, depending on the type of environment. Both theories aim to represent the influence of the coordination environment upon the metal ion.

At all scales, the environment can have an influence on systems of interest. Getting to understand and quantify this influence is the key for scientific rationalization of the properties of compounds. Still, the notion of environment remains vague and the environment is often approximated or even neglected. Moreover, Quantum Chemistry cannot afford to consider the full description of the environment in their calculations. Thus, different approximations are used to take it into account effectively (*e.g.* periodic conditions for materials, Polarizable Continuum Models for solvents...). This allows one to obtain more physical results at an acceptable cost. Yet, the importance of the environment is sometimes reduced and the evaluated quantities can be biased.

The spin state of an environment can influence the electronic structure of a molecule and its resulting spectroscopy. Moreover different spin coupling schemes can arise, tuning further the interactions between the site of interest and its environment. Particularly interesting scenarios arise in open-shell systems. This is the thread that has guided my research during the past three years. This thesis addressed two questions related to the role of the environment on the spectroscopy of spin architectures, one in Organic photoChemistry (1) and the other in Inorganic magnetoChemistry (2). It is organized as follows.

Chapter 1 introduces all the elements and methods needed to understand the further two Chapters. All inspections in this thesis are wavefunction-based. Thus, in section (1.1), a presentation of the electronic problem in a WaveFunction Theory (WFT) perspective starts this Chapter. The main ingredients of WFT used in this thesis are reminded. Then follows, in section (1.2), a brief introduction to wavefunction-based methods, in order to introduce the importance of correlation and post Hartree-

Fock methods. Configuration Interaction (CI) methods and MultiConfigurational Self Consistent Field (MCSCF) methods are explained to better understand the two methods of choice used in this work: the Complete Active Space Self Consistent Field (CASSCF) method, and the Difference Dedicated Configuration Interaction (DDCI) method. Localization is an important concept in Quantum Chemistry which allows an easier readability of wavefunctions, and a possible reduction in the computational cost of calculations. It is thus presented in section (1.3), and the DoLo method of localization is shortly presented. Section (1.4) reminds the spin operators and several elements of spin algebra, *e.g.* Clebsch-Gordan coefficients. Finally it ends by section (1.5) with an introduction to the concept of models in Quantum Chemistry and the resulting model Hamiltonians. The Heisenberg-Dirac-Van Vleck Hamiltonian, a model Hamiltonian of choice for magnetic systems, ends the section and the Chapter.

Chapter 2 is focused on a photo-physical process, Singlet Fission (SF). SF is a promising phenomenon that necessitates at least a dimer (covalent or not) to produce two excitons upon the absorption of a single photon. It has seen an increase in interest over the last decade, both on experimental and theoretical perspectives. Many conditions have been theoretically demonstrated for the SF phenomenon to occur. One of them is the so-called "thermodynamic condition", relative to the energy level positioning of chromophores. However while at least two chromophores are needed for the phenomenon, many theoretical groups investigate possible candidates by calculating the spectroscopy of a monomer, discarding its neighbour. We wondered how much the immediate environment of a given monomer may modulate its spectroscopy. More precisely, we concentrated on the influence of the electronic structure and the resulting spin structure of this environment on a given monomer. This raised the following questions:

1) Does the spin and charge of the environment influence the conditions for the Singlet Fission phenomenon ? How can we quantify and explain this influence ?

To answer the latter, Chapter 2 starts by introducing the Singlet Fission phenomenon and its applications in section (2.1). Then, in section (2.2), a model Hamiltonian is developed. It is based on a minimal model of two hydrogen molecules, with one molecule labelled "active" (whose electronic structure is allowed to relax)

and the other labelled "frozen environment" (whose electronic structure is frozen in a given state). The influence of the spin and the charge of an environment on the spectroscopy of the active monomer is evidenced and sized. This Chapter concludes and proposes self-criticism in section (2.3).

Chapter 3 focuses on a peculiar phenomenon: *spinmerism*. The usual picture in CFT and LFT considers the ligands in a coordination compound as a frozen-spin environment for the metal ion. Depending on its geometry and nature, this coordination environment can influence the spin, electronic and oxidation states of the metal ion. The spin-versatility of the metal ion, its ability to change spin states upon modification of its environment, is an important effect found in Spin CrossOver (SCO) complexes. Yet, this is based on the consideration of a static, tunable, environment. This consideration is accepted and evidenced for the case of closed-shell ligands, but more debatable for the case of open-shells ligands, and more particularly, radical ligands. The environment generated by radical ligands can be spin-versatile due to the couplings between radicals, which question the separation between the metal ion and its environment. This led us to the following two questions:

2) What are the limits of the separation between the coordination environment and the spin-versatile metal ion, when the environment is also spin-versatile ? What is the resulting influence on the spectroscopy of the coordination complex ?

Two coupled spin-versatile entities can give rise to unusual and puzzling scenarios. One unusual scenario is the *spinmerism* phenomenon. This phenomenon can be seen as an analogy of mesomerism, with the different resonance structures being different local spin states distributions. The main ingredients for *spinmerism* where identified as to have at least two coupled spin-versatiles entities. This produces total spin states which are superpositions of different local spin states. Whilst the total spin remains a pure quantum number, the local spins are not anymore. Still, the various couplings between the local spin states of the two entities generate the same total spin state. In this sense, this phenomenon occurs even in the absence of well-known Spin-Orbit Couplings. *Spinmerism* opens up new views towards the notion of environment in coordination compounds and present perspectives towards the design of new spin-qubits devices. Chapter 3 starts, in section (3.1), by an intro-

duction to SCO systems and related phenomena, *e.g.* Light Induced Excited Spin State Trapping (LIESST). This allows for a better understanding of the Valence Tautomerism (VT) phenomenon, and its ingredients: SCO ions and non-innocent ligands. Finally, the *spinmerism* phenomenon is presented in more details and possible applications to Qubits and Quantum Computers are suggested. Then section (3.2) presents a model Hamiltonian-based study of the *spinmerism* phenomenon. It is based on an "artificial" d^2 (or d^8) SCO ion, coordinated to two radical ligands, and is restricted to exchange interactions. Unusual spin state structures emerge and two guiding rules for a consequent *spinmerism* effect are derived. Next, section (3.3) is an *ab initio* study of a Co(II) oxoverdazyl complex, by means of wavefunction-based methods (CASSCF and DDCI). Atypical ground and first excited states are reported, which present a weak *spinmerism* effect. This is the first *ab initio* report of *spinmerism* in a coordination complex. After that, section (3.4) shows an *ab initio* study of a Fe(II) oxoverdazyl complex, using the same approach as in section (3.3). While the low-energy spectrum depicts an usual Heisenberg-Dirac-Van Vleck (HDVV) picture, the higher-lying quintet states are superpositions of local Fe(II) triplet and quintet spin states. This observation is the consequence of *excited state spinmerism*. The modification of Tanabe-Sugano d^6 diagram by the latter effect is discussed, which stimulates new perspectives for spin-versatile environments. A manipulation of *spinmerism* through the mean of LIESST effect is suggested, which would allow for the design of possible spin-qubits candidates. Finally, section (3.5) concludes the Chapter with some self-criticism.

Conclusions and perspectives are finally ending this work.

Chapter 1

WaveFunction Theory and its methods

The aim of this Chapter is to introduce all the elements and methods needed to understand the further theoretical developments in Chapters 2 and 3. It is divided into five sections. In section (1.1), the electronic problem and its constituents are presented. A particular attention is paid to the correction of matrix elements constructed on non-orthonormal orbitals. In section (1.2), the Hartree-Fock (HF) method is shortly presented in order to introduce post-HF methods used in this work. Complete Active Space Self-Consistent Field and Difference Dedicated Configuration Interaction methods are explained in subsection (1.2.5). The last part of this section gives some words to Perturbation Theory. In section (1.3), the concept of localization, and a priori and a posteriori approaches are explained. The DoLo method, an a posteriori method used in Chapter 3, is presented. In section (1.4), spin operators and the important equations for spin coupling are reminded. Finally, section (1.5) presents, in a few words, the concept of models in Quantum Chemistry and the resulting model Hamiltonians. A brief comment is given on effective Hamiltonians, which are not used in this work, and on the Heisenberg-Dirac-Van Vleck Hamiltonian, which is widely used to rationalize magnetic behaviour in this work.

keywords: wavefunction, wavefunction methods, localization, spin coupling, models

1.1 The electronic problem

The main goal in Quantum Chemistry (QC) is to solve the Schrödinger equation. In this interest, we search for solutions of the non-relativistic Schrödinger equation:

$$\hat{H}|\Psi\rangle = E|\Psi\rangle \tag{1.1}$$

where $\hat{H}$ is the Hamiltonian operator.

We will not elaborate on time-dependent quantities as this work concerns only time-independent studies and will stick to time-independent molecular Hamiltonian (in atomic units):

$$\hat{H} = \hat{H}_e + \sum_{B>A} \frac{Z_A Z_B}{R_{AB}} + \hat{T}_n \tag{1.2}$$

with $\hat{H}_e$ the electronic Hamiltonian and $\hat{T}_n$ the nuclear kinetic energy:

$$\hat{H}_e = -\sum_i \frac{1}{2}\nabla_i^2 - \sum_{i,A} \frac{Z_A}{r_{iA}} + \sum_{i>j} \frac{1}{r_{ij}} \qquad \text{and} \qquad \hat{T}_n = -\sum_A \frac{1}{2M_A}\nabla_A^2. \tag{1.3}$$

Where $M_A = \frac{m_A}{m_e}$ is the ratio of the mass of the nucleus A to the mass of an electron. The position vectors $\boldsymbol{r} \equiv \{r_i = (r_{ix}, r_{iy}, r_{iz})\}$ and $\boldsymbol{R} \equiv \{\boldsymbol{R_A} = (R_{Ax}, R_{Ay}, R_{Az})\}$ are, respectively, for electrons and nuclei. Distances between particles are written $r_{ij} = |\boldsymbol{r_i} - \boldsymbol{r_j}|$ (distance between electrons i and j). A similar definition is given for distances r_{iA} and $R_{A,B}$. $\nabla_i^2 = \dfrac{\partial^2}{\partial x_i^2} + \dfrac{\partial^2}{\partial y_i^2} + \dfrac{\partial^2}{\partial z_i^2}$ is the Laplacian of electron i (here in cartesian coordinates).

To solve this many-body problem, different approaches have been derived and will be discussed further in the text. In order to efficiently manipulate the QC operators (such as $\hat{H}$), two type of representation were proposed. The first one, developed by Born, Jordan and Heisenberg in 1925,[27, 28] made use of matrices, the so-called matrix mechanics. This allows the representation of an operator in a defined basis using matrix notations. Then the system is defined following all its inner possible interactions. This information is stored as matrix elements $\langle i|\hat{H}|j\rangle$, which implies that one needs to know how to calculate these matrix elements. Diagonalizing this matrix, one can obtain its eigenvectors (Ψ) and eigenvalues (E), which represent the energy and the wavefunction of each states of the system. Around the same time, Schrödinger proposed its wave formulation (equation 1.1), where he used wave mechanics to describe the QC problem. It is important to note that the matrix

representation was primarily meant for particles, whilst the wave representation for waves. As quantum bodies are a duality between a particle and a wave, Paul Dirac incorporated matrix mechanics and the wave equation of Schrödinger into a single formulation. Matrices are an efficient tool and, through their diagonalization, one can get the quantisized energies of the system. Considering the full system means working with large matrices. However, diagonalizing a $N \times N$ matrix represents a N^3 numerical cost, which becomes a significant limitation for $N > 10^{11}$ (until today, the highest recorded calculation had 10^{12} determinants).[29] This calls for clever implementation of diagonalization methods and mathematical tricks. One of the, in my opinion, most interesting trick is the concept of block-diagonalization: only the most important part of the system will be treated intensively (diagonalization). This is the case of the commonly implemented Jacobi-Davidson method,[30] which reduces the cost of diagonalization to $n.M^3$ (n is the number of iterations and M the size of the working subspace, $M <<< N$). Then, the calculation is corrected extensively using different correction methods. This allows to reduce the numerical cost of the problem while keeping the physics of the system. A strong argument for such approach is the fact that, often, only part of the system's spectrum is of interest, *e.g.* the low-lying energy spectrum. Thus, only a correct description of the states of interest is necessary to render the physics studied. Still, particular care must be given in the selection of the states of interest. In fact, the extensive correction may fail or induce wrong results when particular states, which are important for the physics of the system, are neglected (for example in second-order Perturbation Theory, as discussed in subsection 1.2.6).

1.1.1 Born-Oppenheimer approximation

An electron weights roughly 1836 times less than protons and neutrons. This is the main argument for Born-Oppenheimer (BO) approximation: considering the mass ratio M_A, one can expect the electrons motion to be instantaneous relatively to the nucleus (made of many protons and neutrons). Thus one can assume that electronic and nuclear motions in molecules can be treated separately. This strongly simplifies molecular calculations and allows to separate QC into either static or dynamic pictures. The static viewpoint considers nuclei frozen in space and studies

electronic structures (electronic Schrödinger equation). The dynamic perspective assumes that the electronic structure problem has been solved and studies nuclear dynamics (Schrödinger equation for nuclear motions).

In this regard, the BO approximation separates a molecule's wavefunction of independent coordinates $\{\boldsymbol{r_i}\}$ and $\{\boldsymbol{R_A}\}$ into a product of a nuclear wavefunction Ψ_n of coordinates $\{\boldsymbol{R_A}\}$ and an electronic wavefunction Ψ_e being an implicit function of nuclei coordinates $\{\boldsymbol{r_i}; \{\boldsymbol{R_A}\}\}$. Replacing Ψ by $\Psi_e\Psi_n$ in equation (1.1), different terms appear:

$$\begin{aligned}\hat{H}\Psi_e\Psi_n = &-\sum_i \frac{1}{2}\Psi_n\nabla_i^2\Psi_e + \Psi_e\hat{T}_n\Psi_n \\ &-\sum_A \frac{1}{2M_A}(\nabla_A\Psi_e\nabla_A\Psi_n + \Psi_n\nabla_A^2\Psi_e) \\ &+ V\Psi_e\Psi_n\end{aligned} \tag{1.4}$$

where V is a function of $\{\boldsymbol{r_i}\}$ and $\{\boldsymbol{R_A}\}$ and represent all the potential energy terms. The terms with $\nabla_A\Psi_e$ and $\nabla_A^2\Psi_e$ are not zero because Ψ_e is an implicit function of nuclei coordinates $\{\boldsymbol{R_A}\}$. However, Born and Oppenheimer proposed to neglect these terms, considering that they are small due to $M_A \geq 1836$ appearing in the denominator. Considering that the positions of the nuclei are frozen, the term $\sum_{B>A} \frac{Z_A Z_B}{R_{AB}}$ in V becomes constant and the term $\Psi_e\hat{T}_n\Psi_n$ becomes zero. Thus, they can be treated outside of the electronic problem. This approximation allows then to solve first the electronic problem at frozen nuclei geometry, then the nuclear problem. Yet, it is important to note the different limitations of neglecting the two above terms by BO approximation. The neglected terms may carry more importance as the condition on the mass ratio $M_A >> 1$ is approximated.[31] As soon as the energy difference between two electronic states is of the order of vibrational quanta, the separation between the electrons and nuclei displacements is invalidated.[32] Still, BO approximation was a crucial step in the development of QC and, until today, its computational advantage outweighs its possible limitations.

As this work interest is in the electronic problem for systems with frozen geometries, we will concentrate solely on the electronic Hamiltonian $\hat{H}_e$ and wavefunction Ψ_e. For the sake of simplicity, $\hat{H}_e$ will be referred as $\hat{H}$ in the follow-up and Ψ_e as Ψ.

1.1.2 Antisymmetry or Pauli Exclusion principle

To fully define an electron, it is necessary to specify its spin projection. As an electron has a defined spin $S = \frac{1}{2}$, its spin projection can take the values $\frac{1}{2}$ and $-\frac{1}{2}$. It is then needed to introduce two "spin functions" of an integrating spin parameter ω: $\alpha(\omega)$ and $\beta(\omega)$, respectively for spin up and down. These two spin functions are complete and orthonormal.

$$\int d\omega\ \alpha^\star(\omega)\alpha(\omega) = \int d\omega\ \beta^\star(\omega)\beta(\omega) = 1 \tag{1.5}$$

$$\langle\alpha|\alpha\rangle = \langle\beta|\beta\rangle = 1 \tag{1.6}$$

and

$$\langle\alpha|\beta\rangle = \langle\beta|\alpha\rangle = 0. \tag{1.7}$$

An electron is then defined following the three spatial coordinates $\boldsymbol{r}$ and one spin coordinate ω, denoted as $\boldsymbol{x} = \{\boldsymbol{r}, \omega\}$. This way, the wavefunction of an N-electron system is a function of $\boldsymbol{x_1}, \boldsymbol{x_2}, ..., \boldsymbol{x_N}$, written as $\Psi(\boldsymbol{x_1}, \boldsymbol{x_2}, ..., \boldsymbol{x_N})$. Pauli formulated in 1925 that no two (or more) electrons (more generally fermions, extended in 1940) in the same atom can occupy the same quantum state, meaning they cannot have the same $\boldsymbol{x_i}$ coordinates (so called "Pauli Exclusion Principle"). A beautiful way to proceed is to make the wavefunction antisymmetric.

$$\Psi(\boldsymbol{x_1}, ..., \boldsymbol{x_i}, ..., \boldsymbol{x_j}, ..., \boldsymbol{x_N}) = -\Psi(\boldsymbol{x_1}, ..., \boldsymbol{x_j}, ..., \boldsymbol{x_i}, ..., \boldsymbol{x_N}) \tag{1.8}$$

Then, assuming $\boldsymbol{x_i} = \boldsymbol{x_j}$, the wavefunction becomes zero. This allows to take explicitly into account both the spatial and spin coordinates. For these reasons, *"a many-electron wavefunction must be antisymmetric with respect to the interchange of the coordinate $\boldsymbol{x_i}$ of any two electrons"*, this is the "antisymmetry principle".[33, 34]

1.1.3 Spatial and Spin orbitals

An orbital is defined as a wavefunction for a single particle, an electron. A spatial orbital $\phi_i(\boldsymbol{r})$ is a function of $\boldsymbol{r}$ which describes the spatial distribution of an electron. In this sense, $|\phi_i(\boldsymbol{r})|^2\ d\boldsymbol{r}$ represents the probability density to find an electron in a small volume element $d\boldsymbol{r}$ surrounding $\boldsymbol{r}$. Concerning the electronic problem, it is best to have an orthonormal spatial orbitals set. The importance of having an

orthonormal orbitals set in QC is developed in subsection (1.1.6). For now let us consider having an orthonormal spatial orbitals set $\{\phi_i(\boldsymbol{r})\}$, which means that:

$$\langle \phi_i | \phi_j \rangle = \delta_{ij}. \tag{1.9}$$

This set needs to be infinite to be complete which, until today, is impossible to compute. In practice, we will work with a finite set $\{\phi_{i=1,\ldots,K}(\boldsymbol{r})\}$ of K spatial orbitals. Working with a finite set and fully diagonalizing the complete space lead to "exact" results in the finite set region.

As described in the previous subsection (1.1.2), it is necessary to add the integrating spin parameter ω to fully describe an electron. Thus, we will introduce the set of K spin-orbitals $\chi_i(\boldsymbol{x})$ by multiplying the spatial orbital $\phi_i(\boldsymbol{r})$ by the spin function $\alpha(\omega)$, and the set of K spin-orbitals $\overline{\chi_i}(\boldsymbol{x})$ by multiplying $\phi_i(\boldsymbol{r})$ by $\beta(\omega)$:

$$\left.\begin{aligned} \chi_i(\boldsymbol{x}) &= \phi_i(\boldsymbol{r})\alpha(\omega) \\ \overline{\chi_i}(\boldsymbol{x}) &= \phi_i(\boldsymbol{r})\beta(\omega) \end{aligned}\right\} \text{i=1,...,K.} \tag{1.10}$$

As we study the molecular electronic structure, we will need molecular orbitals. This introduces two usual families in QC: atomic orbitals (AOs) sets and molecular orbitals (MOs) sets. Before pursuing, it is important to say that a "spin-orbital" corresponds to one orbital of the $2K$ set of spin-orbitals whereas an "orbital" means the pair of $\{\chi_i(\boldsymbol{x}); \overline{\chi_i}(\boldsymbol{x})\}$, belonging to the K set of AOs or MOs. When no magnetic field is applied, $\chi_i(\boldsymbol{x})$ and $\overline{\chi_i}(\boldsymbol{x})$ are degenerated.

A molecule is a system made of $n > 1$ atoms, each bringing their atomic electronic structure. In this regard, the first step is to define a K AOs "basis set". Each AO (*e.g.* 1s, 2s, 3d...) can be represented depending on different theories, usually either as Slater orbitals or Gaussian orbitals. As these are common knowledge, we will not describe them in this text but will comment on two facts: 1) Slater orbitals are more physical than Gaussian's. 2) Slater orbitals integration is really difficult whereas Gaussian orbitals integration, being Gaussian functions, is easy to compute. For this reason, the majority of QC have been done using Linear Combination of Gaussian orbitals (so-called contracted orbitals) as AOs sets, to be more physically accurate and to keep the mathematical advantage of Gaussian over Slater orbitals. Even if the contraction of Gaussian orbitals brings more basis

functions to manipulate, the numerical cost is lower than with a smaller basis of Slater orbitals.

Studying $n = 1$ atom, the AOs set is enough to describe the atomic electronic structure as developed above. For molecules, this becomes a many atoms system. In this case, considering a sufficient K_A AOs set on each n atoms, one can construct MOs as a Linear Combination of Atomic Orbitals (LCAO). This allows to build a $\sum_{A=1,...,n} K_A$ MOs set $\{|\psi_i\rangle\}$. Moreover, different AOs sets are not forcibly orthogonal. Doing a LCAO, one is able to introduce orthonormality into the electronic problem, through the generation of an orthonormal MOs set. An orthonormal MOs set is more advantageous for a QC calculation than to a non-orthonormal set, as demonstrated in subsection (1.1.6).

$$|\psi_i\rangle = \sum_{\mu} c_{i,\mu} \, |\chi_\mu\rangle \tag{1.11}$$

where $c_{i,\mu}$ is the LCAO coefficient.

1.1.4 Slater determinants

In order to take into account the antisymmetry of the wavefunction, Slater came up with an original mathematical description: determinants. As stated in subsection (1.1.2), "*a many-electron wavefunction must be antisymmetric with respect to the interchange of the coordinate* $\boldsymbol{x_i}$ *of any two electrons*". One can mathematically prove that any N electronic (antisymmetric) function can be rewritten as a linear combination of so-called "Slater determinants"[1]. Slater proposed to write configurations as determinants where one axis (rows in example below) represents spin-MOs $\{\psi_i\}$ and the other axis (columns in example below) the electrons $\{\boldsymbol{x_j}\}$ of the configuration. This allows to write a one configuration wavefunction as:

$$\Psi(\boldsymbol{x_1}, \boldsymbol{x_2}, ..., \boldsymbol{x_N}) = \frac{1}{\sqrt{N!}} \begin{vmatrix} \psi_1(\boldsymbol{x_1}) & \psi_1(\boldsymbol{x_2}) & \dots & \psi_1(\boldsymbol{x_N}) \\ & \dots\dots\dots\dots & & \\ \psi_N(\boldsymbol{x_1}) & \psi_N(\boldsymbol{x_2}) & \dots & \psi_N(\boldsymbol{x_N}) \end{vmatrix} \tag{1.12}$$

with N the number of spin-MOs. Permuting two columns or two rows in a determinant multiplies it by (-1). Then if two electrons occupy the same spin orbital, the

[1] We will often call them simply "determinants".

determinant becomes zero, which carries Pauli exclusion principle. This long-hand notation above is important when developing the workings behind determinants and their use in QC. However in order to work efficiently with determinants, it is necessary to introduce a short-hand notation for normalized Slater determinants:

$$\Psi(\boldsymbol{x_1}, \boldsymbol{x_2}, ..., \boldsymbol{x_N}) = |\psi_1\ \psi_2\ ...\ \psi_N\rangle. \tag{1.13}$$

One can see that this notation only presents the diagonal elements of the determinant and includes the normalization constant ($N!^{-1/2}$).

1.1.5 One- and two-electron integrals

As presented in subsection (1.1.1), we will apply the electronic Hamiltonian $\hat{H}$ to the electronic wavefunction $\Psi(\boldsymbol{x_1}, ..., \boldsymbol{x_N})$. The electronic Hamiltonian for a many-electron system is often rewritten as:

$$\hat{H} = -\sum_i \frac{1}{2}\nabla_i^2 - \sum_{i,A} \frac{Z_A}{r_{iA}} + \sum_{i>j} \frac{1}{r_{ij}} \tag{1.14}$$

$$= \sum_i \hat{h}(i) + \sum_{i>j} \frac{1}{r_{ij}} \tag{1.15}$$

$$= \hat{\mathcal{O}}_1 + \hat{\mathcal{O}}_2 \tag{1.16}$$

where $\hat{h}(i)$ is the mono-electronic Hamiltonian operator, describing electron i kinetic energy and potential energy in the field of all nuclei. It is usual to split $\hat{H}$ in two sub-parts: $\hat{\mathcal{O}}_1$, the mono-electronic part (one-electron) and $\hat{\mathcal{O}}_2$, the bi-electronic part (two-electrons).

When calculating the matrix element $\langle\Psi|\hat{\mathcal{O}}_1|\Psi\rangle$ and developing $\Psi(\boldsymbol{x_1}, ..., \boldsymbol{x_N})$ as a sum of product, one will observe the appearance of one-electron integrals:

$$\int d\boldsymbol{x_m} \psi_i^\star(\boldsymbol{x_m}) \hat{h}(\boldsymbol{r_m}) \psi_k(\boldsymbol{x_m}) \tag{1.17}$$

with $\psi_i(\boldsymbol{x_m})$ and $\psi_k(\boldsymbol{x_m})$ spin-orbitals. It is important to note that this one-electron integral is directly zero if both spin-orbitals differ in spin.

$$\int d\boldsymbol{r_m} \phi_i(\boldsymbol{r_m}) \hat{h}(\boldsymbol{r_m}) \phi_k(\boldsymbol{r_m}) \cancelto{0}{\int dw\ \alpha(w)\ \beta(w)} \tag{1.18}$$

In this sense, it is often rewritten in a "chemists" notation $[i|\hat{h}|k]$ for spin-orbitals:

$$[\psi_i|\hat{h}|\psi_k] \tag{1.19}$$

Following the same procedure, and developing the matrix element $\langle\Psi|\hat{\mathcal{O}}_2|\Psi\rangle$, two-electron integrals will appear:

$$\iint d\boldsymbol{x_m}\, d\boldsymbol{x_n}\, \psi_i^\star(\boldsymbol{x_m})\psi_k(\boldsymbol{x_m})\, \frac{1}{r_{mn}}\, \psi_j^\star(\boldsymbol{x_n})\psi_l(\boldsymbol{x_n}). \tag{1.20}$$

This time, spin-orbitals $|\psi_i\rangle$ and $|\psi_j\rangle$ need, respectively with $|\psi_k\rangle$ and $|\psi_l\rangle$, to have the same spin for this integral not to be zero. The previous notation is referred as the chemists' notation and is shortened to:

$$[\psi_i\psi_k|\psi_j\psi_l]. \tag{1.21}$$

The wavefunction being antisymmetric, pairs of two-electron integrals will always appear, which calls for an antisymmetrized two-electron integral denoted as:

$$\langle\psi_i\psi_j||\psi_k\psi_l\rangle = [\psi_i\psi_k|\psi_j\psi_l] - [\psi_i\psi_l|\psi_j\psi_k]. \tag{1.22}$$

1.1.6 Importance of orthonormality and General rules for matrix elements

Before presenting briefly the general rules for one- and two-electron integrals, I would like to use the next five pages to present why it is so important to work with orthonormal orbitals. It is a fact which is commonly accepted in the QC community but I find that its explanation nowadays do not give enough credit to the beauty of the mathematics occurring here. Moreover this will be of help for the reader in the Chapter 2.

1.1.6.a Non-orthonormal orbitals

This section presents Slater's derivation [35] of Lowdin's equations [36] for matrix elements for non-orthonormal orbitals.

Assuming a determinantal function $\Psi(\boldsymbol{x_1}, \boldsymbol{x_2}, ..., \boldsymbol{x_N})$ formed of N spin-orbitals, defined as

$$\Psi(\boldsymbol{x_1}, \boldsymbol{x_2}, ..., \boldsymbol{x_N}) = \frac{1}{\sqrt{N!}} \begin{vmatrix} u_1(\boldsymbol{x_1}) & u_1(\boldsymbol{x_2}) & \dots & u_1(\boldsymbol{x_N}) \\ & \dots\dots\dots\dots & & \\ u_N(\boldsymbol{x_1}) & u_N(\boldsymbol{x_2}) & \dots & u_N(\boldsymbol{x_N}) \end{vmatrix} \tag{1.23}$$

where spin-orbitals are not necessarily orthogonal neither normalized. The desired matrix element $\langle\Psi|\hat{K}|\Psi\rangle$, where $\hat{K}$ is any even operator, is described by Slater as

$$\frac{1}{N!}\int \begin{vmatrix} u_1^*(\boldsymbol{x_1}) & u_1^*(\boldsymbol{x_2}) & \dots & u_1^*(\boldsymbol{x_N}) \\ & \dots\dots\dots\dots & & \\ u_N^*(\boldsymbol{x_1}) & u_N^*(\boldsymbol{x_2}) & \dots & u_N^*(\boldsymbol{x_N}) \end{vmatrix} \hat{K} \begin{vmatrix} u_1(\boldsymbol{x_1}) & u_1(\boldsymbol{x_2}) & \dots & u_1(\boldsymbol{x_N}) \\ & \dots\dots\dots\dots & & \\ u_N(\boldsymbol{x_1}) & u_N(\boldsymbol{x_2}) & \dots & u_N(\boldsymbol{x_N}) \end{vmatrix} d\boldsymbol{x_1} d\boldsymbol{x_2} \dots d\boldsymbol{x_N} \tag{1.24}$$

where the volume elements $d\boldsymbol{x_k}$ include summation over spin. It is interesting to see that the left determinant in equation (1.24) can be rewritten. Developing this determinant, one obtain

$$\begin{vmatrix} u_1(\boldsymbol{x_1}) & u_1(\boldsymbol{x_2}) & \dots & u_1(\boldsymbol{x_N}) \\ & \dots\dots\dots\dots & & \\ u_N(\boldsymbol{x_1}) & u_N(\boldsymbol{x_2}) & \dots & u_N(\boldsymbol{x_N}) \end{vmatrix} = \sum_{\hat{P}} (-1)^p \hat{P}(u_1(\boldsymbol{x_1}) u_2(\boldsymbol{x_2}) \dots u_N(\boldsymbol{x_N})) \tag{1.25}$$

with $\hat{P}$ the permutation operator and p the parity of the permutation. $\hat{K}$ being an even operator, permutation of electrons do not affect it ($[\hat{P}, \hat{K}] = 0$), and an interesting derivation arises from equation (1.24). Developing the left determinant and permuting electrons indexes as in equation (1.25), it is possible to obtain $N!$ terms, each having a sign ± 1 in front, depending on their parity. It is interesting to see that for each electrons permutation, this also affects the right determinant, which makes appear a factor ± 1 depending on the permutation parity. These two ± 1 parity signs will then always cancel each other, allowing to simplify equation (1.24) into

$$\int u_1^*(\boldsymbol{x_1}) u_2^*(\boldsymbol{x_2}) \dots u_N^*(\boldsymbol{x_N}) \hat{K} \begin{vmatrix} u_1(\boldsymbol{x_1}) & u_1(\boldsymbol{x_2}) & \dots & u_1(\boldsymbol{x_N}) \\ & \dots\dots\dots\dots & & \\ u_N(\boldsymbol{x_1}) & u_N(\boldsymbol{x_2}) & \dots & u_N(\boldsymbol{x_N}) \end{vmatrix} d\boldsymbol{x_1} d\boldsymbol{x_2} \dots d\boldsymbol{x_N}. \tag{1.26}$$

Developing the above equation, it is now possible to evaluate the three matrices which we will encounter in usual QC when $\hat{K}$ is: a constant operator 1, a sum of one-electron operators $\sum_i \hat{f}_i$, and a double sum of two-electron operators $\sum_{i>j} \hat{g}_{ij}$.

First if $\hat{K}$ is a constant operator, equation (1.26) produces $N!$ terms with a coefficient ± 1 depending on the development of the right determinant. As an example, the term

obtained by taking the diagonal element of the right determinant will be equal to

$$S_{11}S_{22}\dots S_{NN} \tag{1.27}$$

where

$$S_{ij} = \int u_i^*(\boldsymbol{x_1})u_j(\boldsymbol{x_1})d\boldsymbol{x_1}. \tag{1.28}$$

In the end, this is simply the determinant det $|S_{pq}|$, also called the normalization integral. One should then always multiply the determinant in equation (1.23) by (det $|S_{pq}|)^{-\frac{1}{2}}$ to have normalized functions. For sure if spin-orbitals u_i are orthonormal ($S_{ij} = \delta_{ij}$), det $|S_{pq}|$ = det $|\mathbb{1}| = 1$ so the above mentioned function is already normalized.

$$\det |S_{pq}| = \begin{vmatrix} S_{11} & S_{12} & \dots & S_{1N} \\ & \dots\dots\dots & & \\ S_{N1} & S_{N2} & \dots & S_{NN} \end{vmatrix} \tag{1.29}$$

Next let us consider the case where $\hat{K} = \sum_i \hat{f}_i$. As complexity will increase, we will first use the operator $\hat{f}_1$ and the principal diagonal term of the right determinant in equation (1.26), which gives us

$$[1|1]S_{22}\dots S_{NN} \tag{1.30}$$

with

$$[i|j] = \int u_i^*(\boldsymbol{x_1})\hat{f}_1 u_j(\boldsymbol{x_1})d\boldsymbol{x_1}. \tag{1.31}$$

Then we will extend our derivation to all $(N-1)!$ terms containing $u_1(\boldsymbol{x_1})$ in the right determinant. The coefficient multiplying $[1|1]$ becomes the minor of the determinant det $|S_{pq}|$ where the first row and column have been crossed out. We name this minor $|S_{pq}|_{1,1}$, equals to

$$\begin{vmatrix} S_{22} & S_{23} & \dots & S_{2N} \\ & \dots\dots\dots & & \\ S_{N2} & S_{N3} & \dots & S_{NN} \end{vmatrix}. \tag{1.32}$$

In a similar way, we can find the coefficient multiplying $[1|j]$ where j is any spin-orbital. It appears to be the minor $|S_{pq}|_{1,j}$. Afterwards, doing the same derivation with another one-electron operator $\hat{f}_i$, one can observe the general form of the coefficient multiplying $[i|j]$ as the minor of the determinant det $|S_{pq}|$ where the i-th column and the j-ih row have been crossed out, $|S_{pq}|_{i,j}$.

Finally, let us consider the case where $\hat{K} = \sum_{i>j} \hat{g}_{ij}$. Following our previous developments, if we start with $\hat{g}_{12}$ and keep all terms where $u_1(\boldsymbol{x_1})u_2(\boldsymbol{x_2})$ or $u_2(\boldsymbol{x_1})u_1(\boldsymbol{x_2})$, equation (1.26) reduces to

$$[11|22] - [12|21] \tag{1.33}$$

multiplied by the minor of det $|S_{pq}|$ where the first two rows and columns are crossed out.

Generalizing the problem to i, j, k and l indices (with $i > k$ and $j > l$), one can observe that equation (1.26) becomes, when $\hat{K} = \sum_{i>k,j>l} \hat{g}_{ikjl}$, a quadruple sum over $[ij|kl] - [il|kj]$ times the minor determinant obtained by crossing out the i-th and j-th columns and the k-th and l-th rows, multiplied by the parity factor $(-1)^p$ to bring the i-th row and k-th column to the first row and first column and the j-th row and l-th column to the second row and second column:

$$(-1)^p \sum_{i>k,j>l} ([ik|jl] - [il|jk])|S_{pq}|_{(i,j),(k,l)}. \tag{1.34}$$

As stated by Slater,[35] " *We see that in general, with non-orthogonal orbitals, none of the terms we have described will vanish*". This stresses the importance of working with orthonormal spin-orbitals as, in this common case, all previously described minor determinants will be either equal to 0 or 1.

To better grasp the complexity and the workings of equations, a personal attitude is to take a simple but sufficiently complex example and to develop it somewhat brutally. In this regard, let's take two three-electrons determinants $|D_1\rangle = K_1|abc|$ and $|D_2\rangle = K_2|ade|$ made of non-orthogonal orbitals a, b, c, d, e and normalization constants K_1 and K_2, which read

$$|D_1\rangle = \frac{1}{\sqrt{3!}\sqrt{n_1}} \begin{vmatrix} a(\boldsymbol{x_1}) & a(\boldsymbol{x_2}) & a(\boldsymbol{x_3}) \\ b(\boldsymbol{x_1}) & b(\boldsymbol{x_2}) & b(\boldsymbol{x_3}) \\ c(\boldsymbol{x_1}) & c(\boldsymbol{x_2}) & c(\boldsymbol{x_3}) \end{vmatrix} \quad \text{and} \quad |D_2\rangle = \frac{1}{\sqrt{3!}\sqrt{n_2}} \begin{vmatrix} a(\boldsymbol{x_1}) & a(\boldsymbol{x_2}) & a(\boldsymbol{x_3}) \\ d(\boldsymbol{x_1}) & d(\boldsymbol{x_2}) & d(\boldsymbol{x_3}) \\ e(\boldsymbol{x_1}) & e(\boldsymbol{x_2}) & e(\boldsymbol{x_3}) \end{vmatrix} \tag{1.35}$$

with n_1 and n_2 the normalization factors for $|D_1\rangle$ and $|D_2\rangle$. n_1 is obtained after

deriving the equation $\int D_1^* D_1(d\boldsymbol{v})$ with $(d\boldsymbol{v}) = d\boldsymbol{x_1} d\boldsymbol{x_2} d\boldsymbol{x_3}$. In this regard,

$$\begin{aligned}|abc| =& a(\boldsymbol{x_1})b(\boldsymbol{x_2})c(\boldsymbol{x_3}) - a(\boldsymbol{x_1})c(\boldsymbol{x_2})b(\boldsymbol{x_3}) \\ &- b(\boldsymbol{x_1})a(\boldsymbol{x_2})c(\boldsymbol{x_3}) + b(\boldsymbol{x_1})c(\boldsymbol{x_2})a(\boldsymbol{x_3}) \\ &+ c(\boldsymbol{x_1})a(\boldsymbol{x_2})b(\boldsymbol{x_3}) - c(\boldsymbol{x_1})b(\boldsymbol{x_2})a(\boldsymbol{x_3})\end{aligned}$$

and so

$$\begin{aligned}\int D_1^* D_1(d\boldsymbol{v}) = K_1^2 \Bigg(& \int a^*(\boldsymbol{x_1}) b^*(\boldsymbol{x_2}) c^*(\boldsymbol{x_3}) \begin{vmatrix} a(\boldsymbol{x_1}) & a(\boldsymbol{x_2}) & a(\boldsymbol{x_3}) \\ b(\boldsymbol{x_1}) & b(\boldsymbol{x_2}) & b(\boldsymbol{x_3}) \\ c(\boldsymbol{x_1}) & c(\boldsymbol{x_2}) & c(\boldsymbol{x_3}) \end{vmatrix} (d\boldsymbol{v}) \\ & - \int a^*(\boldsymbol{x_1}) b^*(\boldsymbol{x_3}) c^*(\boldsymbol{x_2}) \begin{vmatrix} a(\boldsymbol{x_1}) & a(\boldsymbol{x_2}) & a(\boldsymbol{x_3}) \\ b(\boldsymbol{x_1}) & b(\boldsymbol{x_2}) & b(\boldsymbol{x_3}) \\ c(\boldsymbol{x_1}) & c(\boldsymbol{x_2}) & c(\boldsymbol{x_3}) \end{vmatrix} (d\boldsymbol{v}) \\ & + \dots \Bigg).\end{aligned} \tag{1.36}$$

Permuting electrons 2 and 3 in the second term will transform it into

$$\begin{aligned}-\int a^*(\boldsymbol{x_1}) b(\boldsymbol{x_3})^*(\boldsymbol{x_2})^* \begin{vmatrix} a(\boldsymbol{x_1}) & a(\boldsymbol{x_2}) & a(\boldsymbol{x_3}) \\ b(\boldsymbol{x_1}) & b(\boldsymbol{x_2}) & b(\boldsymbol{x_3}) \\ c(\boldsymbol{x_1}) & c(\boldsymbol{x_2}) & c(\boldsymbol{x_3}) \end{vmatrix} (d\boldsymbol{v}) &= -\int a^*(\boldsymbol{x_1}) b^*(\boldsymbol{x_2}) c^*(\boldsymbol{x_3}) \begin{vmatrix} a(\boldsymbol{x_1}) & a(\boldsymbol{x_3}) & a(\boldsymbol{x_2}) \\ b(\boldsymbol{x_1}) & b(\boldsymbol{x_3}) & b(\boldsymbol{x_2}) \\ c(\boldsymbol{x_1}) & c(\boldsymbol{x_3}) & c(\boldsymbol{x_2}) \end{vmatrix} (d\boldsymbol{v}) \\ &= +\int a^*(\boldsymbol{x_1}) b^*(\boldsymbol{x_2}) c^*(\boldsymbol{x_3}) \begin{vmatrix} a(\boldsymbol{x_1}) & a(\boldsymbol{x_2}) & a(\boldsymbol{x_3}) \\ b(\boldsymbol{x_1}) & b(\boldsymbol{x_2}) & b(\boldsymbol{x_3}) \\ c(\boldsymbol{x_1}) & c(\boldsymbol{x_2}) & c(\boldsymbol{x_3}) \end{vmatrix} (d\boldsymbol{v}).\end{aligned}$$

Repeating these permutations allows us to obtain 3! times the first term of equation (1.36). To have $|D_1\rangle$ normalized, one should then fulfill the equality

$$\int D_1^* D_1(d\boldsymbol{v}) = \frac{1}{n_1} \int a^*(\boldsymbol{x_1}) b^*(\boldsymbol{x_2}) c^*(\boldsymbol{x_3}) \begin{vmatrix} a(\boldsymbol{x_1}) & a(\boldsymbol{x_2}) & a(\boldsymbol{x_3}) \\ b(\boldsymbol{x_1}) & b(\boldsymbol{x_2}) & b(\boldsymbol{x_3}) \\ c(\boldsymbol{x_1}) & c(\boldsymbol{x_2}) & c(\boldsymbol{x_3}) \end{vmatrix} (d\boldsymbol{v}) = 1. \tag{1.37}$$

Developing the part in the integral of the above equation brings

$$\begin{aligned} a^*(\boldsymbol{x_1})b^*(\boldsymbol{x_2})c^*(\boldsymbol{x_3}) \begin{vmatrix} a(\boldsymbol{x_1}) & a(\boldsymbol{x_2}) & a(\boldsymbol{x_3}) \\ b(\boldsymbol{x_1}) & b(\boldsymbol{x_2}) & b(\boldsymbol{x_3}) \\ c(\boldsymbol{x_1}) & c(\boldsymbol{x_2}) & c(\boldsymbol{x_3}) \end{vmatrix} =& a^*(\boldsymbol{x_1})a(\boldsymbol{x_1})b^*(\boldsymbol{x_2})b(\boldsymbol{x_2})c^*(\boldsymbol{x_3})c(\boldsymbol{x_3}) \\ & -a^*(\boldsymbol{x_1})a(\boldsymbol{x_1})b^*(\boldsymbol{x_2})c(\boldsymbol{x_2})c^*(\boldsymbol{x_3})b(\boldsymbol{x_3}) \\ & -a^*(\boldsymbol{x_1})b(\boldsymbol{x_1})b^*(\boldsymbol{x_2})a(\boldsymbol{x_2})c^*(\boldsymbol{x_3})c(\boldsymbol{x_3}) \\ & +a^*(\boldsymbol{x_1})b(\boldsymbol{x_1})b^*(\boldsymbol{x_2})c(\boldsymbol{x_2})c^*(\boldsymbol{x_3})a(\boldsymbol{x_3}) \\ & +a^*(\boldsymbol{x_1})c(\boldsymbol{x_1})b^*(\boldsymbol{x_2})a(\boldsymbol{x_2})c^*(\boldsymbol{x_3})b(\boldsymbol{x_3}) \\ & -a^*(\boldsymbol{x_1})c(\boldsymbol{x_1})b^*(\boldsymbol{x_2})b(\boldsymbol{x_2})c^*(\boldsymbol{x_3})a(\boldsymbol{x_3}) \end{aligned} \tag{1.38}$$

which can be plugged back into equation (1.37) and, applying integrals over $(d\boldsymbol{v})$, can simplify as

$$\begin{aligned} & \frac{1}{n_1} \int \begin{vmatrix} a^*(\boldsymbol{x_1})a(\boldsymbol{x_1}) & b^*(\boldsymbol{x_2})a(\boldsymbol{x_2}) & c^*(\boldsymbol{x_3})a(\boldsymbol{x_3}) \\ a^*(\boldsymbol{x_1})b(\boldsymbol{x_1}) & b^*(\boldsymbol{x_2})b(\boldsymbol{x_2}) & c^*(\boldsymbol{x_3})b(\boldsymbol{x_3}) \\ a^*(\boldsymbol{x_1})c(\boldsymbol{x_1}) & b^*(\boldsymbol{x_2})c(\boldsymbol{x_2}) & c^*(\boldsymbol{x_3})c(\boldsymbol{x_3}) \end{vmatrix} (d\boldsymbol{v}) = 1 \\ \Leftrightarrow n_1 = & \begin{vmatrix} \int a^*(\boldsymbol{x_1})a(\boldsymbol{x_1})d\boldsymbol{x_1} & \int b^*(\boldsymbol{x_2})a(\boldsymbol{x_2})d\boldsymbol{x_2} & \int c^*(\boldsymbol{x_3})a(\boldsymbol{x_3})d\boldsymbol{x_3} \\ S_{ab} & S_{bb} & S_{cb} \\ S_{ac} & S_{bc} & S_{cc} \end{vmatrix}. \end{aligned} \tag{1.39}$$

The same development occurs for $|D_2\rangle$. We will keep the notations n_1 and n_2 in the rest of the derivations.

Now we will develop the matrix element between $|D_1\rangle$ and $|D_2\rangle$ when $\hat{K}$ is the sum of one-electron operators $\hat{K} = \sum_i \hat{f}_i$

$$\langle D_1| \sum_i \hat{f}_i |D_2\rangle \tag{1.40}$$

Let us first develop the case for $\hat{K} = \hat{f}_1$ then generalize it to the sum over $\hat{f}_i$. We can directly use the previous derivation to determine

$$\frac{1}{\sqrt{n_1 n_2}} \int a^*(\boldsymbol{x_1})b^*(\boldsymbol{x_2})c^*(\boldsymbol{x_3})\hat{f}_1 \begin{vmatrix} a(\boldsymbol{x_1}) & a(\boldsymbol{x_2}) & a(\boldsymbol{x_3}) \\ d(\boldsymbol{x_1}) & d(\boldsymbol{x_2}) & d(\boldsymbol{x_3}) \\ e(\boldsymbol{x_1}) & e(\boldsymbol{x_2}) & e(\boldsymbol{x_3}) \end{vmatrix} (d\boldsymbol{v}) = \frac{1}{\sqrt{n_1 n_2}} \begin{vmatrix} \int a^*(\boldsymbol{x_1})\hat{f}_1 a(\boldsymbol{x_1})d\boldsymbol{x_1} & S_{ba} & S_{ca} \\ \int a^*(\boldsymbol{x_1})\hat{f}_1 d(\boldsymbol{x_1})d\boldsymbol{x_1} & S_{bd} & S_{cd} \\ \int a^*(\boldsymbol{x_1})\hat{f}_1 e(\boldsymbol{x_1})d\boldsymbol{x_1} & S_{be} & S_{ce} \end{vmatrix}. \tag{1.41}$$

Developing further, one can see that three one-electron integrals arise from this derivation, each having as multiplying factor the minor determinant obtained by crossing the first column and the j-th row in det $|S_{pq}|$, times $(-1)^p$, taking into account the parity p needed to permute the j-th row with the first one:

$$\frac{1}{\sqrt{n_1 n_2}}\left([a|a]\begin{vmatrix}S_{bd} & S_{cd}\\ S_{be} & S_{ce}\end{vmatrix} - [a|d]\begin{vmatrix}S_{ba} & S_{ca}\\ S_{be} & S_{ce}\end{vmatrix} + [a|e]\begin{vmatrix}S_{ba} & S_{ca}\\ S_{bd} & S_{cd}\end{vmatrix}\right). \tag{1.42}$$

Repeating this for $\hat{f}_2$ and $\hat{f}_3$, one will then obtain two times three other one-electron integrals $[i,j]$, with a factor obtained by crossing the j-th row and, respectively, the second and third column.

In an orthonormal basis set, one can expect at maximum three one-electron integrals as $S_{pq} = \delta_{pq}$ but in a non-orthogonal basis, N^2 one-electron integrals are to be expected, each having a different multiplying factor.

The derivation for the case $\hat{K} = \sum_{j>i} \hat{g}_{ij}$ follows the same logic as for the one-electron operators sum. However some particular care need to be taken as two-electron operators do not allow the splitting of the double-integral $d\boldsymbol{x_i}d\boldsymbol{x_j}$. Let's take for example $\hat{g}_{13}$ operator

$$\begin{aligned}
\langle D_1|\hat{g}_{13}|D_2\rangle =& \frac{1}{\sqrt{n_1 n_2}}\int \hat{g}_{13}\begin{vmatrix} a^*(\boldsymbol{x_1})a(\boldsymbol{x_1}) & S_{ba} & c^*(3)a(\boldsymbol{x_3})\\ a^*(\boldsymbol{x_1})d(\boldsymbol{x_1}) & S_{bd} & c^*(3)d(\boldsymbol{x_3})\\ a^*(\boldsymbol{x_1})e(\boldsymbol{x_1}) & S_{be} & c^*(3)e(\boldsymbol{x_3})\end{vmatrix} d\boldsymbol{x_1}d\boldsymbol{x_2}d\boldsymbol{x_3}\\
=& \frac{-1}{\sqrt{n_1 n_2}}\int \hat{g}_{13}\begin{vmatrix} a^*(\boldsymbol{x_1})a(\boldsymbol{x_1}) & c^*(3)a(\boldsymbol{x_3}) & S_{ba}\\ a^*(\boldsymbol{x_1})d(\boldsymbol{x_1}) & c^*(3)d(\boldsymbol{x_3}) & S_{bd}\\ a^*(\boldsymbol{x_1})e(\boldsymbol{x_1}) & c^*(3)e(\boldsymbol{x_3}) & S_{be}\end{vmatrix} d\boldsymbol{x_1}d\boldsymbol{x_2}d\boldsymbol{x_3}\\
=& \frac{-1}{\sqrt{n_1 n_2}}\begin{pmatrix}[aa|cd]|S_{be}| - [aa|ce]|S_{bd}|\\ -[ad|ca]|S_{be}| + [ad|ce]|S_{ba}|\\ +[ae|ca]|S_{bd}| - [ae|cd]|S_{bd}|\end{pmatrix}\\
=& \frac{-1}{\sqrt{n_1 n_2}}\begin{pmatrix}([aa|cd] - [ad|ca])S_{be}\\ +([ae|ca] - [aa|ce])S_{bd}\\ +([ad|ce] - [ae|cd])S_{ba}\end{pmatrix}\\
=& \frac{-1}{\sqrt{n_1 n_2}}([aa||cd]S_{be} + [ae||ca]S_{bd} + [ad||ce]S_{ba}).
\end{aligned} \tag{1.43}$$

One can see that this operator generates six two-electron integrals $[ik|jl]$, all multiplied by $(-1)^p$ with p the parity to bring i and j in, respectively, the first and second row and k and l in, respectively, the first and second column, and each multiplied by the minor of determinant det $|S_{pq}|$ with i-th and j-th columns and k-th and l-th rows crossed.

In an orthonormal basis set, all these integrals except one would equal 0 as $|D_1\rangle$ and $|D_2\rangle$ differ by two spin-orbitals, whereas $\frac{N!}{2(N-2)!}N(N-1)$ two-electron integrals are expected in a fully non-orthonormal basis.

Moreover due to scaling factors of multideterminantal wavefunctions, it becomes clear that orthonormal basis set are to be prioritized when necessary. However I do think that it is important to grasp the beauty hidden behind the simplification of all these minor determinants to 0 or 1 in an orthonormal basis. In my opinion, this is a good exercise to better understand the matrix elements "selection rules" for determinants, as one can find in p.70 of Modern Quantum Chemistry [33] and reminded in the next subsection, but also to remember the dangerous scaling which can appear in QC.

1.1.6.b General rules for matrix elements

Hoping the reader is convinced on the use of orthonormal basis set in QC, we will quickly summarize some tricks to evaluate efficiently matrix elements. As stated in the previous section, when working with an orthonormal MOs basis set, all multiplying minor determinants will simplify to 0 or 1. This allows to derive four cases and their respective mathematical tricks/rules. These rules are perfectly presented and explained in p.70 of Modern Quantum Chemistry [33] and my position here is to remind them briefly as they are often compared to non-orthonormal rules in Chapter 2.

Let us take two determinants $|A\rangle$ and $|B\rangle$. The rules for evaluating the matrix element $\langle A|\hat{\mathcal{O}}|B\rangle$ depends on whether $\hat{\mathcal{O}}$ is a sum of one-electron operators $\hat{\mathcal{O}}_1$ or a sum of two-electron operators $\hat{\mathcal{O}}_2$, and on the number of spin-orbitals differing from $|A\rangle$ to $|B\rangle$.

The first case, Case 1, is when both determinants are equal. We are thus evaluating

a diagonal matrix element.

$$|A\rangle = |\cdots mn\cdots\rangle \tag{1.44}$$

In this case, the normalization integral (see equation (1.29)) is the determinant of identity $|\mathbb{1}|$, meaning that every diagonal element is 1 and extra-diagonal elements are 0. The resulting minor determinants are therefore non-zero when crossing 1) for $\hat{\mathcal{O}}_1$ the same i^{th} row and column; 2) for $\hat{\mathcal{O}}_2$ the same i^{th} and j^{th} rows and columns.

$$\begin{vmatrix} 1 & 0 & \cdots & 0 \\ 0 & 1 & \cdots & 0 \\ \vdots & \vdots & \ddots & \vdots \\ 0 & 0 & \cdots & 1 \end{vmatrix}$$

The second case, Case 2, is when they differ by one spin-orbital.

$$|A\rangle = |\cdots mn\cdots\rangle$$
$$|B\rangle = |\cdots pn\cdots\rangle$$

One diagonal element is then zero in the normalization integral. All minor determinants except the ones obtained by crossing the line and column of zeroes will be null and will make vanish their resulting integrals.

$$\begin{vmatrix} 1 & \cdots & 0 & \cdots & 0 \\ \vdots & \ddots & & & \vdots \\ 0 & & 0 & & 0 \\ \vdots & & & \ddots & \vdots \\ 0 & \cdots & 0 & \cdots & 1 \end{vmatrix}$$

The third case, Case 3, is when they differ by two spin-orbitals.

$$|A\rangle = |\cdots mn\cdots\rangle$$
$$|B\rangle = |\cdots pq\cdots\rangle$$

Two diagonal elements are zero in the normalization integral. All one-electron integrals' minor determinants will be strictly zero as one needs to cross out two lines and columns. Only one two-electron integral (obtained by crossing out the two lines and columns of zeroes) will survive.

The last case is when they differ by three or more spin-orbitals. In this case, minor determinants obtained by crossing one or two lines and columns will always be zero. This results in the fact that the matrix element of two determinant $|A\rangle$ and $|B\rangle$ which differs by more than two spin-orbitals is always zero.

The two tables below were taken from Ref [33], and summarize the following rules obtained by deriving the three first cases.

$\hat{\mathcal{O}}_1 = \sum_{i=1}^{N} \hat{h}(i)$	
Case 1:	$\|A\rangle = \|\cdots mn\cdots\rangle$
	$\langle A\|\hat{\mathcal{O}}_1\|A\rangle = \sum_{m}^{N}\langle m\|\hat{h}\|m\rangle$
Case 2:	$\|A\rangle = \|\cdots mn\cdots\rangle$
	$\|B\rangle = \|\cdots pn\cdots\rangle$
	$\langle A\|\hat{\mathcal{O}}_1\|B\rangle = \langle m\|\hat{h}\|p\rangle$
Case 3:	$\|A\rangle = \|\cdots mn\cdots\rangle$
	$\|B\rangle = \|\cdots pq\cdots\rangle$
	$\langle A\|\hat{\mathcal{O}}_1\|B\rangle = 0$

Table 1.1: Matrix elements between determinants for one-electron operators.

$\hat{\mathcal{O}}_2 = \sum_{i=1}^{N}\sum_{i>j}^{N} \frac{1}{r_{ij}}$	
Case 1:	$\|A\rangle = \|\cdots mn\cdots\rangle$
	$\langle A\|\hat{\mathcal{O}}_2\|A\rangle = \sum_{m}^{N}\sum_{n>m}^{N}[mm\|nn] - [mn\|nm] = \sum_{m}^{N}\sum_{n>m}^{N}\langle mn\|\|nm\rangle$
Case 2:	$\|A\rangle = \|\cdots mn\cdots\rangle$
	$\|B\rangle = \|\cdots pn\cdots\rangle$
	$\langle A\|\hat{\mathcal{O}}_2\|B\rangle = \sum_{n}^{N}[mp\|nn] - [mn\|np] = \sum_{n}^{N}\langle mn\|\|np\rangle$
Case 3:	$\|A\rangle = \|\cdots mn\cdots\rangle$
	$\|B\rangle = \|\ pq\cdots\rangle$
	$\langle A\|\hat{\mathcal{O}}_2\|B\rangle = [mp\|nq] - [mq\|np] = \langle mn\|\|pq\rangle$

Table 1.2: Matrix elements between determinants for two-electron operators.

1.2 Methods

Now that we possess many tools, we are able to do wavefunction calculations. This section will start with mono-configurational methods (HF) in order to introduce multi-configurational methods (FCI, MCSCF, MRCI) and will finally end on some words regarding second order Perturbation Theory (MP2, CASPT2, NEVPT2).

1.2.1 Hartree-Fock approximation

Coming from experimental chemistry, I can state that the generalized picture of a molecule in its ground state is often the configuration obtained by filling $\frac{N}{2}$ MOs with N electrons from the lowest MO (in energy) to the highest MO. This concept is inspired from the Aufbau principle (which is for atoms and ions) stating that "*a maximum of two electrons are put into orbitals in the order of increasing orbital energy: the lowest-energy orbitals are filled before electrons are placed in higher-energy orbitals*".[8]

Instinctively, chemists represent the ground state of a molecule as a mono-determinantal wavefunction. This is the basis of the Hartree-Fock approximation: assuming that the exact N-electrons wavefunction of a system can be approximated by a single Slater determinant. There is no point in describing HF in details as there is already plenty of literature around it. However HF remains the starting point for almost all QC methods and it is interesting to comment on some of its points.

From my point of view, the most interesting idea carrying HF is to consider each electron of the N-electron system as "feeling" a mean field due to the presence of the other $N-1$ electrons. This allows to decouple the high-dimensional problem of the wavefunction into multiple lower dimensionality problems. To solve the non-linear QC problem and obtain the lowest lying root, one needs to obtain the best wavefunction as stated by the variational principle.

$$E_0 = \frac{\langle \Phi_0 | \hat{H} | \Phi_0 \rangle}{\langle \Phi_0 | \Phi_0 \rangle} \tag{1.45}$$

HF being a mono-determinantal approach, the only parameter able to tune the wavefunction is the definition of MOs. Finding the best Φ MOs brings the lowest

root.

$$\min_{\Phi} \frac{\langle \Phi | \hat{H} | \Phi \rangle}{\langle \Phi | \Phi \rangle} \geq E_0 \tag{1.46}$$

To do such, HF uses a procedure called the Self-Consistent Field (SCF). Briefly, it starts with a guess on MOs from whom the average field, generated by $N-1$ electrons, (and the constant nuclei field) seen by each electron in a MO is calculated. This allows to get the eigenvalue of the system. By promoting an electron into a virtual MO, it is possible to evaluate the energy of a virtual MO. Then MOs are modified and the procedure is repeated iteratively, until self-consistency is reached (*i.e.* the average field does not change and is minimised). In the end, one obtains the HF ground state energy of the system and its respective orthonormal set of MOs.

1.2.2 Drawbacks of HF method

However moving from $2N$ electron systems to $2N-1$, HF becomes unable to treat the system. Same thing happens when searching a state with open-shells. Its concept of single determinant is restricted to a fully doubly occupied determinant. This called for the development of unrestricted Hartree-Fock method,[9] which is able to treat open-shells systems. Though, a new drawback appears due to the use of a single determinant to describe an open-shell system: spin contamination. A mono-determinantal wavefunction is not a satisfactory eigenfunction of the total spin operator $\hat{S}^2$, thus states get spin contaminated.

Another possible trouble in HF method is the mean-field approximation itself. It is a powerful approximation which comes with its responsibilities. In fact it averages electron-electron repulsions by considering the interaction of an electron with an average field generated by $N-1$ electrons. Thus, HF misses the fluctuations of electron-electron repulsions. These fluctuations are particularly important in the description of weak interactions. A famous example is that it badly describes H_2 at the dissociation limit. This is because correlation is needed to describe accurately certain physics.

1.2.3 Correlation

Before continuing, it is important to present a major concept in QC methods: correlation energy. IUPAC defines it as "*the difference between the Hartree–Fock energy calculated for a system and the exact non-relativistic energy of that system*".[10] It arises due to the approximate representation of the electron-electron repulsions in HF method, also called Coulomb correlation. HF substitutes the instantaneous electron-electron interactions by an averaged interaction of an electron with an average field of $N-1$ electrons. Being a mono-determinantal method, it can be seen as a constrained optimization of the exact nonrelativistic Schrödinger equation: it misses electronic correlation. There is a need to retrieve this missing correlation, calling for post-HF methods that are described in the following subsections. Yet before advancing, it is necessary to specify three facts:

1) Correlation is highly basis set dependent. As said in section (1.1.3), the exact non-relativistic energy (E_{exact}) of a system needs an infinite AOs set, which is too computationally expensive. Therefore, correlation is calculated using a finite AOs set large enough to be considered complete. Due to basis set dependence, comparisons between methods should be done in the same complete basis set.

2) Thus, the IUPAC definition for correlation energy (E_c) is usually defined as the energy gain E from HF (E_{HF}).[2]

$$E_c = E_{HF} - E \tag{1.47}$$

3) Often, correlation energy is divided into two types: dynamical correlation and non-dynamical (static) correlation. In both cases, correlation is recovered by going from a mono-determinantal wavefunction to a multi-configurational wavefunction. In other words: mixing more Slater determinants $|\Phi_I\rangle$ to the HF one $|\Phi_{HF}\rangle$.

$$|\Psi\rangle = c_{HF}|\Phi_{HF}\rangle + \sum_I c_I|\Phi_I\rangle \tag{1.48}$$

If c_{HF} is assumed to be close to 1 and numerous excited determinants are added but give a small contribution, then dynamical correlation is primarily treated. On the other hand, if there are some determinants $|\Phi_I\rangle$ with weights c_I close to that

[2]However, the reader may find $E_c = E - E_{HF}$ in the literature.

of $|\Phi_{HF}\rangle$, then static correlation is primarily treated. However these definitions are particularly arbitrary. The limit between dynamical and static correlation is unclear. Degenerated and quasi-degenerated configurations should be accounted in static correlation, but what defines the quasi-degeneracy energy criteria ? Moreover, higher energy configuration that can be considered as perturbations should be accounted for dynamical correlation, but what defines the energy criteria ? In the end, my opinion is that one should be satisfied with his/her own definition. An interesting approach to the arbitrariness of definitions is to adapt dynamically to the system, *i.e.* using a First-Order Interacting Space described in section (1.2.6). In the next part, we present first how to treat both these correlations then methods focused on static correlation, and finally methods focused on dynamical correlation.

1.2.4 Configuration Interaction

Going beyond HF, a method of choice to capture correlation is the so-called Configuration Interaction (CI) method, as described in the previous paragraph (see equation 1.48). It consists of an expansion of the wavefunction through a linear combination of the ground determinant and excited determinants. Then, the c_I coefficients are optimized with respect to the variational principle.

$$\min_{c_I} \frac{\langle \sum_I c_I \Phi_I | \hat{H} | \sum_I c_I \Phi_I \rangle}{\langle \sum_I c_I \Phi_I | \sum_I c_I \Phi_I \rangle} \geq E_0 \tag{1.49}$$

It is conceptually speaking one of the simplest methods. In practice, it represents working with $\binom{2K}{N}$ determinants for $2K$ spin-orbitals and N electrons. This makes it one of the most computationally demanding QC method. A first trick to reduce the size of the problem is to work only in a chosen m_s subspace. As an example, let us assume we are computing a quintet state ($S = 2$). Then, in the absence of any exterior magnetic field, we can reduce the number of determinants to $\binom{K}{4}\binom{K-4}{\frac{N}{2}-2}\binom{K}{\frac{N}{2}-2}$ by taking only $m_s = +2$ determinants. Considering the full excitation space is called Full Configuration Interaction (FCI) method. In comparison to HF theory in which MOs are optimized, it is not necessary in FCI as improving the wavefunction through excitations is equivalent to rotating MOs. However, due to its enormous scaling, it is only possible for small-scale systems.

To save computational time and treat bigger systems, we need to truncate the CI

space. This gives rise to CID method, limited to double excitations, to CISD method, limited to single and double excitations, etc... Though an important problem in truncation is the lost of size-consistency. It means that the energy of two infinitely far subsystems must be equal to twice the energy of a subsystem, and that the total wavefunction must be equal to the product of each individual wavefunction, which get lost by truncation. For this reason, truncated CI methods must be taken with care to study dissociation of molecules. Otherwise one needs to bring proper corrections to get back size-consistency.

There exist different methods to keep size-consistency. Next, we will present one concept proper to Multi-Configurational methods, the Active Space, and its related QC methods.

1.2.5 Multi-Configurational methods

We have seen on one hand that HF uses the SCF method through MOs rotation to minimise the energy. On the other hand, a multi-determinantal wavefunction like the one from CI allows one to retrieve correlation energy. Nevertheless, we cannot afford the computational cost of FCI and truncation looses size-consistency. But would size-consistency be conserved if a FCI in a smaller subspace was realized ? This is what motivated the development of Multi-Configurational Self-Consistent Field (MCSCF) methods. Instead of treating the system as a whole, only a part of it is studied at an exact level. This smaller subspace is the concept of the Active Space.

Very much like when chemists represent a molecule by its valence orbitals, the so-called Active Space (AS) is a slice of the electronic system which is deemed more important than the rest of the system, *i.e.* to study particular properties. Several MCSCF methods exist but only the one used throughout this thesis will be discussed, the Complete Active Space Self-Consistent Field (CASSCF) method. CASSCF is based on the prior definition of a Complete Active Space (CAS). In this sense, MOs are split into three categories:

- virtual MOs, always empty, denoted r, s.
- active MOs, partial electron occupation, denoted a, b.

- inactive MOs, always doubly occupied, denoted p, q.

The CAS is defined by a number n of electrons in the set k of active MOs (*e.g.* CAS[8,7] means 8 electrons in 7 MOs). All the possible excitations inside the CAS are generated (FCI inside the CAS). Different wavefunctions are thus constructed as linear combinations of CAS determinants. To prevent biases, these determinants are treated on an equal footing, which means that they are considered degenerated. Then, CASSCF uses the variational principle to do a double optimization on MOs ψ_i and on the CAS wavefunction $|\Psi_{CAS}\rangle$.

$$\psi_i = \sum_k c_k \, \chi_k \quad \text{and} \quad |\Psi_{CAS}\rangle = \sum_I c_I \, |\Phi_I\rangle \tag{1.50}$$

where $\sum_I c_I^2 = 1$.

The energy of the system is then minimized following this double optimization until convergence.

$$\min_{c_k, c_I} \frac{\langle \Psi_{CAS} | \hat{H} | \Psi_{CAS} \rangle}{\langle \Psi_{CAS} | \Psi_{CAS} \rangle} \geq E_0 \tag{1.51}$$

This allows to retrieve a lot of static correlation and some dynamical correlation. For sure, expanding the CAS to the size of the complete system is equivalent to a FCI (which renders the MOs optimization step useless), which we cannot afford. In this sense CASSCF is an interesting compromise between SCF and FCI methods. It is important to mention that in this case, one may use the State-Average Complete Active Space Self-Consistent method to compute excited states. This method considers N states with the ground state and minimises a total wavefunction being a preset weighted ($\omega_i > 0$) linear combination of these states $|\Psi_i\rangle$.

$$|\Psi\rangle = \sum_{w_i} \omega_i |\Psi_i\rangle = \sum_{w_i} \omega_i \sum_{J_i} c_{J_i} \, |\Phi_{J_i}\rangle \tag{1.52}$$

This method allows for an equal description of the ground state and its excited states by the same set of MOs. It is particularly efficient to compute Conical Intersections. However it needs particular attention in general calculations as it assumes that the ground state and the excited states have the same set of MOs. In general, this is a correct approximation but it has been proven in recent works that this fails terribly in some cases.[37] In order to retrieve more correlation, it is also possible to use Multi-Reference Configuration Interaction (MRCI) methods. Unlike in CI where there is

one HF reference determinant, MRCI uses multiple determinants as reference. Once again, truncation is a need to reduce computational cost. Choosing the proper references, one can balance the correlation of the ground and excited states as single and double excitations will now generate triple and quadruple excitations. Still, the size-consistency problem survives in truncated MRCI. After presenting MCSCF methods, one can see that these methods will generate proper MOs set and multi-determinantal wavefunction. This is a blessing for MRCI methods which need a good MOs set. It is then possible to feed these wavefunctions and MOs to a MRCI method such as the Difference Dedicated Configuration Interaction (DDCI) method to retrieve more dynamical correlation. The truncated MRCI methods are well described in the literature. We will now discuss the MRCI methods implemented in the CASDI code used in the presented works.[38]

In order to generate different excited determinants, different terms are defined: "holes" (h) are excitations of an electron from the inactive orbitals to the AS; "particles" (p) are excitations of an electron from the AS to the virtuals. These excitations are schematized in Figure 1.1.

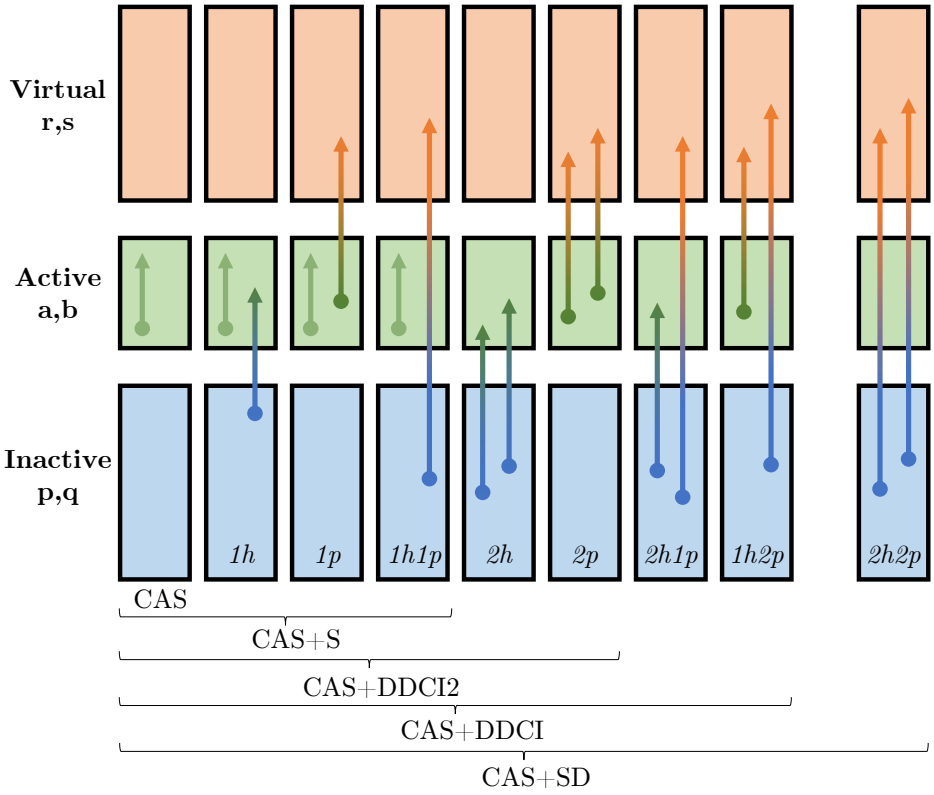

Figure 1.1: Different kind of excitations from CAS to CAS+SD.

Now let us comment on the MRCI methods implemented in CASDI:

1) *CAS*. This is a typical CASCI calculation. Unlike CASSCF where both the wavefunction and MOs are optimized, here the MOs are kept frozen and a FCI is calculated in the CAS subspace.

2) *CAS+S*. This is a MRCIS method. It diagonalizes the Hamiltonian representation in the basis formed by the CAS determinants and all single excitations: $1h$, $1p$ and $1h1p$.

3) *CAS+DDCI2*. This is a truncated MRCISD method. It works with determinants at CAS+S level and adds double excitations from and to the CAS only, such as: $2h$ and $2p$.

4) *CAS+DDCI*. Also called *CAS+DDCI3*. This is the earliest DDCI method,[39, 40] a truncated MRCISD. It uses all previous determinants and generates more double excitations: $2h1p$ and $1h2p$.

One can observe that double excitations outside the CAS are missing: $2h2p$. Adding these excitations makes a MRCISD method (a CAS+SD calculation in CASDI). However, this is not necessary for most of magnetic compounds. Indeed, $2h2p$ excitations, at the second order of perturbation theory, do nearly not contribute to the energy differences of the states. This is presented in detail in the following part on Perturbation Theory.

1.2.6 Perturbation Theory

A computationally cheap way to retrieve dynamical correlation is to use Perturbation Theory. There exist two main types of Perturbation Theories, Rayleigh-Schrödinger Perturbation Theory (RS-PT) and Brillouin-Wigner Perturbation Theory (BW-PT). RS-PT is analytical unlike BW-PT which can only be solved iteratively. The focus will only be on RS-PT as it was applied analytically in Chapter (3), and because it is useful for the QC previously described.

The principle of RS-PT is to split the Hamiltonian $\hat{H}$ into an unperturbed (zeroth-order) Hamiltonian $\hat{H}_0$, and a small perturbation V. Let us suppose we know the

eigenvalues and eigenvectors of $\hat{H}_0$ by means of wavefunction calculations.

$$\hat{H}_0|\Psi_i^{(0)}\rangle = E_i^{(0)}|\Psi_i^{(0)}\rangle$$

RS-PT goal is to improve the eigenvalues and eigenvectors of the system. In this regard, a dimensionless parameter λ is introduced, taking values from 0 (no perturbation) to 1 (full perturbation) such that the perturbed Hamiltonian takes the form:

$$\hat{H} = \hat{H}_0 + \lambda\hat{V}. \tag{1.53}$$

We then wish to solve the following eigenvalue problem:

$$\hat{H}|\Psi_i\rangle = (\hat{H}_0 + \lambda\hat{V})|\Psi_i\rangle = E_i|\Psi_i\rangle. \tag{1.54}$$

It is possible to expand the perturbed eigenvalues and eigenvectors in function of unperturbed ones following a Taylor expansion.

$$E_i = E_i^{(0)} + \lambda E_i^{(1)} + \lambda^2 E_i^{(2)} + \cdots \tag{1.55}$$

$$|\Psi\rangle = |\Psi_i^{(0)}\rangle + \lambda|\Psi_i^{(1)}\rangle + \lambda^2|\Psi_i^{(2)}\rangle + \cdots \tag{1.56}$$

Until this point, this is textbook knowledge. The same goes for the derivations of these equations to first-order, second-order and beyond. A particularly clear development can be found in Chapter 35 of ESQC Book II by Roos and Widmark. Thus, I will only focus on the important concepts that deserve discussion for this thesis. The general formulation for energies up to second-order are:

$$E_i^{(0)} = \langle\Psi_i^{(0)}|\hat{H}_0|\Psi_i^{(0)}\rangle \tag{1.57}$$

$$E_i^{(1)} = \langle\Psi_i^{(0)}|\hat{V}|\Psi_i^{(0)}\rangle \tag{1.58}$$

$$E_i^{(2)} = \langle\Psi_i^{(0)}|\hat{V}|\Psi_i^{(1)}\rangle \tag{1.59}$$

One can see that the system energy is corrected starting at second-order $E_i^{(2)}$ whereas its wavefunction is corrected at first order $|\Psi_i^{(1)}\rangle$. This gives the two general working equations:

$$|\Psi_i^{(1)}\rangle = \sum_{m\neq i} \frac{\langle\Psi_i^{(0)}|\hat{H}|\Psi_m^{(0)}\rangle}{E_i^{(0)} - E_m^{(0)}}|\Psi_m^{(0)}\rangle \tag{1.60}$$

$$E_i^{(2)} = \sum_{m\neq i} \frac{\left|\langle\Psi_i^{(0)}|\hat{H}|\Psi_m^{(0)}\rangle\right|^2}{E_i^{(0)} - E_m^{(0)}} \tag{1.61}$$

because $\langle\Psi_i^{(0)}|\hat{H}|\Psi_m^{(0)}\rangle = \langle\Psi_i^{(0)}|\hat{H} - \hat{H}_0|\Psi_m^{(0)}\rangle = \langle\Psi_i^{(0)}|\hat{V}|\Psi_m^{(0)}\rangle$.

The trick in second-order Perturbation Theory (PT2) is to chose a correct $\hat{H}_0$ which allows for easier developments. PT2 is analytically treated in Møller-Plesset second-order Perturbation Theory (MP2)[41] when there is a HF reference, but becomes more complex for multi-reference wavefunctions.

Starting with MP2, as $|\Psi_i^{(0)}\rangle = |\Phi_{HF}\rangle$, then we construct $\hat{H}_0$ as

$$\hat{H}_0 = \hat{P}_0\hat{F}\hat{P}_0 + \hat{P}_X\hat{F}\hat{P}_X \tag{1.62}$$

where $\hat{P}_0 = |\Psi_{HF}\rangle\langle\Psi_{HF}|$ is a projection operator onto the reference function, $\hat{P}_X$ is a projection operator for the rest of the configuration space, and $\hat{F}$ is the Fock operator. As single excitations are not coupled to the HF reference determinant (Brillouin's theorem), and triple and above excitations are not coupled to Φ_{HF} due to Slater's rules, the perturbation space is comprised only of double excitations. These double excitations are generated using the double excitation operator $\hat{D}_{ab,rs}\Phi_{HF} = \Phi_{ab}^{rs}$ to transform equation (1.59) into

$$E_{\Phi_{HF}}^{(2)} = \sum_{\hat{D}_{ab,rs}\Phi_{HF}} \frac{\left|\langle\hat{D}_{ab,rs}\Phi_{HF}|\hat{V}|\Phi_{HF}\rangle\right|^2}{E_{\Phi_{HF}}^{(0)} - E_{\hat{D}_{ab,rs}\Phi_{HF}}^{(0)}} = \sum_{a>b,r>s} \frac{\langle ab||rs\rangle^2}{\epsilon_a + \epsilon_b - \epsilon_r - \epsilon_s}. \tag{1.63}$$

Then moving to multi-reference wavefunction, it becomes trickier. As presented in subsection (1.2.4), MRCI methods already recover dynamic correlation. Let us discuss Multi-Reference Perturbation Theory methods. Two methods are particularly popular for PT2 corrections of CAS energies: Complete Active Space second-order Perturbation Theory (CASPT2)[42] and N-Electron Valence state second-order Perturbation Theory (NEVPT2).[43, 44] I have however only used CASPT2 as implemented in MOLCAS.[45] Both methods are based on an approximation called the First Order Interacting Space (FOIS). Instead of treating all the "perturbers" (determinants from the perturbation space), FOIS only consider the functions which directly interact with the zeroth-order wavefunction $|\Psi_i^{(0)}\rangle$. It is then spanned by all determinants generated by single and double excitations from the determinants defining $|\Psi_i^{(0)}\rangle$. It is important to state that NEVPT2 comes in two flavours and only Partially Contracted N-Electron Valence state second-order Perturbation Theory (PC-NEVPT2) is commented here. In CASPT2, the model Hamiltonian $\hat{H}_0$

is a one-electron Fock-like operator whereas, in PC-NEVPT2, it has two-electrons components because it uses the Dyall Hamiltonian $\hat{H}^D$.[46]

$$(CASPT2) \qquad \hat{H}_0 = \hat{P}_{\Psi_{CAS}}\hat{F}\hat{P}_{\Psi_{CAS}} + \hat{P}_{FOIS}\hat{F}\hat{P}_{FOIS} \tag{1.64}$$

$$(PC-NEVPT2) \qquad \hat{H}_0 = \hat{P}_{\Psi_{CAS}}\hat{H}^D\hat{P}_{\Psi_{CAS}} + \hat{P}_{FOIS}\hat{H}^D\hat{P}_{FOIS} \tag{1.65}$$

One may note that the FOIS of CASPT2 and PC-NEVPT2 are equivalent. Moreover, the FOIS of the other flavour of NEVPT2, Strongy-Contracted N-Electron Valence state second-order Perturbation Theory, is smaller and gives very similar results with CASPT2 and PC-NEVPT2. However, this is outside of the scope of this PhD as these methods were not used actively. The same goes for Quasi Degenerate Perturbation Theories (QDPT).

It is important to state that RS-PT is size-consistent but not variational, it corrects the energy by an external perturbation. This means that one may underestimate the exact energy of a system. Even worse, if one perturber is close in energy with the perturbed state, then the method may diverge. This is due to the fact, as stated some paragraphs above, that the perturbation must be small in comparison with the perturbed system's energy. If such scenario were to occur, one should include this perturber in the reference space. What about a mono-determinantal wavefunction such as HF ? The answer is simple: MP2 will badly treat this system and QDPT or multi-reference methods must be used.

DDCI demonstration

Now that PT was introduced, it is possible to come back to the proposed demonstration for the use of DDCI instead of MRCISD. Considering a double excitation $2h2p$ outside of the CAS, this is equivalent to applying a double excitation operator $\hat{D}_{pq,rs}$ to the CAS determinants Φ_I. Then, splitting the second-order energy correction $E_i^{(2)}$ and focusing on the $2h2p$ perturbers contribution, one can write

$$(2h2p) \qquad E_i^{(2)} = \sum_{\Phi_\beta \in 2h2p} \frac{\langle \Phi_\beta | \hat{V} | \Psi_i \rangle^2}{E_i^{(0)} - E_{\Phi_\beta}^{(0)}} = \sum_{\substack{p>q \in \text{inactive} \\ r>s \in \text{virtuals}}} \sum_{J \in CAS} \frac{\langle \hat{D}_{pq,rs}\Phi_J | \hat{V} | \sum_{I \in CAS} c_I \Phi_I \rangle^2}{E_i^{(0)} - E_{\hat{D}_{pq,rs}\Phi_J}^{(0)}}. \tag{1.66}$$

Two cases are possible:

1) $I \neq J$, then the two determinants differ by more than three spin-orbitals and $\langle \hat{D}_{pq,rs}\Phi_J | \hat{V} | \Phi_I \rangle = 0$.

2) $I = J$, then they differ by exactly two spin-orbitals and $\langle \hat{D}_{pq,rs}\Phi_I|\hat{V}|\Phi_I\rangle = \langle pq||rs\rangle$.

Now if one assumes that $E_i^{(0)} - E^{(0)}_{\hat{D}_{pq,rs}\Phi_J}$ is a quantity independent of $E_i^{(0)}$ as in MP definition of $\hat{H}_0$. In other words, considering that $E_i^{(0)}$ are quasi-degenerate, then the above expression simplifies as

$$E^{(2)}_{2h2p} = \sum_{\substack{p>q\in\text{inactive}\\ r>s\in\text{virtuals}}} \frac{\langle pq||rs\rangle^2}{\epsilon_p + \epsilon_q - \epsilon_r - \epsilon_s}. \tag{1.67}$$

One may observe that coefficients c_I^2 disappeared from equation (1.66) to (1.67). As each $\hat{D}_{pq,rs}$ excitation on the N determinants of the CAS generates N excited determinants, the summation takes the form $\sum_{\substack{p>q\\ r>s}}\sum_{I}^{N} c_I^2 X = \sum_{\substack{p>q\\ r>s}} X$ because $|\Psi_i\rangle$ is normalized and all X terms are equal.

Then, these perturbers shift all the diagonal elements by the same quantity. As a consequence, energy differences between states are the same at the DDCI and MRCISD level, at the MP2 level.[39, 40] Another advantage for this approximation is the fact that the number of determinants from MRCISD to DDCI importantly decreases, which reduces the cost of computation and the size-consistency error.

1.3 Localization

The question of representability of MOs has been discussed in QC since its beginning. Two philosophies arose: localized *vs.* delocalized MOs. A particularly nice Chapter (p.41-101) from Basis Sets in Computational Chemistry [11] presents the different localization methods and their advantages and disadvantages compared to delocalization. I will summarize the points that are important for this PhD work.

Already in 1930s, Localized Molecular Orbitals (LMOs) interested Quantum Chemists as they allowed for a representation of bonds following the Valence-Bond formalism. However it restricts bonds to an electron pair localized between two specific atoms, which fails for many systems, *e.g.* systems with delocalized electrons. Still, as an approximation, it gives representability to undergraduate students studying QC and remains acceptable for small molecules. On the contrary, the success of Molecular Orbital Theory introduced the notion of MOs delocalized over the entire molecule. This introduced Canonical Molecular Orbitals (CMOs) which are MOs optimized after a wavefunction calculation. CMOs are nowadays more popular than LMOs as the difference between the energy of two CMOs gives the frequency of the electronic transition associated to these two orbitals. However having delocalized MOs is a disadvantage when analyzing the wavefunction as one may only extract global information.[3] The building blocks of the electronic wavefunction are MOs.[4] The freedom of using either localized or delocalized MOs comes from the fact that one can apply an unitary transformation on delocalized MOs to obtain LMOs, and vice-versa. This means that any expectation value, in particular the energy, remains untouched, and only the wavefunction structure is changed. The interest of a local representation is twofold. First it is useful to select molecular regions that are physically "interesting", *e.g.* to study chemical reactions, excited states, magnetic systems... In other words, it may allow a reduction of the active space by working only with a selection of LMOs of interest. This opens the way to a second advantage, namely the possible reduction in the size of the reference space, convenient for MRCI calculations. There exist two main concept of localization: *a posteriori* and *a priori*.

[3] Local information may be too complicated to extract.

[4] MOs serve as a building block for determinants, further building the wavefunction.

In *a posteriori* methods, a set of CMOs is previously calculated then transformed by an unitary transformation to obtain LMOs. Two popular *a posteriori* methods are Foster-Boys,[12] where a functional based on the spatial position of MOs is minimized, and Pipek-Mezey,[13] where a functional based on the partial atomic charges is maximized.

A priori methods are based on chemical intuition: a user-defined guess of LMOs is used as a starting point. One may use directly these LMOs (and correct their possible non-orthogonality) as done in Chapter 2, or converge these LMOs onto the reference CMOs of a wavefunction calculation, on the condition to keep the LMOs as local as possible. An *a priori* method of choice used in Chapter 3 is implemented in the suite of programs DoLo.[14] Its specificity is the separation of inactive, active and virtual orbitals into three classes. It is a two-step method. The first step (i) is to determine a guess of LMOs. Starting from non-orthogonal AOs, one first orthogonalizes each class of AOs (inactive, valence, virtuals) to obtain orthogonal AOs. Then linear combinations of orthogonal AOs, guided by the information on bonds and molecular fragments contained in the one-electron density matrix, are made to produce non-orthogonal LMOs. Finally non-orthogonal LMOs are separated into inactive, active and virtual classes, and each class is orthogonalized, with a different order of priority.[5] The second step (ii) is the optimization of the LMOs. This is done by projecting the LMOs onto reference CMOs (after a previous HF or CASSCF calculation). Projected LMOs may lose their orthogonality, so a final orthogonalization is necessary. This procedure can then be repeated to try to increase the projection of the LMOs onto the CMOs.

A posteriori methods are easier to implement, but more difficult to use to identify physically "interesting" regions as they are not based on chemical intuition. On the contrary, this intuition may be a bias for *a priori* methods. There are many other methods of localization. A brief example is the case of the Natural Bond Orbitals method [15] and its extension, the Natural Localized Molecular Orbitals approach,[16] which produces LMOs optimal for a Lewis structure description. It is also possible to make a "hand-made" *a posteriori* localization by doing a linear

[5]Highest priority is given to the inactive LMOs, then to the active ones, and finally to the virtual ones.

combination of chosen CMOs.

Finally it is important to point out that any LMOs strategy breaks the symmetry of the system. Symmetry is indeed a powerful ally in QC to reduce computational costs. Then one needs to choose between using LMOs to clarify the problem (specific molecular region and MOs) with the help of localization or retaining the ease of handling symmetry. It it important to state that LMOs can potentially reduce the size of the reference space, and thus the computational cost. Implementing LMOs is more demanding than using symmetry, however it has many advantages, particularly for qualitative data analysis.

1.4 Spin

1.4.1 Spin operators

Spin is the intrinsic kinetic momentum of quantum bodies. All bodies are described by a total spin quantum number S, whose values are $0, \frac{1}{2}, 1, \frac{3}{2}, \ldots$, and by a quantum number M_S, with $2S+1$ possible values such that $-S, -S+1, \ldots, S-1, S$. For convention, we will use s and m_s for a single body system, and S and M_S for a many-body system. Let us first take the case of a single body system. Its spin angular momentum is defined by the vector operator $\hat{\boldsymbol{s}}$.

$$\hat{\boldsymbol{s}} = \hat{s}_x \boldsymbol{i} + \hat{s}_y \boldsymbol{j} + \hat{s}_z \boldsymbol{k} \tag{1.68}$$

where $\boldsymbol{i}$, $\boldsymbol{j}$ and $\boldsymbol{k}$ are unit vectors along the x, y and z directions. The components $\hat{s}_x$, $\hat{s}_y$ and $\hat{s}_z$ satisfy the commutation relation:

$$[\hat{s}_x, \hat{s}_y] = i\hat{s}_z. \tag{1.69}$$

The square of $\hat{\boldsymbol{s}}$ operator is a scalar operator $\hat{s}^2$.

$$\hat{s}^2 = \hat{s}_x^2 + \hat{s}_y^2 + \hat{s}_z^2 \tag{1.70}$$

$\hat{s}^2$, $\hat{s}_x$, $\hat{s}_y$ and $\hat{s}_z$ are not a Complete Set of Commuting Observables, because only one projection of $\hat{\boldsymbol{s}}$ commute with $\hat{s}^2$. Considering the z axis as the main spin axis, $\hat{s}_z$ and $\hat{s}^2$ constitute a Complete Set of Commuting Observables, *i.e.* they are diagonalizable simultaneously in the same spin space ($[\hat{s}^2, \hat{s}_z] = 0$).[6] Thus the set of spin states $|s, m_s\rangle$ describing a single body are generally taken to be eigenfunctions of $\{\hat{s}^2, \hat{s}_z\}$ such as

$$\hat{s}^2|s, m_s\rangle = s(s+1)|s, m_s\rangle \tag{1.71}$$

$$\hat{s}_z|s, m_s\rangle = m_s|s, m_s\rangle. \tag{1.72}$$

This work concerns only electrons. An electron has a spin $s = 1/2$ and two possible quantum states $m_s = \pm 1/2$.

$$\{|s, m_s\rangle\} = \{|\frac{1}{2}, \frac{1}{2}\rangle; |\frac{1}{2}, -\frac{1}{2}\rangle\} \tag{1.73}$$

[6] It is possible to consider the x axis, thus all the following equations must be permuted in a circular fashion. This is rarely the case and the z axis is always preferred.

These spin states are eigenfunctions of $\{\hat{s}^2, \hat{s}_z\}$ but not of $\{\hat{s}_x, \hat{s}_y\}$. There is no need for a demonstration as one can find a clear one in p.98 of Modern Quantum Chemistry.[33] Instead of working with $\hat{s}_x$ and $\hat{s}_y$, it is more convenient to introduce the spin ladder operators $\hat{s}_+$ and $\hat{s}_-$:[7]

$$\hat{s}_+ = \hat{s}_x + i\hat{s}_y \tag{1.74}$$

$$\hat{s}_- = \hat{s}_x - i\hat{s}_y \tag{1.75}$$

such that

$$\begin{aligned}
\hat{s}_+|s, m_s\rangle &= \sqrt{s(s+1) - m_s(m_s+1)}|s, m_s+1\rangle \qquad \text{if} \quad m_s < s \\
&= 0 \qquad\qquad\qquad\qquad\qquad\qquad\qquad\qquad\quad \text{if} \quad m_s = s \\
\hat{s}_-|s, m_s\rangle &= \sqrt{s(s+1) - m_s(m_s-1)}|s, m_s-1\rangle \qquad \text{if} \quad m_s > -s \\
&= 0 \qquad\qquad\qquad\qquad\qquad\qquad\qquad\qquad\quad \text{if} \quad m_s = s.
\end{aligned}$$

Interestingly, $\hat{s}_+$ and $\hat{s}_-$ commute and are Hermitian conjugates: $\hat{s}_+ = \hat{s}_-^\dagger$. One may then rewrite expression (1.70) as

$$\hat{s}^2 = \hat{s}_-\hat{s}_+ + \hat{s}_z + \hat{s}_z^2. \tag{1.76}$$

Moving on to a N-electron wavefunction, the total spin angular momentum $\boldsymbol{S}$ is the vector sum of the spin vectors of each electron.

$$\boldsymbol{S} = \sum_i^N \boldsymbol{s}(i) \tag{1.77}$$

Then $\hat{S}_z$, $\hat{S}^2$ and $\hat{S}_\pm$ are easily derived.

$$\hat{S}_I = \sum_i^N \hat{s}_I(i) \qquad I = x, y, z \tag{1.78}$$

$$\hat{S}_\pm = \sum_i^N \hat{s}_\pm(i) \tag{1.79}$$

$$\hat{S}^2 = \hat{S}_-\hat{S}_+ + \hat{S}_z + \hat{S}_z^2 \tag{1.80}$$

As the electronic Hamiltonian $\hat{H}$ we are working with does not contain any spin coordinates, it commutes with $\hat{S}^2$ and $\hat{S}_z$. Thus the eigenfunctions Ψ of $\hat{H}$ are

[7] $\hat{s}_+$ and $\hat{s}_-$ are often named "step up" and "step down" operators.

eigenfunctions of $\{\hat{S}^2, \hat{S}_z\}$.

$$\hat{S}^2|\Psi\rangle = S(S+1)|\Psi\rangle \tag{1.81}$$

$$\hat{S}_z|\Psi\rangle = M_S|\Psi\rangle \tag{1.82}$$

These operators may be manipulated as presented in first quantization but their numerical implementation is eased using second quantization, as presented in Appendix A.

1.4.2 Spin coupling

Some of the following equations can be found at p.367 of Molecular Magnetism [47] but are needed for the spin coupling schemes presented later in this work.

Let us consider two local spins S_A and S_B having, respectively, a set of local spin states $\{|S_A, M_A\rangle\}$ and $\{|S_B, M_B\rangle\}$ (for clarity, M_A and M_B stand for M_{S_A} and M_{S_B}). Coupling these two spin states as a total S spin state,[8] different S values are generated following the expression below:

$$|S_A - S_B| \leq S \leq S_A + S_B. \tag{1.83}$$

The generated spin states are expressed in a set of paired spin states $\{|S_A, S_B, S, M_S\rangle\}$, which are linear combinations of the direct product of the set of local spin states $|S_A, M_A\rangle \otimes |S_B, M_B\rangle$.

$$|S_A, S_B, S, M\rangle = \sum_{M_A, M_B} |S_A, M_A\rangle \otimes |S_B, M_B\rangle C_{C-G} \tag{1.84}$$

The coefficients C_{C-G} of the linear combination are so-called Clebsch-Gordan (C-G) coefficients and are expressed as

$$C_{C-G} = \tag{1.85}$$
$$\delta(M_S, M_A + M_B)\sqrt{\frac{(S_A + S_B - S)!(S + S_A - S_B)!(S - S_A + S_B)!(2S+1)}{(S + S_A + S_B + 1)!}} \times$$
$$\sqrt{(S_A + M_A)!(S_A - M_A)!(S_B + M_B)!(S_B - M_B)!(S + M_S)!(S - M_S)!} \times$$
$$\sum_k \frac{(-1)^k}{k!(S_A + S_B - S - k)!(S_A - M_A - k)!(S_B + M_B - k)!(S - S_B + M_A + k)!(S - S_A - M_B + k)!}$$

[8] We may sometimes call the total spin S as S_{total} for further readability.

where $\delta(M_S, M_A + M_B)$ is the Kronecker symbol.

C-G formula is not trivial as it implies a triple sum, over M_A, M_B and k. For M_A and M_B the values are well-defined and vary by an integer value from, respectively, $-S_A$ to S_A and $-S_B$ to S_B. Having programmed the C-G formula in Python out of curiosity, I can say that the summation over k is not easy. It is extended over all integer k for which every factorial is nonnegative. However, once evaluated, the C-G coefficients remain the same for a given S_A, S_B, S and M_S. The results of some specific cases used in this work are given in Appendix B. I personally find much beauty in this heavy but general formula, as it develops what the community often takes for granted.

A simple example is the case of coupling two spins $S_A = S_B = 1/2$, *i.e.* a copper(II) dimer. Considering no Charge Transfers, chemists will expect one singlet state and one triplet state. The generated wavefunctions will read $|S_A, S_B, S, M\rangle$, where one can see the analytical values of the C-G coefficients:

$$
\begin{aligned}
|S_A, S_B, 1, +1\rangle &= 1|S_A, +1/2\rangle \otimes |S_B, +1/2\rangle \\
|S_A, S_B, 1, 0\rangle &= \sqrt{1/2}|S_A, +1/2\rangle \otimes |S_B, -1/2\rangle + \sqrt{1/2}|S_A, +1/2\rangle \otimes |S_B, -1/2\rangle \\
|S_A, S_B, 1, -1\rangle &= 1|S_A, -1/2\rangle \otimes |S_B, -1/2\rangle
\end{aligned}
$$

$$
|S_A, S_B, 0, 0\rangle = \sqrt{1/2}|S_A, +1/2\rangle \otimes |S_B, -1/2\rangle - \sqrt{1/2}|S_A, +1/2\rangle \otimes |S_B, -1/2\rangle
$$

1.5 Models

1.5.1 Model Hamiltonians and effective Hamiltonians

Understanding complex physical properties of molecules, such as molecular magnetism, spin or aromaticity, using the exact Hamiltonian is particularly tedious. Instead, one may simplify the problem by developing a model Hamiltonian or an effective Hamiltonian.

Here, I would like to summarize the major idea behind models as: "Why bother studying the full system when only some of its properties are of interest ?". In fact, considering all possible interactions in a system may be detrimental as it may overshadow the relevant information under non relevant information. Sweeping away unnecessary elements allows to identify a minimum number of physically sensitive parameters but also to reduce the cost of evaluation down to analytical or low cost numerical resolution. The ability to identify the sensitive parameters of a system opens the way to new molecular design and more critical analysis of phenomena. A model is then a simplification, physical or not, of a full problem which allows to focus solely on some of its properties. It is a toy for scientists to play with, through the use of a model Hamiltonian.

A model Hamiltonian is defined upon a subspace of the exact space, a "model space", where different parameters are chosen to incorporate the physics of the problem. By tuning them, one can explore physics in a simpler way and may identify sensitive parameters. Model Hamiltonians are needed by both the experimental and the theoretical communities. On one hand, experimentalists measure the exact properties of the full system then treat their data assuming a given model Hamiltonian, allowing to extract physically relevant parameters. On the other hand, theoretical calculations being costly, one may develop a model Hamiltonian upon a chemical model in order to have a neater understanding of the mechanisms in play. These Hamiltonians are often proposed following chemical/physical intuitions. However they must reproduce as accurately as possible the energy solutions of a "target space" of the exact Hamiltonian (see Figure 1.2). The targeted energies and wavefunctions are often the ones of low-energy solutions. It is then important for theoretical chemistry

to provide evidence of the validity (or invalidity) of these models. The validity of a model Hamiltonian depends on the type of approximation regarding the studied phenomena: a non-physical approximation often results in a wrong model. When a model is correct, its parameters can be extracted from first principle calculations. When a model is not valid, meaning it does not reproduce the desired physical properties of the system, then theoretical chemists may use different tools to correct and deduce a more accurate model Hamiltonian. One of these tools are so-called effective Hamiltonians. Briefly, an effective Hamiltonian is a contraction of the exact Hamiltonian in a particular model space where all the physics of the problem are taken into account in an effective way. Like model Hamiltonians, effective Hamiltonians are much simpler that the exact Hamiltonian and aim at reproducing targeted solutions. However they use *ab initio* parameters, transformed in the model space to map effectively the rest of the system. In this sense, effective Hamiltonian theories developed by Bloch (non-hermitian version)[48] and des Cloizeaux (hermitian version)[49] showed that the eigenvalues and eigenvectors of an effective Hamiltonian are, respectively, the eigenvalues of the exact Hamiltonian and the projected eigenvectors of the exact Hamiltonian:

$$\hat{H}_{eff}(\hat{P}\Psi_{exact}) = E_{exact}(\hat{P}\Psi_{exact}) \tag{1.86}$$

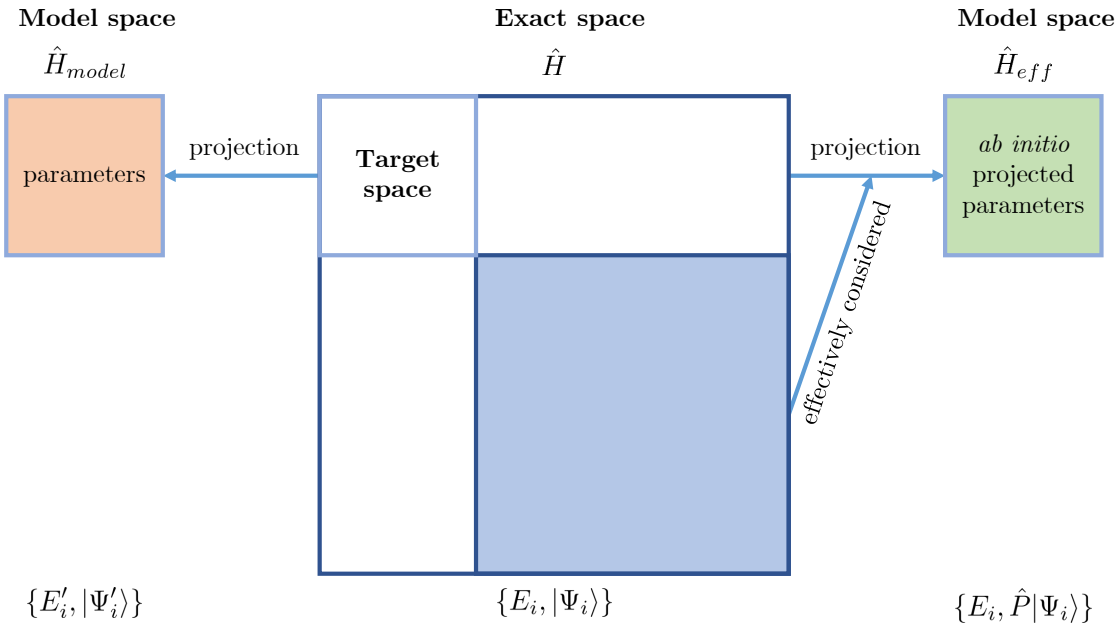

Figure 1.2: Schematic comparison of exact, model and effective Hamiltonians. Adapted from Ref [20].

The main difference between exact, model and effective Hamiltonians are on the type of approximation. Model and effective Hamiltonians are a simplification of the exact Hamiltonian, and aim at reproducing some of its eigenvalues and eigenvectors. On one hand, a model Hamiltonian works in a subpart of the exact space and neglects some interactions on the basis of satisfactory approximations. It uses tunable parameters, physical or not. On the other hand, an effective Hamiltonian also works in a subpart of the exact space but effectively maps all the exterior contributions and effects, *i.e.* not neglecting any interaction. It uses *ab initio* parameters.

There exist numerous model Hamiltonians, *e.g.* Hückel, Hubbard or Heisenberg-Dirac-Van Vleck (HDVV) models.[9] This work presents two model Hamiltonians developed in more details in their respective Chapters (2 and 3). The HDVV Hamiltonian is intensively used in Chapter 3. For this reason, let us present it briefly.

1.5.2 Heisenberg-Dirac-Van Vleck Hamiltonian

The Heisenberg-Dirac-Van Vleck Hamiltonian is a model Hamiltonian formulated by Heisenberg [17] and improved by Dirac [18] and Van Vleck.[19] Originally developed to better understand ferromagnetism, it quickly became useful to treat a lot of ferromagnets and antiferromagnets. It can be derived from an effective Hamiltonian of the exact Hamiltonian and/or from a Generalized Hubbard model followed by RS-PT2.[20, 21] The general form[10] of the HDVV Hamiltonian is

$$\hat{H}_{HDVV} = -\sum_{i>j} 2J_{ij}\hat{\boldsymbol{S}}_{\boldsymbol{i}}\hat{\boldsymbol{S}}_{\boldsymbol{j}} \tag{1.87}$$

with i and j spin active sites ($s_i > 0$ and $s_j > 0$). As $\hat{\boldsymbol{S}}_{\boldsymbol{i}}$ and $\hat{\boldsymbol{S}}_{\boldsymbol{j}}$ are vector operators, it is possible to rewrite the scalar product $\hat{\boldsymbol{S}}_{\boldsymbol{i}}\hat{\boldsymbol{S}}_{\boldsymbol{j}}$ into a more convenient form:

$$\hat{\boldsymbol{S}}_{\boldsymbol{i}}\hat{\boldsymbol{S}}_{\boldsymbol{j}} = \hat{S}_{iz}\hat{S}_{jz} + \frac{1}{2}(\hat{S}_{i+}\hat{S}_{j-} + \hat{S}_{i-}\hat{S}_{j+}). \tag{1.88}$$

[9] More information on model and effective Hamiltonians, out of the scope of this thesis, can be found in the Refs [20, 50].

[10] The literature may add a supplementary $-\frac{n_i n_j}{4}\hat{I}$ term to set the energy of the highest spin multiplicity state to zero. n_i and n_j are the number of unpaired electrons on sites i and j, and $\hat{I}$ is the identity operator.

The literature uses a coefficient $-2J$, $-1J$, $+1J$ or $+2J$, which is just a matter of appreciation. Regarding this PhD work, the coefficient $-2J$ was always considered, for convenience. The term J_{ij} is the magnetic coupling between centers i and j. It incorporates all the discarded physics of the system, such as electron-electron interaction, electron-nuclei interaction and the spatial structure of the system. It is important to comment that it is valid when the studied system is mainly made of neutral configuration (in the sense of limited charge transfer, *i.e.* a small ratio of the hopping integral divided by the coulomb repulsion integral). Experimental deviations from the HDVV Hamiltonian are sometimes reported in the literature. Corrections of the HDVV Hamiltonian by adding a biquadratic term $\sum_{i>j} +2j_{ij}(\hat{\boldsymbol{S}}_{\boldsymbol{i}}\hat{\boldsymbol{S}}_{\boldsymbol{j}})^2$ to the former [22, 23] allowed to identify and take into account the role of non-Hund forms in this deviation.[24] Yet, in systems where direct exchange contribution can be considered as negligible, HDVV Hamiltonian allows to properly represent the physics of the system. A strength of HDVV is that it only works with spin degrees of freedom, as the spatial part dependency is injected in the exchange constant values J_{ij}. This allows one to extract the physical value of the coupling term from *ab initio* calculations or experimental measurements.

Taking as an example a two site A and B system of respective spins S_A and S_B, one can derive the following terms from the equations presented in section (1.4).

$$\hat{\boldsymbol{S}} = \hat{\boldsymbol{S}}_{\boldsymbol{A}} + \hat{\boldsymbol{S}}_{\boldsymbol{B}} \tag{1.89}$$

$$\hat{S}^2 = \hat{S}_A^2 + \hat{S}_B^2 + 2\hat{\boldsymbol{S}}_{\boldsymbol{A}}\hat{\boldsymbol{S}}_{\boldsymbol{B}} \tag{1.90}$$

Then, the HDVV Hamiltonian for this system $\hat{H}_{HDVV} = -2J\hat{\boldsymbol{S}}_{\boldsymbol{A}}\hat{\boldsymbol{S}}_{\boldsymbol{B}}$ may be rewritten as

$$\hat{H}_{HDVV} = -J(\hat{S}^2 - \hat{S}_A^2 - \hat{S}_B^2) \tag{1.91}$$

whose eigenvalues are

$$E(S, S_A, S_B) = -J[S(S+1) - S_A(S_A+1) - S_B(S_B+1)]. \tag{1.92}$$

As all states generated by coupling S_A and S_B only differ by their total spin S, then it is possible to change the origin of the system to have:

$$E(S) = -JS(S+1) \tag{1.93}$$

Finally one sees that depending on the sign of J, either the highest ($J > 0$) or the lowest ($J < 0$) spin state will be the ground state. Following our decision of using a constant of $-2J$, a positive J represents a ferromagnetic coupling whereas a negative J represents an antiferromagnetic coupling.

Appendix A. Clebsch-Gordan coefficients

For the sake of clarity, the labels S_A and S_B have been omitted, and the product $|S_A, M_A\rangle \times |S_B, M_B\rangle$ hs been shortened to $|M_A, M_B\rangle$ such that $|S, M\rangle = \sum_{M_A,M_B} C_{C-G}|M_A, M_B\rangle$. We will present five cases specific to this work but more can be found in C-G tables or at p.368-373 of Molecular Magnetism.[47]

$S_A = 1/2$ and $S_B = 1/2$:

$$
\begin{aligned}
|1,+1\rangle &= |+1/2,+1/2\rangle \\
|1,0\rangle &= \sqrt{1/2}|+1/2,-1/2\rangle + \sqrt{1/2}|-1/2,+1/2\rangle \\
|1,-1\rangle &= |-1/2,-1/2\rangle
\end{aligned}
$$

$$
|0,0\rangle = \sqrt{1/2}|+1/2,-1/2\rangle - \sqrt{1/2}|-1/2,+1/2\rangle
$$

$S_A = 1/2$ and $S_B = 1$:

$$
\begin{aligned}
|3/2,+3/2\rangle &= |+1/2,+1\rangle \\
|3/2,+1/2\rangle &= \sqrt{1/3}|-1/2,+1\rangle + \sqrt{2/3}|+1/2,0\rangle \\
|3/2,-1/2\rangle &= \sqrt{2/3}|-1/2,0\rangle + \sqrt{1/3}|-1/2,-1\rangle \\
|3/2,-3/2\rangle &= |-1/2,-1\rangle
\end{aligned}
$$

$$
\begin{aligned}
|1/2,+1/2\rangle &= \sqrt{2/3}|-1/2,+1\rangle - \sqrt{1/3}|+1/2,0\rangle \\
|1/2,-1/2\rangle &= \sqrt{1/3}|-1/2,0\rangle - \sqrt{2/3}|+1/2,-1\rangle
\end{aligned}
$$

$S_A = 1$ and $S_B = 1$:

$$
\begin{aligned}
|2,+2\rangle &= |+1,+1\rangle \\
|2,+1\rangle &= \sqrt{1/2}|+1,0\rangle + \sqrt{1/2}|0,+1\rangle \\
|2,0\rangle &= \sqrt{1/6}|+1,-1\rangle + \sqrt{2/3}|0,0\rangle + \sqrt{1/6}|-1,+1\rangle \\
|2,-1\rangle &= \sqrt{1/2}|0,-1\rangle - \sqrt{1/2}|-1,0\rangle \\
|2,-2\rangle &= |-1,-1\rangle
\end{aligned}
$$

$$
\begin{aligned}
|1,+1\rangle &= \sqrt{1/2}|+1,0\rangle - \sqrt{1/2}|0,+1\rangle \\
|1,0\rangle &= \sqrt{1/2}|+1,-1\rangle - \sqrt{1/2}|-1,+1\rangle \\
|1,-1\rangle &= \sqrt{1/2}|0,-1\rangle - \sqrt{1/2}|-1,0\rangle
\end{aligned}
$$

$$
|0,0\rangle = \sqrt{1/3}|+1,-1\rangle - \sqrt{1/3}|0,0\rangle + \sqrt{1/3}|-1,+1\rangle
$$

$\underline{S_A = 3/2 \text{ and } S_B = 1}$:

$$
\begin{aligned}
|5/2,+5/2\rangle &= |+3/2,+1\rangle \\
|5/2,+3/2\rangle &= \sqrt{2/5}|+3/2,0\rangle + \sqrt{3/5}|+1/2,+1\rangle \\
|5/2,+1/2\rangle &= \sqrt{1/10}|+3/2,-1\rangle + \sqrt{3/5}|+1/2,0\rangle + \sqrt{3/10}|-1/2,+1\rangle \\
|5/2,-1/2\rangle &= \sqrt{3/10}|+1/2,-1\rangle + \sqrt{3/5}|-1/2,0\rangle + \sqrt{1/10}|-3/2,+1\rangle \\
|5/2,-3/2\rangle &= \sqrt{3/5}|-1/2,-1\rangle + \sqrt{2/5}|-3/2,0\rangle \\
|5/2,-5/2\rangle &= |-3/2,-1\rangle
\end{aligned}
$$

$$
\begin{aligned}
|3/2,+3/2\rangle &= \sqrt{3/5}|+3/2,0\rangle - \sqrt{2/5}|+1/2,+1\rangle \\
|3/2,+1/2\rangle &= \sqrt{2/5}|+3/2,-1\rangle + \sqrt{1/15}|+1/2,0\rangle - \sqrt{8/15}|-1/2,+1\rangle \\
|3/2,-1/2\rangle &= \sqrt{8/15}|+1/2,-1\rangle - \sqrt{1/15}|-1/2,0\rangle - \sqrt{2/5}|-3/2,+1\rangle \\
|3/2,-3/2\rangle &= \sqrt{2/5}|-1/2,-1\rangle - \sqrt{3/5}|-3/2,0\rangle
\end{aligned}
$$

$$
\begin{aligned}
|1/2,+1/2\rangle &= \sqrt{1/2}|+3/2,-1\rangle - \sqrt{1/3}|+1/2,0\rangle + \sqrt{1/6}|-1/2,+1\rangle \\
|1/2,+1/2\rangle &= \sqrt{1/6}|+1/2,-1\rangle - \sqrt{1/3}|-1/2,0\rangle + \sqrt{1/2}|-3/2,+1\rangle
\end{aligned}
$$

$\underline{S_A = 2 \text{ and } S_B = 1}$:

$$
\begin{aligned}
|3,+3\rangle &= |+2,+1\rangle \\
|3,+2\rangle &= \sqrt{1/3}|+2,0\rangle + \sqrt{2/3}|+1,+1\rangle \\
|3,+1\rangle &= \sqrt{1/15}|+2,-1\rangle + \sqrt{8/15}|+1,0\rangle + \sqrt{6/15}|0,+1\rangle \\
|3,0\rangle &= \sqrt{1/5}|+1,-1\rangle + \sqrt{3/5}|0,0\rangle + \sqrt{1/5}|-1,+1\rangle \\
|3,-1\rangle &= \sqrt{6/15}|0,-1\rangle + \sqrt{8/15}|-1,0\rangle + \sqrt{1/15}|-2,+1\rangle \\
|3,-2\rangle &= \sqrt{2/3}|-1,-1\rangle + \sqrt{1/3}|-2,0\rangle \\
|3,-3\rangle &= |-2,-1\rangle
\end{aligned}
$$

$$
\begin{aligned}
|2,+2\rangle &= \sqrt{2/3}|+2,0\rangle - \sqrt{1/3}|+1,+1\rangle \\
|2,+1\rangle &= \sqrt{1/3}|+2,-1\rangle + \sqrt{1/6}|+1,0\rangle - \sqrt{1/2}|0,+1\rangle \\
|2,0\rangle &= \sqrt{1/2}|+1,-1\rangle - \sqrt{1/2}|-1,+1\rangle \\
|2,-1\rangle &= \sqrt{1/2}|0,-1\rangle - \sqrt{1/6}|-1,0\rangle - \sqrt{1/3}|-2,+1\rangle \\
|2,-2\rangle &= \sqrt{1/3}|-1,-1\rangle - \sqrt{2/3}|-2,0\rangle
\end{aligned}
$$

$$
\begin{aligned}
|1,+1\rangle &= \sqrt{3/5}|+2,-1\rangle - \sqrt{3/10}|+1,0\rangle + \sqrt{1/10}|0,+1\rangle \\
|1,0\rangle &= \sqrt{3/10}|+1,-1\rangle - \sqrt{2/5}|0,0\rangle + \sqrt{3/10}|-1,+1\rangle \\
|1,-1\rangle &= \sqrt{1/10}|0,-1\rangle - \sqrt{3/10}|-1,0\rangle + \sqrt{3/5}|-2,+1\rangle
\end{aligned}
$$

Appendix B. Spin operators in second quantization

Second quantization will not be presented because it is textbook knowledge (see the book Molecular Electronic Structure Theory [51, 52]) and because it was only used numerically in this work.

In order to build $\hat{S}^2$ and $\hat{S}_z$ operators, one needs two working equations:

$$\hat{S}_z = \frac{1}{2}\sum_p (\hat{a}^\dagger_{p,\alpha}\hat{a}_{p,\alpha} - \hat{a}^\dagger_{p,\beta}\hat{a}_{p,\beta}) \tag{1.94}$$

$$\hat{S}_+ = \sum_p (\hat{a}^\dagger_{p,\alpha}\hat{a}_{p,\beta}) \tag{1.95}$$

with $\hat{a}^\dagger_p$ creation and $\hat{a}_p$ annihilation operators of an electron in the spin-orbital p. As one can prove that $\hat{S}_- = \hat{S}^\dagger_+$, then, from equation (1.80), one can define $\hat{S}^2$ as

$$\hat{S}^2 = \hat{S}_-\hat{S}_+ + \hat{S}_z(\hat{S}_z + 1). \tag{1.96}$$

Chapter 2

Environmental influence on the Singlet Fission phenomenon

This Chapter tackles the notion of environment using an organic dimer where one molecule is denoted active, while the other is the "environment". It is composed of two parts. It begins with an introduction on the Singlet Fission (SF) phenomenon, its mechanisms and how the environment is considered by the SF community. Then follows a model study on the effects of a neighbour on the thermodynamic condition of SF. The model is based on a H_2 dimer where one hydrogen molecule represents a frozen environment felt by the other molecule, representing an active class I chromophore. The environment molecule is frozen in a given electronic configuration state function of either spin singlet or triplet, which means that charge transfers are not permitted. The influence of different environments on the spectroscopy of the active moiety is studied and different energy matching values $\rho = [E(S_{A,1}) - E(S_{A,0})]/[E(T_{A,1}) - E(S_{A,0})]$ are obtained, depending on the type of environment (open/closed-shell and triplet/singlet). The field generated by a singlet environment improves the ratio ρ up to 6% compared to a free chromophore. This ratio is further improved when the environment is triplet, improving the former by 10%. This indicates that the usual "single chromophore" computational screening for SF candidates may leave out some compounds of interest. Finally, this Chapter is concluded and further personal criticism of the study is discussed.

keywords: singlet fission, class I chromophore, model Hamiltonian, energy spectrum

Part of the content of this Chapter has been published in Ref [53].

2.1 Singlet Fission

Humanity has a need to move away from fossil energies to renewable ones. Nature provides us with various sources of renewable energy such as biomass, hydraulic energy, geothermal energy, wind energy and, finally, solar energy. Over the years, we have seen an awareness raising of the population with regard to renewable energies, and efforts have been put towards them. The source of energy that inspired this Chapter is solar energy. Light has always questioned humans. We see, breathe, and eat thanks to light as it is needed in plant's photosynthesis, which then generates food and oxygen for the livings. It is a wonderful source of energy which we are mainly getting from the Sun. We have been using solar power since ancient times, *i.e.* for drying. However, it is only since the 19th century, when we started using electricity and discovered the photo-electric effect, that solar power appeared as an interesting resource. This gave birth to the field of Photovoltaics ("phos", light and "volt"), which goal is to convert solar power into electricity. The first practical solar cell by Bell Labs in 1954 opened the way for its further developments. The first solar panel used silicon. By producing an exciton (electron-hole pair) upon light absorption, semi-conductors were presented as the base material for solar cells. This is why they still represent 90% of the total world production. However, the recent years have seen different propositions arise with the development of material chemistry and more specifically thin-film technologies. It allowed scientists to come up with novel solar cells such as Multi-Junction solar cells, Perovskites cells, Dye-Sensitized Solar Cells, and Organic PhotoVoltaic cells. By their easy tuning of properties and lower cost, chromophores from Organic Chemistry are candidates of choice for future photovoltaic applications. In parallel, many photo-physical processes have been studied to go beyond the Shockley-Queisser limit, which states that the maximum solar conversion efficiency for a single junction solar cell is 33%.[54] This section will present one of these processes: Singlet Fission.

2.1.1 Introduction

Singlet Fission (SF) is an unique photo-physical process which requires two or more entities, separated or covalently bonded. This phenomenon can be seen as the

conversion of one overall singlet excited state (S^*) into two triplet excited states (T).

$$S^* \longrightarrow T + T \tag{2.1}$$

Considering two identical chromophores A and B both in singlet ground states, $S_{A,0}$ and $S_{B,0}$, the singlet excited state S^* corresponds to the absorption of one photon by a chromophore, promoting it into an excited state (*i.e.* $S_{A,1}$). Usually, one will consider two possible pathways to occur:

1) relaxation to $S_{A,0}$ by either photon-emission (fluorescence) or Internal Conversion (IC).

2) Inter-System Crossing (ISC) to $T_{A,1}$ a triplet state.

However, there is another one. From the general theory of kinetic moments couplings,[47] a system consisting of two local triplet states can give rise to a singlet, a triplet and a quintet overall state. Instead of assuming both chromophores independents, let us consider them coupled. Considering that each chromophore has one local singlet ground state (respectively $S_{A,0}$ or $S_{B,0}$), one local singlet excited state (respectively $S_{A,1}$ or $S_{B,1}$), and one local triplet excited state (respectively $T_{A,1}$ or $T_{B,1}$), 11 total states arise, as can be seen in the Figure 2.1 below.

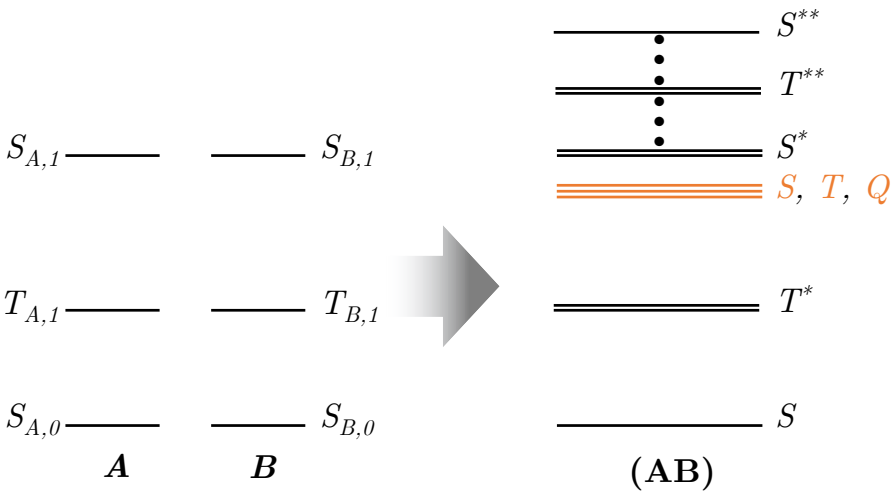

Figure 2.1: (left) From (local) uncoupled states picture to (total) coupled states pictures (right).

The four total states resulting from the coupling of a local singlet state with a local singlet, and the four total states resulting from the coupling a local singlet state with a local triplet state, are readily predicted. However, the coupling of two local triplet

states deserve particular care. Thus, we would like to focus on the appearance of the three nearly degenerated states S, T, Q, and in particular the singlet state S. This state can be rewritten as $^1(TT)$, and is an overall singlet state made of two local triplets. This is the other pathway, which is part of the total SF process: a spin-allowed relaxation from S^* to $^1(TT)$. Then, one may separate this singlet state into its two triplet components, usually spatially.

$$S \xrightarrow{h\nu} S^* \longrightarrow {}^1(TT) \longrightarrow {}^1(T \cdots T) \longrightarrow T + T. \tag{2.2}$$

SF is a spin-allowed process as the total spin never changes, and can be seen as an internal conversion process, *i.e.* a radiationless transition. This makes it very fast, roughly in the picosecond time scale.[55, 56, 57]

2.1.2 Brief history

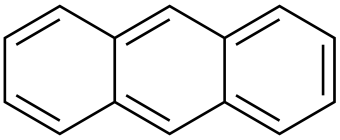

Figure 2.2: Anthracene.

SF dates back to 1965, where it was introduced to explain experimental photophysical data in anthracene crystals.[58] During nearly 40 years, it was observed in few molecular complexes but the community had minimum enthusiasm in its regard, due to the lack of applications. It is in 2006 that a paper awoke the global interest for SF.[59] In this paper, Hanna and Nozik suggested that the conversion of excited singlets into pairs of correlated triplets by SF could drastically improve the efficiency of solar cells. This quantitative analysis showed that the well-known Shockley-Queisser 33% limit [54] of an ideal single junction photovoltaic cell would increase to close to 44% in a SF-based solar cell. This paper attracted the community's interest in SF, but it was really after the first review on SF [60] that the spark was lit. Over the last thirteen years, more than 1500 articles and 90 reviews have been published regarding SF (see Figure 2.3). It is an emerging field with a constant growth of interest for many fundamental and applied research groups.[61, 62, 63, 64, 65, 66]

Besides solar cells, SF has also been considered and applied to organic light-emitting

diodes,[67] organic photo-detectors,[68] and many other applications, such as quantum computing.[69]

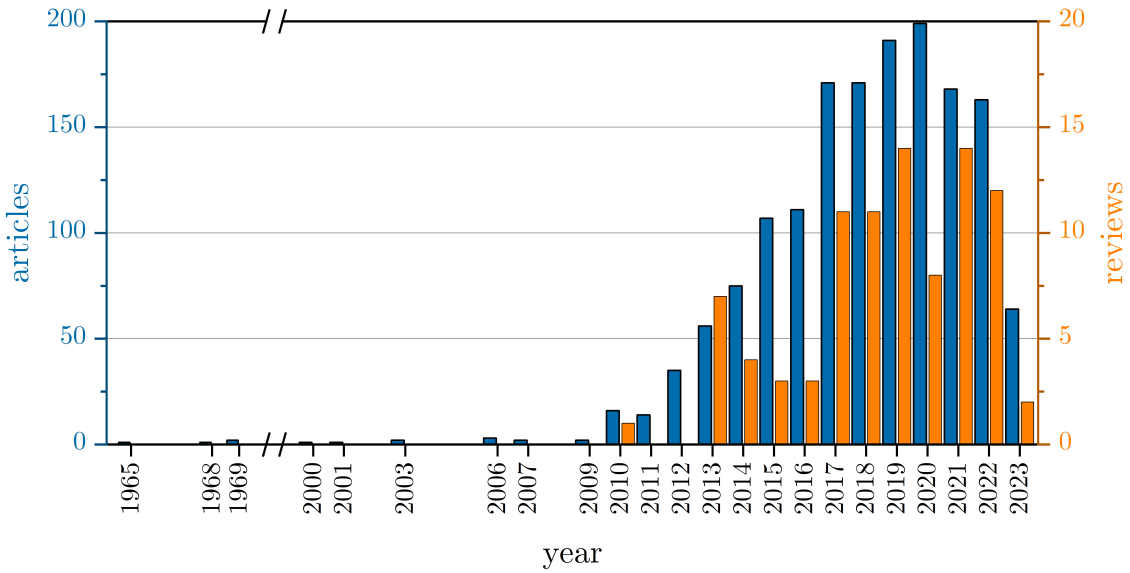

Figure 2.3: Number of articles and reviews published on SF. Source: Clarivate *Web of Science*.

2.1.3 Mechanisms

SF differs from competing Inter-System Crossing (ISC) and Multiple Exciton Generation in inorganic semiconductors, where conversion into vibrational energy occurs. Its mechanism is not yet fully understood and three main propositions have enlivened the community: 1) direct internal conversion as described in subsection (2.1.1). 2) mediation by virtual Charge Transfer (CT) states. 3) sequential two one-electron transfers, having CT states as intermediates. However, this PhD work was not on the SF mechanisms but on its particularities. One can find all the proper details of these propositions in the three excellent reviews of Michl (2010, 2013)[60, 61] and Casanova (2018).[63] For this reason, let us briefly extract some key concepts. Alternant acene-like hydrocarbons are natural target systems; for the excited singlet–triplet, splitting is sizable and connected to a large exchange integral (*ca.* 1 eV) involving the highest occupied molecular orbital (HOMO) and the lowest unoccupied molecular orbital (LUMO), so-called frontier orbitals (see Figure 2.4).[70, 71, 72] SF chromophores may be separated in three classes:

- **Class I**. The first excited state S_1 is mainly a result of a HOMO $\rightarrow$ LUMO transition. Its second excited state S_2 is significantly higher in energy. The transition $S_0 \rightarrow S_1$ allows then to form S^* (*e.g.* anthracene, tetracene, perylene).

- **Class II**. The second or third excited state S_2 or S_3 is mainly a HOMO $\rightarrow$ LUMO transition. The first excited state S_1 is then reached by a fast IC. It can be seen as a linear combination of HOMO $-1 \rightarrow$ LUMO and HOMO $\rightarrow$ LUMO $+1$ (*e.g.* benzene, napthalene, pyrene).

- **Class III**. The second or third excited state S_2 or S_3 is mainly a HOMO $\rightarrow$ LUMO transition. The first excited state S_1 is then reached by a fast IC. It can be seen as a doubly excited state HOMO, HOMO $\rightarrow$ LUMO, LUMO (*e.g.* polyenes and linearly conjugated polymers).

Following the three-class classification of organic chromophores, many theoretical efforts have been dedicated to the positioning of the relevant energy levels (first excited singlet S_1 and triplet T_1 states of a single chromophore), thus to foresee the chemical conditions to stabilize the first excited singlet state S_1. Since the $T_1 - S_1$ energy difference is almost insensitive to the acene size, the so-called "energy matching" or "thermodynamic" condition of the SF $E(S_1) - E(S_0) \geq 2[E(T_1) - E(S_0)]$ is attainable by a reduction of the $S_1 - S_0$ energy gap. However, this condition is an approximation to the more physical thermodynamic condition $E(S^*) \geq E(^1(TT))$, where S^* and $^1(TT)$ are the excited states of the pair of chromophores. While the approximated condition is easier to evaluate as it considers a single chromophore instead of a two or more chromophoric system, the importance of considering the $^1(TT)$ state has been debated in an excellent but critical review.[73]

It is important to state the many deactivation channels that may prevent SF. First, the reverse process may occur, so-called Triplet-Triplet Annihilation, where $^1(TT)$ produces one singlet excited state $S_{A,1}$ and one singlet ground state $S_{B,0}$ (or $S_{B,1}$ and $S_{A,0}$). ISC may do a direct $S^* \rightarrow T_{i,1}$ transition due to an important Spin-Orbit Coupling (SOC). For this reason, organic molecules with their low SOC are good

candidates. Next, Conical Intersections which induce a fast IC from S^* to S can cause trouble. This calls for non-flexible molecules. These conditions are fulfilled by alternant acene-like hydrocarbons.

More recently, biradicaloids molecules have seen an increase in interest [74, 75, 76] thanks to their propensity to fulfill the SF thermodynamic condition. Dimers built on covalently linked monomers have also intrigued the community as they allow to have a direct control on the monomers geometry, and a tuning on inter- and intra-molecular SF.[77, 78, 79, 80]

2.1.4 Environment

In the meantime, the kinetics of the spin-allowed transition was depicted based on electron transfer or energy transfer theories.[81, 82, 83] A critical parameter that governs SF is the coupling between neighbouring units.[84, 85, 86] Following this concern, computational studies have also much contributed to the definition of a well-balanced coupling strength, and to the identification of the best chromophores.[87, 88, 89, 90, 91] While too strong an interaction is not favourable for the triplets to separate and move apart, too weak a coupling reduces the rate of SF.[73, 92, 93, 94] The role of excimer formation in SF still deserves particular attention, indeed its formation is a critical step for the generation of pairs of triplets.[95, 96] The energy matching condition, which approximates the energy positioning from the monomer values, allows for the computational screening of possible SF candidates data sets.[97, 98, 99, 100, 101, 102, 103, 104] Irrespective of the level of theory, wave-function theory or density functional theory (WFT and DFT, respectively) calculations, such an approximation is considered to be satisfactory for molecular crystals, and more questionable in covalent dimers.[84, 105, 106, 107, 108]

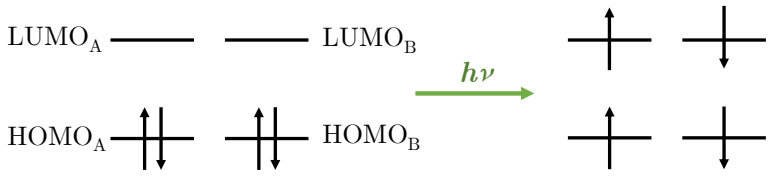

Figure 2.4: Schematic description of the thermodynamic condition of the SF phenomenon from the frontier orbital diagram of a class I compound built on A and B chromophores.

However, one may wonder how much the immediate environment of a given monomer may modulate its spectroscopy. In the design of SF compounds, we felt that attention should be paid to the molecular description, and to go beyond the free monomer description. Practically, one would like to stress, if sizable, the influence of the electronic structure of a monomer spin state (so-called environment) on the relative energies of a given neighbouring unit (so-called active chromophore). The importance of the environment is known and was reported in complex systems for which local and collective effects are likely to compete.[109, 110, 111] Evidently, the appropriate definition of the spin nature of the environment in *ab initio* calculations calls for particular care, not to mention the system size which might make it not tractable from quantum chemistry methods.

2.2 Environmental effects on the thermodynamic condition of the Singlet Fission phenomenon: a model Hamiltonian-based study

In the screening of compounds for Singlet Fission, the relative energies of the constitutive units are decisive to fulfill the thermodynamic rules. From a model Hamiltonian constructed on the local spin states of an active chromophore and its environment, it is suggested that the embedding greatly influences the energy differences of the active monomer spin states. Even in the absence of charge transfer, the field generated by a singlet environment produces an increase of the $[E(S_{A,1}) - E(S_{A,0})]/[E(T_{A,1}) - E(S_{A,0})]$ *critical ratio by up to 6% as compared to the one of a free chromophore. Besides, variations are observed when the intimate electronic structure of the singlet environment is modified. This propensity towards SF is even more pronounced (10%) when the environment is switched to the triplet state. Finally, the embedding is likely to reverse the spin states ordering in the limit of vanishing atomic orbital overlaps. Despite its simplicity, the model stresses the importance of the environment spin nature in the quest for SF candidates, and more generally in spectroscopy analysis.*

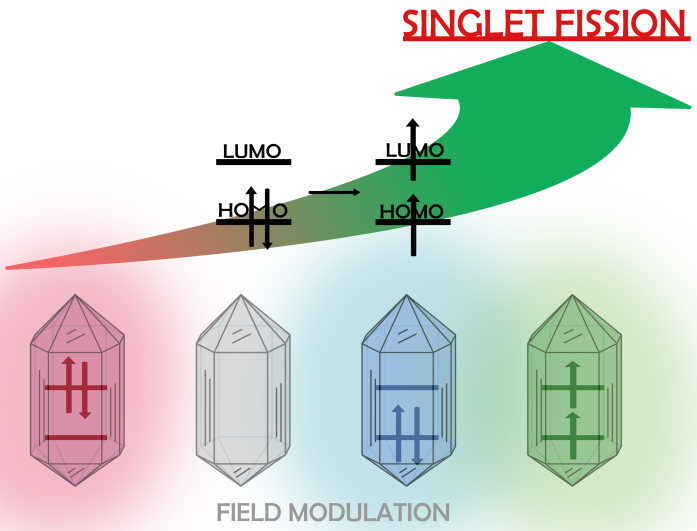

2.2.1 Introduction

Our intention is to set the environment characteristics to foresee its impact on the energies of the active chromophore. For a neighbouring closed-shell chromophore, a single configuration might be an acceptable approximation and one strategy would be to freeze the molecular orbitals (MOs) to mimic such a closed-shell environment. However, the presence of a neighbouring open-shell chromophore (*e.g.* triplet) is more problematic since the electronic structures and spin values of the sub-parts cannot be decided in standard quantum chemistry calculations. Indeed, in a non-relativistic description, the total spin is a good quantum number, and any calculation produces spin eigen-states of the full system.

A model Hamiltonian built on the local spin states of two H_2 sub-systems was considered to complement the current views on molecules with potential applications for SF. A much more sophisticated environment may enrich the description at a cost of a less comprehensive analysis. The model aims at capturing the environment effects using this minimal picture consisting of a single H_2 molecule. An "active" H_2 molecule is then feeling a field generated by an "environment" H_2 molecule. The relevance of traditional approaches based on isolated chromophores can be examined from this simple H_4 model. Following the standard crystal-field theory that relies on a closed-shell structure of the coordination sphere, we wanted to trace the importance of the spin value of the environment, and the resulting modifications of the Coulomb and exchange contributions. In particular, different coupling schemes can arise with the presence of open-shells on both H_2 molecules. The presence of a spin-active environment triggers new interactions and coupling schemes with a spin-active molecule. Such phenomenon is similar to *spinmerism*, a manifestation in particular coordination chemistry compounds presented in the next Chapter.

2.2.1.a Description of the model

Traditionaly, theoretical inspections greatly concentrate on the HOMO and LUMO frontier orbitals.[112, 113, 114, 115] The S_0-S_1 transition in the popular class I of SF chromophores is reasonably described by a HOMO–LUMO electronic transition.[116] Indeed, the most promising candidates are slip-stacked chromophores where the di-

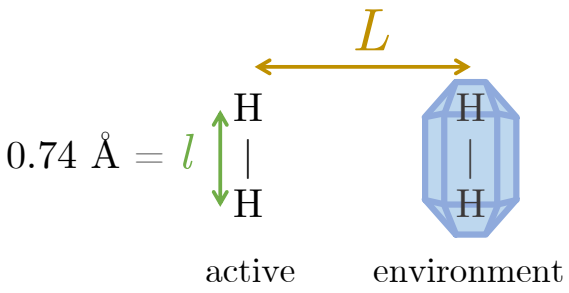

Figure 2.5: Model system built on the active (A) and environment (E) chromophores with relevant geometrical parameters $l = 0.74$ Å (fixed intra-chromophore distance) and L (inter-chromophore distance).

rect mechanism can be optimized.[109, 117, 118, 119] Therefore, Charge Transfer (CT) states which might become competitive were not included in our description by simply constraining the number of electrons on the active chromophore and the environment, a realistic picture when $L >> l$ (see Figure 2.5). The possibility of mediation by the CT mechanism was explored elsewhere in covalent dimers.[83, 105, 106] Thus, the model Hamiltonian is constructed on local spin states of a pair of interacting H_2-like molecules (*i.e.* two electrons in two MOs). For preliminary inspections, SF is limited to the direct coupling mechanism. In summary, the construction is nothing but a projection of the configuration interaction space into a selection of configurations that preserve the electron numbers and spin states on the subunits.

Let us take one AO per hydrogen-site, which makes it a system of four electrons in four AOs. Working with localised orbitals facilitates the wavefunction analysis and its understanding. In this regard, one can either consider to work directly from non-orthogonal AOs or to produce orthonormal MOs.[120] Each approach has its specificity: on one hand, non-orthogonal AOs overlap (s) should be considered and matrix elements for non-orthogonal orbitals need to be built, on the other hand, orthonormal MOs need to be properly localized.

The *a priori* and *a posteriori* localization methods described in section (1.3) are particularly efficient for bigger systems but they must pay an orthogonalization cost: a "delocalization tail" appears in the Localized MOs (LMOs).[1] When π-stacking occurs in noncovalent SF chromophores, the inter-molecular MOs overlap is close

[1]The LMOs of a two-site system (A and B) are a linear combination of the AOS of A and B if their AOs are not strictly orthogonal (in other words, if the AOs overlap is not zero).

to zero due to the packing distance. As there is no exact control on the amount of delocalization during the construction of LMOs, the first approach (non-orthogonal AOs) was chosen. To start from a chemical intuition picture, two locally orthonormal MOs (g_k and u_k) are built on each monomer. Then, the non-orthogonality between the two sub-spaces constructed on each H_2 fragment is taken into account.

Considering a minimal 1s AOs basis i_A, j_A, i_E and j_E (A and E being the active and environment parts, respectively), the bonding (g_A and g_E) and anti-bonding (u_A and u_E) LMOs of the active (A) and environment (E) subunits (see Figure 2.5) can easily be built as

$$g_k = \frac{1}{\sqrt{2(1+s_k)}}(i_k + j_k) \quad \text{and} \quad u_k = \frac{1}{\sqrt{2(1-s_k)}}(i_k - j_i) \tag{2.3}$$

where $s_k = \langle i_k | j_k \rangle$ is the AOs overlap between i_k and j_k, and k is either the A or E subspace.

From a chemist point of view, g_k is the HOMO and u_k is the LUMO of the sub-system. g_k and u_k are, by construction, orthonormal. However, the MOs of the active subunit are not necessarily orthogonal to the MOs of the environment. In fused-benzene compounds, orthogonality between the carbon-2p AOs becomes numerically acceptable in the $\pi - \pi$ interaction regime characterized by ~ 2.5 times the carbon–carbon π-bond distance (1.43 Å). Indeed, the 2p carbon AOs σ-overlap is calculated as 0.01 for $L = 3.6$ Å. At shorter separation distances, the AOs overlaps can no longer be neglected, similarly is the 1s hydrogen AOs overlap in the H_4-model system for distances smaller than $L \sim 2.5l \sim 1.9$ Å. Following the procedure described in subsection (1.1.6), the matrix elements are corrected to account for non-orthogonality.

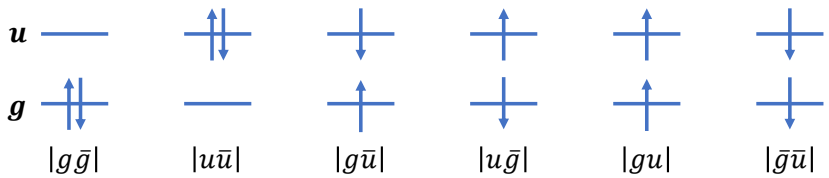

Figure 2.6: Schematic representation of the $m_S = 0$ closed-shell $|g\overline{g}|$, $|u\overline{u}|$, the $m_S = 0$ open-shell $|g\overline{u}|$ and $|u\overline{g}|$, and the $m_S = \pm 1$ $|gu|$ and $|\overline{gu}|$ configurations on a dimer. The $m_S = 0$ singlet and triplet configuration state functions are $\frac{1}{\sqrt{2}}(|g\overline{u}| + |u\overline{g}|)$ and $\frac{1}{\sqrt{2}}(|g\overline{u}| - |u\overline{g}|)$ respectively.

Neglecting the CT mechanisms, each monomer displays six possible local configurations: one $m_S = -1$, four $m_S = 0$, and one $m_S = +1$ (see Scheme 2.6). These local configurations are combined into local configuration state functions Γ_A and Γ_E to span the total tensorial product space $\Gamma_A \otimes \Gamma_E$. This tensorial product space contains $\binom{4}{2}\binom{4}{2} = 36$ determinants, which are referenced in the following Table 2.1.

<table>
<tr><th>$\Gamma_A \otimes \Gamma_E$</th><th>$|g_E\bar{g_E}|$</th><th>$|u_E\bar{u_E}|$</th><th>$|g_E\bar{u_E}|$</th><th>$|u_E\bar{g_E}|$</th><th>$|g_E u_E|$</th><th>$|\bar{g_E}\bar{u_E}|$</th></tr>
<tr><td>$|g_A\bar{g_A}|$</td><td colspan="4" rowspan="4">$\boldsymbol{M_S = 0}$</td><td rowspan="4">$M_S = +1$</td><td rowspan="4">$M_S = -1$</td></tr>
<tr><td>$|u_A\bar{u_A}|$</td></tr>
<tr><td>$|g_A\bar{u_A}|$</td></tr>
<tr><td>$|u_A\bar{g_A}|$</td></tr>
<tr><td>$|g_A u_A|$</td><td colspan="4">$M_S = +1$</td><td>$M_S = +2$</td><td>$\boldsymbol{M_S = 0}$</td></tr>
<tr><td>$|\bar{g_A}\bar{u_A}|$</td><td colspan="4">$M_S = -1$</td><td>$\boldsymbol{M_S = 0}$</td><td>$M_S = -2$</td></tr>
</table>

Table 2.1: The total determinants basis for the configuration state functions Γ_A (rows) and Γ_E (columns). Total spin projection M_S of the tensorial product space $\Gamma_A \otimes \Gamma_E$ is given.

All matrix elements were first analytically calculated as functions of mono-electronic and bi-electronic integrals expressed in the minimal AOs STO-3G basis set. Evidently, the model Hamiltonian parametrization could be used. However, we preferred to introduce the chemical details of the structure, as any *ab initio approach* would do, to possibly extend to any realistic SF chromophore. All integrals are distance-dependent and numerically available from the PSI4 suite of programs [121] (see Figure 2.5).

All determinants are built in the $M_S = 0$ manifold (in **bold** in Table 2.1), and the energies are compared to the ones obtained in the absence of the environment subunit. Within our approach restricted to the direct coupling mechanism (*i.e.* no CT), the singlet state environment S_E is constructed as a contraction on the three configuration state functions (see Figure 2.6):

$$S_E = e_1|g_E\overline{g}_E| + e_2|u_E\overline{u}_E| + e_3\frac{1}{\sqrt{2}}(|g_E\overline{u}_E| + |u_E\overline{g}_E|). \tag{2.4}$$

Such a contraction allows one to (i) generate a given electronic structure that is not affected by the presence of the active chromophore (frozen embedding picture),

and (ii) extend our model to non-symmetric active-environment pairs. By varying the coefficients in the contraction, the nature of the environment can be selectively modified to account for the aggregate formation, and to reproduce different regimes. In contrast, the electronic structures of active chromophore singlets $S_{A,0}$, $S_{A,1}$ and $S_{A,2}$ are fully relaxed as linear combinations of $|g_A\overline{g}_A|$, $|u_A\overline{u}_A|$ and $\frac{1}{\sqrt{2}}(|g_A\overline{u}_A| + |u_A\overline{g}_A|)$ configurations:

$$|S_{A,i}\rangle = a_1|g_A\overline{g}_A| + a_2|u_A\overline{u}_A| + a_3\frac{1}{\sqrt{2}}(|g_A\overline{u}_A| + |u_A\overline{g}_A|). \tag{2.5}$$

Let us mention that a closed-shell S_E environment is readily achieved by freezing the occupied and virtual LMOs of the environment in an *ab initio* procedure. Evidently, the triplet state consists of a single configuration $T_{A,1} = \frac{1}{\sqrt{2}}(|g_A\overline{u}_A| - |u_A\overline{g}_A|)$, the energy of which is immediately calculated in the S_E field.

A similar inspection was then performed when the environment is switched into a triplet state T_E. However, some particular care must be taken since a total triplet state ${}^3(T_{A,1}T_E)$ emerges from the local triplet states $T_{A,1}$ and T_E. Such a triplet can mix in with the triplet state built from the $\frac{1}{\sqrt{2}}(|g_A\overline{u}_A| + |u_A\overline{g}_A|) \times \frac{1}{\sqrt{2}}(|g_E\overline{u}_E| - |u_E\overline{g}_E|)$ configuration (*i.e.* $S_{A,1}\otimes T_E$). Moreover, one overall singlet and one quintet states emerge from the coupling of $T_{A,1}$ and T_E. The eigenvector analysis evidences contributions arising from local singlet and triplet states on the active chromophore.

In this study, we are primarily concerned with the impact of the environment spin structure on the energy level matching conditions. Thus, the objective is to examine the sensitivity of the low-energy state ordering of an active chromophore A in the field generated by a L-distant environment E. In this picture, the thermodynamic condition for SF reads $\rho = [E(S_{A,1}) - E(S_{A,0})]/[E(T_{A,1}) - E(S_{A,0})] \geq 2$.

2.2.2 Results and discussion

Let us first concentrate on the active chromophore energy levels in the field of a singlet state environment S_E. In the $M_S = 0$ manifold, the $S_A \otimes S_E$ space is spanned by three determinants. A single determinant built as $T_{A,1} \otimes S_E$ defines the local triplet state energy on the active chromophore. Overall, three singlet states $S_{A,i}$ and one single triplet $T_{A,1}$ energy are evaluated in the presence of a frozen

singlet environment. All energies depend on the inter-dimer distance L as well as on the contraction coefficients e_1, e_2, and e_3 (see equation (2.4)).

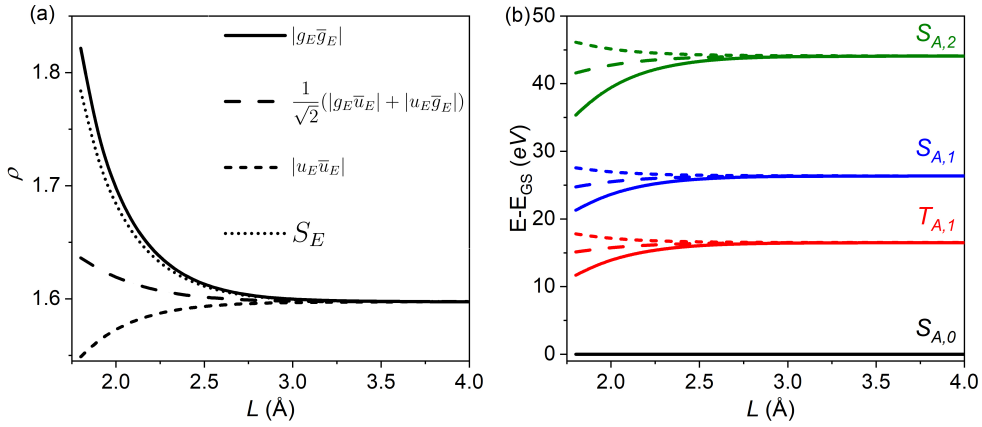

Figure 2.7: (a) Critical ratio $\rho = [E(S_{A,1}) - E(S_{A,0})]/[E(T_{A,1}) - E(S_{A,0})]$ in the field of different singlet environments as a function of the inter-dimer distance L. The singlet environment S_E consists of a contraction $e_1 = 0.91$, $e_2 = 0.27$, and $e_3 = 0.09$. (b) Variations of the singlet and triplet states energies (eV) of the active chromophore in different singlet environments. The energy of the ground state is used as a reference. The intra-chromophore distance l is set to the equilibrium H_2 distance 0.74 Å.

In the long-distance regime ($L > 3.5$ Å), the H_2 monomers do not interact, all integrals becoming vanishingly small. The asymptotic limit of the critical ratio $\rho = [E(S_{A,1}) - E(S_{A,0})]/[E(T_{A,1}) - E(S_{A,0})]$ (*ca.* 1.60) corresponds to the value that is usually reported from calculations performed on a single chromophore. However, ρ is very sensitive to the presence of a surrounding partner (see Figure 2.7(a)), even in this simplified picture. The nature and amplitude of the dipole–dipole interactions are responsible for this differentiating effect. For interacting π-systems, the ratio between the intramolecular carbon–carbon distance and the packing separation is *ca.* 2.5. In analogy, one expects that, below $L \sim 2.5l \sim 1.9$ Å, CT contributions should be included between 1s hydrogen AOs, and our simplified view would be invalidated. However, even at this low-distance limit, ρ is increased up to 1.72 (see Figure 2.7(a)). Figure 2.7(b) shows the variations of the energy levels of the active chromophore in different singlet environments. A closed-shell $|g_E\overline{g}_E|$ environment lower the energy levels of all excited states with respect to the ground state $S_{A,0}$. The

first excited singlet $S_{A,1}$ and triplet $T_{A,1}$ states are equally stabilized with respect to the ground state. However, the gap between $S_{A,1}$ and $T_{A,1}$ is nearly independent from L (standard deviation 0.05). Overall, this favours the SF thermodynamic condition (ρ increases up to 1.75). A closed-shell $|u_E\overline{u}_E|$ environment imposes a weaker but opposite behaviour. Finally, the open-shell singlet environment (long dash lines in Figure 2.7) slightly stabilizes the excited states with respect to the ground state, which slightly improves the SF thermodynamic condition.

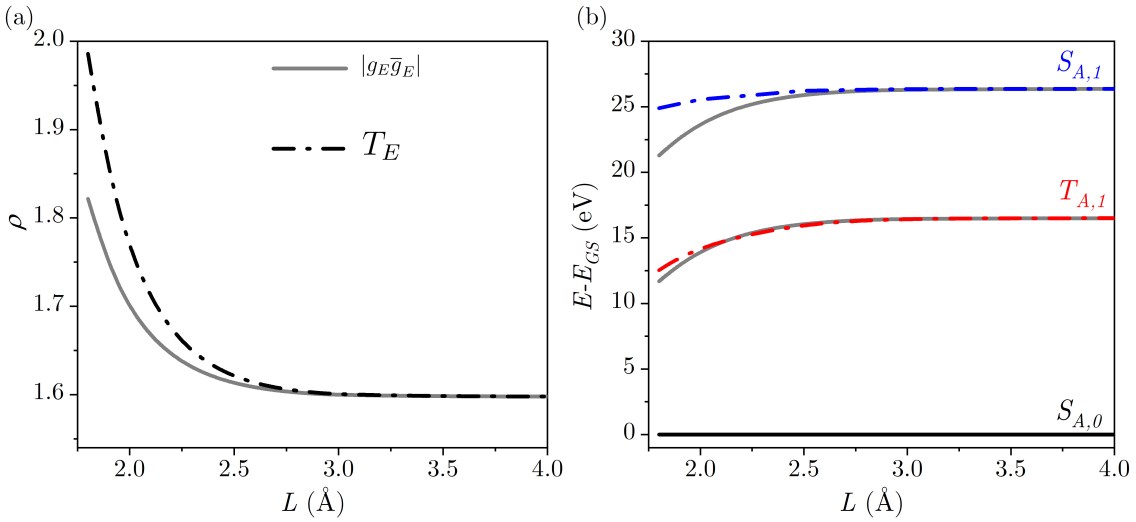

Figure 2.8: (a) Critical ratio $\rho = [E(S_{A,1}) - E(S_{A,0})]/[E(T_{A,1}) - E(S_{A,0})]$ in the field of a triplet environment T_E as a function of the inter-dimer distance L (in dash-dot line). Ratio evaluated in the field of the singlet $|g_E\overline{g}_E|$ environment, from Figure 2.7, is repeated for the sake of comparison (in grey plain line). (b) Variations of the low-lying triplet state energies (eV) for a triplet environment (dash-dot lines). Variations of the low-lying states in the field $|g_E\overline{g}_E|$ environment is repeated for comparison (grey plain lines). The ground state consists of a pure singlet on A, and its energy is used as a reference. The excited triplet states are labelled with the dominant contributions on A. The intra-chromophore distance l is set to the equilibrium H_2 distance 0.74 Å.

As soon as the environment spin state is switched to triplet, the picture is somewhat modified. Irrespective of the inter-dimer distance, the ground state singlet (reference energy in Figure 2.8(b)) is a pure singlet on A dominated by the $|g_A\overline{g}_A|$ configuration. As mentioned before, the excited triplet states result from the mixing between different spin-coupling schemes ($S_{A,i} \otimes T_E$ and $T_{A,1} \otimes T_E$). From our numer-

ical inspections, these states labelled as $T_{A,1}$ and $S_{A,1}$ in Figure 2.8(b) are largely dominated (*ca.* 98% at $L = 2$ Å) by the triplet and singlet on A, respectively. Thus, these energies can be compared to the ones obtained from an isolated chromophore picture for which $\rho = 1.60$ and $T_{A,1} - S_{A,0} = 16.50$ eV. Not only does the $S_{A,1} - T_{A,1}$ energy difference increases with the decreasing inter-chromophore distance (+1.74 eV), but also the SF thermodynamic condition $\rho > 2$ is fulfilled for L values close to 1.9 Å (see Figure 2.8(a)). For comparison, the triplet–singlet energy difference and the ρ value for $L = 3.5$ Å were, respectively, calculated as 16.50 eV and 1.60 at the CAS[4,4]SCF level in a minimal 1s AOs STO-3G basis set.[45] The same results were obtained at the CAS[2,2]SCF level, in the same minimal basis set. In this regime, the contracted view of the model (see Figure 2.8(b)) reproduces the CASSCF energy splitting as well as the asymptotic value $\rho = 1.60$.

Despite its simplicity, our model stresses that the presence of the environment significantly modifies the spin state ordering. As expected, the field generated by the environment depends on its spin state, giving rise to an enhanced SF inclination in the presence of a triplet environment T_E. The observed critical regime of 1.9 - 2.6 Å in the H_4 model agrees with the traditional range of the manifestation of π-stacking interactions in conjugated organic molecules up to a scaling factor based on the intra- and inter-molecular distances ($L \sim 2.5l$).

It is known that realistic synthetic systems for SF are acene-like and our model may look at first over-simplistic. First, the hydrogen 1s AOs σ-overlap is 0.66 for $l = 0.74$ Å, whereas the π-overlap between the 2p carbon AOs is reduced down to 0.19 for a typical carbon–carbon distance. Then, the density of states increases with the number of carbon atoms in a polyacene. Together, these elements favour a reduction of the HOMO–LUMO gap within the chromophore. In the π-stacking acene arrangements, the inter-chromophore interactions are governed by negligible 2p carbon AOs σ-overlap (0.01 for $L = 3.6$ Å). For all these reasons, we felt that setting all overlap values to zero (intra- and inter-chromophores) in our model would allow in making the contact with synthetic compounds, and in analysing the leading mechanisms at work in the hierarchization of the spin states. Importantly, all the one-electron and two-electron energy integrals were maintained as numerically evaluated from PSI4. The former singlet and triplet environments were generated (see Figure 2.9).

In the asymptotic limit (4 Å, see Figure 2.9, upper panel), the spectroscopy evidently does not depend on the environment structure and exhibits a singlet ground state $S_{A,0}$. Nevertheless, the absolute energy of the latter is sensitive to the structure of the environment and, as a consequence, the ρ value is modulated. The spectroscopy of an isolated chromophore in the approximation that all overlap values are zero is calculated as a reference, and the values for the $T_{A,1} - S_{A,0}$ gap and ρ are 9.17 eV and 1.61, respectively. The four different environments create three distinct behaviours, already at $L = 20$ Å (see Figure 2.9, bottom panel). These variations of spectroscopy are mainly shaped by the energies of the closed-shell active states $S_{A,0}$ and $S_{A,2}$.

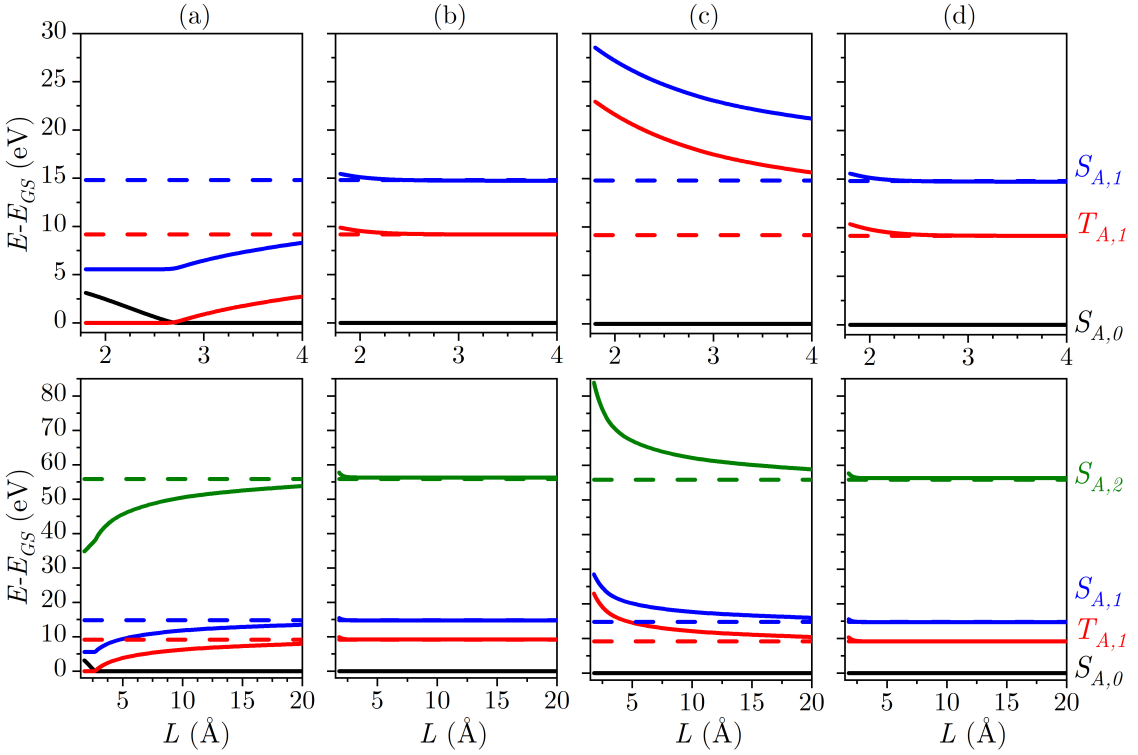

Figure 2.9: Upper panel: Low-lying singlet and triplet states energies (eV) as a function of the inter-dimer distance L in the vicinity of a contracted singlet environment S_E (a,b,c) and a triplet environment (d). (a) $e_1 = 1$ and $e_2 = e_3 = 0$, (b) $e_1 = 0$, $e_2 = 1$, and $e_3 = 0$, and (c) $e_1 = e_2 = 0$ and $e_3 = 1$. All AOs overlaps are set to zero. Following the Tanabe-Sugano representation, the ground state energy E_{GS} is taken as a reference. Horizontal dashed lines represent the spectroscopy of an isolated chromophore. Bottom panel: Extension to the energies of all states beyond the asymptotic limit ($L > 4$ Å), for a clearer reading.

By inspecting the different contributions, the leading one arises from the two-electron integral $[i_A j_A|i_E j_E]$ (see subsection (1.1.5)). This is a slowly decaying $1/L$ integral that destabilizes $|g_A\overline{g}_A g_E\overline{g}_E|$ and $|u_A\overline{u}_A u_E\overline{u}_E|$ configurations, whereas it stabilises $|u_A\overline{u}_A g_E\overline{g}_E|$ and $|g_A\overline{g}_A u_E\overline{u}_E|$ configurations. As a consequence, the energy of the $S_{A,0}$ state increases in the presence of a mono-determinantal singlet environment $|g_E\overline{g}_E|$ ($e_1 = 1$, $e_2 = e_3 = 0$). Conversely, it is lowered for the $|u_E\overline{u}_E|$ environment ($e_1 = 0$, $e_2 = 1$, $e_3 = 0$). For symmetry reasons, the energy of $S_{A,0}$ is not sensitive to the open-shell singlet environment $\frac{1}{\sqrt{2}}(|g_E\overline{u}_E| + |u_E\overline{g}_E|)$ ($e_1 = e_2 = 0$, $e_3 = 1$), neither to the triplet environment. This state of affairs changes for the excited triplet $T_{A,1}$ and singlet $S_{A,1}$ states. Indeed, the dominant integral $[i_A j_A|i_E j_E]$ has no impact on their energies, and the $S_{A,1} - T_{A,1}$ splitting remains constant and equal to $2K_{g_A u_A}$ (exchange integral). As a result of the long-range $1/L$ potential, the critical ratio ρ is still sensitive to the environment even for $L = 20$ Å where $\rho_{|g_E\overline{g}_E|} = 1.70$, $\rho_{|u_E\overline{u}_E|} = 1.53$ and $\rho_{\frac{1}{\sqrt{2}}(|g_E\overline{u}_E|+|u_E\overline{g}_E|} = 1.61$ (see Figure 2.9, bottom panel). A more physical singlet environment is a contraction over the different singlet configuration state functions. Different contracted singlet environment structures were generated by varying the amplitudes e_1, e_2 and e_3 (see Figure 2.10).

For L *ca.* 5 Å, the $\rho > 2$ regime is reached (respectively from (a,b,c) of Figure 2.10, where all AOs overlaps are set to zero, $\rho = 2.33$, 2.28, and 2.10), in sharp contrast with what was observed previously ($\rho = 1.60$ for the different contracted environments in Figure 2.7(a) where AOs overlap are non-zero). When L is further reduced, the energy of the $S_{A,0}$ state continuously increases, and eventually the nature of the ground state switches to high-spin $T_{A,1}$. Such an observation somewhat reconsiders the traditional picture "strong field-low spin" in metal ion coordination compounds. Interestingly, the switching L distance is shifted to lower values (see Figure 2.10) as the weight of the $|u_E\overline{u}_E|$ configuration increases. This is a reflection of the competing effects of the $|g_E\overline{g}_E|$ and $|u_E\overline{u}_E|$ configurations on the stabilization of the $S_{A,0}$ state, observed in Figure 2.10.

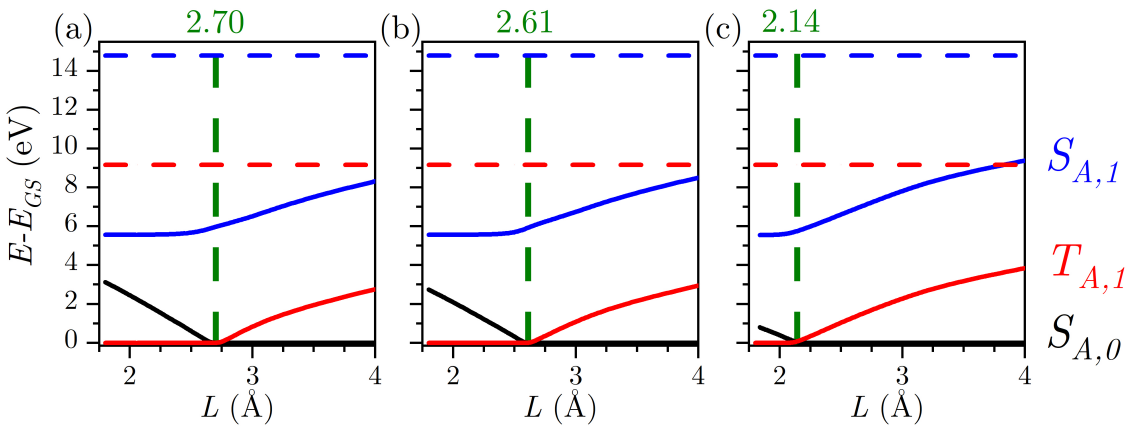

Figure 2.10: Singlet and triplet states energies (eV) as a function of the inter-dimer distance L in the vicinity of a contracted singlet environment S_E with the increasing weight on the $|u_E\overline{u}_E|$ configuration. (a) $e_1 = 1$ and $e_2 = e_3 = 0$, repeated from Figure 2.9 for better comparison of spectra, (b) $e_1 = 0.99$ and $e_2 = e_3 = 0.10$, and (c) $e_1 = 0.95$, $e_2 = 0.29$, and $e_3 = 0.10$. All AOs overlaps are set to zero. Following the Tanabe-Sugano representation, the ground state energy E_{GS} is taken as a reference. Its nature changes for a characteristic L distance which is marked by a vertical dashed line. Horizontal dashed lines represent the spectroscopy of an isolated chromophore.

The examined electronic structure is evidently reminiscent of the one in cyclobutadiene. As seen in Figure 2.10, the ground state of the four-electron four-orbital system is the singlet whatever the structure of the singlet environment. This observation is in agreement with the pseudo Jahn–Teller effect manifestation: the triplet square structure is unstable and a distortion to the rectangular geometry leads to a singlet ground state. In contrast, our constrained wave function description favours a triplet ground state ($T_{A,1} \otimes S_E$) even for strong deviations from the square geometry. The contracted structure of the E part and the resulting absence of CTs are responsible for this behaviour. However, our model highlights the significant impact of the electronic structure of the environment.

2.3 Conclusions

The importance of the spin structure of the environment on the energy states of a two-electron active chromophore was examined by building up a model. The active

chromophore state ordering is much affected in the presence of a triplet or a singlet environment. As a consequence, the critical ratio $\rho = [E(S_{A,1}) - E(S_{A,0})]/[E(T_{A,1}) - E(S_{A,0})]$ defined on the excitation energies of the first singlet and triplet excited states may reach the lower bound $\rho = 2$ value for the SF condition to occur. It is important to remind that the critical $L = 1.9$ Å distance in our model is analogous to the π-stacking distance in a conjugated π-system dimer (3.5 Å). As observed, the environment creates an electronic field influencing the active chromophore already at $L = 3$ Å, equivalent to a 5.7 Å separation of two pentacenes. A simplified description that neglects overlaps leads to an even deeper modification. Moreover, the ground state is switched from the low-spin singlet to the high-spin triplet when the distance between the active chromophore and the environment is *ca.* 2.5 Å. This critical distance is governed by the structure of the singlet state environment acting as a field that controls the spin state hierarchisation. The influence of the slowly decaying $1/L$ two-electron integral $[i_A j_A | i_E j_E]$ on the active subunit is reduced on a more complex description, which does not prevent it from playing a discriminatory role between environments. Even in the absence of charge transfers between the subunits, our model suggests that spin-dependent environment effects should be taken into account. Indeed, a triplet environment favours the SF thermodynamic condition, whereas a closed-shell doubly excited singlet environment disfavours this condition. In the light of the many studies approximating the SF energy condition to the study of a single chromophore, our model highlights the importance of the "discarded" environment chromophore. The simplicity of the H_4-based model brings some insights and means of interpretation that should be transferable in the theoretical quest of SF candidates. Finally, I would like to stress that this model (available online in Appendix C) allows one to study the influence of a 2×2 (2 electrons in a HOMO/LUMO pair) frozen environment chromophore on a 2×2 active chromophore. Then, it is possible to replace the g_k and u_k MOs basis set (constructed on the minimal 1s hydrogen basis set) by any desired g_{phys} HOMO and u_{phys} LUMO basis set. This model corrects non-orthonormality between MOs through its construction of matrix elements, which makes it suited to add more physics (*e.g.* 2p carbon AOs), in the approximation of a 4×4 model Hamiltonian.

Self-criticism is always needed in Science. 1) It is important to mention that only

the commonly used thermodynamic condition $\rho = [E(S_{A,1}) - E(S_{A,0})]/[E(T_{A,1}) - E(S_{A,0})]$ is studied in this problem. A proper comparison with the more physical thermodynamic condition $\rho_{phys} = [E(S^*) - E(S)]/[E(^1(TT) - E(S)]$ would allow to have a reference ρ_{phys}, useful to quantify the variations from one approximation to another. 2) Charge transfers are neglected in the description to facilitate the analysis, and to access a physical undertanding. However, charge transfers states have been suggested in literature to be of importance for SF to occur. Having an environment mainly frozen in a contracted state but with some allowed (*e.g.* 10%) charge transfers contributions may open new understandings on the influence of environments. This idea is inspired from embedding methods, where one can control the amount of charge transfers between an impurity and a bath by tuning their chemical potential. 3) The mono- and bi-electronic integrals calculated consider indirectly the AOs overlaps. Thus, virtually neglecting overlaps in the orthogonalization procedure may induce a bias at shorter distances. 4) The model works in a minimal STO-3G 1s hydrogen AOs basis set, an extended basis set would improve the quality of the electronic spectra. Otherwise, using carbon atoms with 2p AOs such as in an ethylene dimer may bring more physics, differentiating the $\pi - \pi$ interaction for intramolecular bonds from the $\sigma - \sigma$ interaction for intermolecular stacking. Nevertheless, this description would complicate the model, raising the question to move from a model (with or without Perturbation Theory corrections) to a selected-CI approach (where one would select only some electronic configurations). 5) Varying the intramolecular l distance may bring new perspectives to take into account the lowering of the HOMO-LUMO in polyacenes with increasing numbers of carbon atoms. This was in fact explored but not presented as it involves new discussions, less important with regard to the variation of L. 6) The electronic structure is separated into two local structures, but the hydrogen sites remain in a spatially symmetric arrangement. Bringing in asymmetry by having different bonds distances ($l_A \neq l_E$), slip-stacking or rotating the two subunits along an axis, would allow to explore the influence of other types of environment, at the cost of an increase in variability.

Still, our model highlights the influence of a frozen electronic environment on an active subunit. The influence of an electronic environment have applications beyond the SF issues, such as energy and electron transfer mechanisms.

Appendix C. Construction of the model Hamiltonian for SF

My opinion in Science is that, often, codes are written and developed for specific problems but rarely appear when publishing an article or a thesis. For this reason, the codes used in this Chapter have been put on a github page.[122] I would like to take the next few pages to explain the philosophy and details that allowed us to realize such a model study. Our system is a H_4 rectangle. Its symmetry group is D_2. Symmetry arguments allow one to reduce the complexity of a problem, which is the case in our study.

Singlet environment

2.3.0.a Single configuration

Let us first focus on the case where the active monomer is in a Singlet environment. For a single configuration singlet environment (*e.g.* $e_1 = 1$, $e_2 = e_3 = 0$), four determinants are generated in the $M_S = 0$ space.

$\Gamma_A \otimes \Gamma_E$	$\lvert g_E\bar{g_E}\rvert$	$\lvert u_E\bar{u_E}\rvert$	$\lvert g_E\bar{u_E}\rvert$	$\lvert u_E\bar{g_E}\rvert$	$\lvert g_E u_E\rvert$	$\lvert \bar{g_E}\bar{u_E}\rvert$
$\lvert g_A\bar{g_A}\rvert$	A_1					
$\lvert u_A\bar{u_A}\rvert$	B_1					
$\lvert g_A\bar{u_A}\rvert$	C_1					
$\lvert u_A\bar{g_A}\rvert$	D_1					
$\lvert g_A u_A\rvert$						
$\lvert \bar{g_A}\bar{u_A}\rvert$						

Table 2.2: Single configuration singlet environment $e_1 = 1$, $e_2 = e_3 = 0$

A 4×4 resulting matrix is then created, which eigenvalues contains the energies of the three singlet and one triplet states of the active monomer in this field. As we do not introduce any spin-orbit coupling, coupling terms between singlet states and the triplet state are zero. In this sense, this 4×4 matrix can be transformed as two decoupled matrices: a 3×3 singlet matrix, and a 1×1 triplet matrix. It is then necessary to consider a linear combination of C_1 and D_1 determinants, which

transforms our determinant basis ($\{A_1, B_1, C_1, D_1\}$ to a configuration state function basis (singlet basis: $\{A_1, B_1, \frac{1}{\sqrt{2}}(C_1 + D_1)\}$; and triplet basis: $\{\frac{1}{\sqrt{2}}(C_1 - D_1)\}$).

Next, one needs to evaluate the matrix elements following the selection rules for non-orthogonal orbitals stated in subsection (1.1.6). As a concrete example, the $\langle A_1|H|A_1\rangle$ matrix element is developed below.

Though, the first step is to define the secular determinant

$$\begin{array}{c|cccc} & g_A & \bar{g_A} & g_E & \bar{g_E} \\ g_A & 1 & 0 & S_1 & 0 \\ \bar{g_A} & 0 & 1 & 0 & S_1 \\ g_E & S_1 & 0 & 1 & 0 \\ \bar{g_E} & 0 & S_1 & 0 & 1 \end{array} \tag{2.6}$$

with $S_1 = \langle g_A|g_E\rangle$.

Let us start with the one electron operator. As a reminder, the mono-electronic integral $\langle g_A|\hat{h}|g_A\rangle$ have as coefficient the secular determinant above where column g_A and row g_A have been crossed out, which makes

$$\begin{vmatrix} 1 & 0 & S_1 \\ 0 & 1 & 0 \\ S_1 & 0 & 1 \end{vmatrix} = 1 - S_1^2. \tag{2.7}$$

$$\langle g_A\bar{g_A}g_E\bar{u_E}|\hat{\mathcal{O}}_1|g_A\bar{g_A}g_E\bar{u_E}\rangle = 2(1-S_1^2)\langle g_A|\hat{h}|g_A\rangle + 2(1-S_1^2)\langle g_E|\hat{h}|g_E\rangle + 4(S_1 - S_1^3)\langle g_A|\hat{h}|g_E\rangle$$

We remind the reader that we are working with real orbitals ($\langle g_A|\hat{h}|g_E\rangle = \langle g_E|\hat{h}|g_A\rangle$), but also that our system belongs to symmetry group D_2, which allows one to simplify the mono- and bi-electronic integrals, for example: $\langle g_A|\hat{h}|g_A\rangle = \langle g_E|\hat{h}|g_E\rangle$.

It is then important to differentiate inter- from intra-molecular integrals, which we implement by introducing g and u, bonding and anti-bonding molecular orbitals on a given site and j and v, bonding and anti-bonding molecular orbitals on the neighbouring site, with respect to the given site. In this sense, there is no need anymore to differentiate integrals which give the same result, *e.g*:

$$[g_Ag_A|g_Eu_E] = [g_Ag_A|u_Eg_E] = [g_Eg_E|u_Ag_A] = [g_Eg_E|g_Au_A] = [gg|jv] \tag{2.8}$$

Continuing with the two electron operator, the bi-electronic integral $[g_A g_A|\bar{g_A}\bar{g_A}]$ have the secular determinant where columns g_A and $\bar{g_A}$ and rows g_A and $\bar{g_A}$ are crossed out as multiplying factor.

$$\langle g_A\bar{g_A}g_E\bar{u_E}|\hat{\mathcal{O}}_2|g_A\bar{g_A}g_E\bar{u_E}\rangle = 2(3S_1^2-1)[gj|jg]-8S_1[gg|gj]+2(2-S_1^2)[gg|jj]+2[gg|gg]$$

If $S_1 = 0$, then one can observe the textbook selection rules for integrals as described in subsection (1.1.6.b).

$$\begin{aligned}\langle g_A\bar{g_A}g_E\bar{u_E}|\hat{H}|g_A\bar{g_A}g_E\bar{u_E}\rangle =&\epsilon_{g_A} + \epsilon_{\bar{g_A}} + \epsilon_{g_E} + \epsilon_{\bar{g_E}} + [g_A g_A|\bar{g_A}\bar{g_A}] + [g_E g_E|\bar{g_E}\bar{g_E}]\\ &+ [g_A g_A|\bar{g_E}\bar{g_E}] + [\bar{g_A}\bar{g_A}|g_E g_E]\\ &+ [g_A g_A|g_E g_E] - [g_A g_E|g_E g_A] + [\bar{g_A}\bar{g_A}|\bar{g_E}\bar{g_E}] - [\bar{g_A}\bar{g_E}|\bar{g_E}\bar{g_A}]\\ =&4\epsilon_g + 2[gg|gg] + 2(2[gg|jj] - [gj|jg])\end{aligned}$$

There is no need to compute these matrix elements by hand and a working symbolic Python code is available on Github.[122] If the spin of MOs was disregarded, one matrix element for a system as simple as four electrons in four MOs would give rise to 16 mono-electronic integrals and 72 bi-electronic with their respective secular determinant to evaluate.

Concerning the triplet state (and equivalent open-shell singlet), one must evaluate three matrix elements as demonstrated below:

$$\langle\frac{1}{\sqrt{2}}(C_1 \mp D_1)|\hat{H}|\frac{1}{\sqrt{2}}(C_1 \mp D_1)\rangle = \frac{1}{2}(\langle C_1|\hat{H}|C_1\rangle + \langle D_1|\hat{H}|D_1\rangle \mp 2\langle C_1|\hat{H}|D_1\rangle). \quad (2.9)$$

Once the 3×3 singlet and 1×1 triplet matrices are derived in the basis set of the MOs integral, two choices are possible to evaluate these integrals: (i) direct calculation from a QC code, (ii) transformation into AOs integral basis set. The second option was chosen as it allows working in the AOs basis set. This non-orthonormal basis contains AOs localized for the four hydrogen atoms. Above, we explained the symmetry reasons behind the appearance of g, u, j and v in our expressions. These same symmetry reasons can be invoked to write AOs integrals in the basis of $\{i, j, i', j'\}$ such that: i is the AO of a given H atom; j is the AO of its intra-molecular neighbour; i' is the AO of its closest inter-molecular neighbour; and j' is the AO of its farthest inter-molecular neighbour.

From the first step which gave the matrix elements in terms of the MOs integrals, one can obtain a total of $\binom{1}{8}\binom{1}{8} = 64$ mono- and $\binom{1}{8}\binom{1}{8}\binom{1}{8}\binom{1}{8} = 4096$ bi-electronic MOs integrals. This number is reduced, respectively, to 4 and 19 with the help of spin and spatial (D_2) symmetry rules that were presented before. Transforming these MOs integrals to AOs integrals, 4 mono- and 19 bi-electronic AOs integrals are obtained. These important but heavy looking terms are found in Table 2.3. An analytical example is given for $\langle g|\hat{h}|j\rangle$ integral:

$$\begin{aligned}
\langle g|\hat{h}|j\rangle =& \langle \frac{1}{\sqrt{2(1-S_{ij})}}(i+j)|\hat{h}|\frac{1}{\sqrt{2(1-S_{i'j'})}}(i'+j')\rangle \\
=& \frac{1}{2\sqrt{(1-S_{ij})(1-S_{i'j'})}}(\langle i|\hat{h}|i'\rangle + \langle i|\hat{h}|j'\rangle + \langle j|\hat{h}|i'\rangle + \langle j|\hat{h}|j'\rangle) \\
=& \frac{1}{2(1-S_{ij})}(2\langle i|\hat{h}|i'\rangle + 2\langle i|\hat{h}|j'\rangle) \\
=& S_+(2t_{ii'} + 2t_{ij'}).
\end{aligned}$$

By symmetry, $\langle g|\hat{h}|u\rangle$, $\langle g|\hat{h}|v\rangle$, $[gu|gg]$, $[gg|jv]$, $[gj|ju]$, $[gu|uu]$, $[gu|vv]$, $[gv|vu]$ and $[gv|jg]$ are zero.

These integrals were determined using a Psi4 code, which is also uploaded on Github.[122] We have thus fully developed the problem and can now start plugging in the numerical values of AOs integrals to observe the consequence of a frozen singlet environment $|g_E\bar{g_E}|$ on the spectroscopy of an active H_2 molecule.

The same procedure can be repeated when the environment is $|u_E\bar{u_E}|$. Particular care must be taken when the environment is made of multiple frozen determinants such as an open-shell singlet $\frac{1}{\sqrt{2}}(|g_E\bar{u_E}| + |u_E\bar{g_E}|)$. This is demonstrated in the next subsection.

MOs integral	AO integrals basis
$\langle g\|\hat{h}\|g\rangle$	$= S_+(2\epsilon + 2t)$
$\langle u\|\hat{h}\|u\rangle$	$= S_-(2\epsilon - 2t)$
$\langle g\|\hat{h}\|j\rangle$	$= S_+(2t_{ii'} + 2t_{ij'})$
$\langle u\|\hat{h}\|v\rangle$	$= S_-(2t_{ii'} - 2t_{ij'})$
$\langle g\|j\rangle$	$= S_1 = S_+(2S_{ii'} + 2S_{ij'})$
$\langle u\|v\rangle$	$= S_3 = S_-(2S_{ii'} - 2S_{ij'})$
$[gg\|gg]$	$= S_+^2(2U + 2J + 8\lambda_1 + 4K)$
$[gg\|jj]$	$= S_+^2(2J' + 2J_1 + 8\lambda_2 + 4\omega_1)$
$[gj\|jg]$	$= S_+^2(2K' + 2\theta_1 + 8\theta_2 + 2\omega_2 + 2\omega_3)$
$[uu\|uu]$	$= S_-^2(2U + 2J - 8\lambda_1 + 4K)$
$[gg\|uu]$	$= S_+S_-(2U + 2J - 4K)$
$[gu\|ug]$	$= S_+S_-(2U - 2j)$
$[gg\|vv]$	$= S_+S_-(2J' + 2J_1 - 4\omega_1)$
$[gv\|vg]$	$= S_+S_-(2K' - 2\theta_1 + 2\omega_2 - 2\omega_3)$
$[uu\|vv]$	$= S_-^2(2J' + 2J_1 - 8\lambda_2 + 4\omega_1)$
$[uv\|vu]$	$= S_-^2(2K' + 2\theta_1 - 8\theta_2 + 2\omega_2 + 2\omega_3)$
$[gu\|jv]$	$= S_+S_-(2J' - 2J_1)$
$[gv\|ju]$	$= S_+S_-(2K' - 2\theta_1 - 2\omega_2 + 2\omega_3)$
$[gj\|uv]$	$= S_+S_-(2K' + 2\theta_1 - 2\omega_2 - 2\omega_3)$
$[gg\|gj]$	$= S_+^2(2\gamma_1 + 2\gamma_2 + 2\gamma_3 + 2\gamma_4 + 4\gamma_5 + 4\gamma_6)$
$[gj\|uu]$	$= S_+S_-(2\gamma_1 + 2\gamma_2 + 2\gamma_3 + 2\gamma_4 - 4\gamma_5 - 4\gamma_6)$
$[gu\|uj]$	$= S_+S_-(2\gamma_1 - 2\gamma_2 + 2\gamma_3 - 2\gamma_4)$
$[uu\|uv]$	$= S_-^2(2\gamma_1 + 2\gamma_2 - 2\gamma_3 - 2\gamma_4 - 4\gamma_5 + 4\gamma_6)$
$[gg\|uv]$	$= S_+S_-(2\gamma_1 + 2\gamma_2 - 2\gamma_3 - 2\gamma_4 + 4\gamma_5 - 4\gamma_6)$
$[gu\|vg]$	$= S_+S_-(2\gamma_1 - 2\gamma_2 - 2\gamma_3 + 2\gamma_4)$

Acronym	AOs integral
ϵ	$\langle i\|\hat{h}\|i\rangle$
t_{ij}	$\langle i\|\hat{h}\|j\rangle$
$t_{ii'}$	$\langle i\|\hat{h}\|i'\rangle$
$t_{ij'}$	$\langle i\|\hat{h}\|j'\rangle$
S_{ij}	$\langle i\|j\rangle$
$S_{ii'}$	$\langle i\|i'\rangle$
$S_{ij'}$	$\langle i\|j'\rangle$
U	$[ii\|ii]$
J	$[ii\|jj]$
J'	$[ii\|i'i']$
K	$[ij\|ij]$
K'	$[ii'\|ii']$
J_1	$[ii\|j'j']$
λ_1	$[ii\|ij]$
λ_2	$[ii\|i'j']$
ω_1	$[ij\|i'j']$
ω_2	$[ij'\|ij']$
ω_3	$[ij'\|i'j]$
θ_1	$[ii'\|jj']$
θ_2	$[ii'\|ji']$
γ_1	$[ii\|ii']$
γ_2	$[ii\|jj']$
γ_3	$[ii\|ij']$
γ_4	$[ii\|ji']$
γ_5	$[ij\|ii']$
γ_6	$[ij\|ij']$

Table 2.3: (left) MOs integrals transformed into linear combinations of AOs integral basis. $S_+ = \frac{1}{2(1+S_{ij})}$ and $S_- = \frac{1}{2(1-S_{ij})}$. (right) AOs integrals and their acronym used for better readability.

2.3.0.b Multiple configurations

Now let us focus on a multiple configuration singlet environment (*i.e* e_1, e_2 and e_3 are different from 0). There arise 16 determinants as represented in Table 2.4 below.

$\Gamma_A \otimes \Gamma_E$	$\lvert g_E\bar{g_E}\rvert$	$\lvert u_E\bar{u_E}\rvert$	$\lvert g_E\bar{u_E}\rvert$	$\lvert u_E\bar{g_E}\rvert$	$\lvert g_E u_E\rvert$ $\lvert\bar{g_E}\bar{u_E}\rvert$
$\lvert g_A\bar{g_A}\rvert$	A_1	A_2	A_3	A_4	
$\lvert u_A\bar{u_A}\rvert$	B_1	B_2	B_3	B_4	
$\lvert g_A\bar{u_A}\rvert$	C_1	C_2	C_3	C_4	
$\lvert u_A\bar{g_A}\rvert$	D_1	D_2	D_3	D_4	
$\lvert g_A u_A\rvert$ $\lvert\bar{g_A}\bar{u_A}\rvert$					

Table 2.4: Singlet environment

If the environment is not frozen, then a 16×16 matrix need to be built. It is composed of two uncoupled matrices: one 12×12 singlet matrix and one 4×4 triplet matrix. However, as we are freezing the environment, we need to contract these spaces from 12×12 to a 3×3 singlet matrix and from 4×4 to a 1×1 triplet matrix. One naive way to proceed would be to do a linear combination of the four singlet matrices with basis $\{A_i, B_i, \frac{1}{\sqrt{2}}(C_i + D_i)\}$. However, this would neglect the inter-matrices coupling such as $\langle A_1|\hat{H}|A_2\rangle$, which may appear. As an example, the matrix element $\langle A|\hat{H}|A\rangle$ is evaluated in the basis of the 16×16 matrix H, whose elements are denoted as $H_{Y_iZ_j} = \langle Y_i|\hat{H}|Z_j\rangle = H_{Z_jY_i}$ ($Y, Z = A - D$ and $i, j = 1 - 4$).

$$\begin{aligned}|A\rangle &= |e_1|g_A\bar{g_A}g_E\bar{g_E}| + e_2|g_A\bar{g_A}u_E\bar{u_E}| + e_3\frac{1}{\sqrt{2}}(|g_A\bar{g_A}g_E\bar{u_E}| + |g_A\bar{g_A}u_E\bar{g_E}|)\rangle \\ &= |e_1A_1 + e_2A_2 + e_3\frac{1}{\sqrt{2}}(A_3 + A_4)\rangle\end{aligned}$$

$$\begin{aligned}\langle A|\hat{H}|A\rangle &= \langle e_1A_1 + e_2A_2 + e_3\frac{1}{\sqrt{2}}(A_3 + A_4)|\hat{H}|e_1A_1 + e_2A_2 + e_3\frac{1}{\sqrt{2}}(A_3 + A_4)\rangle \\ &= e_1^2H_{A_1A_1} + e_2^2H_{A_2A_2} + \frac{1}{2}e_3^2(H_{A_3A_3} + H_{A_4A_4} - 2H_{A_3A_4}) + 2e_1e_2H_{A_1A_2} \\ &+ \sqrt{2}e_1e_3(H_{A_1A_3} + H_{A_1A_4}) + \sqrt{2}e_2e_3(H_{A_2A_3} + H_{A_2A_4})\end{aligned}$$

This calls for the evaluation of the 136 matrix elements of the 16×16 matrix $\{H_{Y_iZ_j}\}$, then their linear combination to reduce the problem size through contraction. This

is a general way of proceeding which allows one, in the end, to have a global expression of a D_2 symmetric system in terms of $\{e_i\}$, overlaps, mono- and bi-electronic integrals. Being a generalized model, it is possible to use it to describe more complex systems, either stopping at the MOs integrals and using pre-computed HOMO and LUMO MOs or going down to the AOs integrals and studying, for example, the C_4 π-system of a ethylene dimer.

Triplet environment

Let us briefly discuss the case of a triplet environment. It is not necessary to take into account all five possibly generated M_S (-2, -1, 0, 1, 2). We then focus only on the $M_S = 0$ determinants as they give a global picture of all the possible calculated states. The three active singlet states can couple with the triplet environment, producing three singlet states. The active triplet state coupling with a triplet environment generates one singlet, one triplet and one quintet states. One may have observed that our initial determinant basis in Table 2.5 contains ten determinants. Four of the generated determinants belong to the open-shell singlet environment counterpart. A total of six states is to be studied when having a triplet environment.

$\Gamma_A \otimes \Gamma_E$	$\lvert g_E\bar{g_E}\rvert$ $\lvert u_E\bar{u_E}\rvert$	$\lvert g_E\bar{u_E}\rvert$	$\lvert u_E\bar{g_E}\rvert$	$\lvert g_E u_E\rvert$	$\lvert\bar{g_E}\bar{u_E}\rvert$
$\lvert g_A\bar{g_A}\rvert$		A_3	A_4		
$\lvert u_A\bar{u_A}\rvert$		B_3	B_4		
$\lvert g_A\bar{u_A}\rvert$		C_3	C_4		
$\lvert u_A\bar{g_A}\rvert$		D_3	D_4		
$\lvert g_A u_A\rvert$					E_6
$\lvert\bar{g_A}\bar{u_A}\rvert$				F_5	

Table 2.5: Triplet environment in $M_S = 0$.

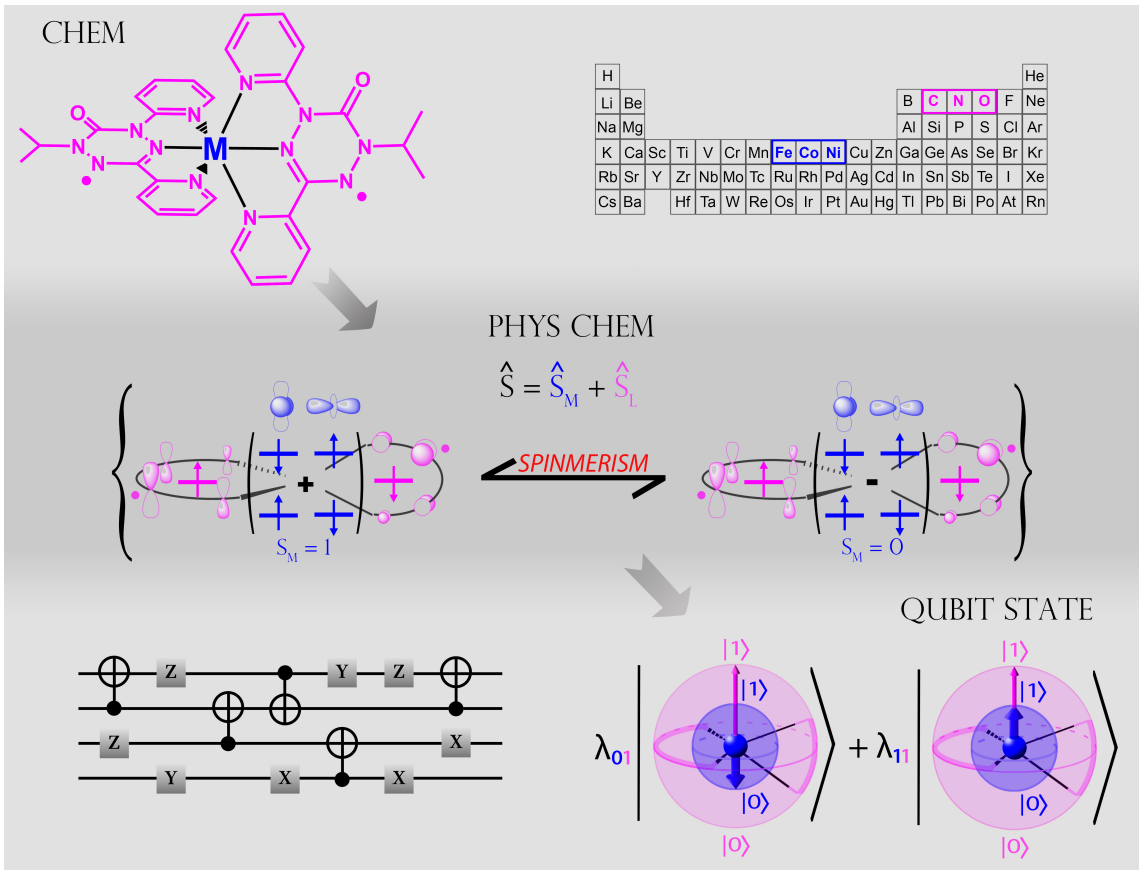
CHEM
M
PHYS CHEM
$\hat{S} = \hat{S}_M + \hat{S}_L$
SPINMERISM
$S_M = 1$
$S_M = 0$
QUBIT STATE
Z
Y
Z
Z
X
Y
X
X
λ_{01}
λ_{11}
|1⟩
|0⟩

Chapter 3

On the rise of *spinmerism*

This Chapter tackles the notion of environment in the point of view of inorganic chemistry: the system of reference is now a metal ion, while the environment is the ligand sphere. It is divided in four parts. First, it introduces the spinmerism phenomenon, studied later in the Chapter, by presenting its various key components. The first part ends with a brief introduction to Quantum Computing. It continues with a model Hamiltonian study of the spinmerism phenomenon, with an extension to possible molecular spin-qubits hardware for Quantum Computing. This is followed by an ab initio wavefunction-based study of a Co(II) oxoverdazyl complex which exhibits a weak spinmerism effect in its ground state. Despite the vanishingly small manifestation of spinmerism observed in this complex, it is the first ab initio observation of this mechanism. Finally, it ends with an ab initio wavefunction-based study of a Fe(II) oxoverdazyl complex that exhibits excited state spinmerism effect. This leads to a comment on the influence of spinmerism on Tanabe-Sugano diagrams (here solely on octahedral d^6 diagram) and its applicability for molecular electronics. This Chapter finishes with a general conclusion and a self-criticism.

keywords: *spinmerism*, wavefunction, model Hamiltonian, *ab initio*, Tanabe-Sugano, spin-qubits

Most of the content of this Chapter has been published in Refs [123, 124, 125].

3.1 An introduction to *spinmerism*

With the fast evolution of science over the last century, many new research areas have emerged, and many older fields have evolved accordingly. Humans have always miniaturized their technology, while increasing its energy consumption. The field of magnetism has a particularly long history. As magnetic materials occur naturally (magnetite), they have been recorded by mankind since 800BC, and used as navigation tools since the 11th century. With the development of advanced theories for magnetism around the 19h century, scientists separated effects from materials. This led to the development of magnetoChemistry.

In recent decades, magnetoChemistry has remained an attractive field of research for the scientific community, especially with the advent of molecular magnetism. Magnetic properties were primarily measured and studied on coordination chemistry complexes of metal ions with unfilled d-orbitals. The synthesis of free radicals has opened the way to new explorations, thanks to the unpaired electrons in the p-orbitals of stable free organic radicals. Association of open-shell fragments, such as transition metal ions and organic free radicals, has led to molecule-based magnetic systems. Magnetic considerations have shifted from a strictly magnetic metal centre to a total ensemble, resulting from the coupling between magnetic centres (metals and/or radicals). Their magnetic properties can be modulated by effectively controlling the nature of the magnetic interactions, and may present extended material properties (*e.g.* low density, transparency, photo-response). They come in a variety of forms: single molecules (zero-dimensional, 0D), chains (1D), layers (2D), and 3D networks structures. The innovative properties of these compounds have opened new perspectives in fields such as molecular electronics and supramolecular chemistry. A significant number of magnetic phenomena (Spin CrossOver, Giant MagnetoResistance, Spin Hall Effect, Tunnel MagnetoResistance...) have contributed to increase the theoretical understanding of magnetism, and to continue the frenetic technological race in the fields of data storage, spintronics and sensors. In recent years, quantum technologies have also manifested their interest for information storage and manipulation possibilities.

This PhD work was inspired by a rather peculiar phenomenon: Valence Tautomerism. Yet, in my opinion, it is easier to tackle this phenomenon after first understanding another phenomenon: Spin CrossOver.

3.1.1 Spin CrossOver Systems

Spin CrossOver (SCO) phenomenon results from molecular bistability of particular compounds. The latter can be defined as "*the ability for a molecular system to exhibit two stable states in a given range of external perturbation*".[126] SCO is mainly observed in coordination complexes with a first row transition metal d^4 to d^7 and a N_6 octahedral environment.[127] These compounds may exhibit a crossover between a low-spin (LS) and a high-spin (HS) states, induced by a variation of temperature, of pressure, and by light irradiation.[128] This crossover is associated with changes in the ligand field strength, molecular structure, volume, magnetic susceptibility, and color. Indeed, LS and HS states have their own (different) ligand equilibrium geometry. This makes them particularly interesting for memory devices and electrical switches applications.[129]

SCO was first observed in 1931, through the temperature-induced interconversion of two spin states of natural Fe(III) complexes.[130] It was then highlighted in other natural iron compounds such as hemoglobin and its derivatives.[131, 132] In the 1960s, some groups studied and reported the crossover region for Fe(II) [133] and Co(II) [134, 135] compounds, but it is truly the development and use of Mössbauer spectroscopy [136] which allowed to study in depth the SCO phenomenom.[137, 138] It was overall mainly studied in Fe(II) compounds,[139, 140, 126] but also in Co(II) compounds,[141] due to their particular properties and because they are the best candidates for Mössbauer spectroscopy. SCO compounds are very diverse, from mononuclear spin transition compounds [142, 143] to polymeric spin transition compounds,[144, 145, 146] but also as thin films, and nanoparticles.[147, 148, 149]

Briefly, one can observe that there is a crossover region in the Tanabe-Sugano diagrams [150] for d^4 to d^7 in an octahedral geometry (see Figure 3.1). Modulating the ligand field allows one to change the spin state of the metal ($\Delta S = 1$ for d^4 and d^7; $\Delta S = 2$ for d^5 and d^6). As stated earlier, this modulation can be tuned by different

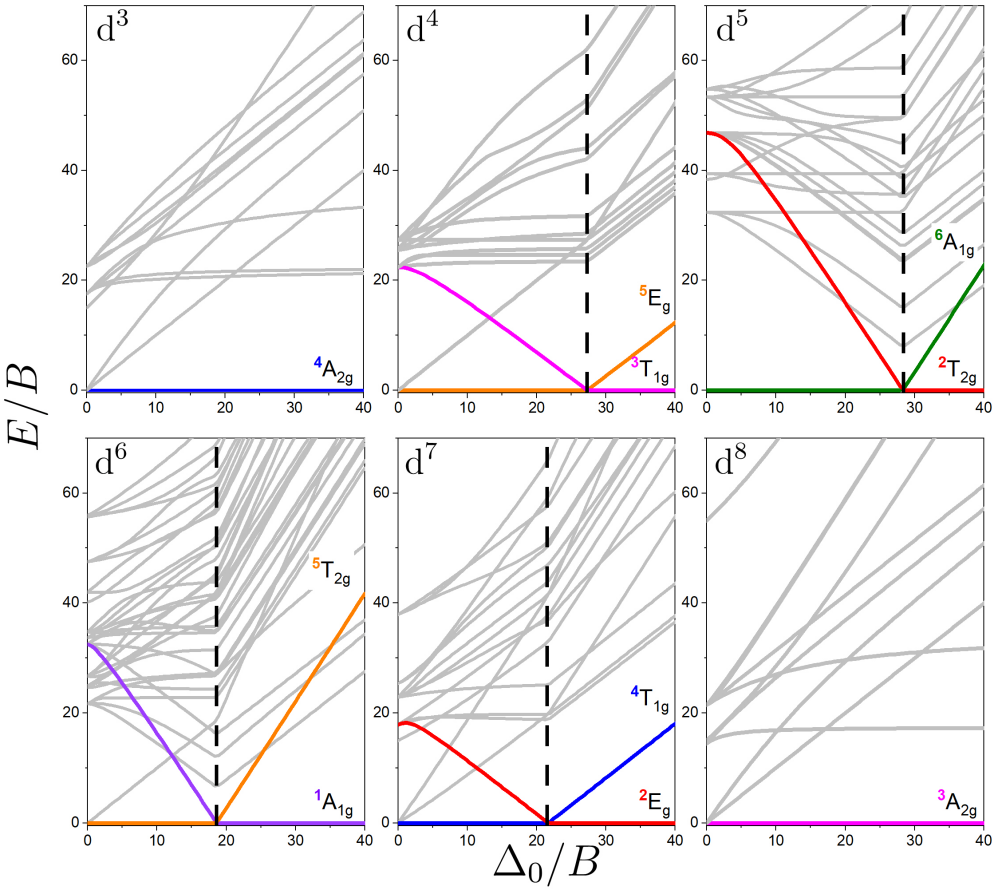

Figure 3.1: Tanabe-Sugano diagrams from d^3 to d^8 octahedral metal complexes. Δ_0 is the ligand field, B is the second Racah parameter, and E is the energy.

external stimuli. If sensitive to temperature, a SCO compound may present a thermal hysteresis. Four criteria [151, 152, 153] are to be fulfilled for the compound to be of interest for thermal devices applications: (i) abrupt transition during heating and cooling. (ii) the transition temperature $T_{1/2}$, at which half of the species are in LS, and the other half in HS, to be around room temperature. (iii) thermal hysteresis width to be of the order of 50 K. (iv) stability of the hysteresis after > 1000 cycles. Pressure variations are more often used as a way to tune thermal hysteresis, and related $T_{1/2}$ in greater depth.[154] Nevertheless some pressure-induced SCO compounds can be found in the literature.[155] Thanks to wavelength tunability, light is a perfect stimuli to select specific transitions (d-d, Metal-to-Ligand Charge Transfer MLCT, Ligand-to-Metal Charge Transfer LMCT).[156] When using wavelengths matching the ligand absorption bands, one can tune the ligand field by inducing ligand configuration changes (photo-isomerization or cyclization). This is the case for Ligand-Driven Light-Induced Spin Change,[157, 158, 159] where SCO

is induced through a photochemical reaction on the ligands, and for Light-Driven Coordination-Induced Spin-State switching,[160, 161] where SCO is induced by a drastic change in the ligand coordination (coordination/dissociation). When using wavelengths matching the d-d bands or the MLCT transitions, transient excited states can be populated, inducing a photo-induced crossover. This is the principle of the Light-Induced Excited Spin-State Trapping effect (LIESST).[162] As it was mainly studied and observed in Fe(II) complexes, let us take one of it as an example (see Figure 3.2). A vertical transition promotes the molecule from the singlet LS state to a singlet excited state, then a first InterSystem Crossing (ISC) $\Delta S = 1$ traps the molecule into an excited triplet state. Finally, a second ISC $\Delta S = 1$ promotes the molecule into the quintet HS state.[163] The switching is really fast ($\sim$ ns) and the quantum yield is high. However, these systems need to be kept at low temperature (< 50 K) to have a neat energy barrier between LS and HS.[126] The reverse process from HS to LS is also possible, and has been named reverse-LIESST.[164]

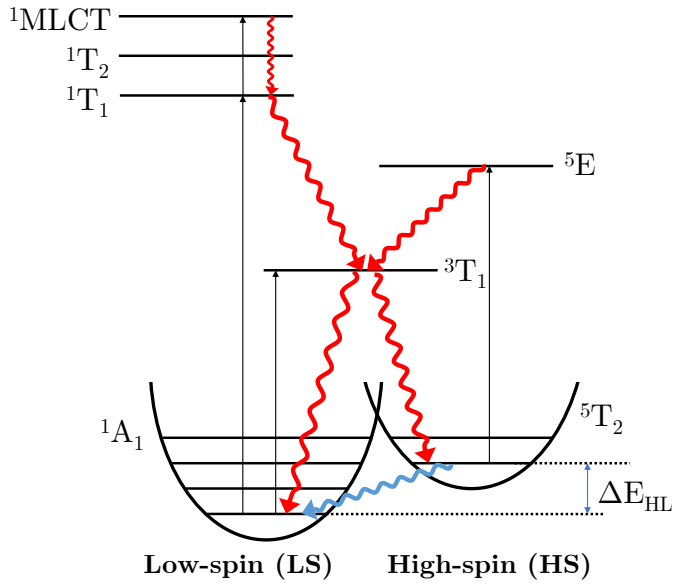

Figure 3.2: LIESST effect in a Fe(II) compound. Wavy arrows are non-radiative transitions, (red) are fast transitions, whereas (blue) is a slow transition.

Another possibility is to use intense light irradiation to heat the sample (photothermal effect), in order to make a thermal SCO using light.[165] Finally, it is important to mention that other processes may induce SCO, generally through an Electron Transfer. This is the case for Valence Tautomerism,[166, 167] presented in the following subsection.

3.1.2 Valence Tautomerism and non-innocent ligands

Valence Tautomerism (VT) is the redistribution of electrons between isomeric forms. It involves the distribution of electrons between a metal centre and redox-active ligands. This gives rise to two different valence tautomers, and consequently different optical, electric, and magnetic properties.[168, 167] It can be induced by external stimuli such as temperature, pressure, and light.[128, 169, 170, 171]

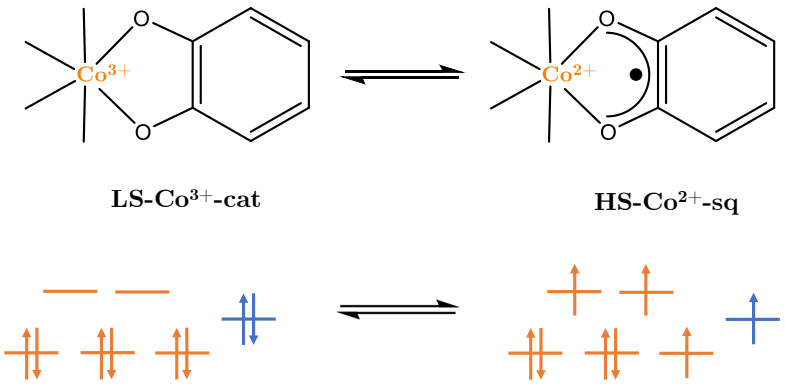

Figure 3.3: Representation of the electronic states associated with a VT transition in cobalt-dioxolene complex. cat = catecholate, sq = semiquinonate. Adapted from Ref [167].

The first reported valence tautomeric compound was an octahedral dioxolene cobalt complex.[166] This paved the way to explore other complexes and ligands.[172] Compounds prone to present VT behaviour are mainly metals from d^3 to d^9 (except d^4), with a variety of redox-active ligands (*i.e.* with an accessible radical form).[170, 167] Candidates of choice are thus the so-called "non-innocent ligands".[173]

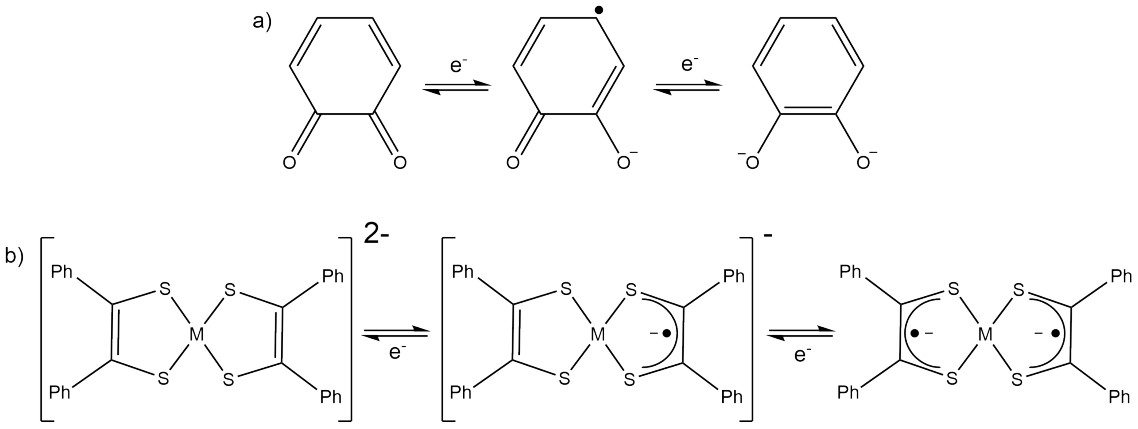

Figure 3.4: Non-innocent behaviour of (a) quinone, and (b) a dithiolene M metal complex.

A non-innocent ligand has the ability to undergo redox reactions under mild conditions, in particular when coordinated to a metal centre. This was first introduced (as "suspect ligands") by Jørgenssen to contrast with "innocent" ligands: "*Ligands are innocent when they allow oxidation states of the central atoms to be defined*".[174] Quinones, dithiolenes, and nitrosyl are perfect examples of the non-innocence of ligands. While for quinones and dithiolenes, a free radical isomer may appear (see Figure 3.4), nitrosyl ligand binds differently to a metal depending on its oxidation state (see Figure 3.5).

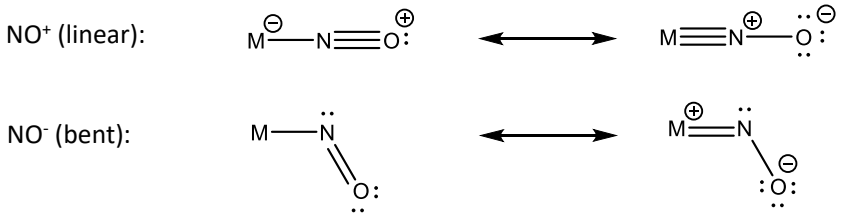

Figure 3.5: Example of different bindings of nitrosyl ligand.

Another way to have a ligand with an accessible radical form would be to directly use a stable radical ligand. Radical organic ligands have been interesting building blocks for molecular materials.[175] The most promising organic free radicals [176] are nitronyl nitroxide,[177] dithiadiazolyl,[178] o-semiquinone,[179] thiazyl,[180] and verdazyls free radicals.[181] In the interest of this work, let us present verdazyl free radicals in the next subsection.

3.1.3 Verdazyl free radicals

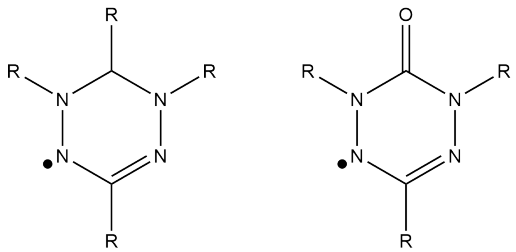

Figure 3.6: (left) verdazyl, and (right) oxoverdazyl compounds.

Verdazyl-free radicals were first reported in 1963.[182] Considered as weakly basic stable radical molecules, the first verdazyl compound was disproportionate[1] at low

[1]also called dismutation, a redox reaction in which a compound acts as both an oxidant and a reductant, forming two species: one reduced, and one oxidized (see Figure 3.7).

pH, which made it difficult to manipulate. Synthesis of the first oxoverdazyl compound in 1980,[183] less prone to disproportionation, showed their potential use as coordination chemistry ligands.

Coordination chemistry of stable radicals has seen much growth in last 40 years, and the most reported radical ligand chemistry is nitronyl nitroxide coordination. The first nitronyl nitroxide coordination complex was synthesized in 1987,[184] whereas the first oxoverdazyl coordination complex appeared ten years later.[185] Shortly after, a variety of oxoverdazyl ligands, and respective complexes arose in the literature: Mn(II), Fe(II), Co(II), Ni(II), Cu(I), Cu(II), Zn(II) complexes, to cite but a few.[181] The resulting coordination compounds present ligand-based redox processes, and non-innocent behavior. Oxoverdazyl being stable radical species, their presence in a coordination complex opens a way to explore magnetic properties.

3.1.4 Recent applications

The synthesis and characterization of molecule-based magnetic systems has been an intense research area for decades, with applications outcomes such as molecular switches,[186] thermal sensors,[167] and photomechanical properties.[187] Recently, it has seen an increase of interest and funding prompted by the need for information storage devices and advances in quantum technologies.[188, 189, 190, 191] The motivations for targeting such complexes stem from their physical-chemical properties ranging from long coherence time [192, 193, 194, 195, 196] to manipulation possibilities.[197, 198, 199, 200, 201, 202]

In this context, various types of molecular systems have been investigated ranging from transition metal complexes to organic magnetic molecules.[203, 204, 205, 206, 207, 208] Natural building blocks are paramagnetic metal ions which can be coupled

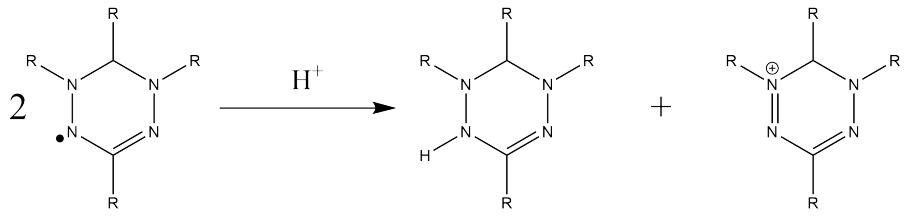

Figure 3.7: Disproportionation of verdazyl radycal, adapted from Ref [181].

through polarizable ligands. Organic radicals have considerably diversified the possibilities offered by 3d ions, not to mention their ability to bind and stabilise high oxidation states of metal ions.[209, 210, 211, 212]

Besides, the resulting transition-metal complexes can be very sensitive to oxidation, and interestingly the oxidative process may involve all partners. As suggested in a metal field,[213] the metal and the ligands should thus be treated on the same footing. As evidenced by means of wavefunction calculations, the spin nature of diradical non-innocent ligands can be controlled by the electrostatic field generated by the metal ion. Such observation had led to the excited state coordination chemistry concept developed for various coordination compounds.[214] Importantly, the redox activity of radical-ligands such as verdazyls [215] is preserved when coordinated to metal centres, introducing exchange interactions between the cation and its coordination sphere. A well-accepted and robust picture to describe magnetic properties is the Heisenberg-Dirac-Van Vleck (HDVV) spin Hamiltonian. Depending on the metal ion, different regimes were reported in verdazyl coordination complexes, ranging from strong ferromagnetic [216] to weak antiferromagnetic [212] interactions between local spin states.

Despite its robustness, deviations from the HDVV spin Hamiltonian were reported and theoretically explained by the appearance of the so-called non-Hund forms. These contributions were first reported in the study of manganese oxides [24] and later evoked to account for non-Heisenberg behaviours.[217, 218, 24, 219] The importance of the three-body operator in three-centre systems was stressed as a major source of deviation. Nevertheless, the direct exchange contributions in these systems were considered as negligible, whereas ferromagnetic interactions are observed in verdazyl-based inorganic compounds.[220] Therefore, direct exchange couplings may dominate, and super-exchange contributions should then be included in a second step. In self-assemblies, the flexibility inherently attributed to the contacts is likely to modulate the inter-unit interactions. This modulation calls for various schemes of rationalization, ranging from exchange interactions coupling to Spin CrossOver phenomenon.

Evidently, a prerequisite is the presence of spin-switchable units, prototypes being

Spin CrossOver ions such as Fe(II) or Co(II) ($3d^6$ and $3d^7$, respectively). Similar observations were reported in Prussian blue analogues where the mobility of the counter cation displacement triggers the low-spin Co(III) to high-spin Co(II) transition within the material.[221, 222] Moreover, external fields such as light or temperature, can control the local spin state of Fe(II) or Co(II) ($3d^6$ and $3d^7$, respectively) ions. Important structural modifications are observed along the $S = 0$ to $S = 2$ spin transition, with changes in bond distances of up to 0.2 Å (*i.e.* 10 %).[223] Furthermore, *ab initio* calculations showed that this transition is not restricted to a mere change in the occupation numbers of the mostly d-type valence molecular orbitals (MOs). Indeed, deep changes in charge distribution (up to 0.5 electrons) were calculated between the Fe(II) centre and its coordination sphere.[224] The latter are responsible for hysteretic behavior in materials,[225] and are known to be the main characteristic of valence tautomers.[167]

At the crossroad of exchange coupled and Spin CrossOver compounds, intriguing Co(II)-based systems have questioned the traditional pictures emerging from a metal ion, either high-spin or low-spin, in the electrostatic field of neighbouring ligands.[220, 123] The amplitudes of the charge transfers (LMCT, and MLCT) determine the geometry, spectroscopy and the spin states orderings in such coordination complexes. Since the ligand field includes Coulomb and exchange contributions in a complex built on spin-coupled partners, one may wonder whether different local spin states may coexist on the metal ion. The introduction of radical ligands may indeed disrupt the assumption of a given spin state on the metal centre. As presented in Chapter 3, *ab initio* calculations have supported such speculation in a Cobalt-verdazyl coordination compound [220] (see Figure 3.8) where coherent explanation had remained elusive so far.

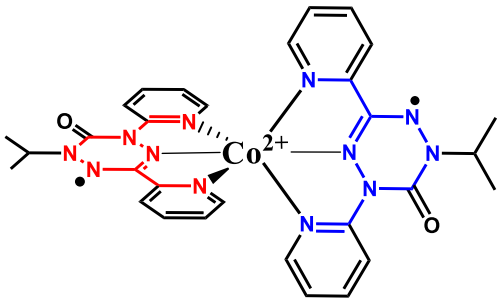

Figure 3.8: $[Co(dipyvd)_2]^{2+}$ (dipyvd = 1-isopropyl-3,5-dipyridyl-6-oxoverdazyl).

3.1.5 The *spinmerism* phenomenon

More recently, transition metal ions combined with organic ligands have been considered as possible targets in the development of molecular-based quantum units of information, *e.g.* qubits or qudits.[188, 189, 190, 191] Theoretical studies have also revealed the potential interest of radical ligands for the manipulation of quantum information via the entanglement of local spin degrees of freedom.[123, 124] A prerequisite is the binding of radical ligands to paramagnetic metal centres without losing their open-shell character. In this respect, oxoverdazyl-based ligands have proven to fulfill such requirements, giving rise to a wealth of magnetic coupling schemes.[226, 227, 228] Furthermore, the ease with which chemical modifications can be made, and the well-established redox activity of organic-based compounds make such materials particularly interesting. Not only can inter-unit interactions be modulated with speculated Spin CrossOver behaviour,[229] but the field generated by several open-shell ligands may give rise to unusual and puzzling scenarios.

In the course of my work, we came up with the concept of *spinmerism*, a phenomenon that can be seen as a direct analogue of mesomerism (involving charge degrees of freedom) for spin-degrees of freedom with entanglement in between two local subparts of a molecule.

Let us consider a molecular complex based on an artifical SCO metal ion that can do a transition between singlet and triplet. In the presence of a spin inactive ligand field ($S_L = 0$), the complex may present a transition from singlet to triplet upon distortion of the ligand field.

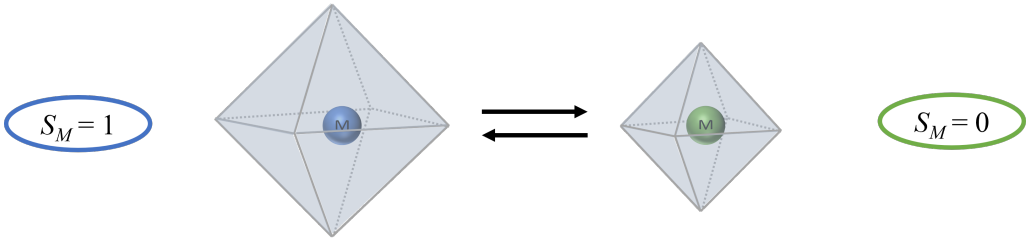

Now, let's consider that the structure is frozen in space (*i.e.*, no distortions allowed). In the absence of Spin-Orbit Coupling (SOC), the non-relativistic electronic Hamiltonian $\hat{H}$ commutes with the spin operator squared $\hat{S}^2$ ($\left[\hat{S}^2, \hat{H}\right] = 0$), and it is impossible to couple two different spins (*e.g.* singlet and triplet as in the Figure

below). The spin of the metal ion, governing the overall spin, is a good quantum number, either $S_M = 0$ or $S_M = 1$.

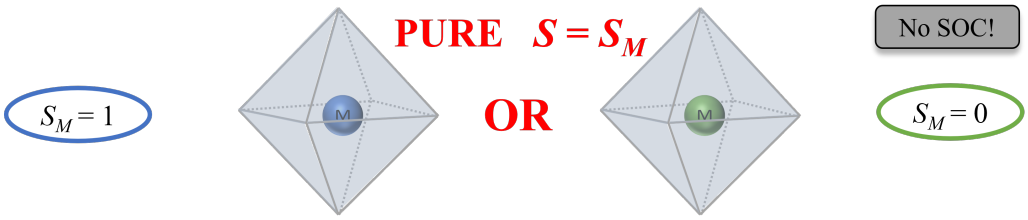

However, if one consider that the ligand field is spin active ($S_L > 0$), new coupling schemes can arise. If the local spin of the active unit S_L is equal to or higher than half of the difference of the two previously described pure spins S_M, then it becomes possible to produce states of same total spin S, but of different local compositions. As an example, we consider two overall triplet states in the Figure below. Within a given total spin multiplicity and spatial symmetry, and if the states are close enough in energy, they can mix in different local spin states. The coefficients of these superpositions may be tuned depending on the competition between the S_M local spin states (*i.e.* energy gap between spin configurations), and on the spin flexibility of the coordination sphere (*i.e.* metal-ligand couplings). This manifestation, that results from spin algebra between different spin holders, was coined into *spinmerism*.

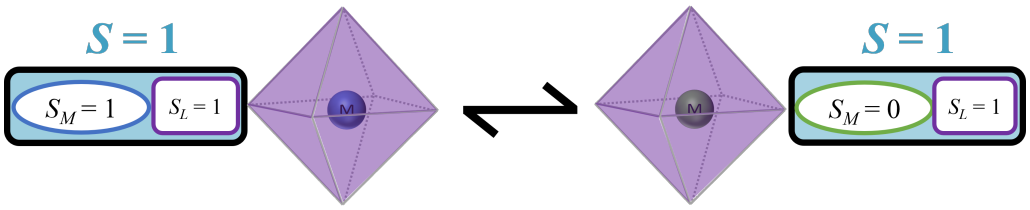

This Chapter gathers all the theoretical explorations done regarding *spinmerism*, first analytically by a model Hamiltonian, then numerically in two metal oxoverdazyl complexes.

It is important to mention that while our explorations were restrained to inorganic complexes, the *spinmerism* phenomenon may be expected for spin active organic complexes (*i.e.*, a dimer such as the one presented in the Chapter 2). However, this was not explored during this PhD work.

3.1.6 Quantum computing and Qubits

As stated in subsection (3.1.4), there has been an increase in research and funding for quantum technologies. It is therefore interesting to briefly present what Quantum Computing is, and what are its devices.

The initial goal of Quantum Computers was to go beyond the limitations of classical computers. Since 1965, the development of computers has followed the trend stated by Moore's law (the number of transistors in an integrated circuit doubles every two years). From tens of microns in the 1970s, the size of silicon etching to create transistors has decreased to 3 nm in 2022 (Samsung, TSMC). However, this trend is about to reach its limit because the miniaturization of integrated circuits and transistors cannot continue: electron leakage from one transistor to another may occur below the nano-scale through tunnelling effects. New limitations appear for technologies in the nanometer region, also called the "molecular level". This calls for research and development in molecular electronics. In the exploration of new molecular-sized components, two approaches were envisioned: top-down, the miniaturization of bulk materials into nanomaterials, and bottom-up, using atoms and molecules to produce nanomaterials. The latter approach inspired the field of Quantum Computing (QCo), *i.e.* using quantum materials and their properties to design a new type of computer. There are two main branches in QCo: hardware, and software. Hardware refers to all the devices that make up a quantum computer, while software refers to the quantum algorithms executed on a quantum computer. Everyday computing is based on the most basic unit of information, the bits (from "binary digits", they can take a value of 0 or 1). QCo, on the other hand, promotes working with quantum information units, such as quantum-bits (qubits), and quantum-dits (qudits). A qubit is the quantum version of classic bit, meaning it can encode any information between 0 and 1. It allows to encode more information than with a normal bit. This is physically achieved through a two-state physical system.[2]

$$\Psi_{qubit} = c_0|0\rangle + c_1|1\rangle$$

Many qubits are then put together to create a quantum circuit, which is used

[2]Qudits are qubits with more than two states.

in a quantum computer. Various physical systems can be used as qubits, such as quantum dots,[230, 231] trapped atoms and ions,[232, 233] superconducting circuits,[234, 235] photons,[236, 237] molecular spins...[188, 238] Qubits alone do not allow to perform computations. It is necessary to manipulate qubits with the help of quantum gates. Quantum gates manipulate the state of qubits by a physical tuning (laser pulses, magnetic field, electric field). As schematized in Figure 3.9, the qubits are first arranged in a defined input state. Then, different operations are performed with the help of diverse quantum gates. Finally, the results are extracted by physically measuring the qubits as an output state. In the case of spin-qubits, spin will be the manipulated and measured quantity.

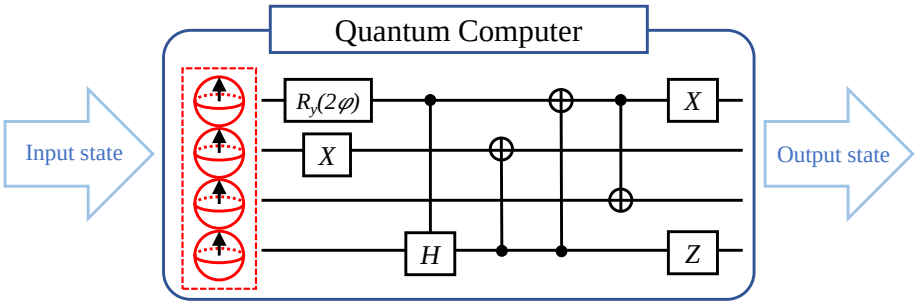

Figure 3.9: Scheme of a Quantum Computer. Qubits are in **red** and quantum gates are in **black**. Adapted from Ref [239], it encodes the superposition of a HF determinant and a HOMO-LUMO singlet CIS state.

From the different possible qubits devices discussed above, molecular quantum magnets, such as SMMs, are promising systems due to their controllable magnetic characteristics by chemical means, and by external stimuli.[238] In this regard, molecular spin-qubits have been separated into two categories: nuclear spin molecular qubits,[240] and electronic spin molecular qubits.[193, 241] Nuclear spin molecular qubits are based on the manipulation of the nucleus' spin through magnetic field, and electromagnetic radiations (radio frequency). They present extremely long coherence time and low error rates,[240] but the small magnetic moments make the interactions between qubits very weak, and complicate their integration to quantum circuits. On the other hand, electronic spin molecular qubits are based on the manipulation of the electronic spin mainly through Electron Paramagnetic Resonance. They can be manipulated at moderate temperature and magnetic fields.[238] The ability to tune them by changing the types of ligands and metals make them ap-

pealing for chemists.[195] However, their major drawback is their important susceptibility to the nuclear spin bath, either from ligands, or from the solvent environment. Rigid structures, with less vibrations of nuclei, are therefore needed. The main examples proposed by the community are $S = 1/2$ systems,[242, 243] usually as iron [244, 245] and chromium/nickel [246] polynuclear complexes, or vanadium [192, 206, 247] and copper mononuclear complexes.[194] More recently, a dithiolene complex with a paramagnetic metal has been presented to suggest the use of radical ligands for spin-qubits.[248] The field of molecular spin qubits is still in its infancy but it opens up a new way of designing possible QCo devices.

The main current challenge for QCo is to maintain the coherence of the qubits long enough to perform computations. Due to interactions with their environment, qubits are susceptible to lose their quantum coherence, which induces errors in the quantum computer. Many ways have been developed in order to protect qubits from decoherence and errors, but we will not discuss them.

The other important part of QCo research is the development of quantum algorithms and softwares. This field programs, either on real or on virtual qubits, algorithms to execute various computations (optimization, cryptography...). Quantum algorithms are out of the scope of this PhD work, which only promotes new devices. As the development of QCo follows the same steps and problems as classical computing (materials, error correction, algorithms...), the QCo community has a critical point of view on its developments, and maintains efforts in all directions. The most emphasized application of QCo is the achievement of the Quantum advantage: solving a problem that no classical computer could solve in a reasonable time.[235] This motivation has prompted governments and big companies (Google, IBM) to invest huge amounts of money in this novel field. However, it is important to mention that QCo is a recent technology that has many advantages, but whose development and induction in our daily life will require many more years, through novel design approaches.

After describing the needs of QCo devices for a controlled superposition of states, we have considered the application of the *spinmerism* phenomenon in the design of new molecular spin-qubits. In fact, the local superposition of $S_M = 1$ and $S_M = 2$

presented in the previous subsection allows one to encode information as a superposition of spin S_M in a total spin S, without applying a magnetic field. This is a different approach than the usual one for electronic spin molecular qubits where quantum information is encoded as a superposition of spin projections M_S in a total spin S, after applying a magnetic field. The applicability of the *spinmerism* phenomenon in QCo devices, and its control through LIESST effect are discussed in the following sections of this Chapter.

3.2 Model Hamiltonian study of *spinmerism* in a fictitious d^2/d^8 SCO complex. Applications to molecular spin-qubits generation.

Molecular platforms are regarded as promising candidates in the generation of units of information for quantum computing. Herein, a strategy combining Spin CrossOver metal ions and radical ligands is proposed from a model Hamiltonian first restricted to exchange interactions. Unusual spin states structures emerge from the linkage of a singlet/triplet commutable metal centre with two doublet-radical ligands. The ground state nature is modulated by charge transfers and can exhibit a mixture of triplet and singlet local metal spin states. Besides, the superposition reaches a maximum for $2K_M = K_1 + K_2$, suggesting a necessary competition between the intramolecular K_M and inter-metal-ligand K_1 and K_2 direct exchange interactions. The study provides insights into spin-coupled compounds and inspiration for the development of molecular spin-qubits.

keywords: *spinmerism*, model Hamiltonian, molecular spin-qubits

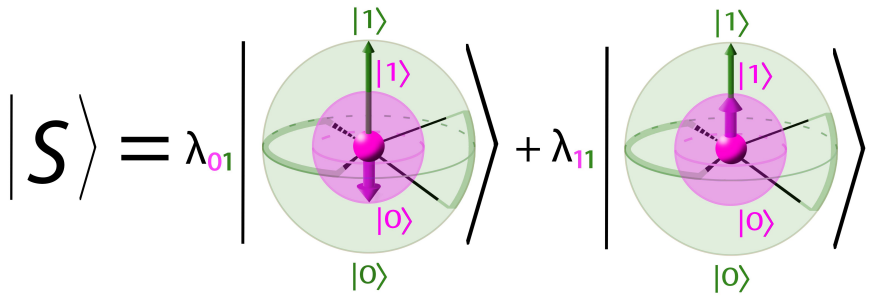

3.2.1 Introduction

Prompted by the originality of coordination compounds built on Spin CrossOver ions and radical ligands, we question the use of such complexes for the development of new quantum unit of information, *i.e.* qubits (for quantum of bits). To this purpose, a model Hamiltonian is derived to account for the suggested *spinmerism* effect (presented in subsection (3.1.5)) and to motivate its potential use for qubit

implementation. If practically accessible, the tunability of the metal local spin states (via the *spinmerism* phenomenon) could provide an innovative way to encode and manipulate information for molecule-based quantum computers. Our intention is to expand the views on related magnetic molecular system by means of a parametrized flexible model in order to identify the regimes where *spinmerism* may be observed. To this purpose, this work concentrates the effort on extracting some rules and synthetic strategy following a zeroth-order description based on direct exchange interactions. Therefore, a three-site model system is considered, including a spin-versatile metal ion $S_M = 0$ or 1 (*e.g.* Ni^{2+} ion in an octahedral environment) and two radical ligands $S_{L_1} = S_{L_2} = 1/2$ (see Figure 3.10). The eigenfunctions of the model Hamiltonian $\hat{H}_0$ written on the neutral configurations (*i.e.* singly occupied on-site orbitals) are decomposed on the local spin states. The contributions of the $S_M = 0$ and $S_M = 1$ components are evaluated in the ground and excited states as a function of the exchange interactions. A key parameter is the metal exchange interaction that not only governs the positions of the non-Hund forms, but also elementary rules that are derived. Then, the energies are corrected using second-order Perturbation Theory to include charge transfers. These contributions account for the fluctuations that must be introduced to go beyond a mean-field picture. The originality of this work stems from the combination of a prototypical Spin CrossOver ion and organic radical ligands, where the weights of the metal local spin states can be modulated. The use of molecular-spin degrees of freedom to encode and/or manipulate quantum information onto magnetic molecules remains a growing field of research.

3.2.2 Description of the model

The system consists of four electrons distributed on ligand- and metal-centred orbitals referred to as φ_{L_1}, φ_{L_2}, φ_M and $\varphi_{M'}$ (see Figure 3.10). In reference to coordination chemistry compounds, the φ_M and $\varphi_{M'}$ orbitals correspond to the d_{z^2} and $d_{x^2-y^2}$ singly occupied atomic orbitals of a tetrahedral d^2 (or octahedral-like d^8) ion. The orbitals φ_{L_1} and φ_{L_2} may be seen as the π-frontier molecular orbitals localised on the radical ligands. In the total spin projection $M_S = 0$ manifold, the zeroth-order Hamiltonian $\hat{H}_0 = \hat{P}\hat{H}\hat{P}$ is built from the full Hamiltonian $\hat{H}$ and

the projector $\hat{P} = \sum_\alpha |\Phi_\alpha\rangle\langle\Phi_\alpha|$ over the subset of six neutral configurations $\{|\Phi_\alpha\rangle\}$ defined as

$$\begin{aligned}\{|\Phi_\alpha\rangle\} = \Big\{ & |\overline{\varphi}_{L_1}\varphi_M\varphi_{M'}\overline{\varphi}_{L_2}|, |\varphi_{L_1}\varphi_M\overline{\varphi}_{M'}\overline{\varphi}_{L_2}|, \\ & |\overline{\varphi}_{L_1}\varphi_M\overline{\varphi}_{M'}\varphi_{L_2}|, |\varphi_{L_1}\overline{\varphi}_M\varphi_{M'}\overline{\varphi}_{L_2}|, \\ & |\overline{\varphi}_{L_1}\overline{\varphi}_M\varphi_{M'}\varphi_{L_2}|, |\varphi_{L_1}\overline{\varphi}_M\overline{\varphi}_{M'}\varphi_{L_2}| \Big\}.\end{aligned} \tag{3.1}$$

This subspace will be referred to as the inner (or model) α-space (following regular notations as used in Ref [249]) characterised by singly-occupied orbitals. The resulting zeroth-order Hamiltonian takes the following form

$$\hat{H}_0 = \sum_{\alpha,\alpha'} H_{\alpha\alpha'} |\Phi_\alpha\rangle\langle\Phi_{\alpha'}| \tag{3.2}$$

From spin coupling algebra $\hat{\boldsymbol{S}} = \hat{\boldsymbol{S}}_{\boldsymbol{M}} + \hat{\boldsymbol{S}}_{\boldsymbol{L_1}} + \hat{\boldsymbol{S}}_{\boldsymbol{L_2}}$, two singlet, three triplet and one quintuplet eigenstates are generated.

The zeroth-order Hamiltonian matrix elements $H_{\alpha\alpha'}$ introduced in equation (3.2) are functions of the on-site energies (one-electron contributions) and positively defined two-electron integrals. The one-electron energies are referenced to the φ_M orbital energy as $\epsilon_{M'}$, ϵ_1 and ϵ_2 for the $\varphi_{M'}$, φ_{L_1} and φ_{L_2} orbitals, respectively (see Figure 3.10). Evidently, the single-occupation of the orbitals in the $\{|\Phi_\alpha\rangle\}$ set of configurations leads to a common $\epsilon_{M'} + \epsilon_1 + \epsilon_2$ value on the diagonal elements of the six-by-six matrix. The off-diagonal matrix elements are linear combinations of the two-electron integrals.

The system may equivalently be examined from two subunits, namely the metal ion centre M and the ligands pair L_1L_2. For the former, the energy difference between the Hund triplet and non-Hund singlet states is $2K_M$, where K_M is the atomic exchange interaction. This is a dominant contribution in free ions, but the energy splitting is evidently much affected by the field generated by the ligands. In Spin CrossOver compounds, the low-spin and high-spin states lie close enough in energy to observe a transition for moderate ligands field modification. In contrast, one would anticipate a negligible Ligand-Ligand exchange integral in synthetic compounds with L_1 and L_2 in trans position (see Figure 3.10). Thus, this integral was set to zero in this model.

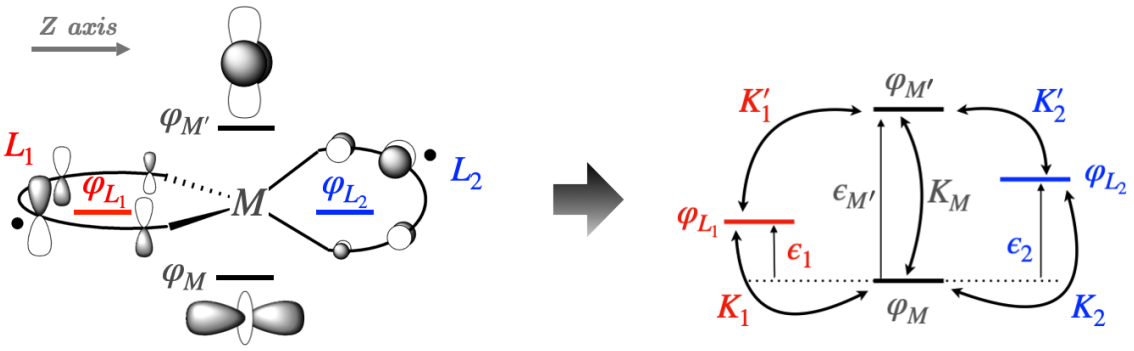

Metal-Ligands molecular complex **Model Hamiltonian with four orbitals**

Figure 3.10: Illustration of a C_{2v}-like symmetry ML_1L_2 model system. (Left panel) representation of the molecular complex composed of a central Spin CrossOver ion M ($S_M = 0$ or 1) coordinated to two radical ligands L_1 and L_2 ($S_{L_1} = S_{L_2} = 1/2$). (Right panel) Associated model Hamiltonian composed of four orbitals. The orbital labels, orbital energies and non-zero direct exchange integrals involved in the zeroth-order Hamiltonian are shown.

After diagonalizing $\hat{H}_0$, the associated eigenvectors $|\Psi\rangle$ (with unperturbed energy E_Ψ) were projected onto the local singlet and triplet states of the M and L_1L_2 subunits. The procedure uses the standard Clebsch-Gordan coefficients algebra presented in subsection (1.4.2). This transformation allows one to evaluate the singlet and triplet weights in the six different states with respect to the parametrization of the model. In the following, all basis set vectors are written as $|S, S_M, S_L\rangle$ where S is the total spin state. S_M and S_L stand for the local spin values on the metal and the ligands pair, respectively. The control of the amount of $S_M = 0$ or 1 (and $S_L = 0$ or 1 on the ligands pair L_1L_2) in the $|S, S_M, S_L\rangle$ wavefunctions makes this class of compounds particularly interesting in molecular magnetism and might enrich the panel of molecular spin-qubits candidates.

After evaluating the eigenstates $|\Psi\rangle$ of the unperturbed Hamiltonian $\hat{H}_0$, the associated zeroth-order energies E_Ψ were corrected using second-order Perturbation Theory to go beyond the mean-field description of the metal-ligands interactions. The fluctuations introducing the electron-electron interactions correspond to charge transfers between the metal centre and the ligands. Following Ref [249], the so-called outer β-space, built from the subset of eight LMCT and eight MLCT perturber configurations $\{|\Phi_\beta\rangle\}$, was introduced. The interaction between the inner α-space and

outer β-space was limited to single charge transfers couplings formally modeled by an interaction Hamiltonian $\hat{V}$ containing a single one-electron hopping integral noted t. In addition, this Hamiltonian was extended to incorporate on-site repulsion parameters U_M (for metal) and U_L (for each ligand).

As described in subsection (1.2.6), the energy correction brought by Perturbation Theory up to second-order reads

$$E_{\Psi}^{PT2} = E_{\Psi} + \sum_{\beta}^{\text{outer-space}} \frac{|\langle \Phi_{\beta}|\hat{V}|\Psi\rangle|^2}{E_{\Psi} - E_{\beta}} \tag{3.3}$$

where $E_{\beta} = \langle \Phi_{\beta}|(\hat{H}_0 + \hat{V})|\Phi_{\beta}\rangle$ is the energy of a given configuration $|\Phi_{\beta}\rangle$. Beyond energy corrections, let us stress that the spin states decomposition is also affected through first-order wavefunction modifications. The perturbers consist of local spin 1/2 states which modify the projection. Nevertheless, the contracted structure leaves the relative weights in the model α-space unchanged.

To conclude, our motivations are twofold. First, it is to trace the arising of *spinmerism* by means of a minimal number of physical parameters (see Fig. 3.10). Proceeding this way naturally offers a great flexibility in terms of explored situations. Specific variations of parameters (more precisely exchange integrals) can reflect the effects of structural changes in realistic molecular systems. The eight-parameter model can be simplified from symmetry arguments keeping only three parameters, and still exotic features are observed. The second motivation of this approach is to open new perspectives in molecular magnetism. The model is inspired from realistic systems including metal centres with two unpaired electrons (*e.g.* analogue to Ni(II) complexes). It extends the traditional views where the local spin multiplicities are fixed quantities. Our intention is to show that significant superpositions of local spin states can be observed in such systems and to unravel the physical conditions that govern such behaviour.

3.2.3 Results and Discussion

All calculations were performed by fixing the K_M value to unity. In the present description, this is the leading parameter that is expected to become vanishingly small for Spin CrossOver ions. The spin states structure is first analyzed from the

zeroth-order Hamiltonian $\hat{H}_0$. Subsequently, the spin states energies are corrected by the outer β-space perturbers to foresee the low-energy spectroscopy of our model system. For $K_M \gg K_i$, K_i' , the spectroscopy splits into two sub-sets identified by the S_M value, $S_M = 1$ and $S_M = 0$. This is the standard situation based on the atomic Hund's states in coordination chemistry compounds. However, the picture might be much different when the direct exchange couplings compete (*i.e.* all K_i and K_i' of the order of K_M), and satisfy particular conditions. In the absence of symmetry (*i.e.* ML_1L_2 compound), the direct exchange couplings are all different and the diagonalization of $\hat{H}_0$ produces eigenvectors which project on pure $S_M = 0$ or $S_M = 1$ states on the metal ion. A strict separation between the Hund and non-Hund states is observed. The systems ruled by such Hamiltonian fall in the traditional category of metal ion complexes where the metal spin state S_M is a good quantum number. Nevertheless, this particular picture is deeply modified as soon as a higher symmetry is introduced by reducing the number of parameters.

Let us first examine the spin states structures for $K_1 = K_2$, while maintaining $K_1' \neq K_2'$. This scenario is expected in spiro-like geometry (such as the Fe(II) and Co(II) complexes studied in Refs [220, 227]) where the interactions are invariant along the z-axis for similar ligands $K_1 = K_{\varphi_{L_1},z^2} = K_{\varphi_{L_2},z^2} = K_2$ whereas they significantly differ in the perpendicular xy-plane ($K_1' = K_{\varphi_{L_1},x^2-y^2} \neq 0$ and $K_2' = K_{\varphi_{L_2},x^2-y^2} \simeq 0$). Both singlet and triplet manifolds exhibit combinations of local singlet and triplet states. In the following, the amplitudes on the $|S = 1, S_M, S_L\rangle$ and $|S = 0, S_M, S_L\rangle$ configurations are written as $\lambda_{S_M S_L}$ and $\mu_{S_M S_L}$, respectively. Thus, the weight on the high-spin ($S_M = 1$) metal centre for the triplet eigenstates given by

$$\begin{aligned} |S = 1, S_M, S_L\rangle = \lambda_{11}|S = 1, S_M = 1, S_L = 1\rangle \\ +\lambda_{10}|S = 1, S_M = 1, S_L = 0\rangle \\ +\lambda_{01}|S = 1, S_M = 0, S_L = 1\rangle \end{aligned} \tag{3.4}$$

reads $\lambda_{11}^2+\lambda_{10}^2$, a value which may differ from zero or one (see Table 3.1). One should note that this mixture does not result from Spin-Orbit Coupling effects which are totally absent in the present description. Such a spin structure that incorporates high-spin ($S_M = 1$) and low-spin ($S_M = 0$) states on the metal centre is expected from spin algebra, but deeply contrasts with the traditional views on inorganic compounds. In analogy with the mesomerism effect that accounts for electronic

charge delocalization, the model highlights the so-called *spinmerism* phenomenon that involves the spin degree of freedom. Finally, the appearance of the $|S = 1, S_M = 1, S_L = 0\rangle$ and $|S = 1, S_M = 0, S_L = 1\rangle$ contributions (λ_{10} and λ_{01} amplitudes, respectively) stresses the arising of entanglement in the state description. Quantum entanglement is here reflected by the correlation arising between both ligands and metal local spin states S_L and S_M that naturally adjust to fulfil a spin $S = 1$ for the full molecular system. Note that, from a pure chemist point of view, spin entanglement would represent a rather unusual picture especially in the case of coordination chemistry compounds where it is usually assumed that local metal and ligand spins states are fixed. This hypothesis however conflicts with fundamental spin and angular momentum algebra which in practice does not forbid the arising of such a feature between two interacting spin subsystems.[250, 251]

	$K_1 = K_2 = 0.25$	$K_1 = K_2 = 0.50$
$S = 1$	81%	90%
$S = 0$	19%	10%

Table 3.1: Metal triplet and singlet proportions in the second lowest lying triplet state (see equation (3.4)), $K'_1 = 0.60$, $K'_2 = 0.80$ (K_M unit).

Moving to Td-symmetry compounds ($L_1 = L_2$) characterised by $K_1 = K_2$ and $K'_1 = K'_2$, the spin states structure gets further modified. Whereas one triplet state simply reads $|S = 1, S_M = 1, S_L = 0\rangle$, the other two exhibit a systematic combination as

$$\begin{aligned} |S = 1, S_M, S_L\rangle = \lambda_{11}|S = 1, S_M = 1, S_L = 1\rangle \\ + \lambda_{01}|S = 1, S_M = 0, S_L = 1\rangle \end{aligned} \tag{3.5}$$

The spectroscopy incorporates local high-spin ($S_M = 1$) and low-spin states ($S_M = 0$) on the metal centre whilst the ligand pair remains $S_L = 1$. As seen in Table 3.2 for $K'_1 = K'_2 = 0.75$, the proportions are much affected by any modification of the $K_1 = K_2$ value. In practice, exchange integrals are very sensitive to the structure (interatomic bond distances) and the chemical details of the radical ligands. Therefore, one may expect to modify the superposition of metal spin states induced by

structural deformations on the coordination complex. In practice, this structural modulation of the system would offer a possible way to encode, and to manipulate, information onto the spin-degree of freedom. The molecular complex behaves as a molecular spin-qubit carrying a quantum superposition of local spin states on the metal with tunable amplitudes.

	$K_1 = K_2 = 0.25$	$K_1 = K_2 = 0.50$
$S = 1$	79%	86%
$S = 0$	21%	14%

Table 3.2: Metal triplet and singlet proportions in the second lowest lying triplet state (see equation (3.4)). $K_1' = K_2' = 0.75$ (K_M unit).

Finally, it can be shown that the mixing reaches a maximum $\lambda_{11}^2 = \lambda_{01}^2$ (equal weights on the $S_M = 1$ and $S_M = 0$) for a first rule $2K_M = K_1 + K_1'$ (see Appendix D). Even though this condition is difficult to achieve from a synthetic point of view, it suggests that at least one ligand-metal direct exchange coupling should be comparable to K_M. Any deviation from $2K_M = K_1 + K_1'$ leads to variations of the metal triplet state component λ_{11}^2 (and singlet λ_{01}^2) which are shown in Figure 3.11 as a function of the dimensionless parameter

$$Q = \frac{K_1' - K_1}{2(K_M - K_1)}. \tag{3.6}$$

For $Q < 1$, *i.e.* $2K_M > K_1 + K_1'$, the second lowest lying triplet state is dominated by the $|S = 1, S_M = 1, S_L = 1\rangle$ configuration, whereas the configuration $|S = 1, S_M = 0, S_L = 1\rangle$ is the leading one for $Q > 1$. In the vicinity of $Q = 0.7$, the changes reach up to 3.5% for deviations smaller than 10%. Therefore, any geometrical change induced by external stimuli (*e.g.* pressure, temperature) is likely to deeply modify the spin state structure whatever the K_M value. This observation makes this class of compounds particularly appealing in the generation of innovative spin-qubits.

Moving away from the Td-symmetry, the $K_1 = K_2 = K_1'$ situation is examined. While the mixing occurred in the triplet manifold, the singlet states are now the

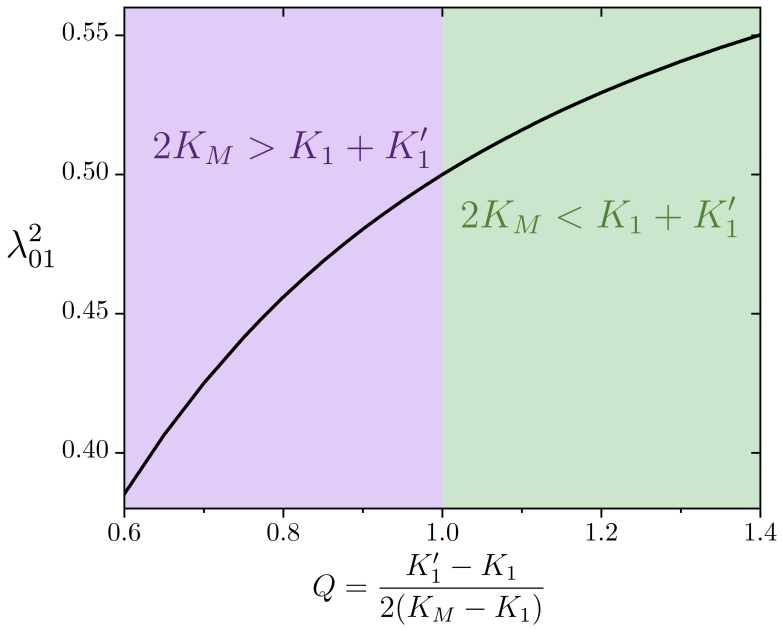

Figure 3.11: Variations of the $S_M = 0$ weight λ^2_{01} as a function of the dimensionless parameter Q (see equation (3.6)) in the second lowest lying triplet state (see equation (3.5)) for a Td compound characterised by $K_1 = K_2$ and $K'_1 = K'_2$. The mixing is maximal ($\lambda^2_{11} = \lambda^2_{01} = 1/2$) for $Q = 1$ (*i.e.* $2K_M = K_1 + K'_1$).

intriguing ones. As a matter of fact, superpositions

$$\begin{aligned} |S = 0, S_M, S_L\rangle = \mu_{11}|S = 0, S_M = 1, S_L = 1\rangle \\ + \mu_{00}|S = 0, S_M = 0, S_L = 0\rangle \end{aligned} \tag{3.7}$$

are observed. A marked difference is the appearance of different spin states on both the metal centre and the ligands pair. The entanglement between these open-shell subunits reaches a maximum $\mu^2_{11} = \mu^2_{00}$ for $2K_M = 3K_2 + K'_2$. Since all exchange values are positive, the condition $K_2 < 2K_M/3$ is necessary for this equality to be fulfilled. For K_2 values larger than $2K_M/3$, the relative weights ratio is reduced until $2K_M = 2K_2 + 2K'_2$, a second rule where $3\mu^2_{11} = \mu^2_{00}$ (see Appendix D). Such condition displayed by less symmetrical ML_1L_2 compounds offers another possibility to address the local spin states superposition. At this stage, the description concentrates on the $\hat{H}_0$ eigenvectors analysis, leaving out the important electronic correlation effects. Therefore, the energies were corrected using second-order Perturbation Theory accounting for charge fluctuations, and depicting a more realistic electronic structure.

Such framework is applicable for large enough energy separations between the $\hat{H}_0$ and the perturbers energies, with respect to the hopping integral t. This picture is not valid for systems governed by superexchange contributions (strong field regime) but applicable to intermediate ligand field regimes where several spin multiplicities compete (*i.e.* Spin CrossOver compounds). The relative weights of the $S_M = 1$ and $S_M = 0$ states are not affected by the outer β-space, but the spin multiplicity of the ground state is likely to be changed.

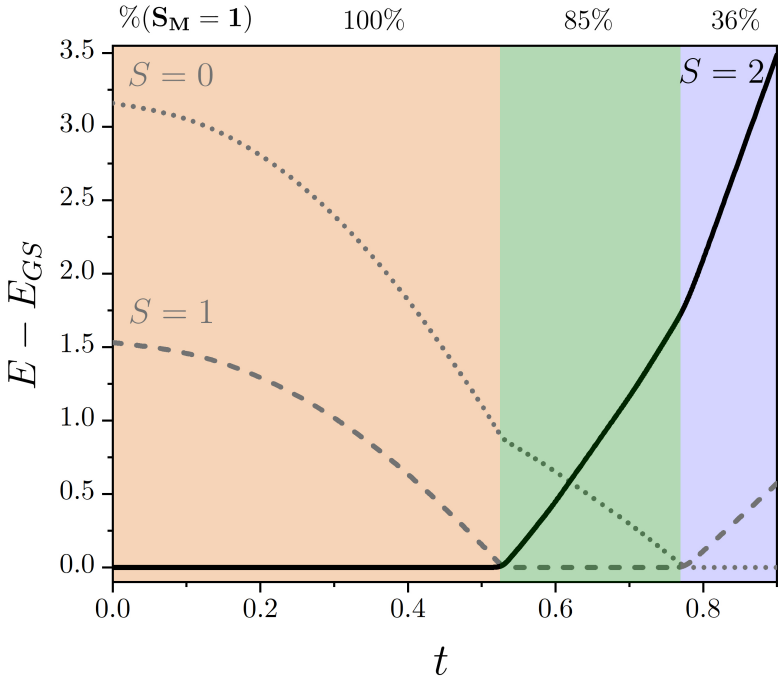

Figure 3.12: Low-lying states energies of a ML_1L_2 system as a function of the hopping parameter t in K_M unit. The $\hat{H}_0$ energies are corrected using second-order Perturbation Theory with the MLCT and LMCT as perturbers with fixed parameters (K_M unit): $U_L = 2.95$, $U_M = 4.0$, $\epsilon_{M'} = 0.80$, $\epsilon_1 = -2.80$ and $\epsilon_2 = -1.50$, $K_1 = 0.35$, $K_2 = 0.10$, $K_1' = 0.58$ and $K_2' = 0.75$. The ground state energy is used as a reference.

As seen in Figure 3.12, the ground state switches from quintet to successively triplet, and singlet as the hopping integral value is increased. For $t = 0.52$, the energy correction to the $S = 1$ state is calculated 33%. This triplet becomes the ground state and is dominated by a $S_M = 1$ spin state (85%). As t is further increased, the ground state switches to a singlet exhibiting a 36% proportion on the local $S_M = 1$. Let us mention that a perturbative treatment in this regime is more than questionable but the picture survives. Not only is the nature of the ground state

sensitive to the strength of the ligand field following traditional pictures, but the metal centre spin states contributions are significantly modified.

Evidently, any realistic system includes both direct exchange and charge transfers contributions which compete to ultimately dictate the ground state and low-lying excited states. However, our model sets the stage to foresee ground states where the local spin on the metal centre is not uniquely defined, being a superposition of different spin multiplicities. The presence of open-shell ligands as entangled partners in the coordination sphere is a prerequisite for this manifestation. Thus, the variability offered by organic radicals combined with mid-series metal ions should give access to original compounds with fundamental and applied interests.

3.2.4 Preliminary conclusion

The spin states structure of a four electron/four orbital coordination compound ML_1L_2 built on a Spin CrossOver metal ion (M =d^2 or d^8 ion such as Ni^{2+}) and radical ligands (L_1 and L_2 such as oxoverdazyl) was examined on the basis of a model Hamiltonian. The zeroth-order structure includes the direct exchange interactions, whereas the LMCT and MLCT accounting for superexchange interactions were treated using second-order Perturbation Theory. From the spin state versatility of the metal ion ($S_M = 0$ or 1), the spin states of the complex combine different local spin multiplicities. Depending on the relative values of the direct exchange interactions, the eigenfunctions of the zeroth-order Hamiltonian can reach an equal mixture of the $S_M = 0$ and 1 metal states entangled with ligands $S_L = 1$ and 0 states. Spin projection gives rise to rules involving the metal atomic exchange interaction K_M and the sum of the ligand-metal K_1 and K_2. Despite its simplicity, the model stresses that under specific conditions (Spin CrossOver ion ferromagnetically interacting with radical ligands) superpositions of local spin states are observed and possibly varied. Evidently, such manifestation of entanglement is anticipated from standard spin algebra. However, conditions for superposition of states are suggested here and enlarge the traditional views in coordination chemistry compounds that usually decide on a given spin state. By experimentally probing the local spin density, such molecular compounds might become original targets for spin-qubits generation. *Spinmerism* behaviour is expected in heavier element-based

compounds where the total angular momenta can vary.[252] However, the mixing between spin-multiplicities might then be dominated by Spin-Orbit effects, which mask the here-reported phenomenon.

Naturally, this work is a first step of a longer run project focused on the utility of *spinmerism* in quantum information technologies. In practice, complementary studies are envisioned to characterize if complex quantum superpositions are possible. *Ab initio* calculations should be performed to assess the changes in the exchange integrals of synthetic metal-ligand compounds and experiments should be conducted to reproduce the here reported *spinmerism* behaviours. On longer terms, quantum dynamical studies should also be considered to determine potential ways to time-control the properties of the systems.

3.3 *Ab initio* study of *spinmerism* in a d^7 Co(II) oxoverdazyl complex.

The spin states of a Co(II) oxoverdazyl compound are investigated by means of wavefunction-based calculations (CAS+DDCI2). Within a ca. 233 K energy window, the ground state and excited states display a structure-sensitive admixture of low-spin $S_M = 1/2$ in a dominant high-spin $S_M = 3/2$ Co(II) ion as indicated by the Localized Molecular Orbitals. The puzzling spin zoology that results from the coupling between open-shell radical ligands and a Spin CrossOver metal ion gives rise to this unusual scenario, which extends the views in molecular magnetism. In agreement with experimental observation, the low-energy spectroscopy is very sensitive to deformations of the coordination sphere, and a growing admixture of Co(II) low-spin is evidenced from the calculations. This is the first time the spinmerism phenomenon is reported in a molecular complex.

keywords: *spinmerism*, *ab initio*, wavefunction methods

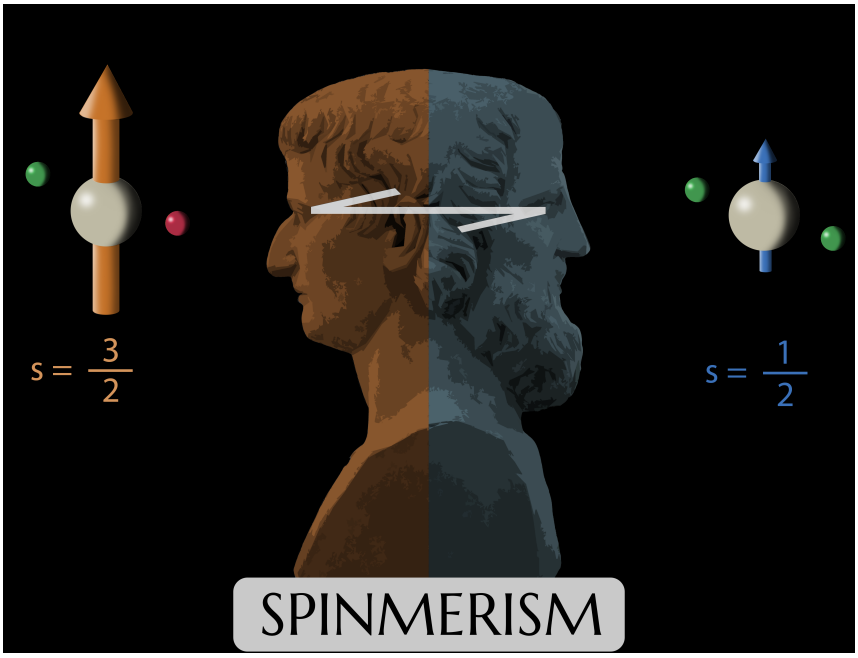

3.3.1 Introduction

In self-assemblies and materials, a spin transition picture may be favoured over exchange-interaction models, reflecting the flexibility of the contacts in purely

organic verdazyl radicals-based materials.[253, 254] In this context, cobalt compounds are known to be interesting targets since valence tautomerization as well as temperature-dependent Spin CrossOver can be triggered by varying the coordination sphere of the Co ion. In coordination chemistry materials, the Co ion has attracted much attention with the growing interest for photomagnetic properties in FeCo Prussian analogue.[222] The cyanide bimetallic network is very sensitive to the alkali environment and a low-spin Co(III) to high-spin Co(II) is observed.[255]

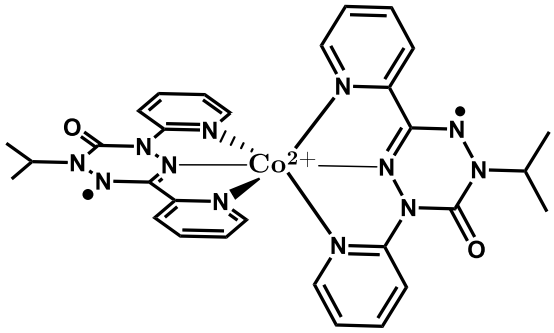

Figure 3.13: Compound **1**.

As a prime example, Valence Tautomerism has been recently reported [256] in the $[Co(dipyvd)_2]^{2+}$ (dipyvd = 1-isopropyl-3,5-dipyridil-6-oxoverdazyl) coordination compound **1** (see Figure 3.13). A combination of magnetic susceptibility, temperature-dependent UV and EPR experiments concluded on a valence tautomeric equilibrium between a high-spin $S_M = 3/2$ Co(II) and a low-spin $S_M = 0$ Co(III). Nevertheless, the occurrence of a high-spin Co(II) in tetragonal environment, not to mention the strong ferromagnetic coupling traditionally observed in cobalt-verdazyl compounds,[257] question the intimate nature of the interactions that characterize this complex. The possibility to manipulate spin state and to trigger Valence Tautomerism in solution makes this cobalt-verdazyl coordination compound particularly fascinating. The authors concluded that there is still to be learned and that a coherent explanation remains elusive. Part of the answer may be found in moving away from overly simplistic models as mentioned by Hicks and coworkers.[258] How much robust is the traditional view of a metal ion, either high-spin or low-spin, in a crystal field? Local singlet and triplet spin values can emerge from the environment generated by two open-shell dipyvd radical ligands. Besides, Co(II) being a Spin CrossOver (SCO) ion, a high-spin $S_M = 3/2$ and a low-spin

$S_M = 1/2$ Co(II) ion (non-Hund form following Bastardis et al. [24]) are likely to compete depending on the crystal field strength. As a consequence, the observed total spin states of the complex may result from several intricated local spin states on the ligands and the metal ion.

3.3.2 Computational details

The presence of open-shells on both the metal ion suggests the use of a wavefunction-based method. Not only can wavefunction-based calculations reach spectroscopic accuracy (a few tens of wave-numbers), but the nature of the spin states can be analyzed based on Localized Molecular Orbitals (LMOs), *i. e.* site orbitals. The energy splittings cannot be reproduced by a mere Heisenberg-Dirac-Van Vleck (HDVV) Hamiltonian picture (see subsection 1.5.2) whilst the structures of the correlated wavefunctions deviate from the picture given by the spin-coupling between a local Co(II) high-spin and dipyvd radicals.

Herein, wavefunction-based calculations (CAS+DDCI) were conducted to examine the electronic structures of low-lying states of **1**. Using such methodology, the microscopic origin of exchange couplings can be investigated, and spin Hamiltonians rationalized or invalidated. In the Complete Active Space Self-Consistent Field method (CASSCF), the Complete Active Space includes the three unpaired electrons on the Co and two on the oxoverdazyl ligands in **1**. The CAS[5,5]SCF hexuplet MOs are then transformed into LMOs, and shown in Figure 3.15. The localization procedure of DoLo (see section 1.3) affords a reading of the multireference wavefunction following a Lewis valence-like picture. CASSCF and MRCI calculations were performed as described in Appendix E. The CI calculations eigenfunctions were projected onto the local spin states of the oxoverdazyl ligands ($s_{L1} = s_{L2} = 1/2$) and the Co(II) ion ($S_M = 1/2$ or $3/2$). This allows for a decomposition into the different intricated metal-ligand contributions. A fictitious $[Zn(dipyvd)_2]^{2+}$ coordination compound **2** was constructed with a closed-shell diamagnetic divalent cation to mimic the electrostatic presence of the Co(II). For this analogue **2**, a similar procedure was used starting from a CAS[2,2]SCF calculation to generate a set of MOs, followed by the CAS[2,2]+DDCI evaluation of the singlet-triplet energy difference.

3.3.3 Results and Discussion

From a traditional crystal field picture, one would naturally start by considering the two radical ligands as the so-called environment of the metal centre. Following this view, the Co(II) ion undergoes a field that is characterized by local singlet or triplet spin multiplicities. Thus, our first intention was to evaluate the energy difference between those local spin states. From a CAS[2,2]SCF calculation performed on **2**, the magnetic orbitals of the local triplet state are essentially the singly occupied MOs localized on each dipyvd radical (see Figure 3.14). As expected, the local singlet and triplet states are quasi-degenerated with a triplet-singlet CAS[2,2]+DDCI energy difference $E_S - E_T = 3$ K. This result suggests that the total spin states in **1** may involve a local $S_L = 1$ as well as a $S_L = 0$ environment. From this point of view, one can anticipate modulations of the crystal field acting on the SCO Co(II) metal centre.

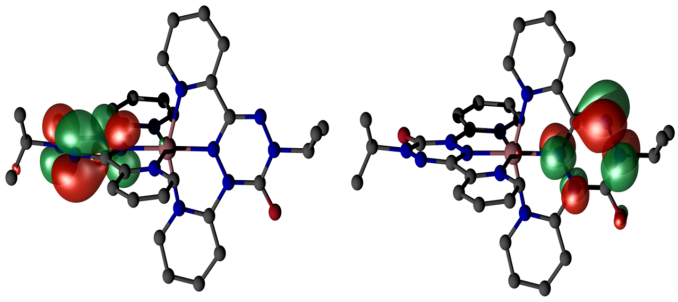

Figure 3.14: CAS[2,2] triplet MOs of the fictitious compound **2**, Zn analogue of **1**.

In order to explore deeper the magnetic behaviour and to provide a spin description of **1**, calculations were then conducted starting from a picture that involves five unpaired electrons in five MOs (CAS[5,5]SCF). Any enlargement of the active space to CAS[9,7]SCF leads to two MOs of d-type character with occupation numbers close to two. The CAS[5,5]SCF MOs were then localized either on the metal centre ($3d_{z^2}$, 0.74 $3d_{xz}$ 0.68 $3d_{x^2-y^2}$, $3d_{xy}$) or on the dipyvd ligands (see Figure 3.15). This procedure allows for a valence-bond like reading of the wavefunctions constructed on orthogonal site-orbitals. Assuming a $S_M = 3/2$ high-spin value on the Co(II) ion, four low-lying spin states S can be anticipated, namely a doublet, two quartets and a hexuplet. A very different scenario holds for a Co(II) low-spin $S_M = 1/2$, resulting in two doublet and a quartet state. Clarifications are readily accessible from *ab initio* CAS[5,5]+DDCI calculations which give access to the low-energy spectrum.

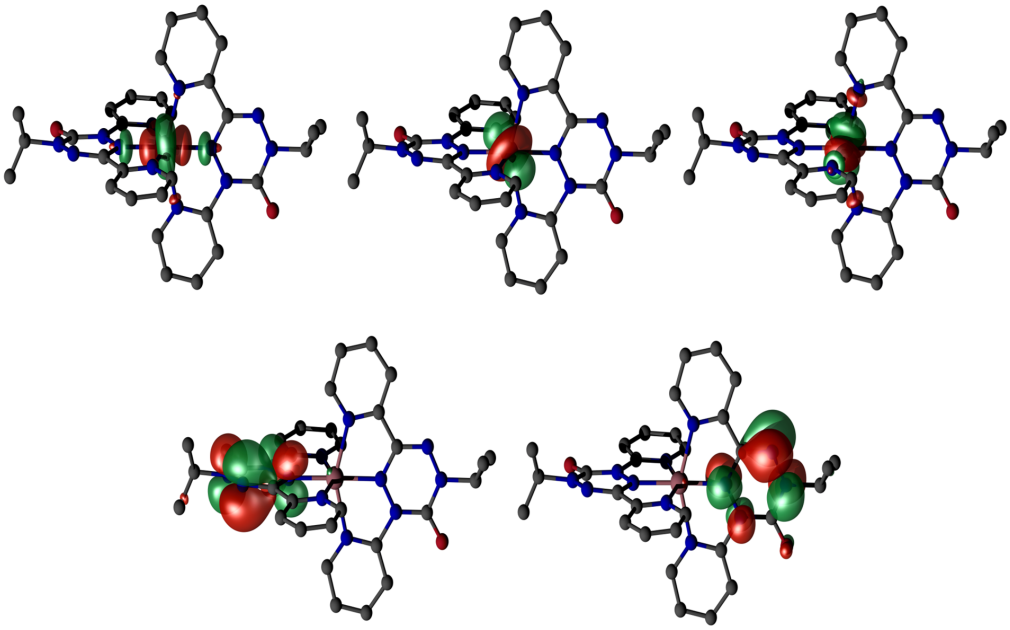

Figure 3.15: CAS[5,5] hexuplet Localized Molecular Orbitals of **1**.

Due to the system size and the number of open-shells, a CAS[5,5]+DDCI level of calculation cannot be reached, and our conclusions are based on CAS[5,5]+DDCI2 spectrum. Even though part of the screening effects is not included, the structures of the wavefunctions are well-defined at this level of approximation. First, the ground state is a doublet (see Figure 3.16) which can be analyzed using the expansion over determinants built on LMOs. It is dominated by a $S_M = 3/2$ Co(II) ion and a $S_L = 1$ environment. A similar analysis holds for the first quartet state, and naturally for the hexuplet state.

Therefore, it is rather tempting to fit the low-energy spectrum using a single-parameter HDVV Hamiltonian $\hat{H}_{1-p} = -2J\hat{\boldsymbol{S}}_{\boldsymbol{M}}\hat{\boldsymbol{S}}_{\boldsymbol{L}}$, where J is the exchange coupling between $S_M = 3/2$ and $S_L = 1$ local spins. Within this description, the ratio between the quartet-doublet and hexuplet-doublet energy differences is readily evaluated 0.375 (see Appendix E). However, the CAS[5,5]+DDCI2 ratio (*ca.* 0.25) strongly deviates from this value, not to mention the presence of a competing quartet state dominated by a $S_L = 0$ environment which cannot be described (see **blue** dashed state in Figure 3.16). Thus, the spin Hamiltonian was extended by the introduction of two exchange coupling constants j_1 and j_2 between the metal centre and the two individual ligands $\hat{H}_{2-p} = -2j_1\hat{\boldsymbol{S}}_{\boldsymbol{M}}\hat{\boldsymbol{s}}_{\boldsymbol{L_1}} - 2\boldsymbol{j_2}\hat{\boldsymbol{S}}_{\boldsymbol{M}}\hat{\boldsymbol{s}}_{\boldsymbol{L_2}}$ (two-parameter HDVV Hamiltonian). Lifting the $S_L = 1$ constraint allows for the description of four

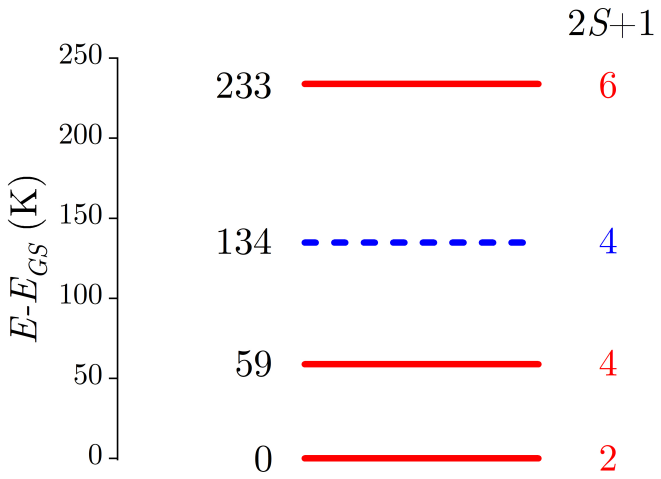

Figure 3.16: Low-energy spectrum of **1** calculated at the CAS[5,5]+DDCI2 level. The ground state energy is used as reference energy. Spin multiplicities $2S+1$ are given.

spin states resulting from $S_M = 3/2$, and $s_{L_1} = s_{L_2} = 1/2$ local spin states. Four CAS[5,5]+DDCI2 energy values give access to three energy differences which can be compared to the analytical expressions of such spin Hamiltonian. A measure of the robustness of this picture is the identification of a set (j_1, j_2) that reproduces the *ab initio* excitation energies. Besides, the geometry of **1** suggests that j_1 and j_2 should be very similar and any strong deviation might not be acceptable from a physical point of view. From the fitting procedure using the $S = 1/2$, first excited 3/2 and 5/2 states, we find $j_1 = -16$ K and $j_2 = -42$ K. Our calculations support that both ligands are antiferromagnetically coupled to the Co ion. This conclusion is to be contrasted with some model that suggested with great care the simultaneous presence of ferromagnetic and antiferromagnetic interactions in some Co analogue.[259] Nevertheless, not only do the antiferromagnetic couplings j_1 and j_2 values strongly differ, but the second excited quartet is then positioned 141 K above the ground state, in disagreement with the calculated value (see Figure 3.16). Finally, the interaction between the ligand spins was introduced in a three-parameter HDVV Hamiltonian $\hat{H}_{3-p} = -2j_1\hat{\boldsymbol{S}}_{\boldsymbol{M}}\hat{\boldsymbol{s}}_{\boldsymbol{L_1}} - 2j_2\hat{\boldsymbol{S}}_{\boldsymbol{M}}\hat{\boldsymbol{s}}_{\boldsymbol{L_2}} - 2j_{12}\hat{\boldsymbol{s}}_{\boldsymbol{L_1}}\hat{\boldsymbol{s}}_{\boldsymbol{L_2}}$ constructed on three coupling constants. Evidently, the three CAS[5,5]+DDCI2 energy differences can be reproduced, and $j_1 = -20$ K, $j_2 = -39$ K and $j_{12} = -20$ K are found. This picture is consistent with spin frustration consideration. However, the exchange couplings ratio j_1/j_2 still deviates from unity without any particular justification. Besides,

the antiferromagnetic coupling between the dipyvd radicals j_{12} is significantly larger than the singlet-triplet energy difference previously calculated in **2**. Whatever the extension of the HDVV Hamiltonian, the fitting to the *ab initio* spectrum leads to some inconsistencies that deserve further investigations.

At this stage, one may wonder whether a given total spin state S may be produced through different spin coupling schemes, involving the contacts between a versatile environment generated by two radical ligands ($S_L = 0$ or 1) and a spin crossover ion ($S_M = 1/2$ or $3/2$). As a matter of fact, ingredients for entanglement manifestation are gathered in this particular compound. While the flexibility of the environment is rather natural and immediately invalidates the single-parameter Hamiltonian $\hat{H}_{1-p} = -2J\hat{\boldsymbol{S}}_{\boldsymbol{M}}\hat{\boldsymbol{S}}_{\boldsymbol{L}}$, ($S_M = 3/2$ and $S_L = 1$), the local spin S_M on the metal centre might not be uniquely defined.

To push further the analysis of the interactions in **1**, the *ab initio* wavefunctions were projected onto the local metal and ligands spin states S_M and S_L. For the $S = 3/2$ (first excited state, or ground state under distortion), the configurations amplitudes are given in Table 3.3 and compared to the ones resulting from a $S_M = 3/2$ and $S_L = 1$ coupling scheme (Clebsch-Gordan coefficients as described in section 1.4.2). Let us mention that the first two configurations necessarily involve a $S_M = 3/2$ spin state on the metal whereas the ligands spin state can be either $S_L = 0$ or 1. The last three configurations are characteristic of $S_L = 1$ and a metal spin state $S_M = 3/2$ or $1/2$. Though small, the observed deviations are indicative of a contribution of $S_M = 1/2$ and $S_L = 0$. Quantitatively, a proportion of 0.06% for $S_M = 1/2$ and 0.001% for $S_L = 0$ were estimated. Remembering the valence tautomeric behaviour of **1** in solution, these contributions might be influenced by structural changes. In particular, it is known that SCO phenomenon is accompanied by modulations of the coordination sphere (*ca.* 0.2 Å variations).[260] Besides, a significant charge redistribution is calculated in this kind of compounds.[261] In the light of the small deviations, one may question the accuracy of our calculations. For all those reasons, the structures of the wavefunctions were examined as the geometry of the complex is varied. First, a breathing deformation that symmetrically modifies the Co-N' axial bonds (slippage in Figure 3.17) was applied to modulate the crystal field generated by the ligands.

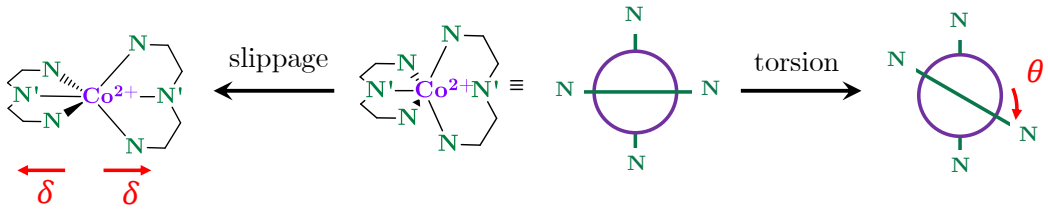

Figure 3.17: Deformations of the coordination sphere of **1**. Left: symmetric slippage of the ligands along the (N'-N') axis. Right: torsion of the two ligands around the (N'-N') axis.

Upon contraction $\delta = -0.15$ Å, the spin state ordering is modified with a $S = 3/2$ ground state dominated by $S_M = 3/2$ and $S_L = 1$. As expected from Tanabe-Sugano view of a d^7 ion, the growth of the $S_M = 1/2$ spin contribution on the Co ion is observed (see Table 3.3), while the so-called high-field regime is reached. The $S_M = 1/2$ weight significantly increases to reach 0.12% for $\delta = -0.15$ Å. On the contrary, this contribution is reduced to 0.04% when the coordination sphere is expanded with $\delta = +0.10$ Å. These variations which agree with an expected trend are a reflection of a physical phenomenon rather than a result of numerical imprecisions. This sensitivity to environment was reported for this particular compound by comparing the solid and solution phases, but also in other organic-based materials.[254, 262] Then, a torsion of the two ligands was applied (see Figure 3.17), and similar conclusions can be drawn. Upon weak distortions, the spin multiplicity of the ground state is changed, and the mixing of different spin states on the metal varies, entangled to the spin environment.

L_1.MMM.L_2	Clebsch-Gordan	Xray	Contraction	Expansion	Torsion
↓.↑↑↑.↑	0.548	0.545	0.400	0.568	0.544
↑.↑↑↑.↓	0.548	0.550	0.674	0.526	0.551
↑.↓↑↑.↑	−0.365	−0.350	−0.353	−0.338	−0.346
↑.↑↓↑.↑	−0.365	−0.362	−0.362	−0.353	−0.358
↑.↑↑↓.↑	−0.365	−0.384	−0.380	−0.384	−0.390

Table 3.3: Wavefunction structure (CAS[5,5]+DDCI2 level) of the $S = 3/2$ state for the Xray structure and distorted geometries $\delta = -0.15$ Å, $\delta = +0.10$ Å, and $\theta = +5°$ (see Figure 3.17).

Despite small deviations observed in Table 3.3, our suggestion is supported by the observed modification of the $S_M = 3/2$ and $S_M = 1/2$ contributions to the $S = 3/2$ state of **1**. Evidently, the electrostatic changes that accompany the $S_L = 1$ to 0 spin change are rather small ($E_S - E_T = 3$ K from our calculations). Should the field generated by the ligands be stronger, the metal ion might consist of a more pronounced weight on the $S_M = 1/2$ state. Such compound that gathers a SCO ion and organic radical ligands offers a variety of spin-coupling schemes that may not be reproduced by a given spin state on the Co centre. This is to be considered as a limiting case where Hund and non-Hund forms are close in energy in an intermediate crystal field produced by radical ligands. These observations put forward the *ab initio* evidence of weak *spinmerism* behaviour in this Co(II) complex.

3.3.4 Preliminary conclusion

While trapped as high-spin in the solid state, the electronic structure of bis(oxoverdazyl) Co(II) compound **1** is deeply modified in solution. This compound is magnetically intriguing and was inspected using the correlated quantum chemistry CAS[5,5]+DDCI2 method. The controversy regarding the magnetic exchange interactions is reflected by a structure sensitive low-energy spectrum. Indeed, the ground state spin multiplicity is switched from a $S = 1/2$ to $S = 3/2$ upon weak distortions. From our *ab initio* calculations, we observed that the spin states emerge from an unusual scenario that combines various local spin states. The manifestation of entanglement results from the simultaneous presence of a SCO Co(II) ion and a crystal field produced by a set of open-shell radicals. The mixing of local high-spin and low-spin states in the construction of the total spin state S is the direct observation of the *spinmerism* phenomenon in a d^7 inorganic complex. Upon weak distortions of the coordination sphere, the superposition of local spin states induced by the *spinmerism* behaviour is tuned. Further studies to quantify the exchange integrals in this complex are to be envisioned, in order to relate with the model Hamiltonian presented in section (3.2). Still, this *ab initio* analysis evidences a weak *spinmerism* effect. These views somewhat extend the traditional picture in transition metal complexes where the spin multiplicity is fixed and governed by the metal ion.

3.4 *Ab initio* study of *spinmerism* in a d^6 Fe(II) oxoverdazyl complex. Modifications of Tanabe-Sugano d^6 diagram by *excited state spinmerism.*

Quantum entanglement between the spin states of a metal centre and radical ligands is suggested in a Fe(II) $[Fe(dipyvd)_2]^{2+}$ compound (dipyvd = 1-isopropyl-3,5-dipyridil-6-oxoverdazyl). Wavefunction ab initio (CAS+DDCI2) inspections were carried out to stress the versatility of local spin states. The construction of Localized Molecular Orbitals allows for a reading of the wavefunctions and projections onto the local spin states. The low-energy spectrum is well-depicted by a Heisenberg-Dirac-Van Vleck picture. A 60 cm^{-1} ferromagnetic interaction is calculated between the radical ligands with the $S = 0$ and 1 states largely dominated by a local low-spin $S_{Fe} = 0$. In contrast, the higher-lying $S = 2$ states are superpositions of the local $S_{Fe} = 1$ (17%, 62%) and $S_{Fe} = 2$ (72%, 21%) spin states, caused by excited state spinmerism. Such mixing extends the traditional picture of a high-field d^6 Tanabe-Sugano diagram. Even in the absence of Spin-Orbit Coupling, the avoided crossing between different local spin states is triggered by the field generated by radical ligands. This puzzling scenario emerges from versatile local spin states in compounds which extend the traditional views in molecular magnetism.

keywords: *excited state spinmerism*, *ab initio*, Tanabe-Sugano, spin-qubits

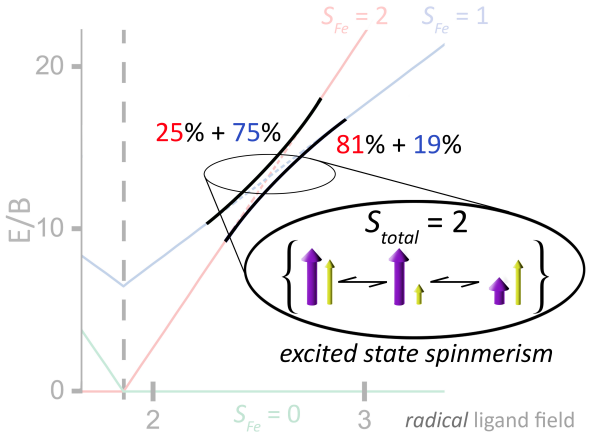

3.4.1 Introduction

The Co(II) oxoverdazyl compound presented in section (3.3) has questioned the traditional picture of a metal ion as either high-spin or low-spin, in the electrostatic field of neighbouring radical ligands. In particular, its ground state displays a structure-sensitive admixture of low-spin $S_{Co} = 1/2$ in a dominant high-spin $S_{Co} = 3/2$, a feature of *spinmerism*. The mixing was further interpreted by inspecting a d^7 Tanabe-Sugano diagram that exhibits a doublet-quartet crossing in the intermediate ligand field regime. Since the ligand field includes Coulomb and direct exchange contributions in a complex built on spin-coupled partners, one may wonder whether different local spin states may coexist on the metal ion. The introduction of radical ligands may indeed disrupt the assumption of a given spin state on the metal centre in the description of ground and excited states. Inspired by these observations,

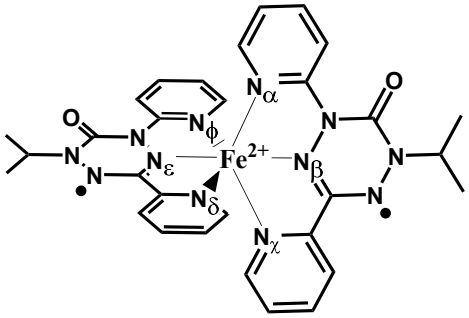

Figure 3.18: $[Fe(dipyvd)_2]^{2+}$ compound **3** from Ref [263]. The Xray Fe-N_i distances $i = \alpha - \phi$ are 1.98, 1.84, 1.95, 2.00, 1.85, and 1.98 Å, respectively.

the pseudo-octahedral Fe(II) oxoverdazyl compound **3** $[Fe(dipyvd)_2]^{2+}$ (dipyvd = 1-isopropyl-3,5-dipyridil-6-oxoverdazyl) was considered as another prototype to be examined (see Figure 3.18).[263] Magnetic and spectroscopic properties were reported in the literature and complemented by density functional theory-based calculations suggesting a low-spin iron centre.[263] Bond lengths (for both ligand and metal ion) are characteristic of a low-spin Fe(II) coordinated to neutral radical verdazyl ligands. In particular, the Fe-N bond distances were reported *ca.* 1.95 Å, as mentioned in Figure 3.18. Such spin picture is also consistent with the IR spectrum, and the 5-300 K magnetic susceptibility measurements support a low-spin metal centre. Fe(II) being a Spin CrossOver metal ion, any intermediate ligand field should be appropriate to observe the coexistence of a $S_{Fe} = 0$ (low spin) and $S_{Fe} = 2$ (high spin).

As seen in Figure 3.19, the d^6 Tanabe-Sugano diagram exhibits a crossing between the excited triplet and excited quintet states. Therefore, a similar manifestation of spin states mixing observed in the ground state of the Co(II) complex might appear in the excited states of this Fe(II) analogue. Guided by this observation in the high-field regime, we thought that *excited state spinmerism* might be anticipated, with total spin states resulting from combinations of local $S_{Fe} = 1$ and $S_{Fe} = 2$. For all these reasons, *ab initio* calculations were carried out to inspect the energy spectrum of **3** (shown in Figure 3.18), dominated by local spins modifications. The examined energy window consists of spin states characterized by similar charge distributions, leaving out ligand-to-metal and metal-to-ligand charge transfer states. The eigen-states were constructed using Localized Molecular Orbitals (LMOs) to allow for projections onto the local spin states of the metal and ligands, S_{Fe} and S_L, respectively.

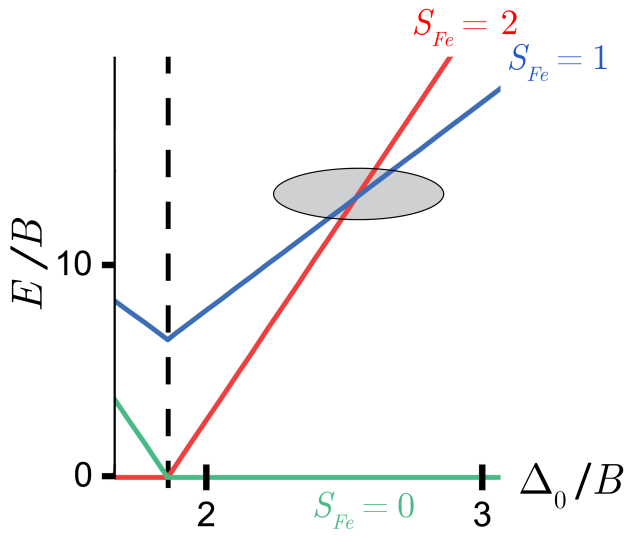

Figure 3.19: Low part of the Tanabe-Sugano diagram of a Fe(II) d^6 ion in an octahedral field. The critical ligand field value marking Spin CrossOver is indicated by a vertical dotted line. The crossing between the excited $S_{Fe} = 1$ and $S_{Fe} = 2$ states is highlighted.

The numerical results presented in this work highlight the presence of a strong quantum entanglement between the local spin states, *i.e.* a *spinmerism* effect, of the metal ion and the radical ligand environment. This evidence reshuffles the standard views in molecular magnetism and simultaneously opens up new perspectives for

technological development at the interface of physics and chemistry. The traditional Tanabe-Sugano diagram concepts might be extended, giving possible out-of-the-box answers to energy spectra governed by ligand fields displaying open-shell character. In Light-Induced Excited Spin-State Trapping (LIESST) experiments,[162] the long-lived excited states at low temperatures would consist of superpositions of $S_{Fe} = 1$ and $S_{Fe} = 2$. Therefore, the variability of local spin states could provide a pathway to encode quantum information on synthetic molecular systems based on this light-induced qubit, presuming that the access to the different local S_{Fe} spin states is available (*e.g.* Fe-N bond stretching frequencies).

3.4.2 Computational details

The presence of multiple open-shells on both metal ion and ligands strongly invites the use of a wavefunction-based method, such as the Complete Active Space Self-Consistent Field (CASSCF) method. The Complete Active Space should include six electrons from the iron centre and two from the oxoverdazyl ligands in seven molecular orbitals (CAS[8,7]). However, the active space was reduced to CAS[6,6] by inspecting the occupation numbers of the active MOs. The CAS[6,6]SCF sextuplet MOs were then transformed into LMOs (following the DoLo procedure presented in section 1.3), which are shown in Figure 3.20. Such transformation allows for a reading of the wavefunctions following a Lewis-like description. In the low-energy spectrum of **3**, we checked that the mostly metal d-type LMOs remained doubly occupied (low-spin Fe(II)), and the active space was even reduced to CAS[2,2]. CASSCF and MRCI calculations were performed as described in Appendix E.

The resulting CI eigenfunctions were projected onto the local spin states of the oxoverdazyl ligands pair ($S_L = 0$ or 1) and the iron ion ($S_{Fe} = 0$, 1 or 2). This procedure allows for a decomposition into the different entangled metal-ligand contributions. To implement these projections and conduct our local spin analysis, the open access package *QuantNBody* [264] was used. This numerical python toolbox has been recently developed by Saad Yalouz, a researcher from LCQS, to facilitate the manipulation of quantum many-body operators and wavefunctions. Based on this tool, matrix representations (in the many-electron basis) of the local metal and ligands spin operators $\hat{S}^2_{Fe}$ and $\hat{S}^2_L$ were built and diagonalized to access the local

spin subspaces. This approach makes it possible to design spin projectors (in the many-electron basis) to target specific local spins contributions for the metal and the ligands in the multi-reference wavefunction.

3.4.3 Results and Discussion

First, CASSCF calculations were conducted on **3**. Inspections based on a CAS[8,7] highlight the presence of a MO mostly localized on a 3d iron atomic orbital with occupation number 1.99. Thus, the active space was reduced down to [6,6]. The CAS[6,6]SCF MOs were localized either on the metal centre or on each individual dipyvd ligand (see Figure 3.20).

Then, the electronic structure of the environment was inspected following the procedure presented in the section (3.3) for a $[Co(dipyvd)_2]^{2+}$ compound (cobalt(II)). Based on a fictitious $[Zn(dipyvd)_2]^{2+}$ (closed-shell divalent metal ion) analogue of the Co(II) compound, it was shown that the singlet-triplet energy difference $E_S - E_T$ is of the order of +2.0 cm^{-1}. Considering the geometry changes moving to compound **3**, a similar inspection was conducted by substituting Fe(II) by Zn(II). A +1.9 cm^{-1} singlet-triplet energy difference was computed at the CAS[2,2]+DDCI level. This negligible exchange coupling value between the radical ligands suggests that any projection of the total spin states of **3** may simultaneously involve the local $S_L = 0$ and $S_L = 1$ states. Besides, this value can be seen as a reference to quantify the role of the electronic structure of the bridging metal ion. Indeed, the nature, and more importantly the spin state, of the metal centre are likely to modify the exchange coupling constant value, a particular issue we wanted to inspect. As reported in the literature, the intramolecular radical-radical exchange couplings were measured in a series of M(II)-$(bipyvd)_2$ complexes (M = Mn, Ni, Cu, Zn; bipyvd = 1,5-dimethyl-3-(2,2'-bipyridin-6-yl)-6-oxoverdazyl) and range from weakly antiferromagnetic (-10 cm^{-1}) to weakly ferromagnetic (+2 cm^{-1}).[228] Due to the system size and the number of open-shells, a CAS[6,6]+DDCI level of calculation is out of reach. Thus, all our conclusions are based on CAS[6,6]+DDCI2 excitation energies and corresponding wavefunctions analysis, as summarized in Table 3.4.

The energy spectrum results from the local spin states $S_{Fe} = 0, 1, 2$ and $S_L = 0, 1$

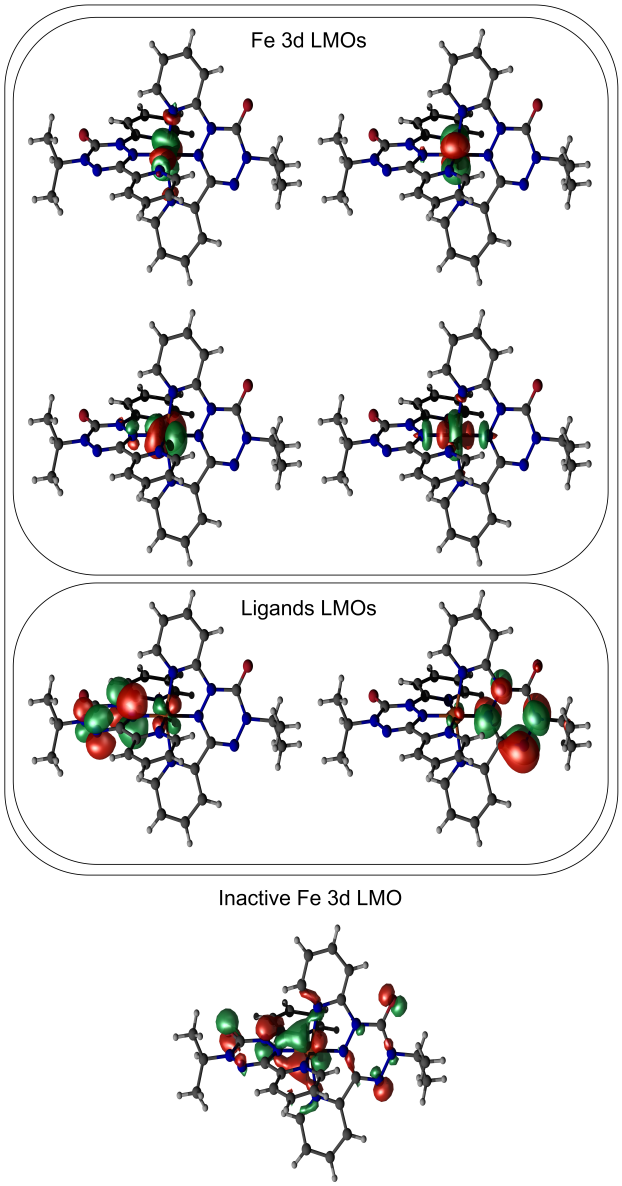

Figure 3.20: Representations of the four mostly metal-type and the two mostly ligand-type LMOs included in the CAS[6,6] generated from a CAS[8,7]SCF calculation for the sextuplet spin state of **3**. The mostly 3d-type inactive LMO is shown below.

which give rise to ten states, namely two singlets (S_i, $i = 0 - 1$), four triplets (T_i, $i = 0 - 3$), three quintets (Q_i, $i = 0 - 2$) and a single heptuplet (H_0). From our calculations, the local spin states display 0, 2 and 4 open-shells on the $S_{Fe} = 0$, $S_{Fe} = 1$ and $S_{Fe} = 2$, respectively (see Figure 3.21). One should stress that the local $S_{Fe} = 1$ spin state involves a single pair of LMOs, a manifestation of the absence of orbital degeneracy as schematically shown in Figure 3.21.

The local spin values can result either from pure spin states or superpositions of different spin multiplicities as manifested in *spinmerism*. Therefore, four different classes can be *a priori* anticipated in the energy spectrum of **3**.

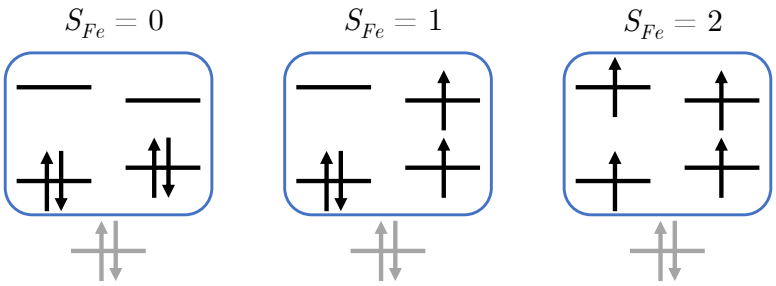

Figure 3.21: Schemes of the leading electronic configurations on the Fe(II) centre, whatever the total spin state in the energy spectrum of **1**. A single mostly d-type LMO essentially doubly occupied (inactive) is shown below. For the sake of simplicity, the maximum spin projections on the local S_{Fe} spin states are shown.

Let us concentrate on the first class of states dominated by pure local spin states S_{Fe} and S_L (see light grey ($\star$) entry in Table 3.4). First, the ground state T_0 is triplet, dominated by the local spin states $S_{Fe} = 0$ and $S_L = 1$, respectively, followed by the singlet S_0 lying 120 cm^{-1} above. This picture is consistent with a d^6 low-spin metal ion in a high-field environment. One should note that small admixtures ($13 - 16\%$) of charge transfers ($S_{Fe} = 1/2$ and $S_L = 1/2$) are evidently observed. Since the CAS[6,6]SCF occupation numbers of the mostly d-type LMOs are larger than 1.98, the $S_0 - T_0$ energy difference was further confirmed from CAS[2,2]+DDCI calculations (CAS[2,2]SCF triplet MOs) and turned out to be 120 cm^{-1}. This value is in reasonable agreement with the reported one which may vary depending on the extraction from density functional theory broken-symmetry calculations.[263] Thus, the low-energy part of the spectrum of **3** can be viewed as two organic radicals coupled through a closed-shell Fe(II) (see Figure 3.22). Evidently, a HDVV Hamiltonian $\hat{H} = -2J\hat{\boldsymbol{s}}_{\mathbf{1}}\hat{\boldsymbol{s}}_{\mathbf{2}}$ can be derived from the singlet-triplet energy difference. The calculated ferromagnetic exchange coupling constant $J = +60$ cm^{-1} is consistent with the experimental value extracted from the magnetic susceptibility fitting (+82 cm^{-1}).[263] This coupling is significantly larger than the reference one we estimated to be +0.95 cm^{-1} for the closed-shell hypothetical Zn(II) complex. The filling of the mostly 3d type e$_g$-orbitals moving from Fe(II) (d^6 ion) to Zn(II) (d^{10} ion) deeply

Label		Energy (cm^{-1})	$2S+1$	$S_{Fe} \bigotimes S_L$	
Q_2	•	10156	5	86% Q	42% S 44% T
S_1	⋆	8603	1	82% T	82% T
T_3	⋆	7691	3	83% Q	83% T
T_2	•	6705	3	87% T	9% S 78% T
H_0	⋆	5326	7	100% Q	100% T
T_1	•	4972	3	81% T	78% S 3% T
Q_1		3323	5	11% Q 10% Q 62% T	11% S 10% T 62% T
Q_0		2906	5	39% Q 33% Q 17% T	39% S 33% T 17% T
S_0	⋆	120	1	84% S	84% S
T_0	⋆	0 (ref.)	3	87% S	87% T

Table 3.4: Energy spectrum of **3**. Quintets and heptuplet energies are calculated at the CAS[6,6]+DDCI2 level. The ground state energy is used as a reference energy. The spin multiplicities $2S+1$ and $S_{Fe} \bigotimes S_L$ decompositions of the wavefunctions are given on the local spin states S_{Fe} and S_L. S, T, Q and H correspond to singlet, triplet, quintet and heptuplet, respectively. The ⋆ symbol is used to refer to states consisting of pure local spin states on both metal and ligand centres. The • symbol refers to states consisting of pure local spin states on the metal centre, and mixed spin values on the ligands. Spin states consisting of mixed spin values on both metal and ligands do not show any symbol, and are manifestation of *excited state spinmerism*.

modifies the electronic structure of the bridging unit (*i.e.*, the metal ion). Similar to the effect of structural modification, such substitution is likely to alter the ex-

change mechanism between the two verdazyl spin holders, and its impact is difficult to anticipate. Such contrast is also found with the experimental values reported in a series of compounds, that not only differ from the relative positions of the verdazyl ligands but also from the absence of the Fe(II) complex in the series.[228] The higher-lying states T_3, S_1 (and evidently the heptuplet H_0) are all characterized by a pure $S_L = 1$ spin state on the coordination sphere. These states are expected from the traditional d^6 Tanabe-Sugano diagram (see Figure 3.19). In a triplet $S_L = 1$ high-field regime, the states ordering follows $S_{Fe} = 0$ (T_0, reference energy), $S_{Fe} = 2$ (T_3, 7691 cm^{-1}), and $S_{Fe} = 1$ (S_1, 8603 cm^{-1}). At this stage, the main difference with usual picture in coordination chemistry compounds lies in the triplet nature of the ligand field, a concept introduced in the literature as "excited state coordination chemistry".[209] One should finally mention the presence of 1.6% singlet state on the metal in S_1. However, this negligible contribution arises from an excited open-shell singlet.

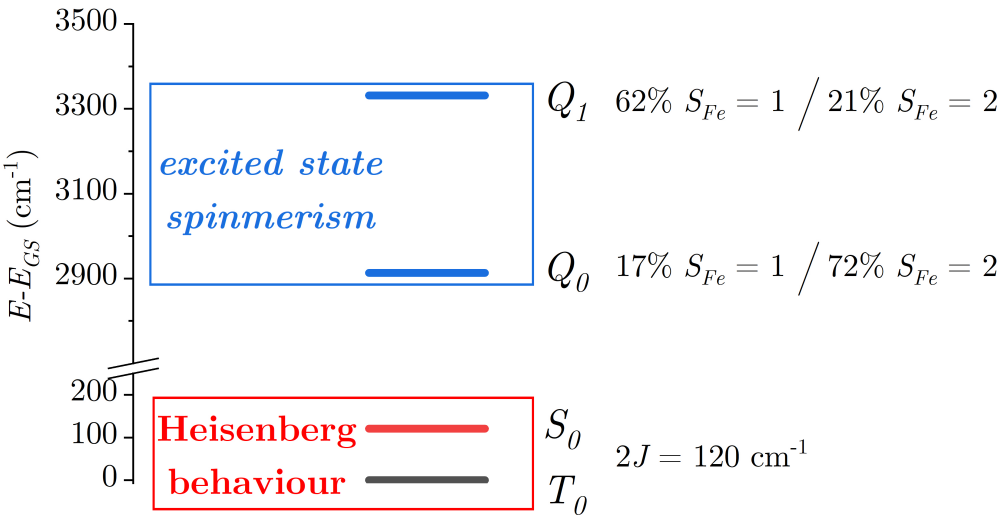

Figure 3.22: Energy spectrum of **3** reflecting a Heisenberg behaviour in the low-energy part with T_0 and S_0 states, whereas *excited sate spinmerism* is observed higher in energy with Q_0 and Q_1 states. The excited quintet states Q_0 and Q_1 exhibit a strong mixing between the $S_{Fe} = 1$ and $S_{Fe} = 2$ local spin states.

Based on this preliminary observation suggesting a $S_L = 1$ ligand field, we now examine the third Q_1 ($2S + 1 = 5$) excited state given in Table 3.4. The Fe(II) spin state is dominated by a $S_{Fe} = 1$ (62%) in the field of a 72% $S_L = 1$. Again, such picture obtained from the spin projections of the wavefunction is consistent

with a high-field d^6 Tanabe-Sugano diagram.[150] However, the quintet state Q_1 in Figure 3.22 exhibits non-negligible contributions from the local $S_{Fe} = 2$ (21%) and $S_L = 0$ (11%) spin states. Such superposition of triplet and quintet metal spin states in the absence of Spin-Orbit Coupling is a manifestation of the *spinmerism* effect. Our analysis supports the appearance of a similar phenomenon in **3**, named as *excited state spinmerism*. This manifestation results from the open-shell character of the environment and the energy crossing between the $S_{Fe} = 1$ and $S_{Fe} = 2$ excited states in the high-field regime of the Fe(II) d^6 diagram (see Figure 3.19). The traditional allowed crossing between different spin multiplicities in the Tanabe-Sugano diagram is lifted from the presence of two radical ligands. As expected, the energy spectrum exhibits a second close-in-energy quintet state resulting from this mixing (see Q_0 in Figure 3.22). The latter is found 2906 cm^{-1} above the ground state, with a dominant $S_{Fe} = 2$ character (72%), and a significant mixing between the environment $S_L = 0$ (39%) and $S_L = 1$ (50%) spin states. This second class of states (Q_0 and Q_1 in Table 3.4) displays entanglement between the spin states of the metal ion and its coordination sphere in the high-field regime. In agreement with the model Hamiltonian-based inspection of section (3.2), the emergence of the two quintet states Q_0 and Q_1 in Figure 3.22 from avoided crossing stresses the importance of not only the magnitude of the ligand field (Coulomb contributions), but also the open-shell character of such field (decisive exchange contributions).

From these numerical inspections, one may further take advantage of the electronic structure changes observed in the photo-induced spin-states of Spin CrossOver compounds (LIESST effect). Under low-temperature irradiation, it is possible to quantitatively achieve a low-spin to high-spin conversion in Fe(II) Spin CrossOver compounds.[162] Very recently, it has been shown that unusually long relaxation times can be reached (*ca.* 20 hours) which makes such complexes particularly encouraging for practical applications.[265] Starting from the ground state T_0 in compound **3**, the spin-allowed transition would lead to the photo-generated T_1 state dominated by a local $S_{Fe} = 1$. The Q_1 state, and to a lesser extent the Q_0 state, exhibit a large proportion of the $S_{Fe} = 1$ local state (62% in Table 3.4). Thus, one may question whether intersystem crossing between T_1 and Q_1 would be enhanced by the presence of *excited state spinmerism*. The mechanism of light-induced Spin CrossOver was

previously studied to calculate intersystem-crossing rates and concluded on a process mediated by a triplet excited state.[266, 267] From the manifestation of the here-proposed *excited state spimnerism* phenomenon, the LIESST effect would produce local superpositions of Fe(II) spin states with potential applications as spin-qubits.

A third class of states in the energy spectrum of **1** is characterized by a pure local spin state on the metal and a superposition of $S_L = 0$ and $S_L = 1$ on the environment (T_1, T_2, Q_2, see dark grey entry (•) in Table 3.4). Such mixture was previously reported in noninnocent ligand-based Fe(III) compounds [213, 268] where the "excited state coordination chemistry" concept [209] was numerically evidenced. In compound **3**, charge transfers are small enough to maintain a formally Fe(II) ion with Spin CrossOver behavior, a prerequisite for *spinmerism* manifestation.

Finally, our analysis of the low-lying spin states does not reflect any representative of the fourth class, characterized by the superposition of S_{Fe} values in the field of a pure S_L value. Evidently, a $S_L = 0$ ligand field would not allow the mixing of different S_{Fe} values. However, the absence of a mixed-spin state on the metal in a $S_L = 1$ ligand field is more puzzling at first. As reported in section (3.2), the entanglement between local spin states is directly controlled by the relative amplitudes of the direct exchange values and conditions which might not be fulfilled in the examined compound **3**.

3.4.4 Preliminary conclusion

The spin states structures of a coordination compound $[Fe(dipvd)_2]^{2+}$ built on a Spin CrossOver ion (Fe(II)) and two radical ligands (oxoverdazyl) were analyzed from CAS[6,6]+DDCI2 wavefunctions calculations. The procedure is based on the generation of Localized Molecular Orbitals, and spin projections onto local spin states. A ground state triplet $S = 1$ characterized by a $S_{Fe} = 0$ local spin state is found, a reflection of a high-field regime. A strong ferromagnetic interaction $J = +60$ cm^{-1} is calculated featuring the coupling of organic radical spin holders through a low-spin metal ion. Even though the low-energy part of the spectrum can be rationalized by a Heisenberg-Dirac-Van Vleck spin Hamiltonian, the magnetic picture delivered by a d^6 Tanabe-Sugano diagram is deeply reshuffled in the next nearest excited states.

The flexibility afforded by the open-shell character of the environment gives rise to marked superpositions of local spin states $S_{Fe} = 1$ and $S_{Fe} = 2$ in the $S = 2$ excited states. The traditional quasi-degeneracy in the high-field regime is lifted by 417 cm^{-1} with significant contributions from both $S_L = 1$ and $S_L = 0$ on the ligand pair. This observation, which we name *excited state spinmerism*, extends the *spinmerism* phenomenon reported in the previous sections. The prerequisite for the manifestation of such entanglement is fulfilled from the presence of a Fe(II) ion and radical organic ligands. By irradiating the sample in the UV-vis or near-IR regions at low temperature, such compounds might be photo-switched and become original targets. Our analysis may stimulate experimentalists to photo-generate slowly decaying excited states consisting of $S_{Fe} = 1$ and $S_{Fe} = 2$ spin states superpositions. Assuming that one can access the proportions of the different local S_{Fe} spin states, the reading of encoded quantum information may become feasible. Therefore, the variability of local spin states could provide a pathway to encode quantum information on synthetic molecular systems. This particular class of coordination chemistry compounds combining versatile local spin states not only enlarges the traditional pictures in molecular magnetism but might become original targets for spin-qubit generation.

3.5 General conclusions

The model Hamiltonian and *ab initio* calculations-based studies highlighted the emergence of a phenomenon we coined into *spinmerism*. The *spinmerism* phenomenon is a superposition of different local spin states that generates a given total spin state, in a sense that it differs from Spin-Orbit effects by keeping the total spin a good quantum number. It can be seen as an extension of mesomerism, with the different resonance structures being different local spin states distributions. Anticipated from standard spin algebra, this work highlights its occurrence in two *ab initio* complexes and aims at elucidating the conditions for its manifestation. *Spinmerism* is based primarily on the coupling of two spin active components whose spin changes are identical. Here the use of a Spin CrossOver metal ion and two radical ligands was a mean to evidence *spinmerism* behaviours.

By concentrating on direct exchange interactions, the first work modelled a complex built on an artificial Spin CrossOver ion (M =d^2 or d^8) and two radical ligands in order to investigate the conditions for the emergence of *spinmerism*. It highlighted two guiding rules for strong *spinmerism* occurrence (50/50). The charge transfer contributions (LMCT and MLCT) were then taken into account in a perturbative manner to get closer to realistic coordination compounds, and stress their influence on the energy spectrum.

The second work presented an *ab initio* inspection of a first molecular complex candidate for *spinmerism*: a Co(II) metal ion coordinated by two radical verdazyl ligands. The Co(II) metal ion may undergo a transition from $S_M = 1/2$ to $S_M = 3/2$, and the verdazyl radicals give rise to $S_L = 0$ or $S_L = 1$ spin-dependent environment. The main ingredients of *spinmerism* are to be found in this particular complex, and a weak *spinmerism* behaviour ($\sim 0.1\%$) was observed by means of wavefunction-based calculations. This pushed forward the fact that the ligand field generated by a set of open-shell radicals cannot be considered as a frozen field according to the usual view of coordination compounds. Still, the observed *spinmerism* behaviour is too weak for potential applications, but extends the traditional picture of the crystal field in transition metal complexes.

Finally, the third work investigated by *ab initio* means another candidate for *spin-*

merism: a Fe(II) metal ion with two verdazyl ligands. The Fe(II) metal ion exhibits an usual spin-transition from $S_M = 0$ to $S_M = 2$. The spin-transition of its ligands does not allow for a superposition of $S_M = 0$ and $S_M = 2$, but does allow the superposition of $S_M = 1$ and $S_M = 2$. Indeed, excited states presenting this superposition are observed, and an important *excited state spinmerism* effect ($\sim 20\%$) is evidenced. Whilst the low-energy spectrum is readily rationalized by a Heisenberg behaviour, the magnetic picture delivered by the excited states reshuffles the views on the d^6 Tanabe-Sugano diagram. The flexibility of the environment opens up new interpretation schemes, contrasting with the usual static view for the crystal field.

Spinmerism is a phenomenon that introduces a different point of view in magnetic complexes. Its strength lies on the fact that it is naturally induced by the structure of the wavefunction, which differentiates it from Spin-Orbit Coupling effects. The spin versatility of the local sites is the major condition for future applications of *spinmerism*. Therefore, the variability of local spin states could provide a pathway to encode quantum information on synthetic molecular systems. By experimentally probing the local spin density, such molecular compounds might become original targets for spin-qubits generation in new Quantum Computers architectures. We suggest the use of Light-Induced Excited Spin State Trapping effect as a possible way to control *spinmeric* compounds, and the information they encode.

Now, let us make some self-criticism regarding the work presented in this Chapter. 1) The developed Model Hamiltonian for *spinmerism* presents two guiding rules depending on the geometry of the system. Real systems may satisfy these symmetries up to a small deviation. The evolution of the conditions for strong *spinmerism* during small deviations from the reference geometry can bring additional information in the search of candidates. A next step is to derive the model into an effective Hamiltonian, using the *ab initio* conditions. This can help to validate the model, and to improve its orientation towards realistic systems. Moreoever, a short screening of possible candidates based on their *ab initio* exchange integrals and energies may pave the way for further *ab initio* studies of *spinmerism*. 2) Spin-orbit coupling is one of the detractor of the *spinmerism* phenomenon. The two phenomena have often been compared by referees to deny *spinmerism*. However, these two effects are unrelated, but are both possible in heavier element-based compounds. Spin-

orbit was always disregarded to focus solely on the *spinmerism* phenomenon. An assessment of the proportion of Spin-Orbit in the complexes previously studied is necessary in order to possibly correct the calculated energy levels. The evolution of the *spinmeric* behaviour as a function of the Spin-Orbit character is an interesting study, as it can guide the theoretical and experimental interpretations towards a more global and physical picture. 3) The other argument for the criticism of *spinmerism* by other referees is the lack of experimental evidence. The main issue with observing a superposition of local spin states is that only the total spin S is an observable, not the local spin states. This problem does not arise for complexes with only one active spin entity, but it does arise for complexes with *spinmerism* because they have more than one active spin entity. One possible idea is as follows: let us measure standards of vibrational frequencies for two possible pure metal spin states (*e.g.* $S_M = 1$ and $S_M = 2$). The measured vibrational frequency of a S spin state built on two different local spin states (*e.g.* S_M) may then be the linear combination of the two vibrational frequencies. This would allow us to experimentally quantify the relative contributions of the local spin states. A deeper literature search and an appropriate study are needed to prove this idea. 4) By considering a molecule in the gas phase, many physical effects are neglected. More advanced calculations taking into account solvent effects and packing in solution or in a crystal may help to demonstrate experimentally *spinmerism*. 5) Finally, the proposal to use *spinmeric* compounds as spin-qubits is tempting, but a number of questions need to be resolved. The stability of these spin-qubits and of their encoded information (decoherence) need to be evaluated. Quantum dynamical studies are needed to assess the evolution of *spinmerism* over time. A first step could be to construct the Potential Energy Surfaces of a candidate, in preparation for future dynamical studies.

In my opinion, *spinmerism* is a phenomenon that will open up new perspectives and interpretations in the field of molecular magnetism. It is still in its infancy, and a first experimental proof may be needed to stimulate the concept among a wider audience.

Appendix D. Model Hamiltonians and equalities

This appendix presents the model Hamiltonians used in section (3.3), to study *spinmerism* and the derived equalities, depending on the geometry of the system.

General case

3.5.0.a Determinant basis

For the sake of notations clarity, the following determinants in $\{|\Phi_\alpha\rangle\}$ basis were renamed:

$$\{|\Phi_\alpha\rangle\} = \Big\{ |\overline{\varphi}_{L_1}\varphi_M\varphi_{M'}\overline{\varphi}_{L_2}|, |\varphi_{L_1}\varphi_M\overline{\varphi}_{M'}\overline{\varphi}_{L_2}|, \quad = \{|\Phi_1\rangle, |\Phi_2\rangle, \tag{3.8}$$

$$|\overline{\varphi}_{L_1}\varphi_M\overline{\varphi}_{M'}\varphi_{L_2}|, |\varphi_{L_1}\overline{\varphi}_M\varphi_{M'}\overline{\varphi}_{L_2}|, \quad |\Phi_3\rangle, |\Phi_4\rangle, \tag{3.9}$$

$$|\overline{\varphi}_{L_1}\overline{\varphi}_M\varphi_{M'}\varphi_{L_2}|, |\varphi_{L_1}\overline{\varphi}_M\overline{\varphi}_{M'}\varphi_{L_2}| \Big\} \quad |\Phi_5\rangle, |\Phi_6\rangle\} \tag{3.10}$$

3.5.0.b General Hamiltonian

Neglecting ϵ_i, the following $H_{\alpha-space}$ is obtained:

$$H_{\alpha-space} = \begin{bmatrix} -K_M & -K'_1 & -K'_2 & -K_1 & -K_2 & 0 \\ -K'_1 & -(K_1+K'_2) & 0 & -K_M & 0 & -K_2 \\ -K'_2 & 0 & -(K_2+K'_1) & 0 & -K_M & -K_1 \\ -K_1 & -K_M & 0 & -(K_2+K'_1) & 0 & -K'_2 \\ -K_2 & 0 & -K_M & 0 & -(K_1+K'_2) & -K'_1 \\ 0 & -K_2 & -K_1 & -K'_2 & -K'_1 & -K_M \end{bmatrix} \tag{3.11}$$

First rule: $2K_M = K_1 + K_1'$

3.5.0.c Inner-space Hamiltonian for $K_1 = K_2$ and $K_1' = K_2'$

In case of Td-symmetry ($L_1 = L_2 \Longrightarrow K_1 = K_2 = K$ and $K_1' = K_2' = K'$), the inner-space Hamiltonian takes the following form:

$$H'_{\alpha-space} = \begin{bmatrix} -K_M & -K' & -K' & -K & -K & 0 \\ -K' & -(K+K') & 0 & -K_M & 0 & -K \\ -K' & 0 & -(K+K') & 0 & -K_M & -K \\ -K & -K_M & 0 & -(K+K') & 0 & -K' \\ -K & 0 & -K_M & 0 & -(K+K') & -K' \\ 0 & -K & -K & -K' & -K' & -K_M \end{bmatrix} \tag{3.11'}$$

3.5.0.d Triplet reference states

Three triplet states are obtained using Clebsch-Gordan coefficients rules for spin algebra.

$$\begin{aligned} |\mathrm{I}\rangle &= |1,0,1\rangle = \tfrac{1}{2}(|\Phi_2\rangle + |\Phi_3\rangle - |\Phi_4\rangle - |\Phi_5\rangle) \\ |\mathrm{II}\rangle &= |1,1,0\rangle = \tfrac{1}{2}(|\Phi_2\rangle - |\Phi_3\rangle + |\Phi_4\rangle - |\Phi_5\rangle \\ |\mathrm{III}\rangle &= |1,1,1\rangle = \tfrac{1}{\sqrt{2}}(|\Phi_1\rangle - |\Phi_6\rangle) \end{aligned}$$

3.5.0.e Triplet only Hamiltonian

Working only in the Triplet inner-space, a 3×3 Hamiltonian is obtained. It was constructed on the $\{|\mathrm{I}\rangle, |\mathrm{II}\rangle, |\mathrm{III}\rangle\}$ basis.

$$H_{triplet} = \begin{bmatrix} -K - K' + K_M & 0 & -\sqrt{2}(K - K') \\ 0 & -K - K' - K_M & 0 \\ -\sqrt{2}(K - K') & 0 & -K_M \end{bmatrix} \tag{3.12}$$

This Hamiltonian was formally diagonalized using WolframAlpha. Three eigenvalues and respective eigenvectors were obtained:

$$\lambda_1 = \frac{1}{2}(-\sqrt{\Delta} - K - K'), \qquad v_1 = (\frac{K + K' - 2K_M + \sqrt{\Delta}}{2\sqrt{2}(K - K')}, 0, 1) \tag{3.13}$$

$$\lambda_2 = \frac{1}{2}(\sqrt{\Delta} - K - K'), \qquad v_2 = (\frac{K + K' - 2K_M - \sqrt{\Delta}}{2\sqrt{2}(K - K')}, 0, 1) \tag{3.14}$$

$$\lambda_3 = -K - K' - K_M, \qquad v_3 = (0, 1, 0) \tag{3.15}$$

with $\Delta = 9K^2 - 14KK' + 9K'^2 - 4KK_M - 4K'K_M + 4K_M^2$

3.5.0.f Resolution of $\lambda_{01}^2 = \lambda_{11}^2 = \frac{1}{2}$

Considering:

- $2K_M = K + K'$

- $K > K'$

One can observe that

$$\Delta = 8K^2 - 16KK' + 8K'^2 = 8(K - K')^2 \Longrightarrow \sqrt{\Delta} = 2\sqrt{2}(K - K') \tag{3.16}$$

and

$$K + K' - 2K_M = 0 \tag{3.17}$$

The former weight on $|\mathrm{I}\rangle$ for (3.13) and (3.14) becomes

$$\frac{K + K' - 2K_M \pm \sqrt{\Delta}}{2\sqrt{2}(K - K')} = \pm 1 \tag{3.18}$$

which reads for v_1 and v_2

$$v_1 = (1, 0, 1) = |\mathrm{I}\rangle + |\mathrm{III}\rangle \tag{3.19}$$

$$v_2 = (-1, 0, 1) = -|\mathrm{I}\rangle + |\mathrm{III}\rangle. \tag{3.20}$$

Due to the normalization condition of the wavefunction, one can see that the former expression becomes

$$v_1 = \frac{1}{\sqrt{2}}|\mathrm{I}\rangle + \frac{1}{\sqrt{2}}|\mathrm{III}\rangle \tag{3.21}$$

$$v_2 = -\frac{1}{\sqrt{2}}|\mathrm{I}\rangle + \frac{1}{\sqrt{2}}|\mathrm{III}\rangle \tag{3.22}$$

$\Longrightarrow$ The following equality is observed $\lambda_{01}^2 = \lambda_{11}^2 = \frac{1}{2}$.

Second rule: $2K_M = 2K_2 + 2K_2'$

3.5.0.g Inner space Hamiltonian for $K_1 = K_2 = K_1'$ and K_2'

In case of $K_1 = K_2 = K_1' = K$, the inner-space Hamiltonian becomes:

$$H"_{\alpha-space} = \begin{bmatrix} -K_M & -K & -K_2' & -K & -K & 0 \\ -K & -(K+K_2') & 0 & -K_M & 0 & -K \\ -K_2' & 0 & -2K & 0 & -K_M & -K \\ -K & -K_M & 0 & -2K & 0 & -K_2' \\ -K & 0 & -K_M & 0 & -(K+K_2') & -K \\ 0 & -K & -K & -K_2' & -K & -K_M \end{bmatrix}. \tag{3.11"}$$

3.5.0.h Singlet reference states

Two singlet states are obtained using Clebsch-Gordan coefficients rules for spin algebra.

$$|\mathrm{IV}\rangle = |0,0,0\rangle = \frac{1}{2}(|\Phi_2\rangle - |\Phi_3\rangle - |\Phi_4\rangle + |\Phi_5\rangle) \tag{3.23}$$

$$|\mathrm{V}\rangle = |0,1,1\rangle = \frac{1}{\sqrt{3}}(|\Phi_1\rangle + |\Phi_6\rangle) - \frac{1}{2\sqrt{3}}(|\Phi_2\rangle + |\Phi_3\rangle + |\Phi_4\rangle + |\Phi_5\rangle) \tag{3.24}$$

3.5.0.i Singlet only Hamiltonian

Working only in the Singlet inner-space, a 2×2 Hamiltonian is obtained. It was constructed on the $\{|\mathrm{IV}\rangle, |\mathrm{V}\rangle\}$ basis.

$$H_{singlet} = \begin{bmatrix} -\frac{3K}{2} - \frac{K_2'}{2} + K_M & -\frac{\sqrt{3}}{2}(K - K_2') \\ -\frac{\sqrt{3}}{2}(K - K_2') & \frac{3K}{2} + \frac{K_2'}{2} - K_M \end{bmatrix} \tag{3.25}$$

This Hamiltonian was formally diagonalized using WolframAlpha. Two eigenvalues and respective eigenvectors were obtained:

$$\lambda_4 = -\sqrt{\Delta'} \qquad v_4 = \left(\frac{3K + K_2' - 2K_M + 2\sqrt{\Delta'}}{\sqrt{3}(K - K_2')}, 1\right) \tag{3.26}$$

$$\lambda_5 = \sqrt{\Delta'} \qquad v_5 = \left(\frac{3K + K_2' - 2K_M - 2\sqrt{\Delta'}}{\sqrt{3}(K - K_2')}, 1\right) \tag{3.27}$$

with $\Delta' = 3K^2 + {K_2'}^2 - 3KK_M - K_2'K_M + K_M^2$.

3.5.0.j Resolution of $\mu_{00}^2 = 3\mu_{11}^2$

Considering:

- $2K_M = 2K + 2K_2'$

- $K > K_2'$

One can observe that

$$\Delta' = K^2 - 2KK_2' + K_2'^2 = (K - K_2')^2 \Longrightarrow \sqrt{\Delta'} = (K - K_2') \tag{3.28}$$

and

$$3K + K_2' - 2K_M = (K - K_2'). \tag{3.29}$$

The former weight on $|\mathrm{IV}\rangle$ for (3.26) and (3.27) reads

$$v_4 = (\sqrt{3}, 1) = \sqrt{3}|\mathrm{IV}\rangle + |\mathrm{V}\rangle \tag{3.30}$$

$$v_5 = (-\frac{1}{\sqrt{3}}, 1) = -\frac{1}{\sqrt{3}}|\mathrm{IV}\rangle + |\mathrm{V}\rangle. \tag{3.31}$$

Due to the normalization condition of the wavefunction, one can see that the former expression becomes

$$v_4 = \frac{\sqrt{3}}{2}|\mathrm{IV}\rangle + \frac{1}{2}|\mathrm{V}\rangle \tag{3.32}$$

$$v_5 = -\frac{1}{2}|\mathrm{IV}\rangle + \frac{\sqrt{3}}{2}|\mathrm{V}\rangle. \tag{3.33}$$

The following equalities are observed for

$\Longrightarrow$ (3.26), the lowest excited singlet state: $\mu_{00}^2 = 3\mu_{11}^2$

$\Longrightarrow$ (3.27), the highest excited singlet state: $3\mu_{00}^2 = \mu_{11}^2$

Appendix E. Details on *ab initio* calculations

All CASSCF calculations were performed on the available Xray structure without any geometry optimization and used the MOLCAS 8.0 package.[45] The Co/Fe and first coordination sphere atoms were described with 4s3p2d and 3s2p1d basis sets, respectively. Smaller basis sets were used for all other atoms, 3s2p whilst hydrogen atoms were depicted with a 1s basis set. Such basis set affords for a balanced description of the iron center and the first coordination sphere atoms fixing the crystal field amplitude.

The dynamical and polarization effects were included following the Difference Dedicated Configuration Interaction (DDCI) method [39, 40] as implemented in the CASDI code [38] and described in subsection (1.2.5). Depending on the classes of configurations involved in the CI expansion, different levels (CAS + S, CAS + DDCI2, and CAS + DDCI) can be reached beyond the CAS picture. This variational method that follows a step-by-step construction of the wavefunction has produced a wealth of interpretations [20, 269, 270] and rationalizations [50, 271] with a systematic relaxation of the wavefunction (so-called "fully decontracted method").

Appendix F. Heisenberg-Dirac-Van Vleck Hamiltonians

This appendix presents the n-parameter Heisenberg-Dirac-Van Vleck Hamiltonians used to fit calculated energy spectra of section (3.3). These matrices were formally diagonalized using WolframAlpha. The obtained eigenvalues λ_i are shown.

One-parameter Hamiltonian: $\hat{H} = -2J\hat{S}_L\hat{S}_M$

$S_M = \frac{3}{2}$ and $S_L = 1$, in $M_s = +\frac{1}{2}$ space:

$$\{|-\frac{1}{2},1\rangle;|\frac{1}{2},0\rangle;|\frac{3}{2},1\rangle\}$$

$$H_{1-p} = \begin{bmatrix} J & -2\sqrt{2}J & 0 \\ -2\sqrt{2}J & 0 & -\sqrt{6}J \\ 0 & -\sqrt{6}J & 3J \end{bmatrix} \tag{3.34}$$

$$\lambda_1 = -3J$$

$$\lambda_2 = 5J$$

$$\lambda_3 = 2J$$

Two-parameter Hamiltonian: $\hat{H} = -2j_1\hat{S}_1\hat{S}_M - 2j_2\hat{S}_2\hat{S}_M$

$S_M = \frac{3}{2}$, $S_1 = \frac{1}{2}$ and $S_2 = \frac{1}{2}$, in $M_s = +1/2$ space:

$$\{|-\frac{1}{2},\frac{1}{2},\frac{1}{2}\rangle;|\frac{1}{2},\frac{1}{2},-\frac{1}{2}\rangle;|\frac{1}{2},-\frac{1}{2},\frac{1}{2}\rangle;|\frac{3}{2},\frac{1}{2},\frac{1}{2}\rangle\}$$

$$H_{2-p} = \begin{bmatrix} \frac{1}{2}(j_1+j_2) & -2j_2 & -2j_1 & 0 \\ -2j_2 & -\frac{1}{2}(j_1-j_2) & 0 & -j_1\sqrt{3} \\ -2j_1 & 0 & \frac{1}{2}(j_1-j_2) & -j_2\sqrt{3} \\ 0 & -j_1\sqrt{3} & -j_2\sqrt{3} & \frac{3}{2}(j_1+j_2) \end{bmatrix} \tag{3.35}$$

$$\lambda_1 = -\frac{3}{2}(j_1 + j_2)$$
$$\lambda_2 = \frac{5}{2}(j_1 + j_2)$$
$$\lambda_3 = \frac{1}{2}(-2\sqrt{4{j_1}^2 - 7j_1j_2 + 4{j_2}^2} + j_1 + j_2)$$
$$\lambda_4 = \frac{1}{2}(2\sqrt{4{j_1}^2 - 7j_1j_2 + 4{j_2}^2} + j_1 + j_2)$$

Three-parameter Hamiltonian:

$$\hat{H} = -2j_1\hat{S}_1\hat{S}_M - 2j_2\hat{S}_2\hat{S}_M - 2j_{12}\hat{S}_1\hat{S}_2$$

$S_M = \frac{3}{2}$, $S_1 = \frac{1}{2}$ and $S_2 = \frac{1}{2}$, in $M_s = +1/2$ space:

$$\{|-\frac{1}{2},\frac{1}{2},\frac{1}{2}\rangle; |\frac{1}{2},\frac{1}{2},-\frac{1}{2}\rangle; |\frac{1}{2},-\frac{1}{2},\frac{1}{2}\rangle; |\frac{3}{2},\frac{1}{2},\frac{1}{2}\rangle\}$$

$$H_{3-p} = \begin{bmatrix} \frac{1}{2}(j_1 + j_2 - j_{12}) & -2j_2 & -2j_1 & 0 \\ -2j_2 & -\frac{1}{2}(j_1 - j_2 - j_{12}) & -j_{12} & -j_1\sqrt{3} \\ -2j_1 & -j_{12} & \frac{1}{2}(j_1 - j_2 + j_{12}) & -j_2\sqrt{3} \\ 0 & -j_1\sqrt{3} & -j_2\sqrt{3} & \frac{3}{2}(j_1 + j_2) - \frac{1}{2}j_{12} \end{bmatrix} \tag{3.36}$$

$$\lambda_1 = \frac{1}{2}(-3j_1 - 3j_2 - j_{12})$$
$$\lambda_2 = \frac{}{2}(5j_1 + 5j_2 - j_{12})$$
$$\lambda_3 = \frac{1}{2}(-2\sqrt{4{j_1}^2 - 7j_1j_2 + 4{j_2}^2 - j_1j_{12} - j_2j_{12} + {j_{12}}^2} + j_1 + j_2 + j_{12})$$
$$\lambda_4 = \frac{1}{2}(2\sqrt{4{j_1}^2 - 7j_1j_2 + 4{j_2}^2 - j_1j_{12} - j_2j_{12} + {j_{12}}^2} + j_1 + j_2 + j_{12})$$

Thesis conclusions

This manuscript is articulated around the notion of environment in complex spin architectures in the field of Organic photoChemistry and Inorganic magnetoChemistry. The following is a brief summary of the main findings and ideas.

In the second Chapter, the construction of a model Hamiltonian allows to qualitatively assess the influence of the spin and charge of different environments on an active chromophore. From a practical point of view, this work highlights the fact that the single chromophore approximation in Singlet Fission (SF) does not reflect reality, and underestimates the ratio of energy gaps which governs the thermodynamic condition of SF. This means that many possible candidates are swept under the carpet due to an erroneous calculation of their energy spectrum and an underestimation of their potential. This point is particularly important in view of the new era of Machine Learning and Computational Screening investigations for SF. The perfect SF material is yet to be discovered, and one is taking the risk of ruling it out by using this approximation. At the fundamental level, this work highlights and quantifies the influence of the spin and the charge of the environment on the spectroscopy of a chromophore. It uses a minimum number of parameters complemented by *ab initio* integral evaluations and, despite this, significant modulations of the energy spectrum are observed. By making the model more complex (*e.g.* slip-stacking, rotation...), other types of environment can be explored, at the cost of greater variability. This would be interesting follow-up works, providing a qualitative overview of the various packings of SF chromophores, and of the mechanisms in play. However, care must be taken when variability increases: an overly complex model Hamiltonian may be less useful than a direct calculation using an *ab initio* Hamiltonian. Still, the developed model is transferable to the study of many class

I SF systems, provided the relevant local HOMOs and LUMOs are given.

In the third Chapter, a model Hamiltonian and *ab initio* calculations studies investigate the *spinmerism* phenomenon. Its emergence opens up new visions with regards to considerations of ligand field and magnetic behaviours. Anticipated from spin algebra, this phenomenon differs from Spin-Orbit Coupling effects because it maintains the total spin as a good quantum number. The particular structure of the wavefunction generated by local spin versatile ligands and metal centre allows various coupling schemes which, under the right conditions, lead to a significant superposition of local spin states. The quantified analysis of local spin states highlights the appearance of *spinmerism*. Still, its inner mechanisms remain poorly understood. Our model Hamiltonian investigation shines light upon the importance of direct exchange interactions in the tuning of *spinmerism*. This is the first step in a longer run aiming to find good candidates for an important manifestation of *spinmerism*. At the applied level, *spinmerism* has potential applications for the design of new molecular spin-qubits, *i.e.* for Quantum Computing. To make progress in this direction, various studies are needed, such as the design of complexes with an easily tunable and quantifiable superposition of local spin states, the measurement of dynamical quantum coherence and, most importantly, experimental studies to probe *spinmerism*. At the fundamental level, this represents a new perspective in the interpretation of magnetic data, and in the study of phenomena induced by a versatile wavefunction. A deeper understanding of *spinmerism* could be the solution to a more correct interpretation of data deemed "non-fittable" by the usual magnetic models. Architectures based on a Spin-CrossOver metal ion coordinated to several open-shell ligands are likely to challenge the traditional frozen-spin pictures. As a consequence, the *spinmerism* phenomenon calls to reconsider the usual view of Tanabe-Sugano diagrams, moving from a strict "ligand field" to more versatile "open-shell ligand field" considerations. However, this phenomenon is still in its infancy, and further theoretical and experimental studies are needed to unravel its mysteries. New projects and collaborations are underway to achieve this goal.

To conclude, this PhD work has studied the importance of open-shell environments and their influence in Organic and Inorganic Chemistry. WaveFunction Theory calculations provided fertile ground for such investigations, at the cost of higher

computational costs. The in-depth calculation and analysis of our systems required appropriate working tools, such as the localization methods and the spin algebra used in this work. On one hand, the environment has a direct influence on the spectroscopy of a molecule (*e.g.* a chromophore, a coordination compound). On the other hand, it plays a major role in the composition of a versatile wavefunction and the induced phenomena associated with it. From my personal point of view, *spinmerism* is an exciting phenomenon that provides a new insight into magnetic compounds, emerging from the combination of radical ligands with a Spin-CrossOver metal ion.

Bibliography

[1] *Climate Change 2022 - Mitigation of Climate Change: Working Group III Contribution to the Sixth Assessment Report of the Intergovernmental Panel on Climate Change*; Cambridge University Press, 2024.

[2] Reichardt, C.; Welton, T. *Solvents and Solvent Effects in Organic Chemistry*; Wiley-VCH, 2010.

[3] Schouten, K. J. P.; Pérez Gallent, E.; Koper, M. T. *J. Electroanal. Chem.* **2014**, *716*, 53–57.

[4] Wurche, F.; Klärner, F.-G. *The Effect of Pressure on Organic Reactions: Basic Principles and Mechanistic Applications*; John Wiley & Sons, Ltd, 2002; Chapter 2, pp 41–96.

[5] Smith, M. B. *March's Advanced Organic Chemistry: Reactions, Mechanisms, and Structure*, 8th ed.; John Wiley & Sons, Inc., 2019.

[6] Bethe, H. *Annalen der Physik* **1929**, *395*, 133–208.

[7] Van Vleck, J. H. *Phys. Rev.* **1932**, *41*, 208–215.

[8] Minkin, V. I. *Pure Appl. Chem.* **1999**, *71*, 1919–1981.

[9] Pople, J. A.; Nesbet, R. K. *J. Chem. Phys.* **1954**, *22*, 571–572.

[10] Verhoeven, J. W. *Pure Appl. Chem.* **1996**, *68*, 2223–2286.

[11] Ben Amor, N.; Evangelisti, S.; Leininger, T.; Andrae, D. *Local Orbitals in Quantum Chemistry*; Springer International Publishing: Cham, 2021; pp 41–101.

[12] Foster, J. M.; Boys, S. F. *Rev. Mod. Phys.* **1960**, *32*, 300–302.

[13] Pipek, J.; Mezey, P. G. *J. Chem. Phys.* **1989**, *90*, 4916–4926.

[14] Maynau, D.; Evangelisti, S.; Guihéry, N.; Calzado, C. J.; Malrieu, J.-P. *J. Chem. Phys.* **2002**, *116*, 10060–10068.

[15] Reed, A. E.; Weinhold, F. *J. Chem. Phys.* **1983**, *78*, 4066–4073.

[16] Reed, A. E.; Weinhold, F. *J. Chem. Phys.* **1985**, *83*, 1736–1740.

[17] Heisenberg, W. *Zeitschrift für Physik* **1928**, *49*, 619–636.

[18] Dirac, P. A. M.; Fowler, R. H. *P. R. Soc. Lond. A-Conta.* **1929**, *123*, 714–733.

[19] Van Vleck, J. H. *Rev. Mod. Phys.* **1945**, *17*, 27–47.

[20] Malrieu, J. P.; Caballol, R.; Calzado, C. J.; de Graaf, C.; Guihéry, N. *Chem. Rev.* **2014**, *114*, 429–492.

[21] Cleveland, C. L.; Medina A., R. *Am. J. Phys.* **1976**, *44*, 44–46.

[22] Kittel, C. *Phys. Rev.* **1960**, *120*, 335–342.

[23] Anderson, P. In *Magnetism*; Rado, G. T.; Suhl, H., Eds.; Academic Press, 1963; pp 25–83.

[24] Bastardis, R.; Guihéry, N.; de Graaf, C. *Phys. Rev. B* **2007**, *76*, 132412.

[25] Griffith, J. S.; Orgel, L. E. *Q. Rev. Chem. Soc.* **1957**, *11*, 381–393.

[26] Lennard-Jones, J. E. *Trans. Faraday Soc.* **1929**, *25*, 668–686.

[27] Fedak, W. A.; Prentis, J. J. *Am. J. Phys.* **2009**, *77*, 128–139.

[28] van der Waerden, B. L.; Weber, R. L. *Phys. Today* **1968**, *21*, 97–97.

[29] Vogiatzis, K. D.; Ma, D.; Olsen, J.; Gagliardi, L.; de Jong, W. A. *J. Chem. Phys.* **2017**, *147*.

[30] G. Sleijpen, G. L.; Van der Vorst, H. A. *SIAM J. Matrix Anal.* **1996**, *17*, 401–425.

[31] Scherrer, A.; Agostini, F.; Sebastiani, D.; Gross, E. K. U.; Vuilleumier, R. *Phys. Rev. X* **2017**, *7*, 031035.

[32] Kerley, G. I.; *On Corrections to the Born-Oppenheimer Approximation*; 2013.

[33] Szabo, A.; Ostlund, N. *Modern Quantum Chemistry: Introduction to Advanced Electronic Structure Theory*; Dover Books on Chemistry; Dover Publications, 1996.

[34] Minkin, V. I. *Pure Appl. Chem.* **1999**, *71*, 1919–1981.

[35] Slater, J. C. *Quantum theory of molecules and solids : Volume 1 : Electronic structure of molecules*; International series in pure and applied physics; McGraw-Hill, 1963.

[36] Löwdin, P.-O. *Phys. Rev.* **1955**, *97*, 1474–1489.

[37] Yalouz, S.; Robert, V. *J. Chem. Theory Comput.* **2023**, *19*, 1388–1392.

[38] Ben Amor, N.; Maynau, D. *Chem. Phys. Lett.* **1998**, *286*, 211–220.

[39] Miralles, J.; Daudey, J.-P.; Caballol, R. *Chem. Phys. Lett.* **1992**, *198*, 555–562.

[40] Miralles, J.; Castell, O.; Caballol, R.; Malrieu, J.-P. *Chem. Phys.* **1993**, *172*, 33–43.

[41] Møller, C.; Plesset, M. S. *Phys. Rev.* **1934**, *46*, 618–622.

[42] Andersson, K.; Malmqvist, P.; Roos, B. O. *J. Chem. Phys.* **1992**, *96*, 1218–1226.

[43] Angeli, C.; Cimiraglia, R.; Evangelisti, S.; Leininger, T.; Malrieu, J.-P. *J. Chem. Phys.* **2001**, *114*, 10252–10264.

[44] Angeli, C.; Cimiraglia, R.; Malrieu, J.-P. *J. Chem. Phys.* **2002**, *117*, 9138–9153.

[45] Aquilante, F.; Autschbach, J.; Carlson, R. K.; Chibotaru, L. F.; Delcey, M. G.; De Vico, L.; Fdez. Galván, I.; Ferré, N.; Frutos, L. M.; Gagliardi, L.; Garavelli, M.; Giussani, A.; Hoyer, C. E.; Li Manni, G.; Lischka, H.; Ma, D.; Malmqvist, P. r.; Müller, T.; Nenov, A.; Olivucci, M.; Pedersen, T. B.; Peng, D.; Plasser, F.; Pritchard, B.; Reiher, M.; Rivalta, I.; Schapiro, I.; Segarra-Martí, J.; Stenrup, M.; Truhlar, D. G.; Ungur, L.; Valentini, A.; Vancoillie, S.; Veryazov, V.; Vysotskiy, V. P.; Weingart, O.; Zapata, F.; Lindh, R. *J. Comput. Chem.* **2016**, *37*.

[46] Dyall, K. G. *J. Chem. Phys.* **1995**, *102*, 4909–4918.

[47] Kahn, O. *Molecular Magnetism*; Wiley-VCH: New York (N.Y.), 1993.

[48] Bloch, C. *Nucl. Phys.* **1958**, *6*, 329–347.

[49] des Cloizeaux, J. *Nucl. Phys.* **1960**, *20*, 321–346.

[50] Maurice, R.; Graaf, C. d.; Guihéry, N. *Phys. Chem. Chem. Phys.* **2013**, *15*, 18784–18804.

[51] Helgaker, T.; Jørgensen, P.; Olsen, J. *Second Quantization*; John Wiley & Sons, Ltd, 2000; Chapter 1, pp 1–33.

[52] Helgaker, T.; Jørgensen, P.; Olsen, J. *Spin in Second Quantization*; John Wiley & Sons, Ltd, 2000; Chapter 2, pp 34–79.

[53] Roseiro, P.; Robert, V. *Phys. Chem. Chem. Phys.* **2022**, *24*, 15945–15950.

[54] Shockley, W.; Queisser, H. J. *J. Appl. Phys.* **1961**, *32*, 510–519.

[55] Yang, C.-H.; Hsu, C.-P. *J. Phys. Chem. Lett.* **2015**, *6*, 1925–1929.

[56] Wilson, M. W. B.; Rao, A.; Clark, J.; Kumar, R. S. S.; Brida, D.; Cerullo, G.; Friend, R. H. *J. Am. Chem. Soc.* **2011**, *133*, 11830–11833.

[57] Chan, W.-L.; Ligges, M.; Jailaubekov, A.; Kaake, L.; Miaja-Avila, L.; Zhu, X.-Y. *Science* **2011**, *334*, 1541–1545.

[58] Singh, S.; Jones, W. J.; Siebrand, W.; Stoicheff, B. P.; Schneider, W. G. *J. Chem. Phys.* **1965**, *42*, 330–342.

[59] Hanna, M. C.; Nozik, A. J. *J. Appl. Phys.* **2006**, *100*, 074510.

[60] Smith, M. B.; Michl, J. *Chem. Rev.* **2010**, *110*, 6891–6936.

[61] Smith, M. B.; Michl, J. *Annu. Rev. Phys. Chem.* **2013**, *64*, 361–386.

[62] Ostroverkhova, O. *Chem. Rev.* **2016**, *116*, 13279–13412.

[63] Casanova, D. *Chem. Rev.* **2018**, *118*, 7164–7207.

[64] Ito, S.; Nagami, T.; Nakano, M. *J. PhotoCh. PhotoBio. C* **2018**, *34*, 85–120.

[65] Krishnapriya, K. C.; Musser, A. J.; Patil, S. *ACS Energy Lett.* **2019**, *4*, 192–202.

[66] Ullrich, T.; Munz, D.; Guldi, D. M. *Chem. Soc. Rev.* **2021**, *50*, 3485–3518.

[67] Nagata, R.; Nakanotani, H.; Potscavage Jr., W. J.; Adachi, C. *Adv. Mater.* **2018**, *30*, 1801484.

[68] Qiao, X.; Ma, D. *Mater. Sci. Eng. R Rep.* **2020**, *139*, 100519.

[69] Smyser, K. E.; Eaves, J. D. *Sci. Rep.* **2020**, *10*, 18480.

[70] Aryanpour, K.; Shukla, A.; Mazumdar, S. *J. Phys. Chem. C* **2015**, *119*, 6966–6979.

[71] Merrifield, R. E. *J. Chem. Phys.* **1961**, *34*, 1835–1839.

[72] Bardeen, C. J. *Annu. Rev. Phys. Chem.* **2014**, *65*, 127–148.

[73] Miyata, K.; Conrad-Burton, F. S.; Geyer, F. L.; Zhu, X.-Y. *Chem. Rev.* **2019**, *119*, 4261–4292.

[74] Akdag, A.; Havlas, Z.; Michl, J. *J. Am. Chem. Soc.* **2012**, *134*, 14624–14631.

[75] Wibowo, M.; Broer, R.; Havenith, R. W. *Comput. Theor. Chem.* **2017**, *1116*, 190–194.

[76] Accomasso, D.; Persico, M.; Granucci, G. *J. PhotoCh. PhotoBio. A* **2022**, *427*, 113807.

[77] Feng, X.; Casanova, D.; Krylov, A. I. *J. Phys. Chem. C* **2016**, *120*, 19070–19077.

[78] Chen, M.; Bae, Y. J.; Mauck, C. M.; Mandal, A.; Young, R. M.; Wasielewski, M. R. *J. Am. Chem. Soc.* **2018**, *140*, 9184–9192.

[79] Millington, O.; Montanaro, S.; Leventis, A.; Sharma, A.; Dowland, S. A.; Sawhney, N.; Fallon, K. J.; Zeng, W.; Congrave, D. G.; Musser, A. J.; Rao, A.; Bronstein, H. *J. Am. Chem. Soc.* **2023**, *145*, 2499–2510.

[80] Wang, T.; Liu, H.; Wang, X.; Tang, L.; Zhou, J.; Song, X.; Lv, L.; Chen, W.; Chen, Y.; Li, X. *J. Mater. Chem. A* **2023**, *11*, 8515–8539.

[81] Berkelbach, T. C.; Hybertsen, M. S.; Reichman, D. R. *J. Chem. Phys.* **2013**, *138*, 114103.

[82] Beljonne, D.; Yamagata, H.; Brédas, J. L.; Spano, F. C.; Olivier, Y. *Phys. Rev. Lett.* **2013**, *110*, 226402.

[83] Alam, B.; Morrison, A. F.; Herbert, J. M. *J. Phys. Chem. C* **2020**, *124*, 24653–24666.

[84] Johnson, J. C.; Nozik, A. J.; Michl, J. *Accounts Chem. Res.* **2013**, *46*, 1290–1299.

[85] Korovina, N. V.; Das, S.; Nett, Z.; Feng, X.; Joy, J.; Haiges, R.; Krylov, A. I.; Bradforth, S. E.; Thompson, M. E. *J. Am. Chem. Soc.* **2016**, *138*, 617–627.

[86] Morrison, A. F.; Herbert, J. M. *J. Phys. Chem. Lett.* **2017**, *8*, 1442–1448.

[87] Shen, L.; Chen, Y.; Li, X.; Li, C. *J. Mol. Graph. Model.* **2016**, *66*, 187–195.

[88] Johnson, J. C.; Michl, J. *Top. Curr. Chem.* **2017**, *375*, 80.

[89] Pradhan, E.; Bentley, J. N.; Caputo, C. B.; Zeng, T. *ChemPhotoChem* **2020**, *4*, 5279–5287.

[90] Sardar, S. *J. Mol. Graph. Model.* **2020**, *98*, 107608.

[91] Zhang, M.; Hua, Z.; Liu, W.; Liu, H.; He, S.; Zhu, C.; Zhu, Y. *J. Mol. Model.* **2020**, *26*, 32.

[92] Stern, H. L.; Cheminal, A.; Yost, S. R.; Broch, K.; Bayliss, S. L.; Chen, K.; Tabachnyk, M.; Thorley, K.; Greenham, N.; Hodgkiss, J. M.; Anthony, J.; Head-Gordon, M.; Musser, A. J.; Rao, A.; Friend, R. H. *Nat. Chem.* **2017**, *9*, 1205–1212.

[93] Korovina, N. V.; Joy, J.; Feng, X.; Feltenberger, C.; Krylov, A. I.; Bradforth, S. E.; Thompson, M. E. *J. Am. Chem. Soc.* **2018**, *140*, 10179–10190.

[94] Sanders, S. N.; Pun, A. B.; Parenti, K. R.; Kumarasamy, E.; Yablon, L. M.; Sfeir, M. Y.; Campos, L. M. *Chem* **2019**, *5*, 1988–2005.

[95] Feng, X.; Krylov, A. I. *Phys. Chem. Chem. Phys.* **2016**, *18*, 7751–7761.

[96] Dover, C. B.; Gallaher, J. K.; Frazer, L.; Tapping, P. C.; Petty, A. J.; Crossley, M. J.; Anthony, J. E.; Kee, T. W.; Schmidt, T. W. *Nat. Chem.* **2018**, *10*, 305–310.

[97] Padula, D.; Omar, O. H.; Nematiaram, T.; Troisi, A. *Energ. Environ. Sci.* **2019**, *12*, 2412–2416.

[98] El Bakouri, O.; Smith, J. R.; Ottosson, H. *J. Am. Chem. Soc.* **2020**, *142*, 5602–5617.

[99] Patil, D. S.; Avhad, K. C.; Sekar, N. *Comput. Theo. Chem.* **2018**, *1138*, 75–83.

[100] Gawale, Y.; Sekar, N. *J. PhotoCh. PhotoBio. B* **2018**, *178*, 472–480.

[101] Fallon, K. J.; Budden, P.; Salvadori, E.; Ganose, A. M.; Savory, C. N.; Eyre, L.; Dowland, S.; Ai, Q.; Goodlett, S.; Risko, C.; Scanlon, D. O.; Kay, C. W. M.; Rao, A.; Friend, R. H.; Musser, A. J.; Bronstein, H. *J. Am. Chem. Soc.* **2019**, *141*, 13867–13876.

[102] Baranac-Stojanović, M. *J. Org. Chem.* **2019**, *84*, 13582–13594.

[103] Liu, Z.; Lin, L.; Jia, Q.; Cheng, Z.; Jiang, Y.; Guo, Y.; Ma, J. *J. Chem. Inf. Model.* **2021**, *61*, 1066–1082.

[104] Weber, F.; Mori, H. *Npj Comput. Mater.* **2022**, *8*, 1–14.

[105] Mauck, C. M.; Bae, Y. J.; Chen, M.; Powers-Riggs, N.; Wu, Y.-L.; Wasielewski, M. R. *ChemPhotoChem* **2018**, *2*, 223–233.

[106] Margulies, E. A.; Miller, C. E.; Wu, Y.; Ma, L.; Schatz, G. C.; Young, R. M.; Wasielewski, M. R. *Nat. Chem.* **2016**, *8*, 1120–1125.

[107] Zeng, T. *J. Phys. Chem. Lett.* **2016**, *7*, 4405–4412.

[108] Minkin, V. I.; Starikov, A. G.; Starikova, A. A. *J. Phys. Chem. A* **2021**, *125*, 6562–6570.

[109] Renaud, N.; Sherratt, P. A.; Ratner, M. A. *J. Phys. Chem. Lett.* **2013**, *4*, 1065–1069.

[110] Wang, L.; Olivier, Y.; Prezhdo, O. V.; Beljonne, D. *J. Phys. Chem. Lett.* **2014**, *5*, 3345–3353.

[111] Young, R. M.; Wasielewski, M. R. *Accounts Chem. Res.* **2020**, *53*, 1957–1968.

[112] Sandoval-Salinas, M. E.; Casanova, D. *ChemPhotoChem* **2021**, *5*, 282–293.

[113] Thomas, A.; Ji, C.; Siddlingeshwar, B.; Manohar, P. U.; Ying, F.; Wu, W. *Phys. Chem. Chem. Phys.* **2021**, *23*, 1050–1061.

[114] Tanaka, K.; Sakamaki, D.; Fujiwara, H. *Eur. J. Chem.* **2021**, *27*, 4430–4438.

[115] Feng, X.; Luzanov, A. V.; Krylov, A. I. *J. Phys. Chem. Lett.* **2013**, *4*, 3845–3852.

[116] Buchanan, E. A.; Havlas, Z.; Michl, J. In *Advances in Quantum Chemistry*; Sabin, J. R.; Brändas, E. J., Eds.; Advances in Quantum Chemistry: Ratner Volume, Vol. 75; Academic Press, 2017; pp 175–227.

[117] Kolata, K.; Breuer, T.; Witte, G.; Chatterjee, S. *ACS Nano* **2014**, *8*, 7377–7383.

[118] Felter, K. M.; Grozema, F. C. *J. Phys. Chem. Lett.* **2019**, *10*, 7208–7214.

[119] Zaykov, A.; Felkel, P.; Buchanan, E. A.; Jovanovic, M.; Havenith, R. W. A.; Kathir, R. K.; Broer, R.; Havlas, Z.; Michl, J. *J. Am. Chem. Soc.* **2019**, *141*, 17729–17743.

[120] Malrieu, J.-P.; Angeli, C.; Cimiraglia, R. *J. Chem. Educ.* **2008**, *85*, 150.

[121] Smith, D. G. A.; Burns, L. A.; Simmonett, A. C.; Parrish, R. M.; Schieber, M. C.; Galvelis, R.; Kraus, P.; Kruse, H.; Remigio, R. D.; Alenaizan, A.; James, A. M.; Lehtola, S.; Misiewicz, J. P.; Scheurer, M.; Shaw, R. A.; Schriber, J. B.; Xie, Y.; Glick, Z. L.; Sirianni, D. A.; O'Brien, J. S.; Waldrop, J. M.; Kumar, A.; Hohenstein, E. G.; Pritchard, B. P.; Brooks, B. R.; SchaeferIII, H. F.; Sokolov, A. Y.; Patkowski, K.; DePrinceIII, A. E.; Bozkaya, U.; King, R. A.; Evangelista, F. A.; Turney, J. M.; Crawford, T. D.; Sherrill, C. D. *J. Chem. Phys.* **2020**, *152*, 184108.

[122] ROSEIRO, P.; *PhdWorks*; 2023. `https://github.com/Pablo-R0/PhdWorks`.

[123] Roseiro, P.; Ben Amor, N.; Robert, V. *ChemPhysChem* **2022**, *23*, e202100801.

[124] Roseiro, P.; Petit, L.; Robert, V.; Yalouz, S. *ChemPhysChem* **2023**, *24*, e202200478.

[125] Roseiro, P.; Yalouz, S.; Brook, D. J. R.; Ben Amor, N.; Robert, V. *Inorg. Chem.* **2023**, *62*, 5737–5743.

[126] Kahn, O. *Curr. Opin. Solid State Mater. Sci.* **1996**, *1*, 547–554.

[127] Gütlich, P.; Garcia, Y.; Goodwin, H. A. *Chem. Soc. Rev.* **2000**, *29*, 419–427.

[128] Sato, O.; Tao, J.; Zhang, Y.-Z. *Angew. Chem., Int. Ed.* **2007**, *46*, 2152–2187.

[129] Gütlich, P.; Goodwin, H. A. *Spin Crossover—An Overall Perspective*; Springer Berlin Heidelberg: Berlin, Heidelberg, 2004; pp 1–47.

[130] Cambi, L.; Szegö, L. *Ber. Dtsch. Chem. Ges.* **1931**, *64*, 2591–2598.

[131] Pauling, L.; Coryell, C. D. *Proc. Natl. Acad. Sci. USA* **1936**, *22*, 210–216.

[132] Coryell, C. D.; Stitt, F.; Pauling, L. *J. Am. Chem. Soc.* **1937**, *59*, 633–642.

[133] Madeja, K.; König, E. *J. Inorg. Nucl. Chem.* **1963**, *25*, 377–385.

[134] Stoufer, R. C.; Busch, D. H.; Hadley, W. B. *J. Am. Chem. Soc.* **1961**, *83*, 3732–3734.

[135] Figgins, P. E.; Busch, D. H. *J. Am. Chem. Soc.* **1960**, *82*, 820–824.

[136] Mössbauer, R. L. *Naturwissenschaften* **1958**, *45*, 538–539.

[137] Frank, E.; Abeledo, C. R. *Inorg. Chem.* **1966**, *5*, 1453–1455.

[138] "König, E.; Madeja, K. *Chem. Commun. (London)* **1966**, 61–62.

[139] Gütlich, P. In *Metal Complexes*; Springer Berlin Heidelberg: Berlin, Heidelberg; pp 83–195.

[140] Gütlich, P.; Hauser, A. *Coord. Chem. Rev.* **1990**, *97*, 1–22.

[141] Goodwin, H. A. *Spin Crossover in Cobalt(II) Systems*; Springer Berlin Heidelberg: Berlin, Heidelberg, 2004; pp 23–47.

[142] Koenig, E.; Madeja, K. *Inorg. Chem.* **1967**, *6*, 48–55.

[143] Boylan, M. J.; Nelson, S. M.; Deeney, F. A. *J. Chem. Soc. A* **1971**, 976–981.

[144] Michalowicz, A.; Moscovici, J.; Ducourant, B.; Cracco, D.; Kahn, O. *Chem. Mater.* **1995**, *7*, 1833–1842.

[145] Martin, J.-P.; Zarembowitch, J.; Dworkin, A.; Haasnoot, J. G.; Codjovi, E. *Inorg. Chem.* **1994**, *33*, 2617–2623.

[146] Enriquez-Cabrera, A.; Rapakousiou, A.; Piedrahita Bello, M.; Molnár, G.; Salmon, L.; Bousseksou, A. *Coord. Chem. Rev.* **2020**, *419*, 213396.

[147] Mahfoud, T.; Molnár, G.; Cobo, S.; Salmon, L.; Thibault, C.; Vieu, C.; Demont, P.; Bousseksou, A. *Appl. Phys. Lett.* **2011**, *99*.

[148] Bousseksou, A.; Molnár, G.; Salmon, L.; Nicolazzi, W. *Chem. Soc. Rev.* **2011**, *40*, 3313–3335.

[149] Murray, K. S. *The Development of Spin-Crossover Research*; John Wiley & Sons, Ltd, 2013; Chapter 1, pp 1–54.

[150] Tanabe, Y.; Sugano, S. *J. Phys. Soc. Japan* **1954**, *9*, 766–779.

[151] Brooker, S. *Chem. Soc. Rev.* **2015**, *44*, 2880–2892.

[152] Kahn, O.; Kröber, J.; Jay, C. *Adv. Mater.* **1992**, *4*, 718–728.

[153] Amin, N. A. A. M.; Said, S. M.; Salleh, M. F. M.; Afifi, A. M.; Ibrahim, N. M. J. N.; Hasnan, M. M. I. M.; Tahir, M.; Hashim, N. Z. I. *Inorganica Chim. Acta* **2023**, *544*, 121168.

[154] Gütlich, P.; Ksenofontov, V.; Gaspar, A. B. *Coord. Chem. Rev.* **2005**, *249*, 1811–1829.

[155] Pinkowicz, D.; Rams, M.; Mišek, M.; Kamenev, K. V.; Tomkowiak, H.; Katrusiak, A.; Sieklucka, B. *J. Am. Chem. Soc.* **2015**, *137*, 8795–8802.

[156] Chastanet, G.; Lorenc, M.; Bertoni, R.; Desplanches, C. *C. R. Chim.* **2018**, *21*, 1075–1094.

[157] Boillot, M.-L.; Roux, C.; Audière, J.-P.; Dausse, A.; Zarembowitch, J. *Inorg. Chem.* **1996**, *35*, 3975–3980.

[158] Boillot, M.-L.; Chantraine, S.; Zarembowitch, J.; Lallemand, J.-Y.; Prunet, J. *New J. Chem.* **1999**, *23*, 179–184.

[159] Boillot, M.-L.; Zarembowitch, J.; Sour, A. *Ligand-Driven Light-Induced Spin Change (LD-LISC): A Promising Photomagnetic Effect*; Springer Berlin Heidelberg: Berlin, Heidelberg, 2004; pp 261–276.

[160] Thies, S.; Sell, H.; Schütt, C.; Bornholdt, C.; Näther, C.; Tuczek, F.; Herges, R. *J. Am. Chem. Soc.* **2011**, *133*, 16243–16250.

[161] Thies, S.; Sell, H.; Bornholdt, C.; Schütt, C.; Köhler, F.; Tuczek, F.; Herges, R. *Eur. J. Chem.* **2012**, *18*, 16358–16368.

[162] Decurtins, S.; Gütlich, P.; Köhler, C.; Spiering, H.; Hauser, A. *Chem. Phys. Lett.* **1984**, *105*, 1–4.

[163] Hauser, A. *Comment Inorg. Chem.* **1995**, *17*, 17–40.

[164] Hauser, A. *Chem. Phys. Lett.* **1986**, *124*, 543–548.

[165] Fouché, O.; Degert, J.; Jonusauskas, G.; Daro, N.; Létard, J.-F.; Freysz, E. *Phys. Chem. Chem. Phys.* **2010**, *12*, 3044–3052.

[166] Buchanan, R. M.; Pierpont, C. G. *J. Am. Chem. Soc.* **1980**, *102*, 4951–4957.

[167] Tezgerevska, T.; Alley, K. G.; Boskovic, C. *Coord. Chem. Rev.* **2014**, *268*, 23–40.

[168] Hendrickson, D. N.; Pierpont, C. G. *Valence Tautomeric Transition Metal Complexes*; Springer Berlin Heidelberg: Berlin, Heidelberg, 2004; pp 63–95.

[169] Sato, O.; Cui, A.; Matsuda, R.; Tao, J.; Hayami, S. *Accounts Chem. Res.* **2007**, *40*, 361–369.

[170] Evangelio, E.; Ruiz-Molina, D. *C. R. Chim.* **2008**, *11*, 1137–1154.

[171] Boskovic, C. *Valence Tautomeric Transitions in Cobalt-dioxolene Complexes*; John Wiley & Sons, Ltd, 2013; Chapter 7, pp 203–224.

[172] Lynch, M. W.; Hendrickson, D. N.; Fitzgerald, B. J.; Pierpont, C. G. *J. Am. Chem. Soc.* **1981**, *103*, 3961–3963.

[173] Kaim, W. *Inorg. Chem.* **2011**, *50*, 9752–9765.

[174] Jørgensen, C. *Coord. Chem. Rev.* **1966**, *1*, 164–178.

[175] Ratera, I.; Veciana, J. *Chem. Soc. Rev.* **2012**, *41*, 303–349.

[176] Vostrikova, K. E. *Coord. Chem. Rev.* **2008**, *252*, 1409–1419.

[177] Rozantsev, E. G.; Ulrich, H. *Nitrogen Oxides and Nitroxyls*; Springer US: Boston, MA, 1970; pp 13–51.

[178] Hearns, N. G. R.; Preuss, K. E.; Richardson, J. F.; Bin-Salamon, S. *J. Am. Chem. Soc.* **2004**, *126*, 9942–9943.

[179] Pierpont, C. G.; Attia, A. S. *Collect. Czechoslov. Chem. Commun.* **2001**, *66*, 33–51.

[180] Preuss, K. E. *Dalton Trans.* **2007**, 2357–2369.

[181] Brook, D. J. R. *Comment. Inorg. Chem.* **2015**, *35*, 1–17.

[182] Kuhn, R.; Trischmann, H. *Angew. Chem., Int. Ed. Engl.* **1963**, *2*, 155–155.

[183] Neugebauer, F. A.; Fischer, H. *Angew. Chem., Int. Ed. Engl.* **1980**, *19*, 724–725.

[184] Caneschi, A.; Gatteschi, D.; Laugier, J.; Rey, P.; Sessoli, R.; Zanchini, C. *Synthetic Pathways to Low-Dimensional Compounds Containing Transition Metal Ions and Nitroxide Radicals*; Springer US: New York, NY, 1987; pp 381–384.

[185] Brook, D. J. R.; Lynch, V.; Conklin, B.; Fox, M. A. *J. Am. Chem. Soc.* **1997**, *119*, 5155–5162.

[186] Ferrando-Soria, J.; Vallejo, J.; Castellano, M.; Martínez-Lillo, J.; Pardo, E.; Cano, J.; Castro, I.; Lloret, F.; Ruiz-García, R.; Julve, M. *Coord. Chem. Rev.* **2017**, *339*, 17–103.

[187] Jung, O.-S.; Pierpont, C. G. *J. Am. Chem. Soc.* **1994**, *116*, 2229–2230.

[188] Gaita-Ariño, A.; Luis, F.; Hill, S.; Coronado, E. *Nat. Chem.* **2019**, *11*, 301–309.

[189] Troiani, F.; Affronte, M. *Chem. Soc. Rev.* **2011**, *40*, 3119–3129.

[190] Stamp, P. C.; Gaita-Arino, A. *J. Mater. Chem.* **2009**, *19*, 1718–1730.

[191] McAdams, S. G.; Ariciu, A.-M.; Kostopoulos, A. K.; Walsh, J. P.; Tuna, F. *Coord. Chem. Rev.* **2017**, *346*, 216–239.

[192] Atzori, M.; Morra, E.; Tesi, L.; Albino, A.; Chiesa, M.; Sorace, L.; Sessoli, R. *J. Am. Chem. Soc.* **2016**, *138*, 11234–11244.

[193] Atzori, M.; Tesi, L.; Morra, E.; Chiesa, M.; Sorace, L.; Sessoli, R. *J. Am. Chem. Soc.* **2016**, *138*, 2154–2157.

[194] Bader, K.; Dengler, D.; Lenz, S.; Endeward, B.; Jiang, S.-D.; Neugebauer, P.; Van Slageren, J. *Nat. Commun.* **2014**, *5*, 1–5.

[195] Graham, M. J.; Zadrozny, J. M.; Shiddiq, M.; Anderson, J. S.; Fataftah, M. S.; Hill, S.; Freedman, D. E. *J. Am. Chem. Soc.* **2014**, *136*, 7623–7626.

[196] Atzori, M.; Benci, S.; Morra, E.; Tesi, L.; Chiesa, M.; Torre, R.; Sorace, L.; Sessoli, R. *Inorg. Chem.* **2018**, *57*, 731–740.

[197] Bayliss, S.; Laorenza, D.; Mintun, P.; Kovos, B.; Freedman, D. E.; Awschalom, D. *Science* **2020**, *370*, 1309–1312.

[198] Carretta, S.; Zueco, D.; Chiesa, A.; Gómez-León, Á.; Luis, F. *Appl. Phys. Lett.* **2021**, *118*, 240501.

[199] Li, J.; Xiong, S.-J.; Li, C.; Jin, B.; Zhang, Y.-Q.; Jiang, S.-D.; Ouyang, Z.-W.; Wang, Z.; Wu, X.-L.; van Tol, J.; et al. *CCS. Chem.* **2021**, *3*, 2548–2556.

[200] Nelson, J. N.; Zhang, J.; Zhou, J.; Rugg, B. K.; Krzyaniak, M. D.; Wasielewski, M. R. *J. Chem. Phys.* **2020**, *152*, 014503.

[201] Thiele, S.; Balestro, F.; Ballou, R.; Klyatskaya, S.; Ruben, M.; Wernsdorfer, W. *Science* **2014**, *344*, 1135–1138.

[202] Hussain, R.; Allodi, G.; Chiesa, A.; Garlatti, E.; Mitcov, D.; Konstantatos, A.; Pedersen, K. S.; De Renzi, R.; Piligkos, S.; Carretta, S. *J. Am. Chem. Soc.* **2018**, *140*, 9814–9818.

[203] Chiesa, A.; Petiziol, F.; Macaluso, E.; Wimberger, S.; Santini, P.; Carretta, S. *AIP Adv.* **2021**, *11*, 025134.

[204] Maylander, M.; Chen, S.; Lorenzo, E. R.; Wasielewski, M. R.; Richert, S. *J. Am. Chem. Soc.* **2021**, *143*, 7050–7058.

[205] Cimatti, I.; Bondi, L.; Serrano, G.; Malavolti, L.; Cortigiani, B.; Velez-Fort, E.; Betto, D.; Ouerghi, A.; Brookes, N.; Loth, S.; et al. *Nanoscale Horiz.* **2019**, *4*, 1202–1210.

[206] Zadrozny, J. M.; Niklas, J.; Poluektov, O. G.; Freedman, D. E. *ACS Cent. Sci.* **2015**, *1*, 488–492.

[207] Lehmann, J.; Gaita-Arino, A.; Coronado, E.; Loss, D. *J. Mater. Chem.* **2009**, *19*, 1672–1677.

[208] Timco, G. A.; Carretta, S.; Troiani, F.; Tuna, F.; Pritchard, R. J.; Muryn, C. A.; McInnes, E. J.; Ghirri, A.; Candini, A.; Santini, P.; et al. *Nat. Nanotechnol.* **2009**, *4*, 173–178.

[209] Ghosh, P.; Bill, E.; Weyhermüller, T.; Neese, F.; Wieghardt, K. *J. Am. Chem. Soc.* **2003**, *125*, 1293–1308.

[210] Tomson, N. C.; Labios, L. A.; Weyhermuller, T.; Figueroa, J. S.; Wieghardt, K. *Inorg. Chem.* **2011**, *50*, 5763–5776.

[211] Berry, J. F.; Bill, E.; Bothe, E.; George, S. D.; Mienert, B.; Neese, F.; Wieghardt, K. *Science* **2006**, *312*, 1937–1941.

[212] Rota, J.-B.; Norel, L.; Train, C.; Amor, N. B.; Maynau, D.; Robert, V. *J. Am. Chem. Soc.* **2008**, *130*, 10380–10385.

[213] Guihéry, N.; Robert, V.; Neese, F. *J. Phys. Chem. A* **2008**, *112*, 12975–12979.

[214] Herebian, D.; Wieghardt, K. E.; Neese, F. *J. Am. Chem. Soc.* **2003**, *125*, 10997–11005.

[215] McKinnon, S. D. J.; Patrick, B. O.; Lever, A. B. P.; Hicks, R. G. *ChemComm* **2010**, *46*, 773–775.

[216] Koivisto, B. D.; Hicks, R. G. *Coord. Chem. Rev.* **2005**, *249*, 2612–2630.

[217] Anderson, P. W.; Hasegawa, H. *Phys. Rev.* **1955**, *100*, 675.

[218] Bastardis, R.; Guihéry, N.; de Graaf, C. *J. Chem. Phys.* **2008**, *129*, 104102.

[219] Papaefthymiou, V.; Girerd, J.; Moura, I.; Moura, J.; Muenck, E. *J. Am. Chem. Soc.* **1987**, *109*, 4703–4710.

[220] Fleming, C.; Chung, D.; Ponce, S.; Brook, D. J. R.; DaRos, J.; Das, R.; Ozarowski, A.; Stoian, S. A. *Chem. Commun.* **2020**, *56*, 4400–4403.

[221] Bordage, A.; Bleuzen, A. *Radiat. Phys. Chem.* **2020**, *175*, 108143.

[222] Cafun, J.-D.; Champion, G.; Arrio, M.-A.; dit Moulin, C. C.; Bleuzen, A. *J. Am. Chem. Soc.* **2010**, *132*, 11552–11559.

[223] Hauser, A. *Ligand Field Theoretical Considerations*; Springer Berlin Heidelberg: Berlin, Heidelberg, 2004; pp 49–58.

[224] Kepenekian, M.; Le Guennic, B.; Robert, V. *J. Am. Chem. Soc.* **2009**, *131*, 11498–11502.

[225] Kepenekian, M.; Le Guennic, B.; Robert, V. *Phys. Rev. B* **2009**, *79*, 094428.

[226] Oms, O.; Rota, J.-B.; Norel, L.; Calzado, C. J.; Rousselière, H.; Train, C.; Robert, V. *Eur. J. Inorg. Chem.* **2010**, *2010*, 5373–5378.

[227] Brook, D. J. R.; Richardson, C. J.; Haller, B. C.; Hundley, M.; Yee, G. T. *Chem. Commun.* **2010**, *46*, 6590–6592.

[228] Barclay, T. M.; Hicks, R. G.; Lemaire, M. T.; Thompson, L. K. *Inorg. Chem.* **2003**, *42*, 2261–2267.

[229] Rota, J.-B.; Le Guennic, B.; Robert, V. *Inorg. Chem.* **2010**, *49*, 1230–1237.

[230] Amico, L.; Fazio, R.; Osterloh, A.; Vedral, V. *Rev. Mod. Phys.* **2008**, *80*, 517–576.

[231] Hendrickx, N. W.; Franke, D. P.; Sammak, A.; Scappucci, G.; Veldhorst, M. *Nature* **2020**, *577*, 487–491.

[232] Ballance, C. J.; Harty, T. P.; Linke, N. M.; Sepiol, M. A.; Lucas, D. M. *Phys. Rev. Lett.* **2016**, *117*, 060504.

[233] Morgado, M.; Whitlock, S. *AVS Quantum Sci.* **2021**, *3*.

[234] Barends, R.; Kelly, J.; Megrant, A.; Veitia, A.; Sank, D.; Jeffrey, E.; White, T. C.; Mutus, J.; Fowler, A. G.; Campbell, B.; Chen, Y.; Chen, Z.; Chiaro, B.; Dunsworth, A.; Neill, C.; O'Malley, P.; Roushan, P.; Vainsencher, A.; Wenner, J.; Korotkov, A. N.; Cleland, A. N.; Martinis, J. M. *Nature* **2014**, *508*, 500–503.

[235] Arute, F.; Arya, K.; Babbush, R.; Bacon, D.; Bardin, J. C.; Barends, R.; Biswas, R.; Boixo, S.; Brandao, F. G. S. L.; Buell, D. A.; Burkett, B.; Chen, Y.; Chen, Z.; Chiaro, B.; Collins, R.; Courtney, W.; Dunsworth, A.; Farhi, E.; Foxen, B.; Fowler, A.; Gidney, C.; Giustina, M.; Graff, R.; Guerin, K.; Habegger, S.; Harrigan, M. P.; Hartmann, M. J.; Ho, A.; Hoffmann, M.; Huang, T.; Humble, T. S.; Isakov, S. V.; Jeffrey, E.; Jiang, Z.; Kafri, D.; Kechedzhi, K.; Kelly, J.; Klimov, P. V.; Knysh, S.; Korotkov, A.; Kostritsa, F.; Landhuis, D.; Lindmark, M.; Lucero, E.; Lyakh, D.; Mandrà, S.; McClean, J. R.; McEwen, M.; Megrant, A.; Mi, X.; Michielsen, K.; Mohseni, M.; Mutus, J.; Naaman, O.; Neeley, M.; Neill, C.; Niu, M. Y.; Ostby, E.; Petukhov, A.; Platt, J. C.; Quintana, C.; Rieffel, E. G.; Roushan, P.; Rubin, N. C.; Sank, D.; Satzinger, K. J.; Smelyanskiy, V.; Sung, K. J.; Trevithick, M. D.; Vainsencher, A.; Villalonga, B.; White, T.; Yao, Z. J.; Yeh, P.; Zalcman, A.; Neven, H.; Martinis, J. M. *Nature* **2019**, *574*, 505–510.

[236] Killoran, N.; Izaac, J.; Quesada, N.; Bergholm, V.; Amy, M.; Weedbrook, C. *Quantum* **2019**, *3*, 129.

[237] Madsen, L. S.; Laudenbach, F.; Askarani, M. F.; Rortais, F.; Vincent, T.; Bulmer, J. F. F.; Miatto, F. M.; Neuhaus, L.; Helt, L. G.; Collins, M. J.; Lita, A. E.; Gerrits, T.; Nam, S. W.; Vaidya, V. D.; Menotti, M.; Dhand, I.; Vernon, Z.; Quesada, N.; Lavoie, J. *Nature* **2022**, *606*, 75–81.

[238] Moreno-Pineda, E.; Godfrin, C.; Balestro, F.; Wernsdorfer, W.; Ruben, M. *Chem. Soc. Rev.* **2018**, *47*, 501–513.

[239] Yalouz, S.; Koridon, E.; Senjean, B.; Lasorne, B.; Buda, F.; Visscher, L. *J. Chem. Theory Comput.* **2022**, *18*, 776–794.

[240] Maurer, P. C.; Kucsko, G.; Latta, C.; Jiang, L.; Yao, N. Y.; Bennett, S. D.;

Pastawski, F.; Hunger, D.; Chisholm, N.; Markham, M.; Twitchen, D. J.; Cirac, J. I.; Lukin, M. D. *Science* **2012**, *336*, 1283–1286.

[241] Yu, C.-J.; Graham, M. J.; Zadrozny, J. M.; Niklas, J.; Krzyaniak, M. D.; Wasielewski, M. R.; Poluektov, O. G.; Freedman, D. E. *J. Am. Chem. Soc.* **2016**, *138*, 14678–14685.

[242] Wasielewski, M. R.; Forbes, M. D. E.; Frank, N. L.; Kowalski, K.; Scholes, G. D.; Yuen-Zhou, J.; Baldo, M. A.; Freedman, D. E.; Goldsmith, R. H.; Goodson, T.; Kirk, M. L.; McCusker, J. K.; Ogilvie, J. P.; Shultz, D. A.; Stoll, S.; Whaley, K. B. *Nat. Rev. Chem.* **2020**, *4*, 490–504.

[243] Atzori, M.; Sessoli, R. *J. Am. Chem. Soc.* **2019**, *141*, 11339–11352.

[244] Takahashi, S.; van Tol, J.; Beedle, C. C.; Hendrickson, D. N.; Brunel, L.-C.; Sherwin, M. S. *Phys. Rev. Lett.* **2009**, *102*, 087603.

[245] Schlegel, C.; van Slageren, J.; Manoli, M.; Brechin, E. K.; Dressel, M. *Phys. Rev. Lett.* **2008**, *101*, 147203.

[246] Troiani, F.; Ghirri, A.; Affronte, M.; Carretta, S.; Santini, P.; Amoretti, G.; Piligkos, S.; Timco, G.; Winpenny, R. E. P. *Phys. Rev. Lett.* **2005**, *94*, 207208.

[247] Atzori, M.; Tesi, L.; Benci, S.; Lunghi, A.; Righini, R.; Taschin, A.; Torre, R.; Sorace, L.; Sessoli, R. *J. Am. Chem. Soc.* **2017**, *139*, 4338–4341.

[248] McGuire, J.; Miras, H. N.; Donahue, J. P.; Richards, E.; Sproules, S. *Eur. J. Chem.* **2018**, *24*, 17598–17605.

[249] Lindgren, I.; Morrison, J. *Atomic many-body theory*; Springer Science & Business Media, 2012; Vol. 3.

[250] Breuer, H.-P. *Phys. Rev. A* **2005**, *71*, 062330.

[251] Breuer, H.-P. *J. Phys. A Math.* **2005**, *38*, 9019.

[252] Briganti, M.; Lucaccini, E.; Chelazzi, L.; Ciattini, S.; Sorace, L.; Sessoli, R.; Totti, F.; Perfetti, M. *J. Am. Chem. Soc.* **2021**, *143*, 8108–8115.

[253] Norel, L.; Rota, J.-B.; Chamoreau, L.-M.; Pilet, G.; Robert, V.; Train, C. *Angew. Chem., Int. Ed.* **2011**, *50*, 7128–7131.

[254] Fumanal, M.; Vela, S.; Novoa, J. J.; Ribas-Arino, J. *ChemComm* **2015**, *51*, 15776–15779.

[255] Krah, T.; Suaud, N.; Zanchet, A.; Robert, V.; Ben Amor, N. *Eur. J. Inorg. Chem.* **2012**, *2012*, 5777–5783.

[256] Fleming, C.; Chung, D.; Ponce, S.; Brook, D. J. R.; DaRos, J.; Das, R.; Ozarowski, A.; Stoian, S. A. *ChemComm* **2020**, *56*, 4400–4403.

[257] Lemaire, M. T.; Barclay, T. M.; Thompson, L. K.; Hicks, R. G. *Inorganica Chim. Acta* **2006**, *359*, 2616–2621.

[258] Barclay, T. M.; Hicks, R. G.; Lemaire, M. T.; Thompson, L. K.; Xu, Z. *ChemComm* **2002**, 1688–1689.

[259] Bowman, A. C.; Milsmann, C.; Bill, E.; Lobkovsky, E.; Weyhermüller, T.; Wieghardt, K.; Chirik, P. J. *Inorg. Chem.* **2010**, *49*, 6110–6123.

[260] Gütlich, P.; Garcia, Y.; Goodwin, H. A. *Chem. Soc. Rev.* **2000**, *29*, 419–427.

[261] Kepenekian, M.; Le Guennic, B.; Robert, V. *J. Am. Chem. Soc.* **2009**, *131*, 11498–11502.

[262] Vérot, M.; Bréfuel, N.; Pécaut, J.; Train, C.; Robert, V. *Chem. Asian J.* **2012**, *7*, 380–386.

[263] Brook, D. J. R.; Fleming, C.; Chung, D.; Richardson, C.; Ponce, S.; Das, R.; Srikanth, H.; Heindl, R.; Noll, B. C. *Dalton Trans.* **2018**, *47*, 6351–6360.

[264] Yalouz, S.; Gullin, M. R.; Sekaran, S. *J. Open Source Softw.* **2022**, *7*, 4759.

[265] Delgado, T.; Tissot, A.; Guénée, L.; Hauser, A.; Valverde-Muñoz, F. J.; Seredyuk, M.; Real, J. A.; Pillet, S.; Bendeif, E.-E.; Besnard, C. *J. Am. Chem. Soc.* **2018**, *140*, 12870–12876.

[266] Sousa, C.; de Graaf, C.; Rudavskyi, A.; Broer, R.; Tatchen, J.; Etinski, M.; Marian, C. M. *Eur. J. Chem.* **2013**, *19*, 17541–17551.

[267] Alías-Rodríguez, M.; Huix-Rotllant, M.; de Graaf, C. *Faraday Discuss.* **2022**, *237*, 93–107.

[268] Messaoudi, S.; Robert, V.; Guihéry, N.; Maynau, D. *Inorg. Chem.* **2006**, *45*, 3212–3216.

[269] Calzado, C. J.; Cabrero, J.; Malrieu, J. P.; Caballol, R. *J. Chem. Phys.* **2002**, *116*, 2728–2747.

[270] Calzado, C. J.; Cabrero, J.; Malrieu, J. P.; Caballol, R. *J. Chem. Phys.* **2002**, *116*, 3985–4000.

[271] Terencio, T.; Bastardis, R.; Suaud, N.; Maynau, D.; Bonvoisin, J.; Malrieu, J. P.; Calzado, C. J.; Guihéry, N. *Phys. Chem. Chem. Phys.* **2011**, *13*, 12314–12320.

Université de Strasbourg

Pablo ROSEIRO

EDSC École Doctorale des Sciences Chimiques

The role of open-shell environments on the spectroscopy of complex spin architectures: wavefunction-based studies.

Résumé

Cette thèse étudie l'influence de l'environnement sur les architectures complexes de spin. Elle se concentre sur les environnements à couche ouverte en Chimie Organique et Inorganique. Elle commence par une présentation des outils et des méthodes de calcul fonction d'onde utilisés dans ce travail. Ensuite, une étude basée sur un Hamiltonien modèle explore qualitativement l'importance des environnements dans la Fission du Singulet. Elle se concentre sur la "condition thermodynamique" et met en évidence les défauts de l'approximation du "chromophore unique". Enfin, un Hamiltonien modèle et deux études *ab initio* étudient l'émergence d'un nouveau phénomène : la *spinmérie*. Les architectures basées sur un ion métallique à transition de spin coordonné à plusieurs ligands à couche ouverte sont susceptibles de générer des états étant une superposition d'états de spin locaux. Cela bouleverse le concept de spins gelés dans les composés de coordination, en particulier dans les diagrammes de Tanabe-Sugano.

Mots-clés : Chimie Quantique, Hamiltonien modèle, calculs *ab initio*, théorie de la fonction d'onde, Fission du Singulet, *Spinmérie*

Abstract

This thesis studies the influence of the environment in complex spin architectures. It focuses on open-shell environments in the fields of Organic and Inorganic Chemistry. It starts off by introducing the basic tools and methods for wavefunction calculations used in this work. Then, a model Hamiltonian-based study qualitatively explores the importance of environments in Singlet Fission. It focuses on the so-defined "thermodynamic condition", and highlights the flaws of the "single chromophore" approximation broadly used in the experimental and theoretical community. Finally, a model Hamiltonian and two *ab initio* studies investigate the emergence of a new phenomenon: *spinmerism*. Architectures based on a Spin CrossOver metal ion coordinated to several open-shell ligands are likely to generate states which are a superposition of local spin states. This reshuffles the traditional frozen-spin picture in coordination compounds, in particular in the Tanabe-Sugano diagrams.

Keywords: Quantum Chemistry, model Hamiltonian, *ab initio* calculations, Wave-Function Theory, Singlet Fission, *Spinmerism*